

**Structural and Functional Characterization
of Adenylosuccinate Synthetase from a
Mesophilic Parasitic Protozoan,
Plasmodium falciparum and a Thermophilic
Archaea, *Methanocaldococcus jannaschii***

A Thesis Submitted for the Award of the Degree of
Doctor of Philosophy

By
Sonali Mehrotra



**Molecular Biology and Genetics Unit
Jawaharlal Nehru Centre for Advanced Scientific Research
(A Deemed University)
Bangalore – 560064, INDIA
May 2008**

Declaration

I hereby declare that this thesis entitled “**Structural and Functional Characterization of Adenylosuccinate Synthetase from a Mesophilic Parasitic Protozoan, *Plasmodium falciparum* and a Thermophilic Archaea, *Methanocaldococcus jannaschii***” is an authentic record of the research work carried out by me under the supervision of Prof. Hemalatha Balaram at the Molecular Biology and Genetics Unit, Jawaharlal Nehru Centre for Advanced Scientific Research, Bangalore, India and that this work has not been submitted elsewhere for the award for any other degree.

In keeping with the general practice of reporting scientific observations, due acknowledgement has been made, wherever the work described has been based on the findings of other investigators. Any omission, which might have occurred by oversight or misjudgement, is regretted.

(Sonali Mehrotra)

Place:

Date:

Acknowledgements

I gratefully acknowledge my supervisor, Prof. Hemalatha Balaram for her constant guidance, encouragement and support. Her amazing patience, even in the face of extreme provocation and, the intellectual freedom she allowed ensured that working in the laboratory was always a pleasure. I take this opportunity to express my gratitude to her.

The inputs and comments that I have received from the faculty members of MBGU- Prof. Anuranjan Anand, Prof. Ranga Uday, Prof. Maneesha Inamdar, Prof. Tapas Kundu, Prof. Namita Surolia, Prof. Kaustav Sanyal and Prof. M. R. S. Rao has greatly improved the quality of this work. I gratefully acknowledge their help during the course of this study. I take this opportunity to thank Prof. Dipankar Chatterji, who has taken an active interest in my work, for his encouragement and advice.

I sincerely thank Prof. Rama Govindarajan, Engineering Mechanics Unit, JNCASR, and Prof. S. Balasubramanian, Chemistry and Physics of Materials Unit, JNCASR, for useful discussions during the mathematical analysis of the kinetic data presented in this thesis. I acknowledge Prof. Jayant B. Udgaonkar, NCBS for providing access to the stopped flow apparatus.

I have had the pleasure of the association of many people during the course of my work. Without the help of Dr. Mylarappa an extensive analysis of *P. falciparum* AdSS mutants would not have been possible. Bopanna has assisted me in the culture experiments that form a part of this thesis. Dr. Amit Mandal, Dr. Pradip and Suma in Prof. Balaram's lab, IISc have helped me with the mass spectrometry experiments. Dr. Pratima Iyengar, MBU, IISc carried out the docking studies. Discussions with Anubhab in Engineering Mechanics Unit, JNCASR have helped in the analysis of the urea unfolding data. Thanks are due to Prof. M. R. N. Murthy and Gayathri for useful inputs

during the attempts to crystallize MjAdSS. I also thank Mousumi, MBU, IISc for her help in carrying out many experiments in IISc.

It has been a memorable experience working in the laboratory, the credit for which is due to all my labmates, both past and present: Dr. Sujay Subbaya, Dr. Priyaranjan Pattanaik, Dr. Jayalakshmi, Dr. Mylarappa, Dr. Chethana, Subhra, Javaid, Vinay, Bharath, Sanjeev, Bimba, Ranjith, Bopanna, Rupa, Shastri and Shilpa. I thank them for the discussions, comments, criticisms and help with experiments. Special thanks are due to my seniors: Dr. Jayalakshmi for all the advice, help and guidance and to Dr. Chethan for his help in conducting various experiments and teaching me the use of various instruments. Special thanks are due to Vinay, Krithika, Subhra and Moumita for painstakingly proof reading the thesis. I wish to thank Subhra and Moumita who have been of immense help during the writing and formatting of this thesis.

Being a part of JNC community has been a wonderful experience. I thank all my batchmates and friends at JNC for making my stay here memorable.

I thank the entire support staff of JNCASR, computer lab personnel, the library and administrative staff who have been highly supportive and helpful throughout.

I acknowledge CSIR and JNCASR for providing financial assistance.

I would have never reached this stage of my carrier if not for the support of my family members. I take this opportunity to thank my father, mother, brother and sister for their constant encouragement and motivation during the course of my Ph.D. and dedicate this thesis to my parents.

Synopsis

Adenylosuccinate synthetase (AdSS) catalyzes the Mg^{2+} dependent condensation of a molecule of IMP with aspartate to form adenylosuccinate (sAMP), in a reaction driven by the conversion of GTP to GDP. This occurs by a concerted two step process, where the first step involves the transfer of γ -phosphate from GTP to IMP resulting in the formation of the intermediate, 6-phosphoryl IMP. Subsequent nucleophilic attack by the α -amino group of aspartate on the C6 position of the phosphorylated purine results in the displacement of the phosphate group and generation of the products sAMP, GDP and Pi. Though AdSS from a vast majority of organisms is 430-457 amino acids in length, the NCBI protein data base contains 38 annotated AdSS sequences that are shorter in length by 90-120 amino acids. The short AdSS sequences which consist of 333-345 amino acids contain two deletions that map to the mid-region and C-terminus of the protein. The effect of these deletions on the structure, function and regulation of AdSS has not been examined.

Though catalyzing the same reaction chemistry, thermophilic and mesophilic enzymes differ in a number of structural and functional properties. Thermophilic enzymes are often smaller and exhibit higher oligomeric states when compared to their mesophilic counterpart. They exhibit remarkable structural stability and catalyze reactions optimally at higher temperatures, where the mesophilic enzymes completely denature and lose activity. To understand the differences in structure and function of AdSS from a mesophilic and a thermophilic source, detailed biochemical characterization of the enzyme from *Plasmodium falciparum*, a mesophilic parasitic protozoan and *Methanocaldococcus jannaschii*, a thermophilic archaea, has been undertaken.

The thesis is divided into six chapters. The first chapter provides an introduction to the life cycle of *Plasmodium falciparum* along with a brief introduction to the

thermophile, *Methanocaldococcus jannaschii*. The chapter also discusses the available literature on adenylosuccinate synthetase. The last section provides a comparative account of the properties of mesophilic and thermophilic proteins and outlines the features of thermozyms that are implicated in thermostability of these proteins.

The second chapter discusses the detailed biochemical characterization of adenylosuccinate synthetase from *Methanocaldococcus jannaschii* and highlights unique features of the archaeal enzyme. The gene encoding AdSS was PCR amplified from *Methanococcus* genomic DNA, cloned in pET23d expression vector and conditions for expression and purification of the enzyme standardized. All well characterized AdSS have been shown to function as homodimers. In contrast, *M. jannaschii* AdSS (MjAdSS) on analytical size exclusion chromatography eluted at a retention volume that was indicative of dimer-tetramer equilibrium. Examination by Dynamic Light Scattering showed that the protein samples were monodispersed with molecular mass of 160 ± 5 kDa (monomer mass 38 kDa) and this result corroborated size exclusion chromatography measurements. Gel filtration studies in the presence of substrates indicated that the tetramer is the catalytically active form of the enzyme. Elucidation of the kinetic mechanism of the three substrate reaction catalyzed by MjAdSS was achieved using initial velocity kinetics and product inhibition studies. Initial velocity kinetics done by the method proposed by Fromm (*Methods in Enzymology* 63,138-159, 1979) and the method proposed by Frieden (*J. Biol. Chem.* 234, 2891-2896, 1959) enabled us to elucidate the kinetic mechanism of the thermophilic enzyme. MjAdSS exhibits rapid equilibrium random AB steady-state ordered C kinetic mechanism (A, B and C denote IMP, GTP and aspartate, respectively). The data were fit to appropriate equations and all kinetic constants governing the reaction elucidated. Further, using product inhibition studies the order of product release was deduced. sAMP and AMP were used as competitive inhibitors of IMP, GDP and GMP, as competitive inhibitors of GTP and in the absence of a product analog of aspartate, the fungal metabolite, hadacidin was used. Competitive inhibitors of IMP and GTP showed noncompetitive inhibition with the other two substrates, whereas hadacidin showed uncompetitive inhibition with IMP and GTP indicating ordered binding of aspartate to E.IMP.GTP complex. The data were fit to equations defining competitive, noncompetitive and uncompetitive inhibition and best fit selected on the basis of statistical significance. Based on the K_i values, we propose that Pi gets

released first from the enzyme active site, followed by random release of GDP and sAMP, which showed similar K_i values.

To explore aspects of regulation of MjAdSS, the effect of the substrate IMP and the glycolytic intermediate, fructose 1,6 bisphosphate (F16BP) was checked on enzyme activity. High concentrations of IMP (>1 mM) at subsaturating concentrations of GTP inhibited MjAdSS activity and this inhibition was relieved at high GTP concentration. Similar feature has been observed in the case of mouse and *P. falciparum* AdSS. Like mouse and rat skeletal muscle AdSS, F16BP inhibits MjAdSS with the inhibition being competitive with respect to IMP and noncompetitive with GTP.

Two important attributes of enzymes from thermophilic organisms are thermophilicity and structural stability. Chapter three outlines the studies carried out to understand these two aspects in AdSS from *M. jannaschii*. MjAdSS shows very weak activity at ambient temperatures where *P. falciparum* AdSS (PfAdSS) exhibits optimum catalysis. Temperature dependence of MjAdSS catalysis exhibited a biphasic Arrhenius Plot with an inflection at 40°C. Non-linearity in Arrhenius Plot could reflect different rate limiting steps across the inflection temperature. AdSS mediated conversion of IMP to sAMP occurs via a two step process, with the first step involving the formation of the intermediate 6-phosphoryl IMP (6P-IMP) and the product GDP which remain bound to the enzyme. We examined the effect of temperature on the first step of catalysis by monitoring the level of GDP formed under steady-state conditions. Thereafter, we also measured the effect of temperature on pre-steady-state kinetics of MjAdSS. GDP formation at the two temperatures, 25 and 70°C was monitored by reverse phase HPLC of reaction mixtures containing equivalent concentrations of enzyme, IMP and GTP incubated at the two temperatures for different time periods. Surprisingly, GDP formation was not instantaneous at either of the two temperatures and the amount of GDP formed increased with time. When hadacidin, which is an aspartic acid analog, was added to the reaction mixture almost complete conversion of GTP to GDP was observed in 30 seconds at both 25 and 70°C. This experiment suggested that at lower temperatures, intermediate formation is not impeded. Temperature dependence of transient kinetics indicated the presence of a “burst” at temperatures between 18-32°C that was absent at and above 35°C, a temperature close to the inflection point in the Arrhenius Plot. Taken together the results suggest that at lower temperatures product release is rate limiting and with increase in temperature

either catalysis or a step preceding it, is the rate determining step in MjAdSS catalyzed reaction.

Thermal unfolding of MjAdSS monitored by circular dichroism spectroscopy, showed a T_m of 85°C, with the process being only partially reversible. Stability of MjAdSS assessed by equilibrium unfolding revealed the robustness of secondary and tertiary structure of the enzyme which remained intact even at 8 M concentration of urea. Guanidinium chloride (GdmCl) induced denaturation of MjAdSS permitted estimation of thermodynamic parameters. Changes in quaternary, tertiary and secondary structure of the enzyme in GdmCl solution were monitored by size exclusion chromatography, fluorescence and circular dichroism spectroscopy. Size exclusion chromatography showed that tetramer dissociation occurred at 0.5 M GdmCl concentration resulting in formation of dimers, which were extremely stable and dissociated only at high denaturant concentrations. The unfolding profiles monitored by fluorescence and CD could be described as a composite of at least two distinct transitions, with a stable intermediate in the unfolding pathway. The first transition corresponds to dimer unfolding and the second to dimer dissociation and monomer unfolding.

The following two chapters of the thesis are centered on characterization of adenylosuccinate synthetase from a mesophilic parasitic protozoan, *Plasmodium falciparum*. Stability of quaternary, tertiary and secondary structure of PfAdSS in urea solution was monitored by size exclusion chromatography, fluorescence and circular dichroism spectroscopy. These studies showed that unlike MjAdSS the association of PfAdSS dimer was weak. Far UV-CD showed two transitions with the first corresponding to dimer dissociation and the second to monomer unfolding and aggregation. Changes in tertiary structure of the protein set in at 0.5 M urea concentration, with the protein showing a continuous multistate transition with increasing urea concentration. Liganding with IMP stabilized the PfAdSS dimer till 1M urea concentration. Earlier studies in the laboratory had shown that PfAdSS rapidly lost activity on storage due to the formation of S-S bonded soluble aggregates. Addition of DTT provided partial protection while inclusion of EDTA in storage buffer increased shelf-life and prevented formation of S-S bonded aggregates. Stabilization seen in the presence of EDTA indicated the role of contaminating metal ions in accelerating the rate of formation of S-S bonded inactive aggregates. AdSS is active as a non-covalently

linked homodimer with the active site at the interface. Inactivation by the cysteine modifying agent, iodoacetate, was accompanied by the destabilization of the dimer as seen on gel filtration chromatography. The substrate, IMP, could protect the protein from inactivation by iodoacetate. These observations implicated interface cysteines in the inactivation process. Three cysteine residues, Cys250, Cys328 and Cys368 were found to lie at the interface of the protein. The crystal structure of PfAdSS solved to 2.0 Å resolution showed additional electron density around the two interface cysteines, Cys328 and Cys368, although the exact nature of the modification could not be mapped. To identify the nature of interface cysteines and to examine their role in maintaining dimer stability, techniques of chemical modification followed by mass spectrometry and site-directed mutagenesis were employed. Cysteines by virtue of possessing an ionizable thiol group in their side chain are highly reactive, oxidizing to S⁻ and S-S, and also higher oxidation states of Cys-SOH, Cys-SO₂H and Cys-SO₃H. Though cysteine sulphonic acids are stable, cysteine sulphenic and sulphinic acids are highly unstable and tend to get reduced to thiols when removed from the native protein environment. The thiol reagent, 7-chloro-4-nitrobenzo-2-oxa-1,3-diazole (NBD chloride), reacts with both cysteine thiols and sulphenic acids at neutral pH and forms adducts which can be differentiated on the basis of mass. Modification studies with PfAdSS showed that Cys328 and Cys368 get only partially modified even after one hour treatment with the reagent, as high intensity peaks corresponding to the unmodified parent peptide containing the two cysteines continued to be present in the mass spectrum. Cys250 remained unmodified while Cys352 showed peptides of mass corresponding to both thiol and sulphenic acid adducts. Hence, this experiment did not provide an unambiguous result on the nature of the cysteines at the interface. Further site-directed mutagenesis was undertaken to probe the nature of interface cysteines and evaluate their role in maintaining dimer stability. For this, cysteine to serine mutants (C328S, C368S and double mutant C328S-C368S) and cysteine to aspartic acid mutants (C328D, C328D-C368D) were made. Though, the urea denaturation profile of C328S mutant was largely similar to the wild type (Wt) protein, gel filtration analysis to evaluate the oligomeric status of interface cysteine to serine mutants showed that C328S and the double mutant exhibit a shift in monomer-dimer equilibrium with clear appearance of monomers seen in the double mutant. In proteins, where cysteine reactivity affects structural stability, cysteine to serine mutations often impart stability.

Only exceptions are the cases where ionized or higher oxidation states of cysteines are essential for structural integrity. Cysteine side chain thiol has a pK_a of 8.4 whereas serine side chain hydroxyl has a very high pK_a and does not ionize easily. Studies on cysteine to serine mutants of PfAdSS possibly implicate a negatively charged cysteine in maintaining dimer stability of PfAdSS. To verify the possible role of a negative charge, cysteine to aspartic acid mutants (C328D and C328D-C368D) were made. Aspartic acid side chain has a pK_a of 3.9 and hence, at ambient pH could impart a negative charge at its location. Unlike, the Wt protein which dissociates to form monomers with increasing ionic strength of the buffer, C328D mutant did not dissociate even in the presence of 1.5 M NaCl. The stability of C328D mutant was also reflected in urea denaturation studies which showed stabilization of the dimer till 1.5 M urea concentration in size-exclusion chromatography, CD and fluorescence measurements. The C328D-C368D mutant showed interesting features. Mutation of two interface cysteines to aspartic acid resulted in modulation of monomer-dimer equilibrium rates in PfAdSS, and as a consequence in size-exclusion chromatography two peaks, one corresponding to dimer and other to monomer could be observed. With increasing ionic strength of buffer, the equilibrium shifted towards the monomer but even in presence of 1.5 M NaCl considerable dimeric population was evident.

Protein interfaces maintain geometric as well as electrostatic complementarity. Any perturbation in charge balance at the interface could lead to destabilization of protein structure. We have introduced two negative charges at the interface and were able to obtain a functionally active dimeric protein. Chapter 4 of the thesis describes the studies carried out on interface cysteine to serine and aspartic acid mutants which largely indicate that negatively charged cysteines may be necessary to maintain dimer integrity and stability in PfAdSS. Infact, the positively charged dimer interface of PfAdSS evident in the crystal structure, could be the right environment to stabilize the negative charge on the interface cysteine.

Two differences in catalytic properties of *P. falciparum* AdSS are; 1) Unlike AdSS studied from *E. coli*, mouse, azotobacter, human and yeast, PfAdSS exhibits ordered substrate binding. Both initial velocity kinetics and product inhibition studies suggested that IMP binds first to the enzyme, followed by GTP and then aspartate. 2) The glycolytic intermediate, fructose 1,6 bisphosphate (F16BP) is an inhibitor of *M. jannaschii*, mouse and *E. coli* AdSS. However, F16BP was found to be an activator of

PfAdSS. This activation was evident only at subsaturating GTP concentration when the reaction was initiated with aspartate. Molecular docking studies predicted binding of this molecule to the aspartate loop. To gain further insight into these two aspects, we resorted to site-directed mutagenesis. Comparison of fully liganded PfAdSS structure with similarly liganded complexes of other AdSS permitted identification of residues, Asn429, Lys62 and Thr307 making unique H-bonds with ligands or other loop residues in PfAdSS and hence, these were subjected to mutational analysis. Kinetic characterization of the mutants indicated that the unique contacts in PfAdSS indeed modulate the affinity of the enzyme for the substrates. In the Thr307 mutant, which showed a high aspartate K_m value, F16BP failed to activate the enzyme. Unlike the Wt protein which showed 50% activation at 1.5 mM F16BP, the T307V mutant showed about 50% inhibition at 7 mM F16BP concentration. This indeed provided support for our previous observations and docking studies, which implicated F16BP in modulating aspartate affinity of PfAdSS. In addition to the above nonconserved residues, two conserved residues, Arg155, which is involved in dimer cross-talk and contacts IMP in the active site of the neighboring subunit, and Thr309, have also been mutated and kinetically characterized. T309V mutant, like in *E. coli* AdSS, was completely inactive. The R155 mutants (R155K, R155A and R155L) exhibited 50-100 fold drop in k_{cat} value. This is unlike the observation in *E. coli* AdSS, where the corresponding arginine mutants exhibit high IMP K_m values but no change in catalytic efficiency. The kinetic characterization of the active site PfAdSS mutants is described in Chapter 5 of the thesis.

The last chapter deals with the molecular dissection of the purine salvage pathway in *Plasmodium falciparum* with an aim to identify alternate routes for AMP production in the parasite. The parasite lacks the *de novo* purine nucleotide biosynthetic pathway and depends exclusively on the salvage of preformed purine bases from the host to meet its requirement for adenine and guanine nucleotides. Hypoxanthine, the major purine base available to the parasite, is converted to IMP by the enzyme hypoxanthine guanine phosphoribosyltransferase (HGPRT). IMP serves as a precursor for both AMP and GMP. Conversion to AMP, proceeding in two steps, involves the enzymes adenylosuccinate synthetase (AdSS) and adenylosuccinate lyase (ASL). Conversion to GMP is mediated by inosine monophosphate dehydrogenase (IMPDH) and GMP synthetase. Using a combination of efficient transporters and salvage

enzymes, the parasite is able to meet its purine nucleotide requirements. In addition to the pathway listed above, alternate routes for AMP production involve the enzymes, adenosine kinase, which directly converts adenosine to AMP and adenine phosphoribosyltransferase, which converts adenine to AMP. These enzymes are unannotated in the Plasmodium genome database. However, weak APRT activity has been earlier detected in the parasite lysate using tritiated adenine. We used radiolabeled precursors to look for the presence of alternate routes for AMP production, if any, in the parasite. The flux through the HGPRT pathway was blocked by using two strategies, 1) xanthine oxidase which depletes hypoxanthine from the culture and 2) using hadacidin which inhibits AdSS and in turn blocks the route for AMP production. Both xanthine oxidase and hadacidin were found to be potent inhibitors of intraerythrocytic Plasmodium in culture and also, saponin released parasites free of the erythrocyte compartment. Uptake of adenine was observed in saponin released free parasites along with incorporation of the label in the DNA pool. To identify the route of adenine metabolism in erythrocyte free parasite, 2 mM cold adenine was added to hadacidin treated culture and incorporation followed using labeled adenine. Unlike the drug treated controls which showed loss of viability of the parasites, adenine supplemented culture showed 35-40% increase in parasite survival. Our observations indicate the presence of an APRT like enzyme activity in the parasite.

List of Publications

- [1] Kinetic characterization of adenylosuccinate synthetase from the thermophilic archaea *Methanocaldococcus jannaschii*. **Mehrotra S** and Balaram H, *Biochemistry* (2007) 46(44):12821-12832.

- [2] Unique kinetic mechanism of *Plasmodium falciparum* adenylosuccinate synthetase. Raman J, **Mehrotra S**, Anand RP and Balaram H, *Molecular and Biochemical Parasitology* (2004) 138(1):1-8

- [3] *Methanocaldococcus jannaschii* adenylosuccinate synthetase: Studies on temperature dependence of catalytic activity and structural stability. **Mehrotra S** and Balaram H (manuscript communicated).

- [4] Mutational Analysis of Cysteine 328 and Cysteine 368 at the interface of *Plasmodium falciparum* adenylosuccinate synthetase. **Mehrotra S**, Mylarappa BN, Jayalakshmi R, Anand RP and Balaram H (Manuscript under preparation).

- [5] Role of nonconserved active site residues in catalysis by *Plasmodium falciparum* adenylosuccinate synthetase. **Mehrotra S**, Mylarappa BN and Balaram H (Manuscript under preparation).

- [6] Molecular dissection of the purine salvage pathway in *Plasmodium falciparum*. **Mehrotra S**, Bopanna MP and Balaram H (Manuscript under preparation).

List of Abbreviations

AdSS	Adenylosuccinate synthetase
PfAdSS	<i>P. falciparum</i> adenylosuccinate synthetase
MjAdSS	<i>M. jannaschii</i> adenylosuccinate synthetase
PhAdSS	<i>P. horikoshii</i> adenylosuccinate synthetase
APRT	Adenine phosphoribosyltransferase
HGXPT	Hypoxanthine guanine xanthine phosphoribosyltransferase
ADA	Adenosine deaminase
ASL	Adenylosuccinate lyase
PNP	Purine nucleoside phosphorylase
IMPDH	Inosine 5'-monophosphate dehydrogenase
AK	Adenosine kinase
ENT	Equilibrative nucleoside transporter
DTT	Dithiothreitol
IPTG	Isopropyl thio- β -D-galactopyranoside
PEI	Polyethyleneimine
HDA	Hadacidin
IMO/6P-IMP	6-phosphoryl IMP
IAA	Iodoacetic acid
IAM	Iodoacetamide
IMP	Inosine monophosphate
GTP	Guanosine triphosphate
GDP	Guanosine diphosphate
GMP	Guanosine monophosphate
AMP	Adenosine monophosphate
sAMP	Succinyl AMP
MES	2-Morpholinoethanesulfonic acid
F16BP	Fructose 1,6 biphosphate

Contents

Declaration	i
Certificate	ii
Acknowledgements	iii
Synopsis	v
List of publications	xiv
List of Abbreviations	xv
1. Introduction	
1.1 Adenylosuccinate Synthetase	1
1.1.1 Isozymes	6
1.1.2 Oligomeric status	6
1.1.3 Reaction mechanism	7
1.1.4 Kinetic mechanism	9
1.1.5 Enzyme structure and ligand induced conformational changes	9
1.1.6 Substrate specificity	11
1.1.7 Regulation of enzyme activity	12
1.2 Diversity of Life	14
1.2.1 Phylogenetic Classification: Position of Archaea	15
1.2.3 <i>Methanocaldococcus jannaschii</i> , a thermophilic archaea	16
1.2.4 <i>Plasmodium falciparum</i> , a mesophilic parasitic protozoan	17
1.3 Thermozyymes and Mesozyymes	19
1.3.1 Protein sequence length in thermophiles	21
1.3.2 Oligomerization	21
1.3.3 Amino acid composition	22
1.3.4 Additional interactions contributing to stability	23
1.3.5 Metal binding	24
1.3.6 Higher packing efficiency and reduction of solvent accessible surface area	25

1.3.7	Increased secondary structure content and stability	26
1.3.8	High rigidity	27
1.4	Thermophilicity	28
2	Kinetic Characterization of Adenylosuccinate Synthetase from the Thermophilic Archaea <i>Methanocaldococcus jannaschii</i>	
2.1	Introduction	29
2.1.1	Classification of kinetic mechanisms	31
2.1.2	Elucidation of kinetic mechanism	32
2.1.3	<i>Methanocaldococcus jannaschii</i> Adenylosuccinate Synthetase	36
2.2	Materials and Methods	40
2.2.1	MjAdSS cloning and purification	40
2.2.2	Size exclusion chromatography	41
2.2.3	Circular dichroism spectroscopy	42
2.2.4	Dynamic light scattering	42
2.2.5	Enzyme assays	43
2.2.6	pH dependence of MjAdSS kinetics	43
2.2.7	Initial velocity measurement and inhibition studies	44
2.2.8	Data analysis	44
2.3	Results	45
2.3.1	Protein expression, purification and preliminary characterization	45
2.3.2	Quaternary structure of MjAdSS	48
2.3.3	Kinetic mechanism of MjAdSS	50
2.3.4	Modulation of MjAdSS activity by metabolites	60
2.4	Discussion	64
2.4.1	Structural implications for the observed kinetic mechanism of MjAdSS	67

3	Studies on Temperature Dependence of Catalytic Activity and Structural Stability of <i>M. jannaschii</i> Adenylosuccinate Synthetase	
3.1	Introduction	69
3.2	Materials and Methods	72
3.2.1	Protein purification	73
3.2.2	Temperature dependence of MjAdSS activity	73
3.2.3	Reverse Phase HPLC	73
3.2.4	Transient kinetics	74
3.2.5	Thermostability of MjAdSS	75
3.2.6	Size exclusion chromatography	75
3.2.7	Equilibrium unfolding measurements	75
3.2.8	Analysis of equilibrium unfolding data	76
3.3	Results	77
3.3.1	Temperature dependence of MjAdSS catalytic activity	77
3.3.2	Effect of temperature on 6-phosphoryl IMP formation	79
3.3.3	Effect of temperature on pre-steady-state kinetics	82
3.3.4	Thermal stability	83
3.3.5	Equilibrium unfolding using chemical chaotropes	85
3.3.6	Unfolding in guanidinium chloride	86
3.4	Discussion	90
4	Studies on Active Site Mutants of <i>P. falciparum</i> Adenylosuccinate Synthetase: Insights into Enzyme Kinetics and Activation	
4.1	Introduction	97
4.1.1	Ligand binding pockets: A comparison of <i>E. coli</i> and <i>P. falciparum</i> enzyme	99
4.1.2	Dynamic loops in adenylosuccinate synthetase	103
4.1.3	Mutational analysis	105
4.1.4	Kinetic mechanism of adenylosuccinate synthetase	110
4.1.5	Effect of glycolytic intermediates on the activity of adenylosuccinate synthetase	110
4.2	Materials and Methods	111

4.2.1	Site-directed mutagenesis	112
4.2.2	Protein expression and purification	114
4.2.3	Circular dichroism and fluorescence spectroscopy	115
4.2.4	Analytical size exclusion chromatography	116
4.2.5	Enzyme assays and kinetics	116
4.2.6	Initial velocity measurements and inhibition studies	117
4.2.7	Fructose 1,6 bisphosphate activation	117
4.3	Results and Discussion	118
4.3.1	Initial velocity kinetics to elucidate the kinetic mechanism of <i>P. falciparum</i> adenylosuccinate synthetase	118
4.3.2	Structural basis of ordered substrate binding in PfAdSS	119
4.3.3	Conservation of Asn429, Lys62 and Thr307 in adenylosuccinate synthetase	122
4.3.4	Protein expression and purification of PfAdSS mutants	123
4.3.5	Structural integrity of the active site mutants	123
4.3.6	Kinetic characterization of wild type and mutant adenylosuccinate synthetase	126
4.3.7	Characterization of N429V mutant	128
4.3.8	Characterization of K62L mutant	130
4.3.9	Characterization of T307V mutant	131
4.3.10	Production inhibition studies with PfAdSS mutants	133
4.3.11	Arg155 and Thr309 mutants: Sequence comparison	134
4.3.12	Characterization of Arg155 mutants	136
4.3.13	Characterization of T309V mutant	140
4.3.14	Activation of PfAdSS by fructose 1,6 bisphosphate	142
4.3.15	Molecular docking	143
4.3.16	Fructose 1,6 bisphosphate activation of the mutants	146
4.3.17	Physiological implications of the activation of PfAdSS by fructose 1,6 bisphosphate	148
4.4	Conclusion	148

5	Studies on Interface Cysteine Mutants of <i>P. falciparum</i> Adenylosuccinate Synthetase	
5.1	Introduction	150
5.1.1	Cysteines	150
5.1.2	Protein association and interfaces	156
5.1.3	Dimerization in adenylosuccinate synthetase	157
5.1.4	Structural and functional role of cysteines in <i>P.falciparum</i> AdSS	160
5.2	Material and Methods	161
5.2.1	Site-directed mutagenesis	162
5.2.2	Protein expression and purification	163
5.2.3	Enzyme assays and kinetics	163
5.2.4	Size exclusion chromatography	164
5.2.5	Cysteine modification	164
5.2.6	Equilibrium unfolding	165
5.3	Results	166
5.3.1	Mass spectrometry	167
5.3.2	Interface cysteine mutants	172
5.3.3	Kinetic characterization of C328D and C328D-C368D mutants of PfAdSS	173
5.3.4	Oligomeric status	175
5.3.5	Stability of wild type and mutants to urea induced denaturation	177
5.3.6	Urea induced unfolding of PfAdSS and the mutants monitored by size exclusion chromatography	178
5.3.7	Urea induced unfolding of PfAdSS and the mutants monitored by tryptophan fluorescence	183
5.3.8	Unfolding of wild type PfAdSS and the mutants monitored by far UV-CD spectroscopy	189
5.3.9	Structural features of the unfolding intermediate	192
5.4	Discussion	192
5.4.1	Importance of negatively charged cysteine/cysteines in maintaining dimer integrity of PfAdSS	192
5.4.2	Urea unfolding	194

5.4.3	Electrostatic complementarity at subunit interfaces	196
5.4.4	Dimer interface in <i>P. falciparum</i> AdSS	198
6	Molecular Dissection of the Purine Salvage Pathway in <i>P. falciparum</i>	
6.1	Introduction	200
6.1.1	Nucleotide metabolism in parasitic protozoa	201
6.1.2	Nucleoside/nucleobase transporters in parasitic protozoa	202
6.1.3	Purine transporters in <i>P. falciparum</i>	205
6.1.4	Purine salvage in parasitic protozoa	207
6.1.5	Purine salvage in <i>Plasmodium falciparum</i>	210
6.2	Materials and Methods	214
6.2.1	In vitro <i>P. falciparum</i> culture	215
6.2.2	Saponin lysis	215
6.2.3	Separation of infected erythrocytes from uninfected erythrocytes using percoll gradient centrifugation	216
6.2.4	Antiplasmodial activity and IC ₅₀ determination	216
6.2.5	Hypoxanthine and adenine uptake	218
6.2.6	Hadacidin inhibition and adenine supplementation	218
6.2.7	Parasite lysate pull down using AMP-affinity beads	218
6.3	Results	219
6.3.1	Effect of hadacidin and xanthine oxidase on parasite growth	220
6.3.2	Adenine uptake and incorporation in <i>P. falciparum</i>	223
6.3.3	Route of adenine metabolism	225
6.3.4	AMP-affinity pull down of <i>P. falciparum</i> lysate	228
6.4	Discussion	229
6.4.1	Purine metabolism in human erythrocytes	229

Chapter 1

Introduction

This chapter provides an introduction to the enzyme adenylosuccinate synthetase which forms the theme of the studies reported in this thesis. This is followed by a general description of the life style of the two organisms; Methanocaldococcus jannaschii, a thermophilic archaea, and Plasmodium falciparum, a mesophilic parasitic protozoan. The last section of the chapter provides a comparative account of the properties of mesophilic and thermophilic proteins and outlines the features of thermozyms that are implicated in thermostability of these proteins.

1.1 Adenylosuccinate synthetase

Adenylosuccinate synthetase (AdSS) [IMP:L-aspartate ligase (GDP-forming) (EC 6.3.4.4)] catalyzes the Mg^{2+} dependent condensation of a molecule of IMP with aspartate to form adenylosuccinate (sAMP), in a reaction driven by the conversion of GTP to GDP (Figure 1.1). Adenylosuccinate is then cleaved by adenylosuccinate lyase to form AMP and fumarate. Adenylosuccinate synthetase is present in all known organisms and tissues, except mature red cells (Stayton *et al.*, 1983; Honzatko *et al.*, 1999).

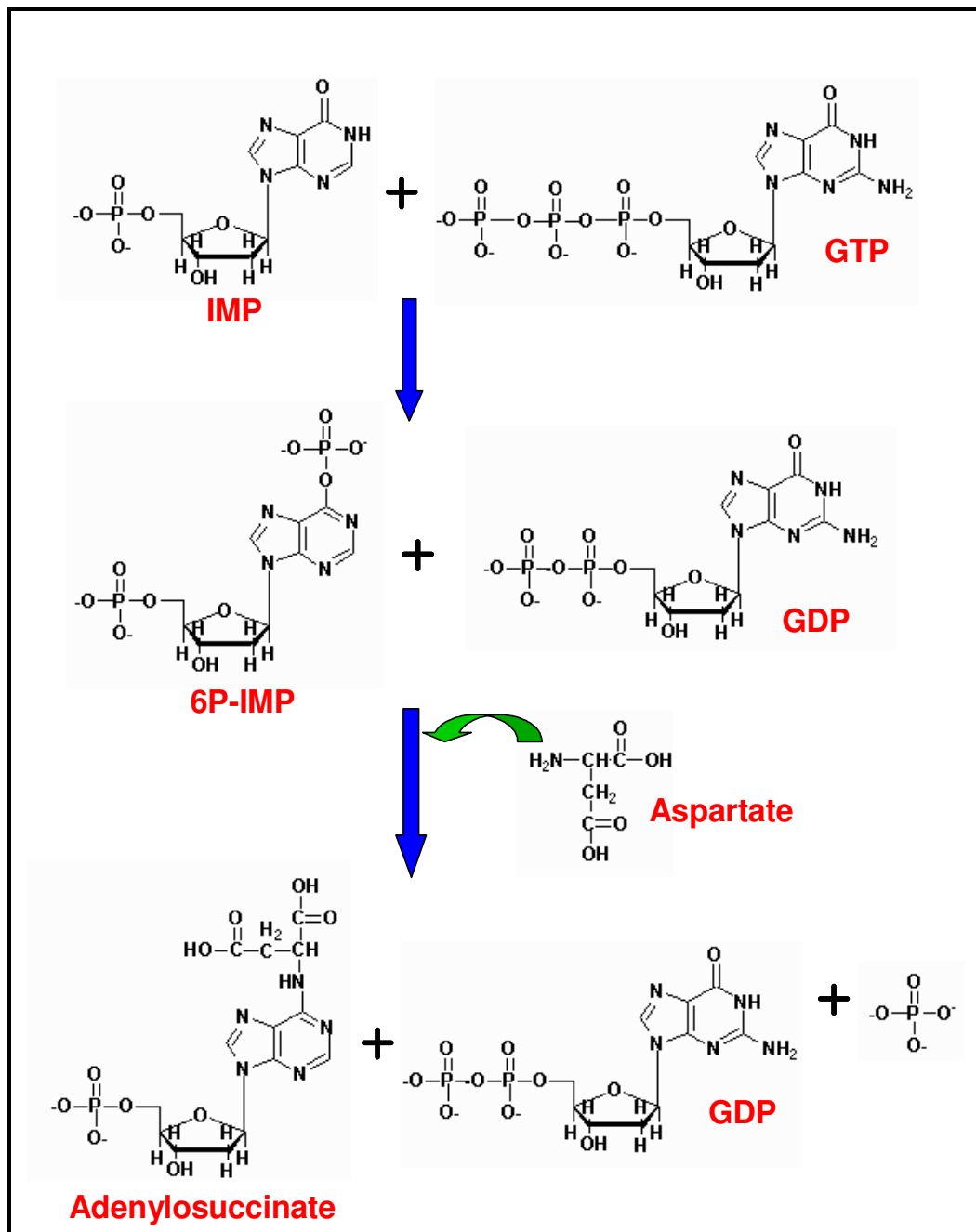
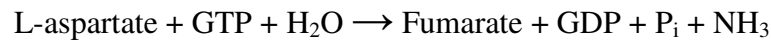


Figure 1.1: The reaction catalyzed by adenylosuccinate synthetase

Adenylosuccinate synthetase plays two major metabolic roles: a) it is a branch point enzyme that commits IMP to AMP formation during purine nucleotide biosynthesis, and b) it is a component of the purine nucleotide cycle (PNC) which in addition to AdSS involves the enzymes adenylosuccinate lyase and AMP deaminase in the following reaction:



The functions of the purine nucleotide cycle are as follows; 1) it is a pathway for the liberation of ammonia from amino acids, 2) it provides the TCA cycle intermediate, fumarate, in tissues that lack pyruvate carboxylase, 3) it is a pathway that regulates the relative levels of adenine nucleotides, AMP, ADP, and ATP, and 4) it aids in the control of phosphofructokinase activity and hence of glycolysis (Lowenstein, 1972). The PNC is active in muscle, brain, kidney, liver and pancreatic islets.

Comparison of the primary sequence of AdSS from different sources shows a high degree of sequence similarity (~ 30-50% in a pair-wise comparison) (Figure 1.2). The conserved sequence stretches correspond to the regions that have been implicated in substrate binding and catalysis by biochemical and crystallographic studies.

```

S.citri          .....MSGTNYRTLAIVGSQ
H.pylori        .....MADVVVGIQ
S.cerevisiae    .....MVNVVVGSGQ
C.albicans      .....MCDVVVLSQ
Mus_musculus    .....MSGTRASNDRPPGTGGVKRGLQKAAATGSRVTVVVGAQ
Homo_sapiens    .....MAFAETYPAASSLPNGDCGRPRAAGGNRVTVVGAQ
A.niger         .....MGVTIVVLSQ
A.thaliana      MSLSSLTLDNPRFAVGGPYHRRYPPLHHRSPFVSCSAKRPAVSASLSVAADSAATESLGRIGSLSQVSGVLGCQ
Zea_mays        ...MSLSTLSHPAAAAAGSGKSLFPAGPAAQSVHFPPKARLPV...AAVSAATAAVHAEDRVSSLTQVSGVLSQ
D.discoideum    .....MASIIIGSQ
P.falci-parum   .....MNIFDHQIKNVDKGNVVAILGAQ
E.coli          .....MGNNVVVLTQ
H.influenzae   .....MGKSVVILGAQ
V.cholerae     .....MGNNVVVLTQ
A.vinelandii   .....MGKNNVVVLTQ
L.pneumophila   .....MGKNNVVVLTQ
B.subtilis     .....MSSVVVVGTQ
B.licheniformis.....MSSVVVVGTQ
C.botulinum    .....MSAFIVLGAQ
M.leprae       .....MPAVVLI GAQ
Methanosarcina.....MFTIITGAQ
M.mazei        .....MFTIITGAQ
A.fulgidus     .....MGATIIVGGF
M.jannaschii   .....MKKVLLTCTIIVGQ
P.furiosus     .....MPSVIVVGGQ

```


Chapter 1

S. citri **WGDEGKGI**TDYFAQQADLIVRWAG. **GDNAGHT**TIVIK. RNKYKLSIVP**SGAFN**KKSMNVIGMVVVNLRKLSYG
H. pylori **WGDEGKGI**VDRIAKDYDFVVRVYQ. **GHNAGHT**TIVHK. GVKHSLHLM**PSGLV**YPCKNISSAVVVSIKDLC. E.
S. cerevisiae **WGDEGKGI**LDVLLVGVKDIIVARCAG. **GNNAGHT**TIVVD. GVKYDFHML**PSGLV**NPNCQNLGGVVIHVPSFFKE
C. albicans **WGDEGKGI**KLVLDLCCDDIDVCARCQ. **GNNAGHT**TIVVG. KVKYDFHML**PSGLV**NPCKQNLVGSVVVHVPSFFAE
Mus musculus **WGDEGKGI**KVVVDLLATDADIVSRCCQ. **GNNAGHT**TIVVD. GKEYDFHLL**PSGI**INTKAVSFIGNGVVIHLPGLFEE
Homo sapiens **WGDEGKGI**KVVVDLLAQDADIVCRCCQ. **GNNAGHT**TIVVD. SVEYDFHLL**PSGI**INPNVTAFIGNGVVIHLPGLFEE
A. niger **WGDEGKGI**TDMLAQATLCCRAAG. **GNNAGHT**TIVHG. DKTDFHLL**PSGLV**SPSCVNLIGAGTVVHVPSFFKE
A. thaliana **WGDEGKGI**VDILAQHFIVARCQ. **GANAGHT**IYNSEGKFFALHLV**PSGIL**NEDTTCVINGVVIHLPGLFEE
Zea mays **WGDEGKGI**KLVVDLAFRFDIVARCQ. **GANAGHT**IYNSEGKFFALHLV**PSGIL**HEGTLCCVVGNAVIVHVPGFFGE
D. discoideum **WGDEGKGI**LDVILSQQFVVARCQ. **GANAGHT**TIVVD. GKKIALHL**PSGI**LNEKASCILGNGMVIHLPTFFKE
P. falciparum **WGDEGKGI**IDMLSEYSDITCRFNG. **GANAGHT**ISVN. DKKYALHL**PCGLV**YDNNISVLGNGMVIHVKSLEME
E. coli **WGDEGKGI**KIVDILLTERAKYVVRVYQ. **GHNAGHT**TLVINGEK. TVLRL**PSGI**LRENVTSIIGNGVVLSPAALMKE
H. influenzae **WGDEGKGI**KIVDILLTDRVKYVVRVYQ. **GHNAGHT**TLVINGEK. TVLRL**PSGI**MLHPNVTCLIGNGVVSPEALMKE
V. cholerae **WGDEGKGI**KIVDILLTDAKIVVRVYQ. **GHNAGHT**TLVINGEK. TVLRL**PSGI**LNNVKCIIGNGVVLSPAALMKE
A. vinelandii **WGDEGKGI**KIVDILLTDAKIVVRVYQ. **GHNAGHT**TLVINGEK. TVLRL**PSGI**LNNVKCIIGNGVVLSPAALMKE
L. pneumophila **WGDEGKGI**KIVDILLTDAKIVVRVYQ. **GHNAGHT**TLVINGEK. TVLRL**PSGI**LNNVKCIIGNGVVLSPAALMKE
B. subtilis **WGDEGKGI**KIVDILLTDAKIVVRVYQ. **GHNAGHT**TLVINGEK. TVLRL**PSGI**LNNVKCIIGNGVVLSPAALMKE
B. licheniformis **WGDEGKGI**KIVDILLTDAKIVVRVYQ. **GHNAGHT**TLVINGEK. TVLRL**PSGI**LNNVKCIIGNGVVLSPAALMKE
C. botulinum **WGDEGKGI**KIVDILLTDAKIVVRVYQ. **GHNAGHT**TLVINGEK. TVLRL**PSGI**LNNVKCIIGNGVVLSPAALMKE
M. leprae **WGDEGKGI**KIVDILLTDAKIVVRVYQ. **GHNAGHT**TLVINGEK. TVLRL**PSGI**LNNVKCIIGNGVVLSPAALMKE
Methanosarcina **WGDEGKGI**KIVDILLTDAKIVVRVYQ. **GHNAGHT**TLVINGEK. TVLRL**PSGI**LNNVKCIIGNGVVLSPAALMKE
M. mazei **WGDEGKGI**KIVDILLTDAKIVVRVYQ. **GHNAGHT**TLVINGEK. TVLRL**PSGI**LNNVKCIIGNGVVLSPAALMKE
A. fulgidus **WGDEGKGI**KIVDILLTDAKIVVRVYQ. **GHNAGHT**TLVINGEK. TVLRL**PSGI**LNNVKCIIGNGVVLSPAALMKE
M. jannaschii **WGDEGKGI**KIVDILLTDAKIVVRVYQ. **GHNAGHT**TLVINGEK. TVLRL**PSGI**LNNVKCIIGNGVVLSPAALMKE
P. furiosus **WGDEGKGI**KIVDILLTDAKIVVRVYQ. **GHNAGHT**TLVINGEK. TVLRL**PSGI**LNNVKCIIGNGVVLSPAALMKE

S. citri **NWV**. IYKQHGFDLLKNLRISDRVHLIFPY**HMKI**DELQEEYRQK. . . . **DSIG**TTKK**GI**PCYQDKAE**RIG**IRLIG
H. pylori **EISAFED**LENRLFISDRAHVILPY**HAKK**DAFKEKSO. . . . **NIG**TTKK**GI**PCYEDKMARSGIRMG
S. cerevisiae **LET**. LEAKGLKNARSRLVSSRAHLVDFD**HQV**TDKIRELELSGRSKDGNIG**TTGK**GIPTYSTKAS**RS**GLRVH
C. albicans **LEN**. LEAKGLD. CRDRLFVSSRAHLVDFD**HQV**TDKIRELELSGRSKDGNIG**TTGK**GIPTYSTKAS**RS**GLRVH
Mus musculus **AEKNE**KKK. LKDWKRLIISDRAHVILPY**HAKK**DAFKEKSO. . . . **GKNIG**TTKK**GI**PTYSTKAS**RS**GLRVH
Homo sapiens **AEKNV**QKGGKLEGEWEKRLIISDRAHVILPY**HAKK**DAFKEKSO. . . . **GKNIG**TTKK**GI**PTYSTKAS**RS**GLRVH
A. niger **LAS**. LEDKLEGGAGKRIFISDRAHVILPY**HAKK**DAFKEKSO. . . . **VG**TT**GI**PCYSDKAARSGVRMG
A. thaliana **IDG**. . . . **LESNGV**SCCKRILVSDRAHLVDFD**HQV**TDKIRELELSGRSKDGNIG**TTGK**GIPTYSTKAS**RS**GLRVH
Zea mays **IDG**. . . . **LESNGV**SCCKRILVSDRAHLVDFD**HQV**TDKIRELELSGRSKDGNIG**TTGK**GIPTYSTKAS**RS**GLRVH
D. discoideum **VQG**. . . . **LQDG**INYGKRLVSDRAHLVDFD**HQV**TDKIRELELSGRSKDGNIG**TTGK**GIPTYSTKAS**RS**GLRVH
P. falciparum **IES**. . . . **VGK**LLDRLVLSNKAHLVDFD**HQV**TDKIRELELSGRSKDGNIG**TTGK**GIPTYSTKAS**RS**GLRVH
E. coli **MKE**. . . . **LED**RG. IPVRERLISEACPLILPY**HVAL**DQAREAAARGKKA. . . . **IG**TT**GR**GI**GPAY**EDKVAR**RG**LRVG
H. influenzae **MGE**. . . . **LES**RG. IKVRERLISEACPLILPY**HVAL**DQAREAAARGKKA. . . . **IG**TT**GR**GI**GPAY**EDKVAR**RG**LRVG
V. cholerae **MSG**. . . . **LED**RG. VVRERLISEACPLILPY**HVAL**DQAREAAARGKKA. . . . **IG**TT**GR**GI**GPAY**EDKVAR**RG**LRVG
A. vinelandii **IAK**. . . . **LE**EKG. VVRERLISEACPLILPY**HVAL**DQAREAAARGKKA. . . . **IG**TT**GR**GI**GPAY**EDKVAR**RG**LRVG
L. pneumophila **IKE**. . . . **LE**NG. VNVRERLISEACPLILPY**HVAL**DQAREAAARGKKA. . . . **IG**TT**GR**GI**GPAY**EDKVAR**RG**LRVG
B. subtilis **LAY**. . . . **LH**ER. NVSTDNLRISNRAHLVILPY**HKL**DVAVEEERKGAN. . . . **IG**TT**GR**GI**GPAY**EDKVAR**RG**LRVG
B. licheniformis **LAY**. . . . **LH**ER. NVSTDNLRISNRAHLVILPY**HKL**DVAVEEERKGAN. . . . **IG**TT**GR**GI**GPAY**EDKVAR**RG**LRVG
C. botulinum **INQ**. . . . **LE**SLGVEITPDRLIISDRAHVILPY**HVAL**DQAREAAARGKKA. . . . **IG**TT**GR**GI**GPAY**EDKVAR**RG**LRVG
M. leprae **IQG**. . . . **LE**SR. GVDTSQLLISADAHLLVDFD**HQV**TDKIRELELSGRSKDGNIG**TTGK**GIPTYSTKAS**RS**GLRVH
Methanosarcina **IAM**. . . . **FEK**HGIQVNAEKLGVDAKTSIIMPY**HI**EMDGLREESREK. . . . **IG**TT**GR**GI**GPAY**EDKVAR**RG**LRVG
M. mazei **IEM**. . . . **FEK**HGVKVNSEKLVDAKTSIIMPY**HI**EMDGLREESREK. . . . **IG**TT**GR**GI**GPAY**EDKVAR**RG**LRVG
A. fulgidus **VEL**. . . . **LV**GV. . . . **DR**ARVDYRCATIEPK**HE**ADKGEHLSKKIG. . . . **TT**GT**CG**PANVDRV**IL**KQAK
M. jannaschii **VEM**. . . . **LK**DFNVKERLIVDYRCATIEPK**HE**ADKGEHLSKKIG. . . . **TT**GT**CG**PANVDRV**IL**KQAK
P. furiosus **LEH**. . . . **LK**DFNVAERVGDYRCATIEPK**HE**ADKGEHLSKKIG. . . . **TT**GT**CG**PANVDRV**IL**KQAK

S. citri **D**LF. . . . **E**KGFLQKLENNLKFNEVLQKFLIVK. DLTKINLKRIFWHYFQ**QIK**SLV**TD**TSILVDNAIHNH. **QK**
H. pylori **D**LL. . . . **D**TILEEKLNAHFKAIEPPREAYDLGE. DYEKD. LREYFKQYTPKIRPF**IKD**TTSMLEIANQKG. **AK**
S. cerevisiae **H**LVNDQP**AW**EEFVARYKRLLETRRQRYGDFEYD. . . . **F**EAKLAEYKLLREQLKPFV**VD**SVVFMHNAIEAK. **KK**
C. albicans **H**LVNDQP**AW**EEFVARYKRLLETRRQRYGDFEYD. . . . **F**EAKLAEYKLLREQLKPFV**VD**SVVFMHNAIEAK. **KK**
Mus musculus **D**LLS. . . . **D**FDEF SARFKNLAHQHSMEPTLEID. . . . **V**EGQLKRLKGFARIRPM**VD**GVVFMYEAALHGPPK
Homo sapiens **D**LVS. . . . **D**FDGFSERFKVLANQYKSIYPTLEID. . . . **I**EGELQKLGKYM**EK**IKPM**VD**GVVFMYEAALHGPPK
A. niger **E**ILD. . . . **E**ALFERKRLSLDAGYRARFGELEYN. . . . **V**EEELARFKEYRKR**LG**PIV**VD**QLAFLOK**Y**KDAP. **IN**
A. thaliana **D**LRH. . . . **M**DTLPQKLDLLSAAAR**Q**GFQYTP. . . . **E**MLREEVEAYKRYADR**LE**PI**TD**TVHFINDSISQK. **KK**
Zea mays **D**LRH. . . . **M**DTLPQKLDLLSAAAR**Q**GFQYTP. . . . **E**MLREEVEAYKRYADR**LE**PI**TD**TVHFINDSISQK. **KK**
D. discoideum **D**LVS. . . . **P**EHFRKTFTRLVFNKHKR**GF**SEFYD. . . . **V**EALKRYQ**FA**EMLKPFV**VD**SVVFMHNAIEAK. **KK**
P. falciparum **T**LKN. . . . **F**ENFNMYSLKIDHMLDLYNITEYD. . . . **K**EKELNLFYNYH**IK**LRD**RI**VDV**IS**FMMNTLNN. **KK**
E. coli **D**LF. . . . **K**ETFAEKLKEVMYHN**F**QLVNYKAE. AVDYQKVLDD**T**MAVAD**IL**TS**MV**VD**VS**DLDDQAR**Q**RG. **DF**
H. influenzae **D**LFN. . . . **K**EFAEKLKEVMYHN**F**QLVNYKAE. AVDYQKVLDD**T**MAVAD**IL**TS**MV**VD**VS**DLDDQAR**Q**RG. **DF**
V. cholerae **D**LF. . . . **M**ASFAEKLQEVMAFHN**F**QLVNYKAE. AVDYQKVLDD**T**MAVAD**IL**TS**MV**VD**VS**DLDDQAR**Q**RG. **DF**
A. vinelandii **D**LFN. . . . **P**ERFAKLLHELE**Y**HN**F**QLVNYKAE. AVDYQKVLDD**T**MAVAD**IL**TS**MV**VD**VS**DLDDQAR**Q**RG. **DF**
L. pneumophila **D**LFH. . . . **R**DRFANKLE**Y**HN**F**QLVNYKAE. AVDYQKVLDD**T**MAVAD**IL**TS**MV**VD**VS**DLDDQAR**Q**RG. **DF**
B. subtilis **D**LL. . . . **R**DAFAEKLERNLE**Y**HN**F**QLVNYKAE. AVDYQKVLDD**T**MAVAD**IL**TS**MV**VD**VS**DLDDQAR**Q**RG. **DF**
B. licheniformis **D**LL. . . . **R**DVFEELKARNLE**Y**HN**F**QLVNYKAE. AVDYQKVLDD**T**MAVAD**IL**TS**MV**VD**VS**DLDDQAR**Q**RG. **DF**
C. botulinum **D**LH. . . . **K**EVFEENL**Y**HN**F**QLVNYKAE. AVDYQKVLDD**T**MAVAD**IL**TS**MV**VD**VS**DLDDQAR**Q**RG. **DF**
M. leprae **D**VLE. . . . **P**ELTHKIEA**Y**HN**F**QLVNYKAE. AVDYQKVLDD**T**MAVAD**IL**TS**MV**VD**VS**DLDDQAR**Q**RG. **DF**
Methanosarcina **E**LV. . . . **Q**ERFLARLE**Y**HN**F**QLVNYKAE. AVDYQKVLDD**T**MAVAD**IL**TS**MV**VD**VS**DLDDQAR**Q**RG. **DF**
M. mazei **E**LV. . . . **K**ERFLARLE**Y**HN**F**QLVNYKAE. AVDYQKVLDD**T**MAVAD**IL**TS**MV**VD**VS**DLDDQAR**Q**RG. **DF**
A. fulgidus **D**IPE. . . . **L**KDYLA**Y**HN**F**QLVNYKAE. AVDYQKVLDD**T**MAVAD**IL**TS**MV**VD**VS**DLDDQAR**Q**RG. **DF**
M. jannaschii **D**IE. . . . **L**KDYLA**Y**HN**F**QLVNYKAE. AVDYQKVLDD**T**MAVAD**IL**TS**MV**VD**VS**DLDDQAR**Q**RG. **DF**
P. furiosus **D**IKE. . . . **L**KDYLA**Y**HN**F**QLVNYKAE. AVDYQKVLDD**T**MAVAD**IL**TS**MV**VD**VS**DLDDQAR**Q**RG. **DF**

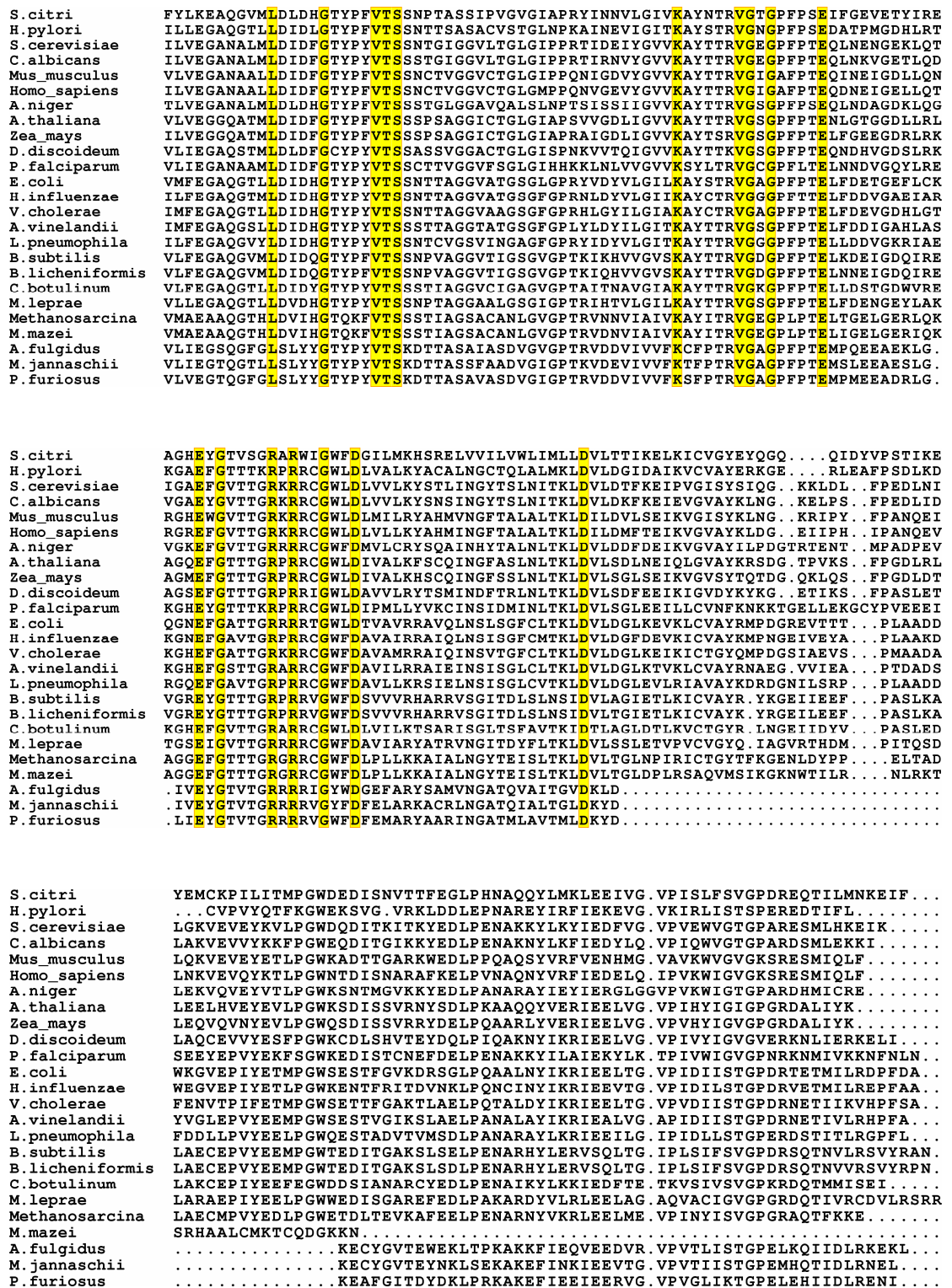


Figure 1.2: Sequence alignment of AdSS from different species. The conserved residues are shaded in yellow. The alignment was generated using CLUSTAL W (Thompson *et al.*, 1994) and represented using ESPRIPT (Gouet *et al.*, 1999).

The enzyme, adenylosuccinate synthetase forms the main theme of the studies presented in this thesis. Biochemical characterization of the enzyme from a thermophilic archaea and a parasitic protozoan has been carried out. The following section summarizes the literature on AdSS.

1.1.1 Isozymes

Adenylosuccinate synthetase plays a dual metabolic role in the cell. It forms an integral part of the *de novo* and salvage pathways for purine nucleotide synthesis and also functions in the purine nucleotide cycle. Matsuda *et al.* reported the existence of two isozymes of adenylosuccinate synthetase, present in roughly equal amount in rat liver and could be distinguished by isoelectric focusing. The first isozyme, which they designated as Type L, is an acidic protein and exhibits a pI of 5.9, while the other isozyme, designated as Type M, is a basic protein and exhibits a pI of 8.9 (Matsuda *et al.*, 1977). Further characterization of the two isozymes showed that the acidic isozyme exhibits a lower K_m value for IMP and a higher K_m value for aspartate when compared to the basic AdSS. The acidic protein was found to be more potently inhibited by nucleotides but exhibited lower inhibition by fructose 1,6 bisphosphate. On the basis of these properties, the acidic isozyme was assigned to the purine nucleotide biosynthesis pathway, whereas, the basic isozyme was associated with the purine nucleotide cycle (Matsuda *et al.*, 1977). While the basic isozyme is abundant in skeletal and heart muscle, the acidic isozyme has a more general tissue distribution. Kidney and brain have predominantly acidic isozyme, with the liver having equal amount of both (Stayton *et al.*, 1983).

1.1.2 Oligomeric status

At high concentration, all characterized AdSS are homodimers. *E. coli* AdSS exhibits monomer-dimer equilibrium in solution with the K_d for dimer dissociation being 10 μM (Wang *et al.*, 1997a). Presence of active site ligands, IMP, GTP, succinate and Mg^{2+} , results in a dramatic drop in K_d for dimer dissociation, implying

ligand induced dimerization in AdSS. Based on crystal structure analysis, the conserved residues, Arg143 and Asp231 (*E. coli* numbering) have been implicated in dimer stabilization. Arg143 directly interacts with IMP in the active site of the symmetry related subunit, whereas, Asp231 forms an intersubunit salt bridge with Lys140. Mutation of Arg143 and Asp231 perturbed the monomer-dimer equilibrium in *E. coli* AdSS and resulted in an increase in the IMP and GTP K_m values with the k_{cat} and aspartate K_m values not being significantly affected (Wang *et al.*, 1997a). Further, chemical modification of Lys140 resulted in complete loss of enzyme activity (Dong & Fromm, 1990). These studies implicated the role of AdSS dimer in catalysis. Kang *et al.* showed by means of subunit complementation that *E. coli* AdSS contains two shared active sites at the dimer interface. Mixing two inactive mutants (R143L and D13A) resulted in the formation of heterodimers that exhibited specific activity which was one-half that of the wild type enzyme. Pre-incubation with IMP and GTP increased the activity of the heterodimers, implicating their role in dimer stabilization (Kang *et al.*, 1996).

Like in *E. coli*, yeast and *P. falciparum* AdSS also exhibit monomer-dimer equilibrium in solution (Jayalakshmi *et al.*, 2002; Lipps & Krauss, 1999), while *Azotobacter vinelandii* AdSS (Markham & Reed, 1977), rat skeletal muscle protein (Ogawa *et al.*, 1977) and mouse acidic and basic isozymes (Borza *et al.*, 2003) are predominantly dimeric in nature. The monomer-dimer equilibrium has been implicated in regulation of the enzyme activity in vivo (Wang *et al.*, 1997a).

1.1.3 Reaction mechanism

Three alternative reaction mechanisms have been proposed for adenylosuccinate synthetase. Lieberman, in 1956, proposed a mechanism for adenylosuccinate formation that involves the participation of a 6-phosphoryl IMP intermediate. He found that when IMP was labeled with ^{18}O on the C-6 position, then after the reaction the label was associated with inorganic phosphate. In addition, there was no exchange of [^{32}P]-inorganic phosphate into GTP in a partial reaction that contained enzyme, MgCl_2 , GTP, IMP and [^{32}P]-inorganic phosphate. On the basis of

these observations he proposed that the reaction involves a nucleophilic attack by O-6 of IMP on the γ -phosphoryl group of GTP to yield 6-phosphoryl IMP intermediate. The second step involves the nucleophilic attack by the aspartate nitrogen on C-6 of the phosphorylated intermediate resulting in the elimination of inorganic phosphorous (Lieberman, 1956). The second mechanism was proposed by Miller and Buchanan. They proposed a concerted one step mechanism which involves the simultaneous participation of the carboxyl and nitrogen bearing substrates along with the nucleoside phosphate. According to this mechanism, α -nitrogen of aspartate makes a nucleophilic attack on C-6 of IMP and at the same time O-6 of IMP attacks the γ -phosphorous of GTP, thus leading to a tetrahedral transition state (Miller & Buchanan, 1962). The third mechanism proposed by Markham and Reed, argued against the formation of 6-phosphoryl IMP intermediate. Rather they proposed an alternative mechanism involving an intermediate formed by the nucleophilic attack of the α -nitrogen of aspartate on C-6 of IMP. The intermediate is subsequently phosphorylated by GTP leading to a tetrahedral transition state which then gives rise to the products, sAMP, GDP and Pi (Markham & Reed, 1978).

The participation of 6-phosphoryl IMP as an obligate intermediate in the reaction catalyzed by AdSS, comes from positional isotope exchange studies and X-ray crystallography. Bass *et al.* used isotope scrambling experiments to elucidate the kinetic mechanism of rat muscle AdSS. [γ - ^{18}O] GTP was incubated with Mg^{2+} and the enzyme in the presence of various ligands. Isotope exchange between the β - γ bridge and the β nonbridging positions of GTP took place in the presence of AdSS and IMP or when enzyme, IMP and succinate were present but not in the presence of enzyme and GTP alone. The finding that the exchange occurs only in the presence of IMP was indicative of the formation of 6-phosphoryl IMP intermediate (Bass *et al.*, 1984). Crystals of AdSS grown in the presence of GTP, 6-thio IMP and hadacidin showed 6-thiophosphoryl IMP, GDP and hadacidin in the active site, providing additional support for the mechanism suggested by Lieberman (Poland *et al.*, 1997). A number of crystal structures have now been solved which show the phosphorylated intermediate in the active site (Eaazhisai *et al.*, 2004; Choe *et al.*, 1999; Iancu *et al.*,

2002; Iancu *et al.*, 2006). However, chemical synthesis or direct spectroscopic observation of this intermediate has not been reported till date.

1.1.4 Kinetic mechanism

Extensive kinetic studies have been carried out on *E. coli* AdSS by Fromm and co-workers. The kinetic mechanism of the enzyme was established using initial velocity kinetics and inhibition studies with products and substrate analogs. The enzyme exhibited a rapid equilibrium random sequential mechanism (Rudolph & Fromm, 1969). Similar studies with human, *Schizosaccharomyces pombe* and *Dictyostelium discoideum* AdSS indicated a random sequential mechanism for the forward reaction (Van der Weyden & Kelly, 1974; Nagy *et al.*, 1973; Jahngen & Rossomando, 1984). AdSS catalyzes a reversible reaction and elucidation of the steady-state kinetic mechanism of *Azotobacter vinelandii* AdSS in both directions by initial velocity kinetics and inhibition methods, highlighted random sequential binding for both forward and reverse reactions (Markham & Reed, 1977). While similar results were obtained for rat muscle AdSS by equilibrium isotope exchange, these studies highlighted a preference for the binding of aspartate to E.IMP.GTP complex (Cooper *et al.*, 1986). In contrast, an ordered binding of substrates to the *P. falciparum* enzyme was observed by product inhibition studies, with IMP binding first followed by GTP and then aspartate (Raman *et al.*, 2004).

1.1.5 Enzyme structure and ligand induced conformational changes

E. coli and mouse AdSS have been extensively studied and various crystal structures of these enzymes including unliganded (Iancu *et al.*, 2001; Silva *et al.*, 1995; Poland *et al.*, 1993), partially liganded (Iancu *et al.*, 2002; Hou *et al.*, 2002; Poland *et al.*, 1996c) and fully liganded (Iancu *et al.*, 2002; Poland *et al.*, 1996a; Poland *et al.*, 1997) are available. In addition, structures of AdSS from two plant species, *Arabidopsis thaliana* and *Triticum aestivum* (Prade *et al.*, 2000), and a parasitic protozoan, *Plasmodium falciparum* (Eaazhisai *et al.*, 2004) are also

available. These structures show that the basic polypeptide fold is similar across AdSS from different sources. A central β -sheet comprising of 10 strands forms the core of the protein. The first nine strands of the sheet are mutually parallel with the tenth being antiparallel to the rest. The strands are connected by segments of the polypeptide chain that range in size from short loops to subdomains comprising of various secondary structural elements (Prade *et al.*, 2000; Eaazhisai *et al.*, 2004; Poland *et al.*, 1993; Iancu *et al.*, 2001). Availability of various liganded structures of AdSS allows analysis of structural movements associated with substrate binding as well as catalysis. The conformational changes induced by substrate binding are restricted to regions connecting the strands of the central β -sheet. Comparison of various liganded and unliganded structures of AdSS reveals that there are 5 loops which respond to substrate binding namely, the Switch loop, IMP loop, GTP loop, Aspartate loop and Valine loop (Poland *et al.*, 1996a; Iancu *et al.*, 2002). IMP bound structures of *E. coli* and mouse AdSS indicate that IMP binding is sufficient to organize all loops except the Aspartate loop that responds to hadacidin (an aspartate analog) binding (Iancu *et al.*, 2002; Hou *et al.*, 2002).

Availability of various crystal structures of *E. coli* AdSS and biochemical data from mutational analysis has enabled a comprehensive understanding of the catalytic process in terms of ligand induced conformational changes in the protein and the chemical transformation of substrates into products. A conserved histidine (His41 in *E. coli*) and aspartic acid (Asp13 in *E. coli*) have been implicated as catalytic acid and base, respectively. Asp13 forms a hydrogen bond with the N1 position of IMP. The abstraction of a proton from N1 of IMP results in the formation of 6-oxyanion of IMP. The oxyanion displaces GDP from γ -phosphate of bound GTP, resulting in formation of the reaction intermediate, 6-phosphoryl IMP. Coordination of Mg^{2+} directly to the β,γ -bridging oxygen of GTP stabilizes charge development on the oxygen. His41 hydrogen bonds to a terminal oxygen on the β -phosphoryl group of GTP and acts as a catalytic acid in the phosphotransfer reaction. After the formation of 6-phosphoryl IMP intermediate, Asp13 (now protonated) moves into the coordination sphere of the catalytic Mg^{2+} . As a consequence, Asp13 becomes a catalytic acid and re-protonates the N1 atom of 6-phosphoryl IMP, thereby generating the C-6 cation of the

intermediate. Binding of aspartate initiates the next step of catalysis. Nucleophilic attack by the α -amino group of aspartate on C-6 of 6-phosphoryl IMP displaces the phosphate group leading to the formation of adenylosuccinate.

1.1.6 Substrate specificity

The enzyme exhibits high specificity for its substrates, IMP, GTP, aspartate and Mg^{2+} . No product formation was detected when L-aspartate was replaced by D-aspartate, L-glutamate, L-glutamine, L-asparagine, L-malate, NH_3 and β -alanine (Lieberman, 1956; Muirhead & Bishop, 1974; Markham & Reed, 1977). However, hydroxylamine could substitute for aspartate to a significant degree (Lieberman, 1956). While the *E. coli* enzyme showed a two fold drop in k_{cat} value when aspartate was replaced by hydroxylamine, the K_m value of the enzyme for hydroxylamine was 1000 fold higher than that for aspartate (Gorrell *et al.*, 2002). Nitroalanine (k_{cat}/K_m ~30% that for aspartate) and cysteine sulfinic acid (having 5.5% of the activity for aspartate) substituted for aspartate in reactions involving *Azotobacter vinelandii* AdSS (Porter *et al.*, 1983). Triphosphates of adenosine, cytidine, uridine and inosine were incapable of replacing GTP (Lieberman, 1956; Muirhead & Bishop, 1974; Markham & Reed, 1977). GTP could however, be replaced by dGTP (Muirhead & Bishop, 1974) and GTP γ S (Markham & Reed, 1978).

Several IMP analogs with N, S and C atoms substituting for one of the phosphoryl oxygens were weak substrates of the enzyme (Hampton & Chu, 1970). IMP could not be replaced by hypoxanthine, inosine, IDP, ITP, UMP, GMP or XMP (Markham & Reed, 1977; Lieberman, 1956; Muirhead & Bishop, 1974). However, 2'-dIMP and β -D-arabinosyl-IMP were found to be substrates for adenylosuccinate from rabbit and mouse muscle and *E. coli* (Spector & Miller, 1976; Iancu *et al.*, 2006). Recombinant synthetase from *E. coli* and mouse muscle exhibited similar K_m values for 2'-deoxy-IMP and IMP. Both enzymes, however, showed a 29-57 fold increase in their K_m values for L-aspartate and K_i values for hadacidin when 2'-deoxy-IMP replaced IMP (Spector & Miller, 1976). A structural explanation for this observation was found by Iancu *et al.* While no significant conformational differences were

observed in crystal structures of *E. coli* AdSS bound to GDP, hadacidin and 6P-IMP or 2'-deoxy-6P-IMP, except for a cavity created by the loss of the hydroxyl group of IMP, crystalline complexes of the mouse muscle synthetase without hadacidin, but having bound GDP and either 6P-IMP or 2'-deoxy-6P-IMP showed significant differences. Disorder in the L-aspartate binding pocket was observed in 2'-deoxy-6P-IMP complex implicating the role of hydroxyl group in IMP in the recognition of L-aspartate and in turn explaining the increase in aspartate K_m value when 2'-dIMP replaces IMP (Iancu *et al.*, 2006).

AdSS requires divalent cation for activity with maximum activity being obtained in the presence of magnesium. In case of rabbit skeletal muscle AdSS replacement of $MgCl_2$ by $MnCl_2$ or $CaCl_2$ gave reaction rates approximately 15% and 20% of the standard, respectively (Muirhead & Bishop, 1974). In *E. coli* AdSS, Mg^{2+} could not be replaced by Co^{2+} or Zn^{2+} , but with Mn^{2+} and Ca^{2+} the rate of adenylosuccinate synthesis was 64% and 40%, respectively, of that with Mg^{2+} (Lieberman, 1956). In the enzyme from Yoshida sarcoma ascites tumor cells Mg^{2+} could be partially replaced by Mn^{2+} , Co^{2+} , Ba^{2+} , Ca^{2+} or Cu^{2+} (10-40% activity). However, Cd^{2+} , Pb^{2+} , Hg^{2+} and Zn^{2+} completely inhibited enzyme activity (Matsuda *et al.*, 1980). Human AdSS also showed maximum activity in the presence of Mg^{2+} with Mn^{2+} , Co^{2+} , Ca^{2+} , Ba^{2+} and Ni^{2+} supporting lesser degree of activity (Van der Weyden & Kelly, 1974). Similar reaction rates were observed with magnesium acetate and manganese acetate in *A. vinelandii* AdSS with calcium acetate giving 20% of this rate (Markham & Reed, 1977).

1.1.7 Regulation of enzyme activity

AdSS lies at a regulatory point in purine metabolism and commits IMP to the formation of AMP. Hence, its tight regulation is vital for maintaining adenine and guanine ratios in the cell. AdSS is subjected to feedback and product inhibition by AMP, GMP, GDP and sAMP. In addition, the substrate, IMP has been found to be an inhibitor of AdSS. Borza *et al.* showed that high concentrations of IMP at saturating concentration of GTP inhibit mouse basic isozyme but not the acidic isozyme.

However, at subsaturating GTP concentrations both acidic and basic isozymes were inhibited (Borza *et al.*, 2003). A similar phenomenon has been demonstrated with *P. falciparum* AdSS (Raman *et al.*, 2004). These observations imply IMP binding to the GTP site at subsaturating concentrations of GTP. This alternate binding mode of IMP was also evident in the crystal structure of an IMP complex of mouse basic AdSS (Iancu *et al.*, 2002).

In addition, the role of glycolytic intermediates in the regulation of enzyme activity has been examined. Ogawa *et al.* examined the effect of various glycolytic intermediates on the activity of adenylosuccinate synthetase purified from rat skeletal muscle. Fructose 1,6 bisphosphate (F16BP) showed 80% inhibition at 2 mM concentration and was found to be a noncompetitive inhibitor of all three substrates. 2,3-diphosphoglycerate, 3-phosphoglycerate, 2-phosphoglycerate and phosphoenolpyruvate showed 15-20% inhibition of enzyme activity at 2 mM concentration, while intermediates like glucose-6-phosphate, fructose-6-phosphate, dihydroxyacetone phosphate, glyceraldehyde-3-phosphate, pyruvate and lactate had no significant effect on enzyme activity (Ogawa *et al.*, 1976). Further they demonstrated that F16BP is more potent inhibitor of the basic isozyme ($K_i = 0.6$ mM) when compared to the acidic isozyme ($K_i = 1.6$ mM) (Matsuda *et al.*, 1977). They proposed that the inhibition of AdSS by F16BP allowed synchronization of purine nucleotide cycle and glycolysis. Studies on mouse isozymes resulted in K_i values for F16BP in the low μ M range. At low IMP concentrations, F16BP exhibited competitive inhibition with respect to IMP. However, the inhibition became noncompetitive at saturating IMP concentration (Borza *et al.*, 2003).

AdSS exhibits monomer-dimer equilibrium and this has been implicated in regulation of enzyme activity in vivo (Wang *et al.*, 1997a). Studies on *E. coli* AdSS have shown that the monomers are inactive and substrates induce dimerization of the enzyme. Thus, the enzyme primarily exists as a monomer at physiological concentration and the formation of IMP activates the enzyme.

Hadacidin (N-formyl N-hydroxyglycine), a secondary metabolite from *Penicillium frequentans* (Kaczka *et al.*, 1962) is a potent inhibitor of AdSS competing for the aspartate binding pocket (Shigeura & Gordon, 1962a; Shigeura & Gordon,

1962b). A number of analogs and precursors of hadacidin, like N-acetyl-N-hydroxyglycine, N-formylglycine, N-acetylglycine, N-hydroxyglycine and N-acetylhydroxyaminoacetate inhibit AdSS but not as potently as hadacidin (Shigeura, 1963; Jahngen & Rossomando, 1984).

ppGpp is an unusual guanine nucleotide produced by *E. coli* under conditions of nutrition deprivation. ppGpp in turn dramatically influences a broad range of metabolic processes including ATP and GTP biosynthesis. It was observed that ppGpp inhibits the activity of adenylosuccinate synthetase and IMP dehydrogenase, which are the first enzymes that commit IMP for the synthesis of AMP and GMP, respectively (Gallant *et al.*, 1971; Pao & Dyess, 1981). Kinetic analysis revealed that ppGpp is a competitive inhibitor of GTP and noncompetitive inhibitor of IMP and aspartate (Stayton & Fromm, 1979). Consistent with kinetic evidence, crystals of *E. coli* AdSS grown in presence of IMP, hadacidin, Mg^{2+} and NO_3^- and then soaked in ppGpp revealed electron density corresponding to guanosine 5'-diphosphate 2':3'-cyclic monophosphate in the GTP binding pocket (Hou *et al.*, 1999).

The thesis describes the biochemical characterization of the enzyme, adenylosuccinate synthetase, from a thermophilic archaea and a parasitic protozoan. The next section provides a brief introduction to the two organisms, *M. jannaschii* and *P. falciparum*. The discussion brings forth the large difference in the growth conditions, especially with respect to temperature in which the two organisms survive and propagate.

1.2 Diversity of Life

Life is known to exist in temperatures ranging from $-40^{\circ}C$ to as high as $130^{\circ}C$ (Georlette *et al.*, 2003; Jaenicke & Bohm, 1998; Ehrlich, 2002). No organism however spans the entire temperature range. This is because proteins and some other structural components of the cell require somewhat different compositions and structures for stability and activity in different temperature ranges (Brock, 1967; Tansey & Brock, 1972). Depending on their optimum growth temperature, organisms

can be classified into the following three groups: Psychrophiles, which grow in a range from below 0°C to about 20°C, with an optimum growth temperature of 15°C or lower. Mesophiles are microbes that grow in the range of 15-45°C, with an optimum range for some of about 25-30°C and for others about 37-40°C. Thermophiles are microbes that live in a temperature range of 42-130°C, but the range for any given thermophile is considerably narrower. Thermophiles can be further classified depending upon their growth temperature as follows: thermophiles, that live above 55°C, moderate thermophiles living above 65°C, extreme thermophiles above 75°C and hyperthermophiles above 90°C (Vieille & Zeikus, 2001; Imanaka & Atomi, 2002). Most hyperthermophiles belong to the phylogenetic domain of archaea with *Thermotogales* and *Aquificales* belonging to bacteria (Vieille & Zeikus, 2001). Generally, thermophilic photosynthetic prokaryotes cannot grow at temperatures higher than 73°C. In contrast, thermophilic eukaryotic algae cannot grow at temperatures higher than 56°C. Thermophilic fungi generally exhibit temperature maxima around 60°C and thermophilic protozoa around 50°C. Only nonphotosynthetic thermophilic prokaryotes exhibit temperature maxima that may be as high as 130°C (Ehrlich, 2002). For growth at temperatures at or above the boiling point of water, elevated hydrostatic pressure is needed to keep the water liquid which is a requirement for life. Protozoans, like bacteria, can be either mesophilic or thermophilic. However, most protozoa are mesophilic, having maximum temperature for growth around 40°C.

1.2.1 Phylogenetic Classification: Position of Archaea

The three-kingdom classification of living organisms was put forth by Carl Woese (Woese & Fox, 1977). A phylogenetic analysis based upon ribosomal RNA sequence characterization revealed a tripartite phylogenetic structure of the living world: (i) the eubacteria, comprising all typical bacteria; (ii) the archaebacteria, containing methanogenic bacteria; and (iii) the eukaryotes. However, he could not establish the evolutionary relationship among the primary kingdoms, because the root of the tree could not be determined. This issue was solved by Iwabe *et al.* (Iwabe *et*

al., 1989) and Gogarten *et al.* (Gogarten *et al.*, 1989). Iwabe *et al.* compared a pair of duplicated genes, elongation factors Tu and G, and the alpha and beta subunits of ATPase, whereas, Gogarten *et al.* compared vacuolar H⁺-ATPase and inferred that archaeobacteria are more closely related to eukaryotes than to eubacteria. They proposed that eubacteria branched first from the universal tree with archaeobacteria and eukaryotes as sister groups. The rooting of the universal tree was further analyzed by Brown and Doolittle who used aminoacyl-tRNA synthetase genes and showed that archaeobacteria are the closest living prokaryote relatives of eukaryotes (Brown & Doolittle, 1995). Woese, Kandler and Wheelis had given the name archaea to archaeobacteria. They introduced a new taxon called “domain” above the level of kingdoms. Thus according to this system of classification life on the planet would be divided into three domains, archaea, bacteria and eucarya, each containing two or more kingdoms (Woese *et al.*, 1990). They subdivided the archaea into two kingdoms, Euryarchaeota, which comprises of methanogens and their phenotypically diverse relatives and Crenarchaeota, which consists of extremely thermophilic archaeobacteria. A comprehensive understanding of the nature of archaea and its relationship to bacteria and eukaryotes came from the genome sequencing of a representative member of Archaeal family, *Methanocaldococcus jannaschii*. This opened up opportunities to compare the biochemical pathways among the three domains of life, bacteria, eukaryotes and archaea.

1.2.2 *Methanocaldococcus jannaschii*, a thermophilic archaea

Methanocaldococcus jannaschii was isolated by J. A. Leigh from a sediment sample collected from the sea floor at the base of a "white smoker" chimney on the East Pacific Rise at a depth of 2600 meters. *M. jannaschii* can grow in habitats with pressure more than 200 atm and a temperature range between 48 and 94°C, with the optimum growth temperature being 85°C. The optimum pH for growth of *M. jannaschii* is 6.0 with little or no growth being observed at pH values greater than 7.0. It is a single celled microbe with a complex flagellar system. The cells are osmotically fragile and irregular cocci shaped (Figure 1.3). *M. jannaschii* exhibits a doubling time

of 26 minutes at 85°C, pH 6.0. It is a strict anaerobe and produces energy by reduction of CO₂ with H₂ resulting in the formation of methane (Jones *et al.*, 1983).

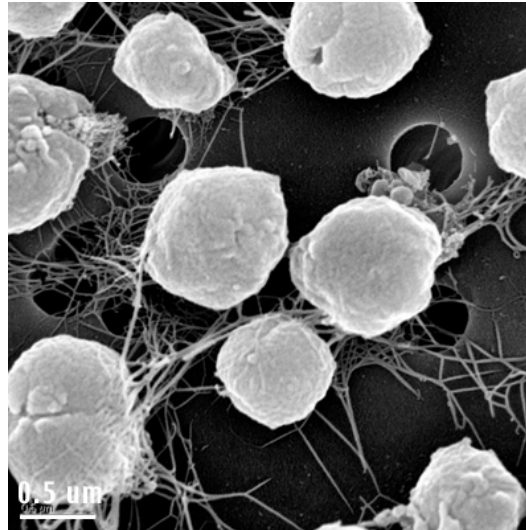


Figure 1.3: Scanning electron micrograph of *Methanocaldococcus jannaschii*. Image taken from www.microbewiki.kenyon.edu, courtesy of Boonyaratanakornkit B. & Clark D.S., University of California, Berkeley.

The archaeal genome consists of three distinct elements: a) a large circular chromosome, b) a large circular extrachromosomal element and c) a small circular extrachromosomal element. These elements are A+T rich and have a G+C content between 28-32%. Analysis of genes encoded in the *M. jannaschii* genome reveals that at the molecular level archaea more closely resemble eukaryotes (Bult *et al.*, 1996).

1.2.3 *Plasmodium falciparum*, a mesophilic parasitic protozoan

Human malaria is caused by four species of Plasmodium; *Plasmodium falciparum*, *Plasmodium malariae*, *Plasmodium vivax* and *Plasmodium ovale*. These four species differ morphologically, immunologically, in their geographic distribution, in relapse pattern and drug response. *P. falciparum* is the causative agent of the most fatal form of malaria causing deaths in young children in Africa. The life cycle of the parasite is extremely complex and requires a vertebrate and an invertebrate host (Figure 1.4). The parasite enters the blood stream of the human host

through the bite of an infected female *Anopheles* mosquito which injects a small amount of anticoagulant-containing saliva and haploid infective sporozoites in the host. The sporozoites reach the liver, penetrate the hepatocytes and trigger exo-erythrocytic schizony. Each sporozoite undergoes asexual replication to produce thousands of merozoites and each merozoite is capable of invading an RBC when released from the liver. This phase takes about 8-25 days in case of *P. falciparum*. All clinical symptoms and pathogenic manifestations associated with mammalian malaria infections are caused by the asexual erythrocytic phase of the Plasmodium life cycle. Merozoites enter the erythrocytes and develop through different stages. The early trophozoite is referred to as “ring” because of its characteristic morphology. Ring enlargement to form mature trophozoites is accompanied by active metabolism which includes active glycolysis, ingestion of host cytoplasm and proteolysis of hemoglobin into amino acids. At the end of the trophozoite stage, there are multiple rounds of nuclear division without cytokinesis resulting in the formation of schizonts. Each schizont contains about 20 mononucleate merozoites which get released into the blood stream after lysis of the erythrocyte. The erythrocyte stage is cyclic and repeats every 48 to 72 hours, depending upon the species of Plasmodium involved. The sudden release of merozoites, toxins and erythrocyte debris triggers an increase in body temperature, which is characteristic of malaria.

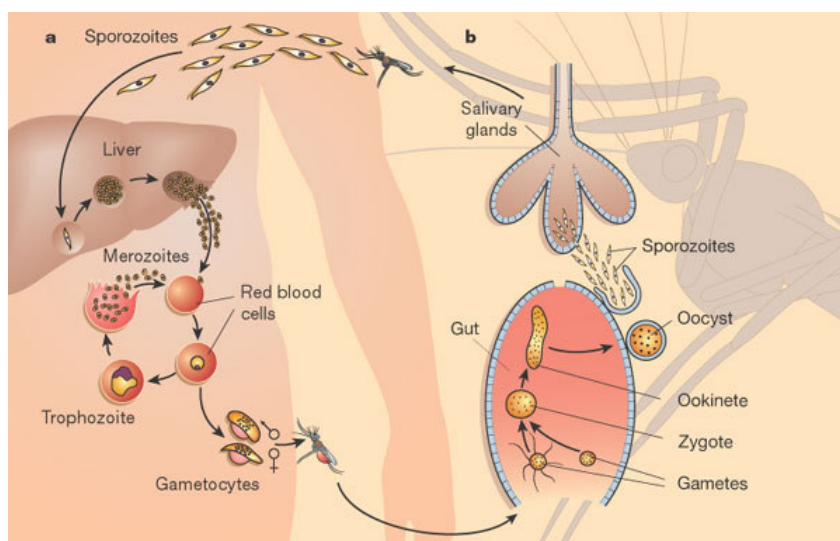


Figure 1.4: Life cycle of *Plasmodium falciparum*. a) Human stages and b) Mosquito stages. Figure taken from Wirth D.F., 2002.

Occasionally, merozoites differentiate into macrogametocytes and microgametocytes, which do not rupture the erythrocyte. Ingestion of gametocytes by the mosquito vector induces gametogenesis which results in development of micro and macrogametes (male and female gametes, respectively). In the mosquito's gut the infected erythrocytes lyse and the gametes fuse to form a diploid zygote which transforms into a motile ookinete. The ookinete migrates to the mosquito's gut, penetrates the gut epithelial cell and forms an oocyst on its outer wall. In a process called sporogony, the oocyst undergoes meiosis and forms sporozoites that migrate to the salivary glands of the mosquito. The cycle is complete and when the mosquito bites another human host, a new cycle begins.

P. falciparum cycles between a poikilothermic mosquito vector and a homoeothermic human host. The parasite is exposed to wide temperature fluctuations during its life cycle, ranging from 25°C in the mosquito vector and 37°C in humans. Subsequently, during its intra-erythrocytic growth in the human, it undergoes repeated exposure to heat shock in the form of episodes of fever suffered by the patient, where the human body temperature goes up to 41°C. Therefore, exposure to frequent temperature fluctuations is an inherent part of the parasite life cycle.

Unlike *Methanocaldococcus jannaschii* which lives under conditions of high temperature and pressure, *P. falciparum* does not experience temperatures greater than 41°C during its life cycle. Thus, the cellular machinery of the two organisms is adapted to function at their optimal growth temperature. Enzymes which are biological catalysts are sensitive to environmental conditions. To function at high temperatures proteins adopt various strategies which are discussed below.

1.3 Thermozymes and Mesozymes

Enzymes produced by thermophiles and hyperthermophiles are known as “thermozymes” and those produced by mesophiles are known as “mesozymes” (Vieille *et al.*, 1996). Although the overall structure of orthologous thermophilic and mesophilic proteins are quite similar, there are intrinsic differences that allow

thermozymes to maintain structural stability and activity at elevated temperatures. Protein stability at extreme temperatures has been attributed to a number of factors like, a) amino acid composition, b) hydrophobic interactions, c) increased aromatic interactions, ion pairs and salt bridge network, d) oligomerization and intersubunit interactions, e) compact packing of the core and reduction in solvent exposed surface area, f) decrease in volume and number of internal cavities, g) decrease in number and size of surface loops, h) modification in α -helix and β -sheet content and i) a general shortening of length (Jaenicke & Bohm, 1998; Kumar & Nussinov, 2001; Li *et al.*, 2005). Apart from the above mentioned factors, *in vivo* stability of a protein is influenced by macromolecular crowding and naturally occurring small molecules such as sugars and other metabolites (Eggers & Valentine, 2001; Ellis, 2001; Vieille & Zeikus, 2001).

The property of thermostability seems to be encoded in the primary amino sequence of the protein, as a large number of studies aimed at elucidating factors responsible for extreme stability of thermostable proteins have not led to the identification of any new amino acid, covalent modification or structural motif that could be responsible for structural stabilization of these proteins. Infact, it is believed that variation in amino acid composition and redistribution of intramolecular interactions required for structural stabilization at moderate temperatures are sufficient to maintain structural stability at extremes of temperature (Fields, 2001).

The major bottleneck in understanding molecular determinants of thermostability in proteins has been the lack of availability of a large dataset of structures of homologous proteins from thermophiles and mesophiles. Thus, studies involving structural comparisons have used one or few protein structures. This limitation has been partly overcome by genome sequencing of organisms adapted to different modes of life. Comparison of ORFs corresponding to proteins with known structures enables correlation of structural context of the observed sequence differences.

The following section discusses the factors implicated in enhancing thermostability of proteins.

1.3.1 Protein sequence length in thermophiles

Thermophilic organisms have significantly higher proportion of smaller proteins when compared to mesophilic organisms (Thompson & Eisenberg, 1999; Chakravarty & Varadarajan, 2000). Shortening of coding sequences is believed to be a determinant of thermal stability of proteins. A study involving a large dataset of proteins from 56 species showed that the mean protein lengths in thermophiles and mesophiles are 283 ± 5.8 and 340 ± 9.4 , respectively (Tekaiia *et al.*, 2002). There is an increased propensity for sequence deletions to occur in the exposed loop regions in thermophilic proteins (Thompson & Eisenberg, 1999; Stieglitz *et al.*, 2005). Loop truncations have been noted in several studies comparing crystal structures from mesophilic and thermophilic sources (Russell *et al.*, 1997; Auerbach *et al.*, 1997; Tahirov *et al.*, 1998).

1.3.2 Oligomerization

A number of thermophilic proteins are known to exhibit a higher oligomerization state than their mesophilic homologs and this is one of the features that has been implicated in stabilization of these proteins (Ogasahara *et al.*, 2001; Villeret *et al.*, 1998; Lokanath *et al.*, 2004; Grabarse *et al.*, 1999; Hess *et al.*, 1995; Sterner *et al.*, 1996). This hypothesis has been experimentally tested in phosphoribosylanthranilate isomerase (PRAI), which is monomeric and labile in most mesophilic microorganisms, but dimeric and stable in the hyperthermophile, *Thermotoga maritima* (tPRAI). Thoma *et al.* engineered monomeric variants of tPRAI by site directed mutagenesis. These monomeric variants were as active as the wild type protein but their kinetic stability at 85°C decreased by several fold (Thoma *et al.*, 2000). Another evidence comes from studies on the repressor of primer (ROP) protein. ROP is an all helical homodimeric protein that denatures at 71°C. Removal of five amino acids from a surface loop converted the protein into a homotetramer with the T_m increasing to 101°C (Lassalle *et al.*, 1998).

1.3.3 Amino acid composition

Hydrophobic residues are found in the interior and polar residues on the surface of globular proteins. While maintaining the basic fold characteristics of the protein family, thermophilic proteins show preferences for certain amino acids. The hydrophobic amino acid content is marginally higher in thermophiles (Chakravarty & Varadarajan, 2000; Sadeghi *et al.*, 2006) when compared to mesophiles, as these residues can increase rigidity and hence stability of the protein. Isoleucine and valine have higher frequency of occurrence in thermophilic proteins (Chakravarty & Varadarajan, 2000; Haney *et al.*, 1999). Proline, which has the lowest conformational entropy, occurs at a higher frequency in thermostable proteins (Pack & Yoo, 2004; Sadeghi *et al.*, 2006). Appropriate positioning of proline residues results in a more rigid and structured polypeptide which does not unfold easily.

Thermostable proteins show a decrease in content of polar uncharged amino acids like serine, threonine, and glutamine (Chakravarty & Varadarajan, 2000; Kumar *et al.*, 2000; Pack & Yoo, 2004; Sadeghi *et al.*, 2006; Tekaiia *et al.*, 2002; Haney *et al.*, 1999). Asparagine and glutamine are thermolabile amino acids due to their tendency to undergo deamination at higher temperatures. These replacements also minimize problems of deamination of asparagine and glutamine by serine and threonine at high temperatures (Tomazic & Klibanov, 1988). Methionine and cysteine, which contain a sulphur atom in the side chain, are also thermolabile by virtue of their property to undergo oxidation at higher temperature. Hence, they have a lower frequency of occurrence in thermostable proteins (Kumar *et al.*, 2000; Zhou *et al.*, 2008).

Thermophiles show an increase in polar charged amino acid content by virtue of their ability to contribute to electrostatic interactions. There is a higher occurrence of glutamic acid and arginine residues in thermophilic proteins (Zhou *et al.*, 2008; Chakravarty & Varadarajan, 2000; Haney *et al.*, 1999). Arginine seems to be substituted for lysine because the bulky guanidine group gives a greater positively charged surface for stabilizing interactions and its higher pK_a enables it to maintain a net positive charge and hence ion pairs at elevated temperatures. Higher ratio for charged amino acids increases ionic interactions and enhances occurrence of salt

bridges and ion pairs in thermophilic proteins which results in increase in thermostability of these proteins.

Hyperthermophilic proteins also show a marginal increase in their aromatic residue content, especially tyrosine (Kumar *et al.*, 2000; Vieille & Zeikus, 2001). In addition to aromatic interactions, aromatic residues are also involved in making π -cation interactions which impart stability to the protein (Ma & Dougherty, 1997).

1.3.4 Additional interactions contributing to stability

The three dimensional structure of proteins is stabilized by two classes of non-covalent interactions, electrostatic and hydrophobic. Electrostatic interactions include ion pairs, hydrogen bonds and weak polar interactions. Enhanced stability of thermostable protein molecules involves only a marginal increase in free energy, equivalent to a small number of interactions which includes a few hydrogen bonds, hydrophobic interactions or ion pairs. Increase in hydrogen bonds, ion pairs and hydrophobic interactions have been considered as a means to enhance protein thermostability. A prominent role for ion pairs and ion pair networks in stabilization of proteins at or above 100°C has been inferred from crystal structures of several proteins from thermophiles (Karlstrom *et al.*, 2006; Miyazono *et al.*, 2005; Sakuraba *et al.*, 2008; Vitali *et al.*, 2007; Salminen *et al.*, 1996; Knapp *et al.*, 1999). One of the enzymes where this feature has been explored in detail is glutamate dehydrogenase (GDH). *Pyrococcus furiosus*, *Pyrococcus kodakaraensis* and *Thermococcus litoralis* glutamate dehydrogenase are 83-87% identical. However, the three enzymes differ in their thermostability, with *P. furiosus* GDH being most stable followed by *P. kodakaraensis* GDH and *T. litoralis* enzyme. Homology-based modeling, structure comparison and site directed mutagenesis aimed at addition or removal of ion pair networks established a positive correlation between intersubunit ion-pair networks and hyperthermostability in these proteins. The mutations, Glu158Gln and Thr138Glu add and remove ion pairs, respectively, at the hexamer interface of *P. kodakaraensis* GDH. Thr138Glu mutation increased the thermostability while Glu158Gln decreased the thermostability of the mutant when compared to the wild type protein (Rahman *et*

al., 1998). An ion pair network involving six charged residues is present only in *P. furiosus* GDH. Using site directed mutagenesis the same network was created in *T. litoralis* and *P. kodakaraensis* GDH and this resulted in stabilization of the two enzymes indicating that intersubunit ion pairs play an important role in stabilization of GDH (Vetriani *et al.*, 1998). When compared to *Clostridium symbiosum* glutamate dehydrogenase, which has 107 salt bridges, *P. furiosus* enzyme has 168 salt bridges (Yip *et al.*, 1995). The salt bridges in the Pyrococcus enzyme form extensive networks and are highly stabilizing when compared to the mesophilic enzyme (Kumar *et al.*, 2000). In addition, a stabilizing function for buried ion pairs has been proposed in *P. kodakaraensis* O⁶-methylguanine-DNA methyltransferase and *Thermosphaera aggregans* β-glycosidase (Hashimoto *et al.*, 1999; Chi *et al.*, 1999). Szilagyi and Zavodszky showed a positive correlation between growth temperature and number of ion pairs in proteins (Szilagyi & Zavodszky, 2000)

Charged residues play a dual role in stabilization of proteins by participating not only in salt links but also in hydrogen bonds with a neutral partner (charged neutral H-bonds; i.e. bond between a side chain atom of a charged residue and either a main chain atom of any residue or side chain atom of a neutral residue). Tanner *et al.* showed a strong correlation between thermostability of glyceraldehyde-3-phosphate dehydrogenase and the number of charged neutral H-bonds (Tanner *et al.*, 1996). An increased number of charged neutral H-bonds are also found in *T. maritima* ferredoxin and *Thermoanaerobacter brockii* NADP(H)-dependent alcohol dehydrogenase (Macedo-Ribeiro *et al.*, 1996; Korkhin *et al.*, 1999).

1.3.5 Metal binding

Metals are known to stabilize and activate enzymes (Lim *et al.*, 2007; Potter *et al.*, 2007; Burmeister *et al.*, 1994; Bogumil *et al.*, 1998; Housley *et al.*, 1993; Tainer *et al.*, 1992). A study on *Bacillus licheniformis* xylose isomerase in the presence and absence of metal ions showed that both kinetic and thermodynamic stability of the enzyme were functions of the nature of metal ion present (Vieille *et al.*, 2001).

Some thermophilic and hyperthermophilic enzymes contain metal atoms that are not present in the mesophilic counterpart. Ferredoxin from *Sulfolobus* sp. strain 7 contains an extra 40 residue N-terminal extension that is linked to the protein core by a zinc binding site. The zinc atom is coordinated by three histidine residues in the N-terminal domain and an aspartic acid residue from the core domain. The N-terminal extension and zinc binding site is absent in eubacterial homologs (Fujii *et al.*, 1997). N-terminal deletion and site directed mutagenesis of the histidine residues coordinating the zinc atom showed that the zinc ion and certain parts of the extra sequence stretch in the N-terminal domain are responsible for thermal stabilization of the molecule (Kojoh *et al.*, 1999). A thermostable subtilase (protein of subtilisin superfamily) from *Bacillus* sp. Ak.1, contains three calcium ion binding sites against two present in thermitase and the mesophilic subtilisins (Smith *et al.*, 1999). The Ak.1 protease is significantly more stable than thermitase in the presence of Ca^{2+} indicating the role of additional metal ion in enhanced thermostability.

1.3.6 Higher packing efficiency and reduction of solvent accessible surface area

Molecular compactness can be achieved by shortening of loops, increasing the number of atoms buried in the protein interior, optimized packing of amino acid side chains in protein core and elimination of cavities (Russell *et al.*, 1997). Thermostable proteins often have a larger and more hydrophobic core, due to an increase in aliphatic amino acid content and aliphatic side chain volume (Haney *et al.*, 1997; Haney *et al.*, 1999). A comparison of citrate synthase from hyperthermophilic (*Pyrococcus furiosus*), thermophilic (*Thermoplasma acidophilum*) and mesophilic organism (pig) indicated that increased compactness of the enzyme is an important factor contributing to the stability at high temperature (Russell *et al.*, 1997). A decrease in number and volume of internal cavities has been observed in certain hyperthermophilic enzymes like lactate dehydrogenase from *Thermotoga maritima* (Auerbach *et al.*, 1998) and glutamate dehydrogenase from *Thermococcus litoralis* (Britton *et al.*, 1999). A study involving eight amidotransferases derived from

hyperthermophiles, thermophiles and mesophiles showed that the increase in the optimum growth temperature of the organism was accompanied by an increase in molecular compactness, surface hydrophilicity and ratio of buried polar contacts in the protein (Matsui & Harata, 2007). Gain in stability by better packing of residues in protein interior has been experimentally demonstrated. A solvent accessible cavity in *Methanobacterium formicicum* histone is filled by a bulky hydrophobic side chain in *M. fervidus* protein. The mutations, Ala31Ile and Lys35Met increased the *M. formicicum* T_m by 11 and 14°C, respectively, while the mutations Ile31Ala and Met35Lys decreased *M. fervidus* histone T_m by 4 and 17°C, respectively (Li *et al.*, 1998; Li *et al.*, 2000).

Thermostable enzymes generally have a smaller and more hydrophilic exposed surface. Hyperthermophilic aldehyde ferredoxin oxidoreductase has 17% smaller accessible surface area when compared to a water soluble oligomeric protein of comparable size (Chan *et al.*, 1995). Since surface hydrophobic residues cannot participate in stabilizing interaction with the solvent, they are detrimental to protein stability and solubility. A number of hyperthermophilic proteins show significantly reduced hydrophobic accessible surface area (Auerbach *et al.*, 1998; Knapp *et al.*, 1999; He *et al.*, 2007). Increased polar surface area contributes to greater stability of thermophilic protein due to added hydrogen bonding density to water (Vogt *et al.*, 1997; Haney *et al.*, 1997).

1.3.7 Increased secondary structure content and stability

Some thermophilic proteins show more extensive secondary structure and better capped helices than their mesophilic counterparts. An increase in secondary structure content, especially α -helices, has been reported for lactate dehydrogenase and phosphoribosylanthranilate isomerase from *T. maritima* (Auerbach *et al.*, 1998; Hennig *et al.*, 1997) and glyceraldehyde-3-phosphate dehydrogenase from *Sulfolobus solfataricus* (Isupov *et al.*, 1999).

α -helix stabilization can be achieved by substituting residues with low helical propensity with residues that have a high helical propensity. Distribution of amino

acids in α -helices of thermophilic proteins is significantly different from the helices in mesophilic proteins. Thermophilic helices favor arginine, which is a helix favoring residue, and avoid histidine, proline and cysteine, which are helix disfavoring residues (Kumar *et al.*, 2000). Helices in thermophilic proteins also show a decrease in content of β -branched residues (valine, isoleucine and threonine) which are not well tolerated in helices (Facchiano *et al.*, 1998; Chakravarty & Varadarajan, 2000). α -helices carry a considerable dipole moment and helix dipole can be stabilized by negatively charged residues near the N-terminal end and positively charged residues near the C-terminal end. Improved stabilization by capping has been observed in indole-3-glycerol phosphate synthase from *Sulfolobus solfataricus* (Hennig *et al.*, 1995), ferredoxin from *Thermotoga maritima* (Macedo-Ribeiro *et al.*, 1996) and phosphoglycerate kinase from *B. stearothermophilus* and *T. maritima* (Auerbach *et al.*, 1997), when compared to mesophilic homologs.

1.3.8 High rigidity

Thermozymes are more rigid than mesozymes. The increased rigidity is essential to preserve the three dimensional structure of the enzyme at high temperature which in turn is essential for catalytic activity. Enhanced rigidity of thermozymes has been demonstrated by reduced hydrogen-deuterium exchange rates, lower susceptibility to protease digestion, resistance to denaturation induced by chemical denaturants and high T_m values (Tehei & Zaccari, 2007; Zavodszky *et al.*, 1998; Khajeh *et al.*, 2001; Bonisch *et al.*, 1996; Daniel *et al.*, 1982). The rigidity of structure arises due to the different kinds of stabilizing interactions that these proteins exhibit.

The above section summarizes the factors exploited by proteins from thermophiles to enhance structural stability at high temperatures. Thermophilic proteins use a combination of factors to maintain structural integrity under extreme conditions with no single universal mechanism implicated in imparting stability to thermozymes.

1.4 Thermophilicity

Another important feature of thermophilic enzymes is their ability to catalyze reactions at elevated temperatures, a phenomenon termed as “thermophilicity”. Protein function relies on a delicate balance between macromolecular stability and micromolecular flexibility. The structural similarity of the active site and conservation of catalytic residues between mesophilic and thermophilic counterparts leads one to expect similar catalytic rates at a given temperature. However, enzymes from thermophiles are barely active at ambient temperatures where the mesophilic enzymes exhibiting similar function are optimally active. Cold denaturation cannot explain this phenomenon as crystal structures of thermostable enzymes solved at low temperatures show a fully folded conformation state of these proteins. Thermostability is achieved by a combination of factors discussed above which in turn decrease the structural flexibility of the protein. Conformational flexibility has an impact on structural stability as well as catalysis. Protein dynamics has been implicated to play a key role in substrate binding, product release and even in the process of chemical conversion (Benkovic & Hammes-Schiffer, 2003; Eisenmesser *et al.*, 2005; Hammes-Schiffer & Benkovic, 2006). The increased conformational rigidity which serves to stabilize thermophilic proteins at extreme temperatures often results in differences in their temperature optima from that of the mesophilic counterparts (Fields, 2001; Georlette *et al.*, 2003; Vihinen, 1987; Zavodszky, 1998; Merz *et al.*, 2000; Wolf-Watz *et al.*, 2004). However, a “corresponding state” with respect to flexibility and hence, catalytic activity is achieved at the respective temperature optimum of the two enzymes.

Studies of structural stability and thermophilicity of *M. jannaschii* AdSS are presented in Chapter 3 of this thesis.

Chapter 2

Kinetic Characterization of Adenylosuccinate Synthetase from the Thermophilic Archaea *Methanocaldococcus jannaschii*

This chapter discusses the biochemical characterization of adenylosuccinate synthetase from the thermophilic archaea, M. jannaschii. Studies with the archaeal enzyme highlight certain unique kinetic and regulatory features of this protein. Unlike the monomer-dimer equilibrium reported for mesophilic AdSS, M. jannaschii AdSS exhibits dimer-tetramer equilibrium with the tetramer being the catalytically active form of the enzyme. The enzyme shows rapid equilibrium random binding of IMP and GTP with the binding of aspartate to E.IMP.GTP complex being steady-state ordered. The substrate, IMP, the glycolytic intermediate, fructose 1,6 bisphosphate and the products of the reaction were found to be effective regulators of enzyme activity. The data presented in this chapter have been published (Mehrotra S. and Balaram H., 2007, Biochemistry, 46(44):12821-12832).

2.1 Introduction

Enzymes are efficient biological catalysts and like all other catalysts, speed up the rate of a chemical reaction without being used up in the process. Like all other catalysts they do not alter the equilibrium constant for the reaction but only affect the rate at which the reaction proceeds towards equilibrium. However, enzymes do differ

from most other catalysts in being highly specific. All processes in a biological cell need enzymes in order to occur at significant rates. Since enzymes are extremely selective for their substrates and speed up only a few reactions from the large set of reactions occurring in a living cell, the set of enzymes expressed in a cell determines which metabolic pathways occur in that cell at a given time.

The complete description of an enzyme catalyzed reaction involves:

i) Elucidation of catalytic mechanism which includes analysis of all chemical transformations, that is the bond breaking and bond making events, involved in the conversion of substrates to products and the elementary reactions comprising the reaction scheme. It involves an understanding of the thermodynamic properties of the reaction, the energetics of the rate determining step, the structure of the intermediates and the transition state, and the effect of temperature, pH, solvent and other factors on the rate of the reaction.

ii) Elucidation of kinetic mechanism which explains more than mere changes in covalent structure of the reactants. To understand how an enzyme acts as a catalyst and how it is regulated in vivo, knowledge of the enzyme's kinetic mechanism is essential. Kinetic mechanism of an enzyme provides information on the chemical mechanism, substrate specificity, aspects of regulation, allosteric properties and the acidic and basic groups associated with catalysis. Infact, it explains the role of the enzyme in catalysis.

Enzyme kinetics is a branch of enzymology which deals with factors affecting the rates of enzyme catalyzed reactions. The most important among these are enzyme concentration, ligand concentration, pH, ionic strength and temperature. Proper analysis of these factors provides enormous information on the nature of the enzyme reaction and the in vivo regulation of the enzyme activity. Studying enzyme kinetics is of importance in biochemistry because:

1. Kinetics provides information on binding affinities of substrates and inhibitors and the catalytic efficiency of the enzyme. Using this information the intracellular concentration of the substrates and products can be guessed and the physiological direction of the reaction determined.
2. Information on enzyme kinetics coupled with chemical and structural studies on the enzyme enable elucidation of enzyme's catalytic mechanism.
3. Using data from kinetics, the kinetic mechanism of an enzyme can be elucidated which in turn provides information on the various enzyme-substrate and enzyme-product complexes that can form and the nature of the transition state. This knowledge can be exploited to design effective inhibitors of the reaction.
4. Most enzymes are constituents of metabolic pathways and hence, enzyme kinetics leads to an understanding of the role of an enzyme in a metabolic process.

2.1.1 Classification of kinetic mechanisms

Multisubstrate enzyme mechanisms can be segregated into two broad classes, Sequential and Ping Pong (Alberty, 1953). Sequential mechanism can be further classified as ordered and random, depending upon the substrate binding pattern.

i) **Sequential Mechanism.** In a sequential mechanism all substrates must be present simultaneously at the enzyme's active site before product formation occurs. Sequential mechanisms exhibit intersecting line patterns in double reciprocal plots of $1/\text{velocity}$ versus $1/[\text{substrate}]$ at different fixed concentrations of the other substrate/substrates. The lines intersect at a common point either to the left or on the y-axis. In an ordered mechanism, binding of one substrate brings about a conformation change in the enzyme which exposes the site for other substrate to bind. Hence, there is a preferred order of substrate binding to the enzyme. In contrast, in a random sequential mechanism, substrates add randomly to the enzyme with no preferential order.

ii) **Ping Pong Mechanism.** In a ping pong mechanism a product dissociates from the enzyme before the second substrate forms a Michaelis complex with the enzyme. The lines in double reciprocal plots of $1/v$ versus $1/\text{substrate concentration}$ are parallel in the case of ping pong mechanism.

2.1.2 Elucidation of kinetic mechanism

Reaction mechanisms can be elucidated using following two approaches

- 1) Initial velocity kinetics
- 2) Product inhibition

A) *Initial Velocity Kinetics*

Initial velocity is defined as the reaction rate at the early phase of enzymatic catalysis during which the formation of product is linear with respect to time. Initial rate persists for a time during which the substrate concentration is within 10% of initial value and the influence of complicating factors such as effects of reversible reaction, product inhibition and progressive inactivation of the enzyme are negligible. Initial velocity kinetics serves as a useful tool to dissect the kinetic mechanism of an enzyme catalyzed reaction. Initial rate data permits evaluation of the kinetic parameters, binding sequence and kinetic mechanism of a reaction. For a bisubstrate reaction, evaluation of enzyme kinetic mechanism involves the measurement of initial reaction velocity at varying levels of one substrate and at different fixed concentrations of the second substrate. For a three substrate reaction there are two different procedures that are widely used. According to Frieden's method, one substrate is varied at different fixed concentrations of the second substrate with the third being held at fixed saturating concentration (Frieden, 1959). In this way the three substrate system reduces to pseudo-two-substrate reaction. A second method was proposed by Fromm and co-workers (Rudolph & Fromm, 1969; Rudolph & Fromm, 1979). Here one substrate is varied while the other two substrates are maintained constant in the general concentration range of their Michaelis constant.

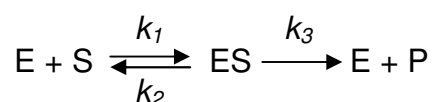
This experiment is then repeated with different concentrations of fixed substrates with care being taken to maintain the ratio of fixed substrates constant. This procedure is repeated until all substrates are varied.

Graphical and/or numerical analysis of initial rate data allows differentiation between sequential and ping pong mechanisms. Line patterns in double reciprocal plots of 1/velocity versus 1/varied substrate are diagnostic of sequential or ping pong mechanism. Further, the intersection points of the double reciprocal plots for sequential mechanism have defined kinetic relationship and are diagnostic of particular mechanisms. Secondary plots of slope and intercept derived from primary double reciprocal data are very useful in elucidating the kinetic mechanism of complex three substrate reactions. Thus, initial rate data defines a reaction mechanism in totality.

Numerical values of certain kinetic constants or the relationship between different groups of kinetic constants determined by mathematical analysis of the initial rate data provides information on whether the reaction follows a rapid equilibrium or steady-state assumption. This information comes from the fit of initial rate data to appropriate rate equations. A rate equation is a mathematical expression that depicts a kinetic model in terms of various rate constants and reactant concentrations. Initial velocity equations are derived based on two basic assumptions,

i) Rapid equilibrium assumption

This concept was proposed by Henri, Michaelis and Menten. The simplest scheme for an enzyme catalyzed reaction is given by



In rapid equilibrium treatment it is assumed that there is a slow catalytic conversion step (k_3) with the enzyme-substrate association and dissociation steps (k_1 and k_2) being relatively fast, resulting in the establishment of equilibrium between E, S and ES, where E denotes the enzyme and S, the substrate.

ii) Steady-state assumption

This assumption was first proposed by G. E. Briggs and James B. S. Haldane. In this, the concentration of various enzyme intermediates (like ES) is assumed to be constant over most of the course of the reaction. This implies that rate of appearance of an intermediate is equal to its rate of disappearance (ie. $k_1 = k_3$).

However, multisubstrate reactions often exhibit complex reaction mechanisms. The reactions may involve two or more rapid equilibrium segments isolated by one or more steady-state steps. These are known as partial equilibrium mechanisms and a combination of rapid equilibrium and steady-state approach is needed to derive the rate equations that define the kinetic mechanism. Steady-state treatment of complicated reaction mechanisms leads to equations and constants that are quite complex to work with. For this reason equations derived on the basis of rapid equilibrium assumption are more useful. However, a simplified procedure was described by Cha, where all the rapid equilibrium segments are treated as a single enzyme species at steady-state with the other species. (Cha, 1968)

B) *Product Inhibition*

Products usually bear resemblance to the substrates from which they are derived and hence, may occupy the substrate binding site resulting in the formation of dead-end complex. The mode of inhibition observed depends on the type of enzyme-product complex that can be formed (Segel, 1975). Products of a reaction can be used to investigate the order of substrate binding. Alberty proposed that bisubstrate sequential mechanisms could be differentiated by product inhibition studies (Alberty, 1958) and this concept was first applied by Fromm in studies on characterization of ribitol dehydrogenase and lactate dehydrogenase (Fromm & Nelson, 1962; Zewe & Fromm, 1962). For a multisubstrate enzyme the experiment involves measurement of initial velocity at varying concentrations of one substrate with the product being held at different fixed concentrations. The other substrate or substrates in the reaction are held at constant subsaturating concentration. The pattern of inhibition is determined

by plotting double reciprocal plots of $1/v$ versus $1/\text{varied substrate}$. It is extremely important to hold the nonvaried substrates at subsaturating concentration in the region of their Michaelis constant to avoid erroneous results. There are three general types of inhibition observed with product inhibitors and these can be defined by their effect on slope and intercept of double reciprocal plots.

i) Competitive inhibition. A competitive inhibitor is a substance that binds to the free enzyme and excludes substrate binding at the active site. This type of inhibition can be overcome by sufficiently high concentrations of the substrate which competes out the inhibitor. A competitive inhibitor may be a nonmetabolizable analog or derivative of the true substrate, an alternative substrate or the product of the reaction. Competitive inhibition increases K_m (i.e., the inhibitor interferes with substrate binding), but does not affect V_{\max} (the inhibitor does not hamper catalysis) of the reaction. Hence, only the slope of the double reciprocal plot is affected in the presence of the inhibitor.

ii) Uncompetitive inhibition. An uncompetitive inhibitor is a compound that binds reversibly to the enzyme-substrate complex yielding an inactive ESI complex. The inhibitor does not bind to the free enzyme. Presence of an uncompetitive inhibitor affects only intercepts and not slopes in double reciprocal plots. This results in a series of parallel lines at different product concentrations. Both V_{\max} and K_m values decrease in the presence of an uncompetitive inhibitor.

iii) Mixed inhibition. Mixed-type inhibitors bind to both E and ES, but their affinities for these two forms of the enzyme are different. Thus, mixed-type inhibitors interfere with substrate binding (increase K_m) and hamper catalysis (decrease V_{\max}). Both slopes and intercepts of double-reciprocal plots are affected by the presence of mixed type inhibitor resulting in a family of lines that intersect to the left of the vertical axis. The intersection can be above, below or on the horizontal axis. Non-competitive inhibition is a form of mixed inhibition where the binding of the inhibitor to the enzyme reduces its activity but does not affect the binding of the substrate. Both

substrate and inhibitor bind reversibly and independently at different sites. As a result, the extent of inhibition depends only on the concentration of the inhibitor.

The inhibition patterns can be further analyzed by replots of slopes and intercepts of the reciprocal plots versus the inhibitor concentration. The replots are often linear but sometimes parabolic line patterns are obtained which may arise due to binding of two molecules of inhibitor to the enzyme or abortive complex formation with products (Rudolph, 1979). Evaluation of the effect of saturation of substrates on the inhibition pattern often results in change in inhibition pattern and this can be used to further distinguish between the various reaction mechanisms. Product inhibition studies have proved extremely useful in elucidating substrate binding order in complex three substrate reactions. Uncompetitive inhibition patterns generated are diagnostic of substrate binding order. However, this technique is limited by the availability of product mimics for each substrate. Alternately, competitive inhibitors of substrates can be used and their inhibition patterns with respect to all substrates determined by methods described above (Fromm, 1979).

2.1.3 *Methanocaldococcus jannaschii* Adenylosuccinate Synthetase

A) *Sequence comparison*

The sequence lengths of AdSS from many bacteria and eukaryotes are similar ranging from 430-457 amino acids (Honzatko *et al.*, 1999; Stayton *et al.*, 1983) with an identity of 30-50% across sequences. Plant chloroplast AdSS differ in having an amino terminal extension that serves as the signal peptide for targeting the enzyme to the organelle (Fonne-Pfister *et al.*, 1996; Prade *et al.*, L., 2000). *Leishmania major* has a significantly longer AdSS with 710 amino acids and the experimentally determined molecular mass of *L. donovani* enzyme is >250,000 Da (Spector *et al.*, 1979). AdSS from *Salinispora tropica* strain CNB-440, a marine actinomycete, is 807 amino acids long. However, the significance of the additional amino acids in context of protein structure and function has not been examined in any case.

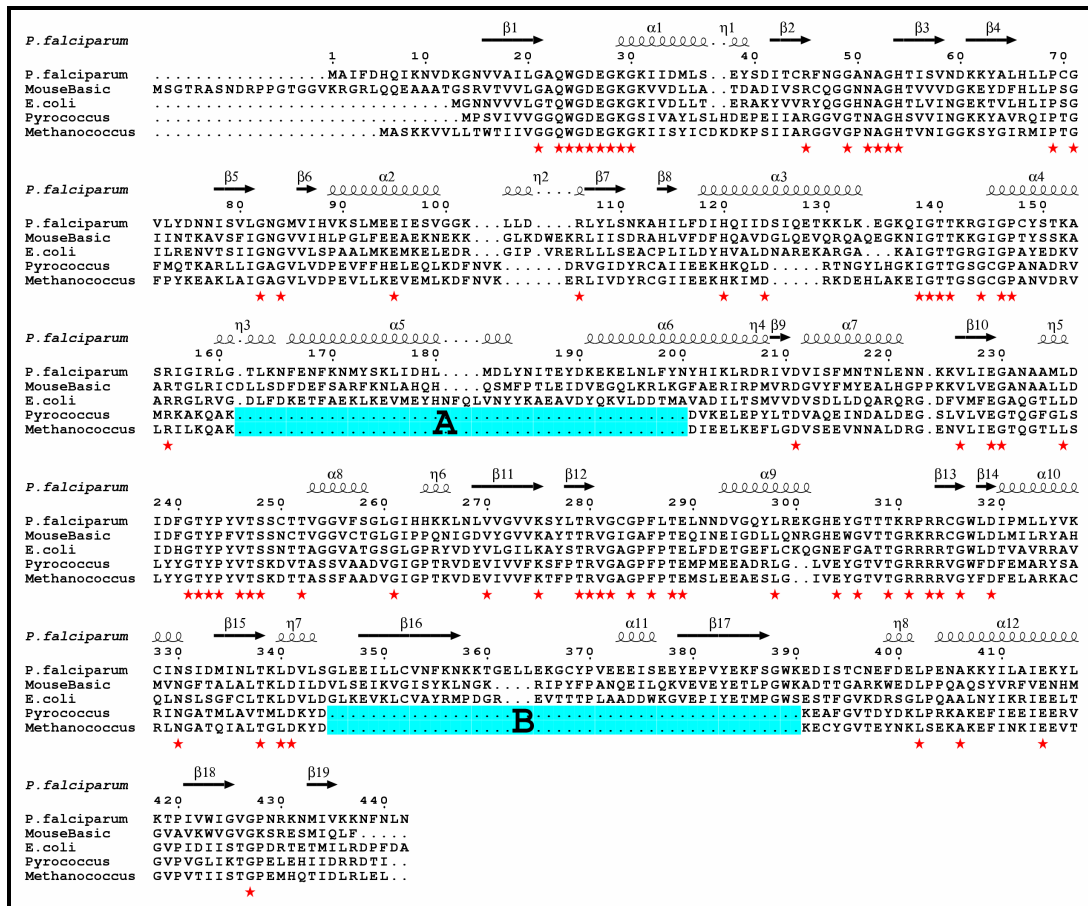


Figure 2.1: Alignment of amino acid sequences of adenylosuccinate synthetase. The alignment was generated using CLUSTAL W (Thompson *et al.*, 1994) and represented using ESPRIPT (Gouet *et al.*, 1999). The sequence numbering and secondary structure assignments on the top correspond to the *P. falciparum* AdSS sequence. α , represents alpha helices; η , represents 3_{10} helices; β , represents sheets, and stars in red mark conserved residues. Boxed regions (A and B) highlight the deletions in *Pyrococcus* and *Methanococcus* AdSS sequences.

Though the AdSS sequence from a vast majority of organisms is 430-457 amino acids in length, the NCBI protein data base contains 38 annotated AdSS sequences that are shorter in length by 90-120 amino acids. Thus, based upon sequence length, AdSS from different organisms can be grouped into 2 clades. Clade 1 comprises of enzymes that are 430-457 amino acids long and Clade 2 consists of enzymes that are 330-350 amino acids in length. Clade 2 AdSS are largely from archaea, however, this is not an exclusive feature of thermophiles as certain thermophilic archaea have longer AdSS sequence. First report of a short AdSS sequence was from *Pyrococcus* species strain ST700 (Bouyoub *et al.*, 1996) followed

by that from *Pyrococcus furiosus* (Cann *et al.*, 1998). *M. jannaschii* has a single AdSS gene that codes for the short, Clade 2 AdSS. Figure 2.1 shows the multiple sequence alignment of the short AdSS sequences from *M. jannaschii* and *P. furiosus* with the longer homologs from *P. falciparum*, *E. coli* and mouse. The short AdSS sequences are characterized by two major deletions (labeled as A and B in Figure 2.1) that map to the mid-region and C terminus of the protein. Loss of segment A leads to loss of α 5, 6 and η 3 while loss of segment B results in deletion of β 16, 17 and α 11 (Figure 2.1 and Figure 2.2) when compared to the *P. falciparum* AdSS structure.

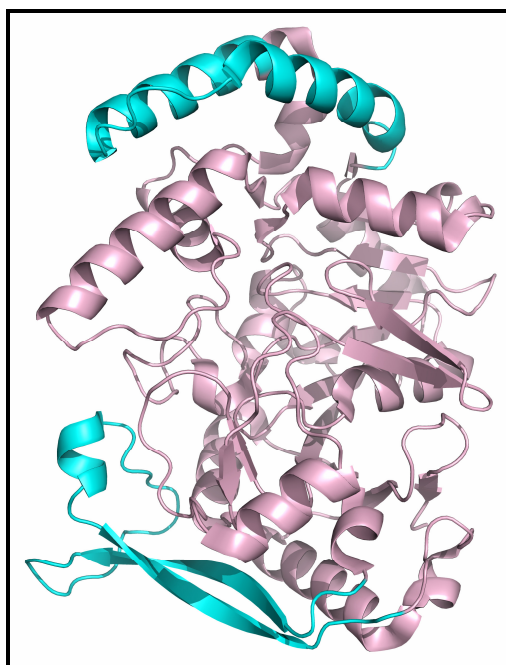


Figure 2.2: Ribbon representation of PfAdSS monomer. Marked in cyan are the segments deleted in MjAdSS. The figure was generated using PyMOL (DeLano, 2002).

In addition to Clade 1 and Clade 2 AdSS, NCBI database has two AdSS sequences, one from *Methanosarcina mazei* and other from *Thermotoga maritima* whose lengths are 379 and 397 amino acids, respectively. While *T. maritima* is a bacterium with an optimum growth temperature of 80°C, *M. mazei* is an archaea, whose genes show strong similarity to the bacterial genes (Deppenmeier *et al.*, 2002). Completion of the *T. maritima* genome has also revealed a high level of similarity of the bacterium with Archaea in terms of gene content and overall genome organization (Nelson *et al.*, 1999). Although the core of *T. maritima* is eubacterial, almost one

quarter of the genome is archaeal in nature. *M. mazei* AdSS completely lacks the first deletion seen in Clade 2 sequences (Figure 2.3), while *T. maritima*, has a nine residue first deletion and 20 residue second deletion (Figure 2.3).

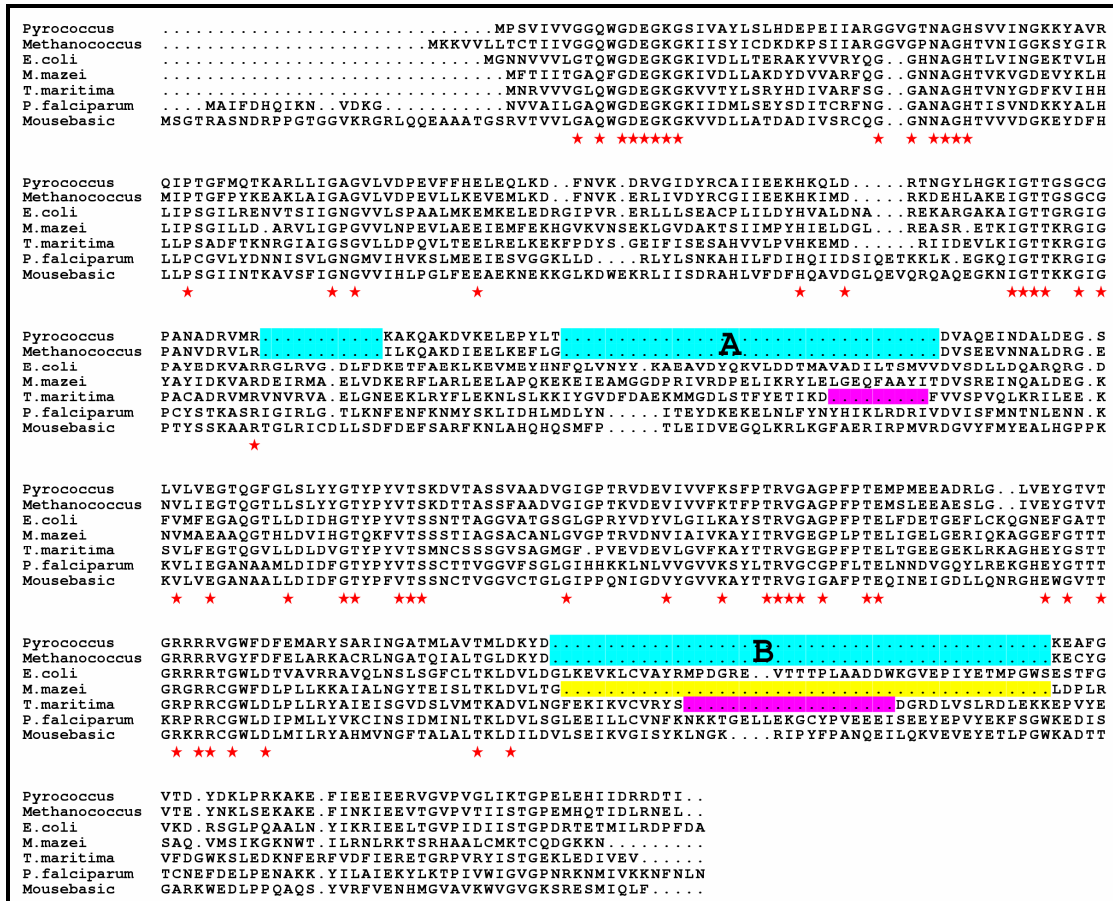


Figure 2.3: Alignment of amino acid sequences of adenylosuccinate synthetase. Boxed regions (A and B) highlight the deletions in *Pyrococcus* and *Methanococcus* AdSS sequences. Regions in pink show the deletions in *T. maritima* AdSS and the regions in yellow show deletions in *M. mazei* AdSS sequence. The alignment was generated using CLUSTAL W (Thompson *et al.*, 1994) and represented using ESPRIPT (Gouet *et al.*, 1999).

Though Clade 1 AdSS have been well studied in terms of structure and function, biochemical characterization of any short AdSS is lacking. This chapter describes the detailed biochemical characterization of *M. jannaschii* adenylosuccinate synthetase.

2.2 Materials and Methods

All media components were purchased from HiMedia Laboratories (Mumbai, India). Pfx polymerase was procured from Invitrogen (California, USA), restriction enzymes and T4 DNA ligase were from Bangalore Genei Pvt. Ltd., (Bangalore, India) and oligonucleotides from Microsynth AG (Balgach, Switzerland). Substrates and inhibitors used in kinetic studies and protein markers were from Sigma Chemical Company (St.Louis, MO). Hadacidin was a kind gift from the Developmental Therapeutics Program, National Cancer Institute, NIH, Bethesda, MD. *Methanocaldococcus jannaschii* genomic DNA was purchased from ATCC (Manassas, USA). Akta Basic HPLC, Sephadex G25, Q-sepharose, Sephacryl 200 and Superdex 200 were from Amersham Pharmacia (Uppsala, Sweden). All assays were done using Hitachi U2010 (Hitachi High-Technologies Corporation, Tokyo, Japan) spectrophotometer fitted with a water circulated cell holder. MALDI-MS spectra of the protein were recorded on Ultraflex II TOF/TOF mass spectrometer (Bruker Daltonics, Bremen, Germany).

2.2.1 MjAdSS cloning and purification

The open reading frame encoding MjAdSS was PCR amplified from *M. jannaschii* genomic DNA using forward

5' **TATCCATGGCTAGCAAAAAGGTGGTTTTATTGACTTGC** 3' and reverse

5'- **TGCGGATCCTTATAGCTCGAGTCTTAAATCAATTGTTTGGTG** 3' primers.

The sequences in bold indicate *Nco*I and *Bam* HI restriction sites that were used to clone the gene into pET23d expression vector (Novagen, Madison, USA). The protein was expressed in *E. coli* BL21(DE3) cells that were grown at 37°C for 10 hours. The cells were harvested by centrifugation, resuspended in lysis buffer (50 mM

Tris HCl, pH 7.4, 10% glycerol, 300 mM NaCl, 0.2 mM PMSF and 2 mM DTT) and lysed using French press. After separation of the debris, the supernatant was first treated with 0.01% polyethylenimine to remove nucleotides and then subjected to thermal precipitation at 70°C for 10 minutes. This was followed by 40% and then 75% ammonium sulphate precipitation. The protein pellet was dissolved in 20 mM Tris HCl, pH 6.9, 10% glycerol, 2 mM DTT and 0.1 mM PMSF and desalted on Sephadex G-25 column equilibrated with the same buffer. The desalted protein was put through Q-sepharose anion exchange chromatography. The protein was eluted using a linear gradient of NaCl with buffer A (20 mM Tris HCl, pH 6.9, 10% glycerol, 1 mM DTT and 0.1 mM PMSF) as solvent system and was found to elute between 250-280 mM NaCl. The fractions containing the protein were pooled, concentrated and further purified through Sephacryl 200 gel filtration chromatography using 20 mM Tris HCl, pH 7.4, 10% glycerol, 1 mM EDTA, 0.1 mM PMSF and 2 mM DTT as the buffer. The samples were analyzed by SDS-PAGE (Laemmli, 1970), pure fractions concentrated and stored at -20°C. The protein concentration was estimated by the method of Bradford using BSA as standard (Bradford, 1976). To obtain the mass spectrum of MjAdSS, the protein was extensively dialyzed against distilled water to remove all additives. 1 µl of protein sample at 4.2 mg ml⁻¹ concentration was mixed with 1 µl of sinapinic acid prior to spotting on target plate. Spectra were acquired in positive ion mode.

2.2.2 Size exclusion chromatography

Size exclusion chromatography was carried out on an analytical Superdex 200 (1 cm * 30 cm) column attached to Akta Basic HPLC using 20 mM Tris HCl, pH 7.4 as the solvent system. The runs were performed at 0.5 ml min⁻¹ and the protein elution was monitored simultaneously at 280 and 220 nm. The column was calibrated with β-amylase (200 kDa), alcohol dehydrogenase (150 kDa), bovine serum albumin (66 kDa), carbonic anhydrase (29 kDa) and cytochrome c (12.4 kDa). To monitor the effect of NaCl on the quaternary structure of MjAdSS, 18 µM protein was incubated with the appropriate concentration of salt for 30 minutes at room temperature and injected into column pre-equilibrated with same NaCl concentration in 20 mM Tris HCl, pH 7.4. To monitor the effect of ligand binding on the oligomeric status of

MjAdSS, 12 μ M protein was incubated with 2 mM magnesium acetate, 60 μ M IMP or 60 μ M GTP in different combinations for 30 minutes at room temperature and chromatographed with the appropriate ligand in the running buffer. All chromatographic runs were performed at 25°C.

2.2.3 Circular dichroism spectroscopy

Far-UV CD spectra of 5 μ M MjAdSS in 20 mM Tris HCl, pH 7.4 and different concentrations of NaCl were recorded on Jasco J-810 spectropolarimeter (JASCO, Corporation, Tokyo, Japan), after preincubation of the protein at room temperature for 30 minutes with the appropriate concentration of NaCl. Spectra of suitable blanks were subtracted from the protein spectra.

2.2.4 Dynamic light scattering

Dynamic light scattering measurements were performed on Nano Zetasizer (Malvern Instruments, Malvern, Worcestershire, UK) with a He-Ne laser, operating at 532 nm. The scattering signal for size analysis was measured at 90°. All measurements were carried out at 25°C in size measurement and protein mode. Each measurement was an average of 14 different scans between 0.5-10⁷ μ s. An exponential decay function was generated from the scattering data and the rate of decay of this function was used to calculate translational diffusion coefficient, D_{τ} . The radius of hydration, R_H , was then calculated using the relationship, $D_{\tau} = kT/6\pi\eta R_H$, where k is the Boltzmann constant, T is the temperature in Kelvin and η is the solvent viscosity. Refractive index of water and solvent viscosity were set to 1.33 and 0.8872, respectively. The molecular weight (M_r) of the proteins was estimated using M_r versus R_H calibration curve made using globular proteins of known molecular weights and size (Huffman *et al.*, 2001). Measurements were made at a protein concentration of 5 μ M in 20 mM Tris HCl, pH 7.4 with or without 100 mM NaCl .

2.2.5 Enzyme Assays

All assays were done at 70°C using water circulated cell holder fitted to Hitachi U2010 spectrophotometer. The temperature was maintained with Julabo F25 (JULABO Labortechnik GmbH, Seelbach, Germany) circulating water bath. The assays were performed in 30 mM MES, pH 6.5 (pH 6.0 at 70°C) and 15 mM magnesium acetate. 0.65-0.85 µg of enzyme was used in a volume of 300 µl and the reaction mix preincubated at 70°C for 30 seconds before initiation with GTP. The reaction rates were monitored as an increase in absorbance at 290 nm and ΔC of 3390 M⁻¹cm⁻¹ (Carey & Mandel, 1961; Kang & Fromm, 1995) was used to calculate the amount of product (sAMP) formed. For the determination of kinetic constants, IMP concentration was varied between 25 and 750 µM, GTP between 10 and 300 µM and aspartate between 0.25 and 10 mM, while their concentrations when fixed were, 500 µM, 250 µM and 10 mM, for IMP, GTP and aspartate, respectively. The data were analyzed by fits to Michaelis Menten equation (equation 1) using GraphPad Prism, version 4 (GraphPad Software, Inc., San Diego, CA).

$$v = V_{\max}[S] / K_m + [S] \quad \text{Equation 1}$$

where v and V_{\max} are the initial velocity and maximum velocity respectively, K_m is the Michaelis constant and S is substrate concentration.

2.2.6 pH dependence of MjAdSS kinetics

The effect of pH on enzyme activity was monitored at fixed substrate concentrations of 500 µM IMP, 250 µM GTP and 10 mM aspartate. Acetate was chosen as buffer for the pH range 4-5, MES for the pH range 5.5-6.5 and Tris HCl for the pH range 7.0-8.5. The data were fit to BELL equation (Tipton & Dixon, 1979) using GraphPad Prism, version 4.

$$\log(y) = \log(c / (1 + H/K_1 + K_2/H)) \quad \text{Equation 2}$$

where y is the pH dependent parameter, c is the pH independent value of the parameter, $[H]$ is the hydrogen ion concentration and K_1 and K_2 are the ionization constants for the two ionizable groups involved in catalysis.

2.2.7 Initial velocity measurement and inhibition studies

For the determination of initial velocity patterns, concentration of one substrate was varied keeping the concentration of the other two substrates in a fixed ratio at different levels in the range of their Michaelis constant. Initial rates were also measured by varying the concentration of one substrate at different fixed concentrations of the second substrate with the third substrate held at saturating concentration.

Inhibition patterns with the products sAMP, GDP and the aspartate analog, hadacidin, were determined by measuring the initial rate at variable concentrations of one substrate, fixed subsaturating concentrations of the other two substrates and at different fixed concentrations of the inhibitor. Inhibition studies with the nucleotides, AMP and GMP were also done in a similar manner. Phosphate (P_i) and fructose 1,6 bisphosphate (F16BP) inhibition studies were carried out by the method of Dixon (Dixon, 1953), where the inhibitor concentration was varied at different fixed concentrations of one substrate with the other two substrates maintained at twice their K_m values. Substrate (IMP) inhibition was examined by measuring the initial rates at different fixed concentrations of GTP, with aspartate concentration being held constant at 10 mM. The assay conditions were as described in Section 2.2.5 and the reactions were carried out at 70°C. Concentrations of substrates and inhibitors used in specific assays are indicated in the figures or figure legends.

2.2.8 Data analysis

All initial rate data were first analyzed by double reciprocal plots of velocity versus substrate concentration and associated secondary plots. Initial rate data of inhibition by P_i and F16BP were analyzed by $1/v$ versus $[I]$ plots. The data were then fitted by non-linear regression to standard kinetic models using GraphPad Prism, version 4. The best fit models were selected on the basis of goodness-of-fit (extra

sum-of-squares F test) and P values. The kinetic parameters obtained by non-linear regression analysis were in agreement with the values obtained by Lineweaver-Burk plots and related secondary plots.

2.3 Results

2.3.1 Protein expression, purification and preliminary characterization

M. jannaschii is an anaerobic thermophilic archaea. BLAST search of *M. jannaschii* genome using *E. coli* AdSS sequence as the query retrieved a protein sequence of 345 amino acids annotated as putative AdSS. For the purpose of generating recombinant *M. jannaschii* AdSS (MjAdSS), the gene was amplified from *M. jannaschii* genomic DNA, cloned into pET23d expression vector and confirmed by DNA sequencing. The protein was expressed in BL21(DE3) strain of *E. coli* cells, which were grown at 37°C and since the level of leaky expression was high induction with IPTG was omitted. Purification of the heat (70°C) treated soluble fraction of the cell lysate using Q-sepharose anion exchange chromatography followed by gel filtration yielded protein of >95% purity (Figure 2.4a) as judged by SDS-PAGE. MALDI mass spectrometric analysis of the recombinant protein yielded a subunit molecular mass of 37855 ± 20 Da (Figure 2.4b). The predicted molecular weight based on its amino acid sequence is 38060 Da. Thus, the experimentally obtained mass corresponds to protein devoid of first two amino acids, methionine and alanine. Similar mass was obtained with different batches of purified enzyme.

The protein was stable at -20°C without any drop in activity for at least six months. Preliminary activity measurements under varied reaction conditions enabled the optimization of enzyme assay methodology. The protein showed a continuous increase in activity till 80°C (Figure 2.5a). All kinetic studies reported in this paper are from activity measurements done at 70°C in 30 mM MES, pH 6.5 and 15 mM magnesium acetate. Phosphate was found to be an inhibitor of enzyme activity and hence, its use during protein purification and in assay solutions was avoided. pH dependence of enzyme activity (Figure 2.4c) when fitted to the BELL equation

(equation 2) yielded pK_1 and pK_2 values of 4.92 and 7.33, respectively. In all AdSS a conserved histidine and aspartic acid have been implicated to function as catalytic acid and base, respectively (Poland *et al.*, 1996a; Kang *et al.*, 1997; Choe *et al.*, 1999). These residues in MjAdSS correspond to His51 and Asp21.

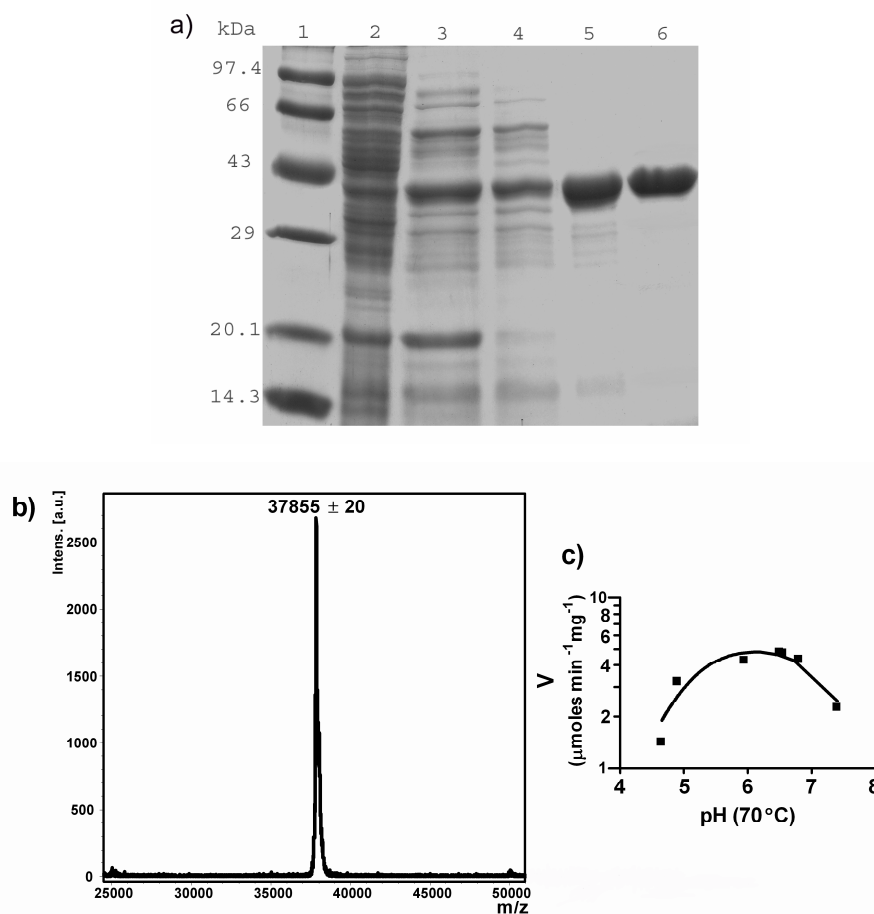


Figure 2.4: Purification and preliminary characterization of MjAdSS. a) Electrophoretic analysis of purification of recombinant MjAdSS. Lane 1, marker; lane 2, crude lysate; lane 3, supernatant after thermal precipitation; lane 4, precipitate from 70% ammonium sulfate fraction; lane 5, Q-sepharose purification; Lane 6, Sephacryl 200 fraction. b) MALDI-MS spectra of purified recombinant MjAdSS. c) pH profile of MjAdSS activity. pH values of buffers used were taken at 70°C.

Like all other AdSS, the *M. jannaschii* enzyme requires Mg^{2+} for catalysis with maximum activity obtained at 15 mM magnesium acetate (Figure 2.5b). The Mg^{2+} dependence of MjAdSS activity exhibits a Hill coefficient of 1 indicating the presence of only one Mg^{2+} binding site in each subunit, a feature similar to mouse

acidic and basic isozyme (Borza *et al.*, 2003). The crystal structures of liganded AdSS also contain one Mg^{2+} bound to α and β -phosphoryls of GDP (Eaazhisai *et al.*, 2004; Poland *et al.*, 1996a; Choe *et al.*, 1999; Poland *et al.*, 1996b; Iancu *et al.*, 2002). However, kinetic analysis on the Mg^{2+} dependence of *E. coli* AdSS activity showed the involvement of two Mg^{2+} ions for each subunit. The second metal ion has been proposed to interact with the substrate aspartate in the enzyme active site (Kang & Fromm, 1995).

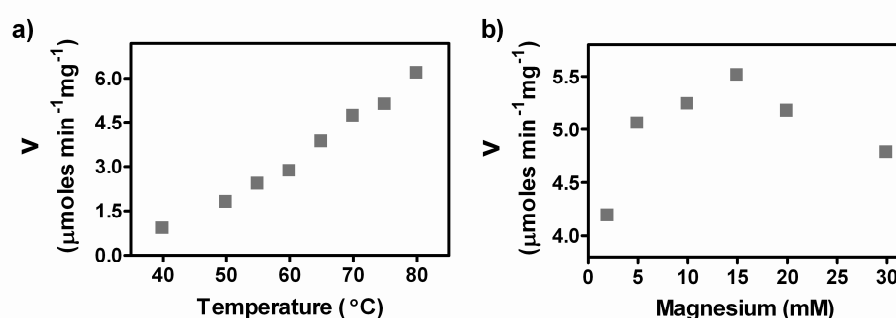


Figure 2.5: Effect of a) temperature and b) magnesium ion concentration on MjAdSS activity

Table 2.1: Comparison of kinetic parameters of MjAdSS with *P. falciparum*, *E. coli* and Mouse AdSS.

Enzyme	k_{cat} (s^{-1})	K_m (μM)		
		IMP	GTP	Aspartate
<i>M. jannaschii</i> ^a	4.2 ± 0.1	75.5 ± 4.6	42.6 ± 2.8	1079 ± 74
<i>P. falciparum</i> ^b	1.1 ± 0.03	23 ± 4	18.4 ± 2.0	1800 ± 50
<i>E. coli</i> ^c	1.0 ± 0.05	30 ± 0	26.2 ± 2.3	230 ± 40
Mouse (basic) ^d	5.4 ± 0.4	45 ± 7	12 ± 2	140 ± 20
Mouse (acidic) ^e	4.2 ± 0.4	12 ± 2	15 ± 2	950 ± 50

^a Values taken from present study. ^b values taken from Raman *et al.*, 2004; ^c values taken from Wang *et al.*, 1997a; ^{d,e} values taken from Borza *et al.*, 2003.

K_m and k_{cat} values for MjAdSS obtained from initial rate data at saturating concentration of two substrates with the third as variable and fit to Michaelis Menten

equation (equation 1) are summarized in Table 2.1. The K_m values for IMP and GTP are in the μM range, while that for aspartate is 1 mM. The k_{cat} value for MjAdSS at 70°C is 4.2 sec^{-1} which reduces to about 0.45 sec^{-1} at 25°C.

2.3.2 Quaternary structure of MjAdSS

The predicted subunit molecular mass of MjAdSS is 38 kDa. On a precalibrated Superdex 200 column, the protein eluted as a single peak at a volume of 13.0 ml which corresponds to a mass of 112 kDa (Figure 2.6a). Repeated runs on calibrated Superdex 200 columns were highly reproducible with only minor variation in molecular mass ranging from 104 to 115 kDa. Variation in protein concentration from 10 to 0.96 μM did not lead to any change in elution profile. However, on addition of 50 and 100 mM NaCl, the protein peak shifted to higher elution volumes of 14.0 ml and 14.2 ml, corresponding to a mass of 79 kDa and 70 kDa, respectively. Further increase in NaCl concentration upto 1.2 M did not lead to a significant change in retention volume (Figure 2.6a). The effect of salt on protein secondary structure monitored by circular dichroism spectroscopy, showed no change in spectral pattern but for a minor increase in molar ellipticity at 220 nm (Figure 2.6b). MjAdSS contains two tryptophans per monomer. Examination of fluorescence spectra of MjAdSS, upon excitation at 290 nm, showed neither a shift in emission maximum nor a change in fluorescence intensity in the presence and absence of NaCl. This indicates the absence of gross secondary and tertiary structural changes in the protein upon addition of NaCl. The gel filtration profiles thus indicate that in the absence of NaCl, MjAdSS is an equilibrium mixture of dimers and tetramers. Presence of NaCl breaks the tetramer to dimers without further dissociation on increase in salt concentration.

The tetrameric nature of MjAdSS was further validated by dynamic light scattering (DLS) measurements. On a standard curve made using standard globular proteins in the mass range 12.5 to 200 kDa, the radius of MjAdSS in 20 mM Tris HCl, pH 7.4 corresponds to a molecular mass of 160 ± 5 kDa. On addition of 100 mM NaCl, the radius drops to half and corresponds to a protein having a molecular mass of 79 ± 3 kDa. The measurements were done in duplicates on three independently

purified batches of protein and each measurement was an average of 14 different scans. Hence, like size exclusion chromatography, DLS measurements also showed that MjAdSS exists as a tetramer which dissociates to dimers in the presence of salt.

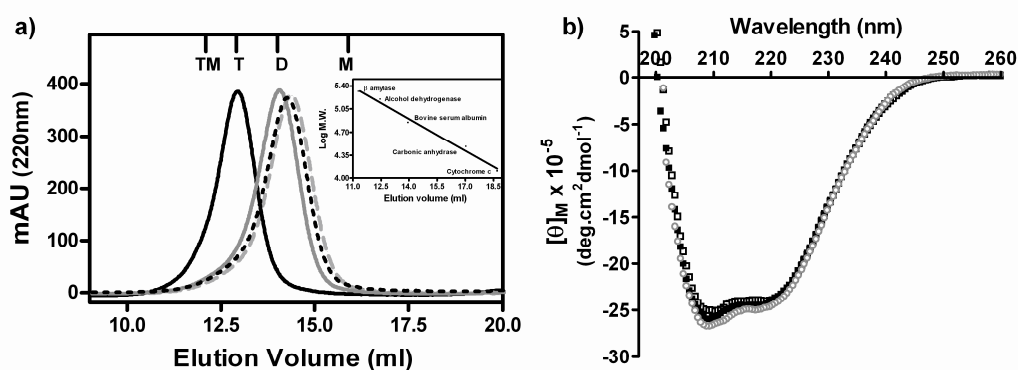


Figure 2.6: Effect of NaCl on the quaternary and secondary structure of MjAdSS. a) Elution profile of MjAdSS on an analytical Superdex 200 column in the presence of different NaCl concentrations; —, 0 mM NaCl; — —, 50 mM NaCl; ·····, 100 mM NaCl, and - · - ·, 1.2 M NaCl. Inset shows the calibration curve of log MW of standard proteins versus elution volume. M, monomer; D, dimer; T, trimer; TM, tetramer, indicated on top of the panels correspond to calculated elution volumes for the monomer, dimer, trimer and tetramer of MjAdSS. b) Far-UV CD spectra of MjAdSS in 20 mM Tris HCl, pH 7.4 and 0 mM NaCl (□), 300 mM NaCl (■) and 1.2 M NaCl (○).

This is the first report of a homotetramer of AdSS. Essentiality of the homotetramer for enzyme activity was monitored by measuring activity in the presence of increasing salt concentration. The enzyme lost 30% activity at low NaCl concentration of 100 mM while at 300 mM only 25% of activity was retained (Figure 2.7b). Studies on mouse AdSS have shown that chloride ions inhibit enzyme activity (Borza *et al.*, 2003), a feature not seen with MjAdSS as substitution of magnesium acetate with $MgCl_2$ in the assay mixture did not result in any change in enzyme activity. Gel filtration chromatography in the presence of ligands also supported the essentiality of an association state higher than a dimer for activity. Inclusion of 2 mM magnesium acetate shifted the protein peak to a larger elution volume when compared to that of the unliganded protein. However, on addition of IMP and GTP in the presence of magnesium, the protein eluted at a lower retention volume and hence, a higher oligomeric form, indicating that substrates mediate association of MjAdSS

dimers to form a tetramer (Figure 2.7a). This substrate driven shift to tetramer indicates that the catalytically active form of the enzyme at 70°C could also be expected to be the higher oligomeric state, as the dimer-tetramer equilibrium would exist even at high temperature.

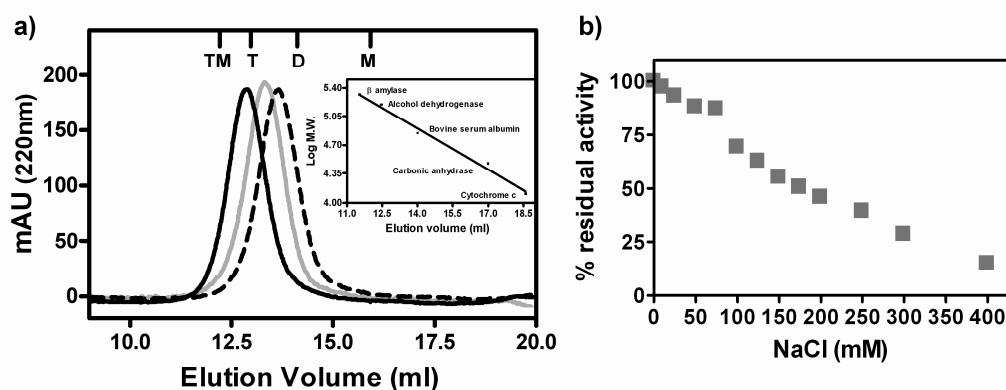


Figure 2.7: a) Effect of substrates on the quaternary structure of MjAdSS. Elution profile of MjAdSS on an analytical Superdex 200 column with and without substrates. —, protein alone; ----, protein with 2 mM magnesium acetate and —, protein with magnesium acetate, IMP and GTP. Inset shows the calibration curve of log MW of standard proteins versus elution volume. M, monomer; D, dimer; T, trimer; TM, tetramer, indicated on top of the panels correspond to calculated elution volumes for the monomer, dimer, trimer and tetramer of MjAdSS. b) Effect of NaCl on MjAdSS activity. Activity in the absence of NaCl was taken as 100 %.

2.3.3 Kinetic mechanism of MjAdSS

A) Initial velocity studies and kinetic parameters

The kinetic mechanism of *E. coli*, mouse and *P. falciparum* AdSS that belong to the subfamily of long AdSS is well characterized (Rudolph and Fromm, 1969; Cooper *et al.*, 1986; Raman *et al.*, 2004). However, the short AdSS from thermophilic organisms have not been studied. Enzyme kinetic mechanisms can be modeled on rapid equilibrium or steady-state assumptions. Steady-state models invoke rate constants for the equilibrium between species in the kinetic scheme and these are well derived for uni and bireactant systems (Leskovac, 2003). However, in trisubstrate

reactions steady-state models lead to initial velocity equations with large number of parameters that cannot be easily determined from kinetic studies. Rapid equilibrium assumptions reduce the number of constants in the rate equation (Leskovac, 2003).

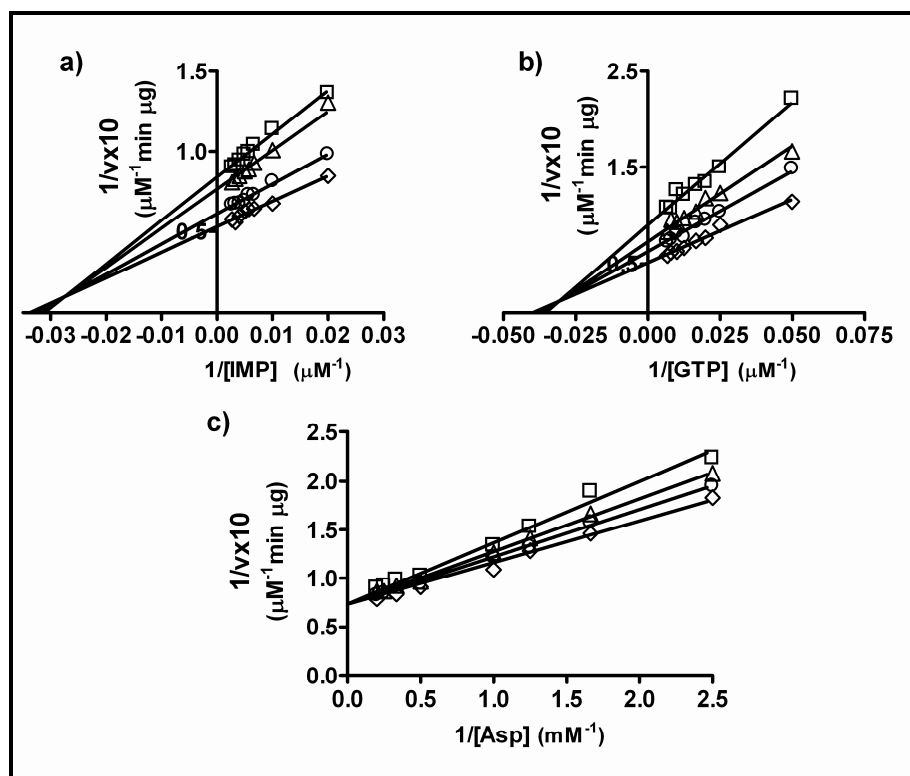


Figure 2.8: Plots of reciprocal of initial velocity (v) with respect to reciprocal of substrate concentration. a-c represent plots from initial velocity measurements where two substrates were varied in a fixed ratio. a) IMP concentration was varied from 50-375 μM and the respective concentrations of aspartate and GTP were, 1.2 mM and 65 μM (\square); 1.65 mM and 90 μM (Δ); 2.4 mM and 133 μM (\circ) and 4.0 mM and 220 μM (\diamond). b) GTP concentration was varied from 20 to 150 μM . The respective concentrations of aspartate and IMP were, 1.2 mM and 100 μM (\square); 1.65 mM and 137.5 μM (Δ); 2.4 mM and 200 μM (\circ) and 4.0 mM and 335 μM (\diamond). c) Aspartate concentration was varied from 0.45 mM to 5 mM. The respective concentrations of IMP and GTP were, 80 and 40 μM (\square); 120 and 60 μM (Δ); 170 and 85 μM (\circ) and 320 and 160 μM .

To deduce the kinetic mechanism of MjAdSS, initial velocity measurements were made following the method developed by Fromm (Rudolph & Fromm, 1969; Rudolph & Fromm, 1979). IMP, GTP and aspartate were varied in separate experiments, where the concentration of the other two substrates was varied simultaneously in a fixed ratio around their respective K_m values. The results are

summarized in Figure 2.8 (a-c). The absence of parallel pattern in the plots indicates that no product is released before the binding of all three substrates, thereby ruling out a ping-pong mechanism. Convergence of lines in each of the plots in Figure 2.8 and 2.9 is indicative of a sequential mechanism. The lines in double reciprocal plots of initial velocity versus IMP or GTP concentration converged in the second quadrant whereas lines in plots of $1/v$ versus $1/[Asp]$ intersected on the y-axis (Figure 2.8). Similar intersection pattern with variable aspartate was obtained in two independent experiments using enzyme from two different batches of purification. The crossover point of $1/v$ versus $1/[Asp]$ plots continued to be on the y-axis when either IMP or GTP were held at constant saturating concentration (Figure 2.9c). This intersection pattern obtained with aspartate as the variable substrate rules out a number of kinetic models viz. a rapid equilibrium completely random mechanism, steady-state completely ordered mechanism, a completely ordered mechanism where E-EA or EA-EAB forms are in rapid equilibrium, a random AB mechanism where E-EA and E-EB forms are in rapid equilibrium, a rapid equilibrium random BC or random AC mechanism and a random BC model where EA-EAC and EA-EAB (\pm EABC) forms are in rapid equilibrium from consideration, as these models would require a family of lines intersecting to the left of $1/v$ axis with all three variable substrates. Therefore, these results are indicative of either (i) completely ordered mechanism where all enzyme forms or E-EA-EAB are in rapid equilibrium or (ii) random AB ordered C kinetic mechanism where all enzyme forms or E, EA, EB and EAB are in rapid equilibrium and EABC is in steady-state (Segel, 1975). Here, A, B and C indicate IMP, GTP and aspartate, respectively. The equations for rapid equilibrium completely ordered (equation 3) and rapid equilibrium random AB ordered C (equation 4) terreactant systems are given below. The equation for partial rapid equilibrium reaction where E, EA, EB and EAB are in rapid equilibrium and $EAB + C \rightarrow EABC$ and its interconversion in steady-state, has the same form as that for the full rapid equilibrium random AB ordered C system (equation 4) (Segel, 1975)

$$v/V_{\max} = [A][B][C] / (K_A K_B K_C + K_B K_C [A] + K_C [A][B] + [A][B][C]) \quad \text{Equation 3}$$

$$v/V_{\max} = [A][B][C] / (\alpha K_A K_B K_C + \alpha K_B K_C [A] + \alpha K_A K_C [B] + K_C [A][B] + [A][B][C])$$

Equation 4

In the above equations, A, B and C are as described earlier, v is the initial velocity, V_{\max} is the maximum velocity. K_A , K_B and K_C in equation 3 are the Michaelis constants for A, B and C, respectively. In equation 4, K_A and K_B denote the dissociation constants for substrates A and B, respectively, whereas, αK_A , αK_B and K_C are Michaelis constants for the three substrates.

To further distinguish between the above two models the initial velocity measurements were made using the method proposed by Frieden where one substrate was held constant and the other two were varied (Frieden, 1959) (Figure 2.9 a-d). A family of lines intersecting in the third quadrant was obtained when aspartate was held saturating and GTP was varied at different fixed concentrations of IMP (Figure 2.9d). This pattern is clearly indicative of a random AB ordered C mechanism. For a completely ordered mechanism, the lines would intersect on the y-axis (Segel, 1975). When IMP or GTP was held saturating with aspartate as the fixed variable, the family of lines again converged close to the horizontal axis, in the second and third quadrant, respectively (Figure 2.9a,b). Under these conditions the system can be treated as a bireactant system. The data were fit to equations 5 and 6 which denote a rapid equilibrium ordered and steady-state ordered bisubstrate reaction, respectively.

$$v/V_{\max} = [A][C] / (K_A K_C + K_C [A] + [A][C]) \quad \text{for variable A, at saturating B}$$

$$v/V_{\max} = [B][C] / (K_B K_C + K_C [B] + [B][C]) \quad \text{for variable B, at saturating A}$$

Equation 5

$$v/V_{\max} = [A][C] / (K_A K_C + K_C [A] + \alpha K_A [C] + [A][C]) \quad \text{for variable A, at saturating B}$$

$$v/V_{\max} = [B][C] / (K_B K_C + K_C [B] + \alpha K_B [C] + [B][C]) \quad \text{for variable B, at saturating A}$$

Equation 6

The constants K_A , K_B , K_C , αK_A and αK_B in equations 5 and 6 are as defined earlier. The fit to equation 5 yielded inferior results and negative values for at least

one constant. The data fitted well to equation 6, the results of which are summarized in Table 2.2.

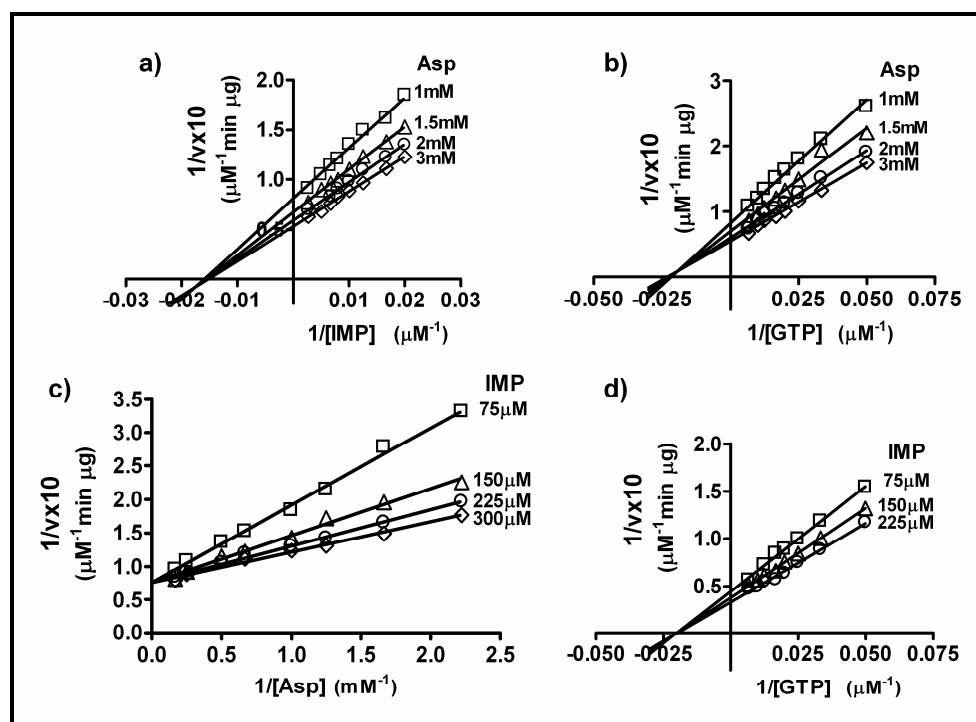


Figure 2.9: Plots of reciprocal of initial velocity (v) with respect to reciprocal of substrate concentration. a-d are plots from initial velocity measurements where one substrate was held at saturating concentration. a) IMP concentration was varied from 50-375 μM and GTP was held constant at 250 μM . The fixed concentration of aspartate is indicated against each line. b) GTP concentration was varied from 20-150 μM and IMP was held constant at 500 μM . The fixed concentration of aspartate is indicated against each line. c) Aspartate was varied from 0.45 mM to 6.0 mM and GTP was held constant at 250 μM . The fixed concentration of IMP is indicated against each line. d) GTP was varied from 20-150 μM and aspartate was fixed at 10 mM. The fixed concentration of IMP is indicated against each line.

The k_{cat} values obtained from fits agree well with those reported in Table 2.1. The K_C value is close to the K_m for aspartate and, the αK_A and αK_B values for IMP and GTP agree with their K_m values in Table 2.1. α value close to 1 indicates that IMP and GTP bind independently to the enzyme. Steady-state ordered binding of aspartate is also supported by the intersection of lines in the second and third quadrant in plots of $1/v$ versus $1/[\text{GTP}]$ and $1/[\text{IMP}]$, respectively at different fixed concentrations of aspartate and saturating concentration of the third substrate (Figure 2.9a,b). Taken

together the initial velocity data indicate that IMP and GTP bind randomly to the enzyme and binding of aspartate to E.IMP.GTP complex is steady-state ordered. Thus, MjAdSS exhibits rapid equilibrium random AB steady-state ordered C kinetic mechanism.

Table2.2: Rapid equilibrium Random AB Steady-state Ordered C kinetic model for MjAdSS.

Equilibrium	Constant	Value from fits
	V_{\max}	$26.0 \pm 2.0 \mu\text{M min}^{-1} \mu\text{g}^{-1}$ $26.0 \pm 0.9 \mu\text{M min}^{-1} \mu\text{g}^{-1}$ Mean = $26.0 \mu\text{M min}^{-1} \mu\text{g}^{-1}$
	$k_{\text{cat}}^{\#}$	5.0 sec^{-1}
EA = E + A	K_A	$64.4 \pm 12.3 \mu\text{M}$
EB = E + B	K_B	$58.03 \pm 17.4 \mu\text{M}$
EAB = EB + A	αK_A	$70.2 \pm 7.1 \mu\text{M}$
EAB = EA + B	αK_B	$44.9 \pm 8.6 \mu\text{M}$
EABC = EAB + C	K_C	$1.0 \pm 0.2 \text{ mM}$ $1.0 \pm 0.1 \text{ mM}$ Mean = 1.0 mM
	$\alpha = \alpha K_A / K_A$	1.1
	$\alpha = \alpha K_B / K_B$	0.8 Mean = 0.95

The symbol E represents MjAdSS; A, B and C represent IMP, GTP and aspartate, respectively. The kinetic constants are defined explicitly with reference to Scheme1.

$$^{\#} k_{\text{cat}} = V_{\max} / [E]_T$$

B) Product inhibition studies

Products and substrate analogs when used as inhibitors in initial velocity measurements serve to confirm the order of substrate binding in multisubstrate reactions. (Fromm, 1967; Rudolph, 1979). In a rapid equilibrium random AB steady-state ordered C kinetic mechanism, a competitive inhibitor of A or B would show

noncompetitive inhibition with the other two substrates and a competitive inhibitor of C would be an uncompetitive inhibitor of A and B (Segel, 1975). The products of the reaction catalyzed by AdSS are sAMP, GDP and P_i. P_i, not being a specific mimic of any of the three substrates does not serve to confirm the order of substrate binding. Hadacidin (N-formyl N-hydroxyglycine), a secondary metabolite from *Penicillium frequentans* (Kaczka *et al.*, 1962) is a potent inhibitor of AdSS competing for the aspartate binding pocket (Shigeura & Gordon, 1962a; Shigeura & Gordon, 1962b; Clark & Rudolph, 1976; Markham & Reed, 1977; Matsuda *et al.*, 1980; Jayalakshmi *et al.*, 2002). Hence, inhibition patterns with the products sAMP, GDP and the aspartate mimic, hadacidin were examined for MjAdSS. The double reciprocal plots of the initial velocity in the presence of the inhibitors are summarized in Figure 2.10. The data were analyzed by fits to the kinetic models for competitive, non competitive and uncompetitive inhibition (equations 7-9).

$$v = V_{\max} [S] / \{K_m (1+I/K_i) + [S]\} \quad \text{competitive inhibition} \quad \text{Equation 7}$$

$$v = V_{\max} [S] / \{K_m (1+I/K_i) + [S] (1+I/K_i)\} \quad \text{noncompetitive inhibition} \quad \text{Equation 8}$$

$$v = V_{\max} [S] / \{K_m + [S] (1+I/K_i)\} \quad \text{uncompetitive inhibition} \quad \text{Equation 9}$$

where v and V_{\max} are initial and maximum velocities, respectively, I is inhibitor concentration, S is the variable substrate concentration, K_i is the inhibition constant and K_m is the Michaelis constant for the variable substrate. The best fits were selected on the basis of F test and P values. Table 2.3 lists the K_i values and the inhibition pattern obtained from non-linear regression fit of the data to appropriate models.

sAMP, a competitive inhibitor of IMP was a noncompetitive inhibitor of GTP and aspartate (Figure 2.10, Ia-c). GDP which was a competitive inhibitor of GTP showed noncompetitive inhibition with IMP and aspartate (Figure 2.10, IIa-c). This pattern of inhibition supports random binding of IMP and GTP to the enzyme. However, hadacidin which was a competitive inhibitor of aspartate showed uncompetitive inhibition with IMP and GTP (Figure 2.10, IIIa-c). The family of parallel lines indicate that both V_{\max} and K_m are modulated with IMP and GTP as the variable substrates.

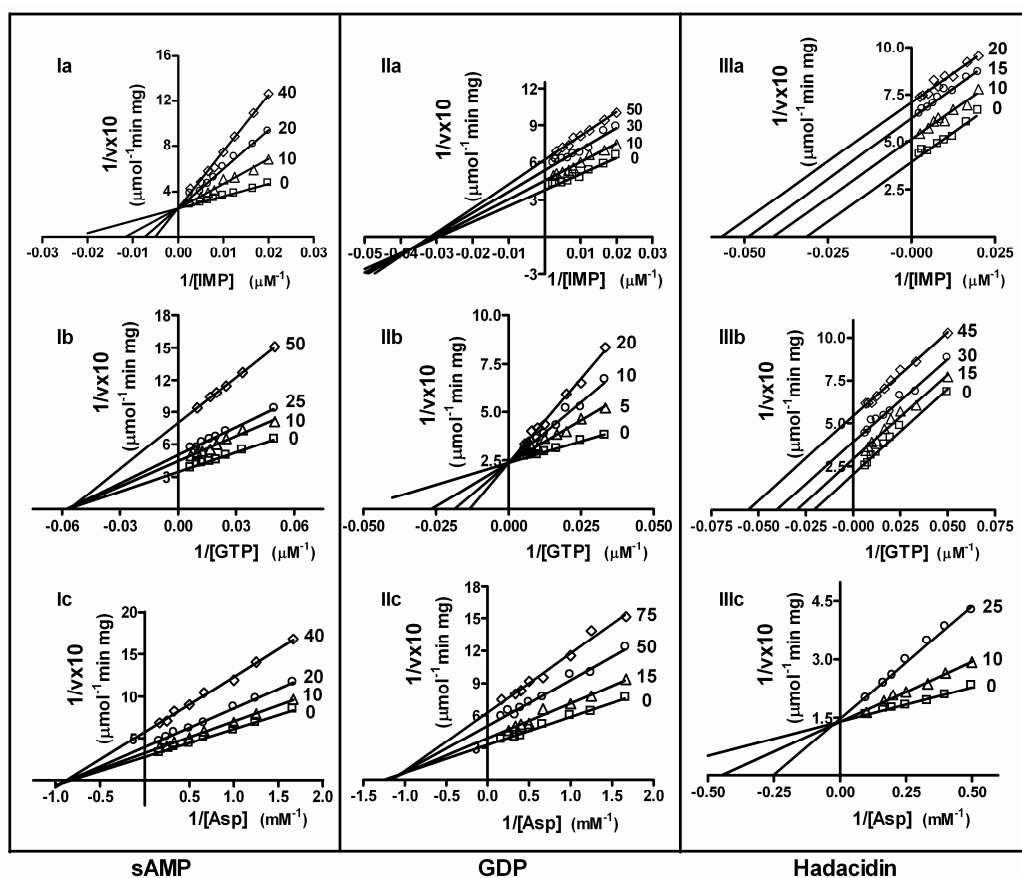


Figure 2.10: Lineweaver-Burk plots for inhibition of MjAdSS by products and substrate analogs; I) adenylosuccinate (sAMP), II) GDP, and III) Hadacidin. The micromolar concentrations of inhibitors are indicated against each line. Ia) GTP and aspartate were held constant at 80 μM and 4.5 mM respectively, and IMP was varied from 50 to 375 μM ; Ib) Aspartate and IMP were held constant at 4.5 mM and 100 μM respectively, and GTP was varied from 20 to 150 μM ; Ic) IMP and GTP were held constant at 150 μM and 80 μM respectively, and aspartate was varied from 0.6 mM to 6 mM. IIa) Aspartate and GTP were held constant at 1.5 mM and 60 μM respectively, and IMP was varied from 50 μM to 400 μM ; IIb) Aspartate and IMP were held constant at 5.4 mM and 100 μM respectively, and GTP was varied from 20 μM to 175 μM ; IIc) IMP and GTP were held constant at 100 μM and 80 μM respectively, and aspartate was varied from 0.6 mM to 6.0 mM. IIIa) Aspartate and GTP were held constant at 1.5 mM and 60 μM respectively, and IMP was varied from 50 μM to 400 μM ; IIIb) Aspartate and IMP were held constant at 3.6 mM and 375 μM respectively, and GTP was varied from 20 μM to 150 μM ; IIIc) IMP and GTP were held constant at 500 μM and 250 μM respectively, and aspartate was varied from 2 mM to 10 mM.

Similar results were obtained when the two fixed substrates (either IMP and aspartate or GTP and aspartate) were held at saturating concentrations with respect to their K_m values. This shows that hadacidin and hence, aspartate binding is conditional to the

catalytic pocket being occupied by both IMP and GTP. This further supports the random AB ordered C substrate binding seen from initial velocity measurements.

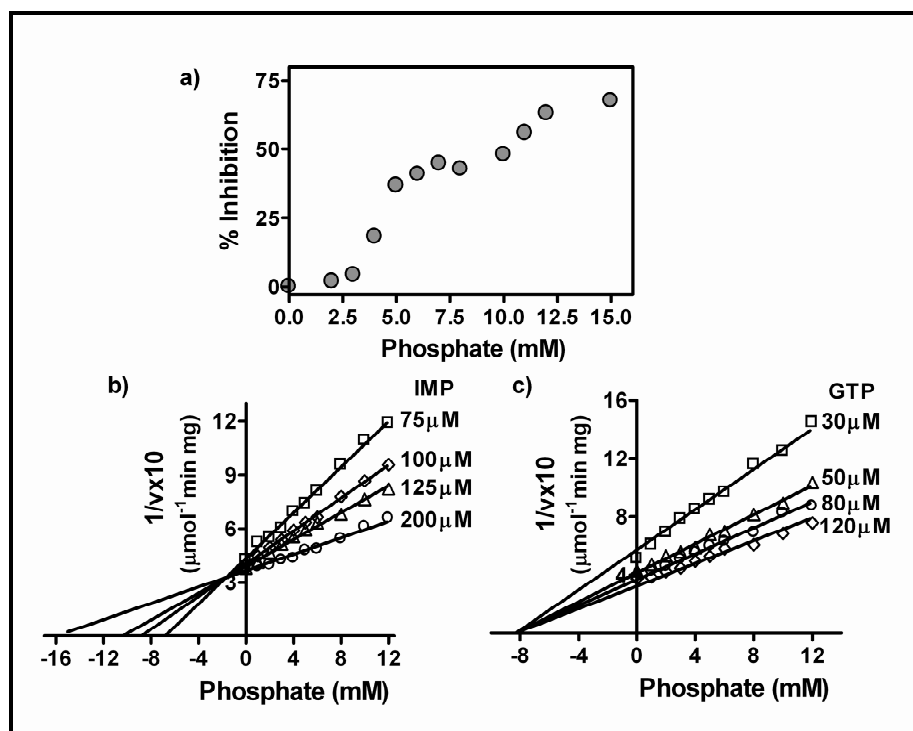


Figure 2.11: a) Effect of increasing P_i concentration on MjAdSS activity. Activity in the absence of P_i was taken as 0% inhibition. b,c) Dixon analysis of the inhibition of MjAdSS by P_i . b) Aspartate and GTP were held constant at 2 mM and 80 μ M, respectively. The fixed concentration of IMP is indicated against each plot. c) Aspartate and IMP were held constant at 2 mM and 150 μ M, respectively. The fixed concentration of GTP is indicated against each plot.

P_i , a product of AdSS catalyzed reaction, was found to be an inhibitor of MjAdSS with the concentration dependence of P_i on enzyme activity showing a biphasic trend (Figure 2.11a). Intersection patterns on Dixon plots were characteristic of competitive inhibition with IMP and noncompetitive inhibition with respect to GTP (Figure 2.11 b,c). To determine the K_i values, the data were fit to equations 10 and 11.

$$1/v = \{K_m / (V_{\max} [S] K_i)\} [I] + \{1/V_{\max} (1 + K_m/[S])\} \quad \text{for competitive inhibition}$$

Equation 10

$$1/v = \{(1+K_m/[S]) / V_{\max} K_i\} [I] + \{1/V_{\max} (1 + K_m/[S])\} \text{ for noncompetitive inhibition}$$

Equation 11

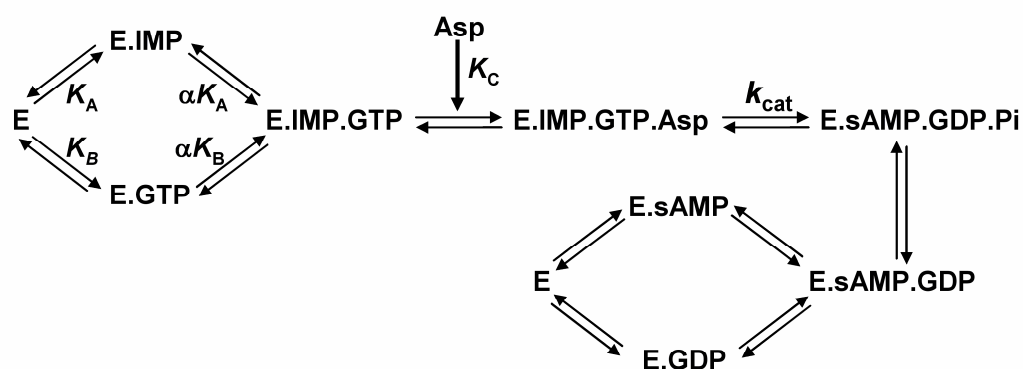
The apparent K_i values for IMP and GTP were determined to be 1.9 ± 0.2 mM and 8.3 ± 0.4 mM, respectively. Among the K_i values for the products, that for P_i is the highest followed by GDP and sAMP having similar but significantly lower values (Table 2.3). This indicates that P_i is liberated first from the enzyme followed by sAMP and GDP adopting a random order of release from MjAdSS. The overall kinetic mechanism as deduced from initial velocity and product inhibition studies for MjAdSS, is shown in Scheme 1.

Table 2.3: Summary of MjAdSS inhibition kinetics using products and substrate analogs.

Inhibitor	Substrate		
	IMP	GTP	Aspartate
sAMP^a	Competitive $K_{iapp} = 9.4 \pm 0.9$	Noncompetitive $K_{iapp} = 42.9 \pm 2.4$	Noncompetitive $K_{iapp} = 42.6 \pm 2.1$
GDP^a	Noncompetitive $K_{iapp} = 82.2 \pm 3.9$	Competitive $K_{iapp} = 7.0 \pm 0.8$	Noncompetitive $K_{iapp} = 82.1 \pm 4.2$
Hadacidin^a	Uncompetitive $K_{iapp} = 26.4 \pm 1.2$	Uncompetitive $K_{iapp} = 26.9 \pm 1.4$	Competitive $K_{iapp} = 10.5 \pm 1.0$
Phosphate^b	Competitive $K_{iapp} = 1.9 \pm 0.2$	Noncompetitive $K_{iapp} = 8.3 \pm 0.4$	ND

K_{iapp} is the apparent inhibition constant; ^a K_{iapp} values in μM ; ^b K_{iapp} values in mM; ND- not determined.

Scheme1. Proposed Kinetic Mechanism for *M. jannaschii* Adenylosuccinate Synthetase catalyzed reaction^a.



^aThe enzyme follows Rapid Equilibrium Random AB Steady-State Ordered C kinetic mechanism, where A, B and C represent IMP, GTP and aspartate, respectively.

2.3.4 Modulation of MjAdSS activity by metabolites

AdSS is a branch point enzyme with its substrate IMP also being utilized by inosine monophosphate dehydrogenase, the enzyme that catalyzes the first step in the biosynthesis of GMP. Hence, regulation of AdSS activity by various metabolites becomes an important feature in the context of cellular biochemistry. Metabolites that are known to modulate AdSS activity are GDP, sAMP, GMP, AMP, IMP and F16BP (Stayton *et al.*, 1983). Tables 2.3 and 2.4 provide a summary of the K_i values of these inhibitors for MjAdSS.

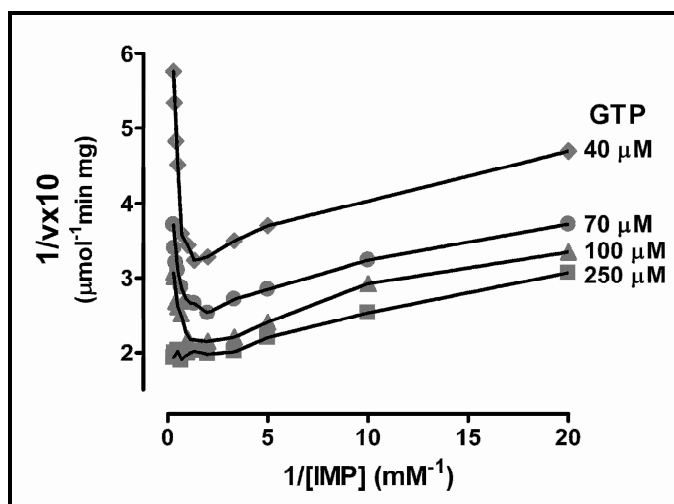


Figure 2.12: Inhibition of MjAdSS by IMP. Double reciprocal plot of initial velocity and IMP concentration at different fixed concentrations of GTP. Aspartate concentration was held constant at 10 mM.

High concentrations of IMP (>1 mM) at subsaturating concentrations of GTP inhibited MjAdSS, and this inhibition was relieved at high GTP concentration. The $1/v$ versus $1/[IMP]$ curves at different fixed concentrations of GTP showed parabolic behaviour characteristic for substrate inhibition where $AdSS.(IMP)_2$ dead end complex is formed (Figure 2.12). Secondary plot of $slope_{1/GTP}$ versus $1/[IMP]$ was also parabolic reinforcing $AdSS.(IMP)_2$ dead end complex formation (Cleland, 1979; Leskovic, 2003). Inhibition of MjAdSS by AMP like sAMP, was competitive with respect to IMP and noncompetitive with GTP and aspartate (Figure 2.13, Ia-c). However, unlike sAMP, AMP was a weak inhibitor with a K_i value of 58.2 μM (Table 2.4). Like GDP, GMP inhibition was competitive with respect to GTP and noncompetitive with IMP and aspartate (Figure 2.13, IIa-c). The inhibition patterns seen with AMP and GMP also support the random binding of the substrates IMP and GTP to MjAdSS.

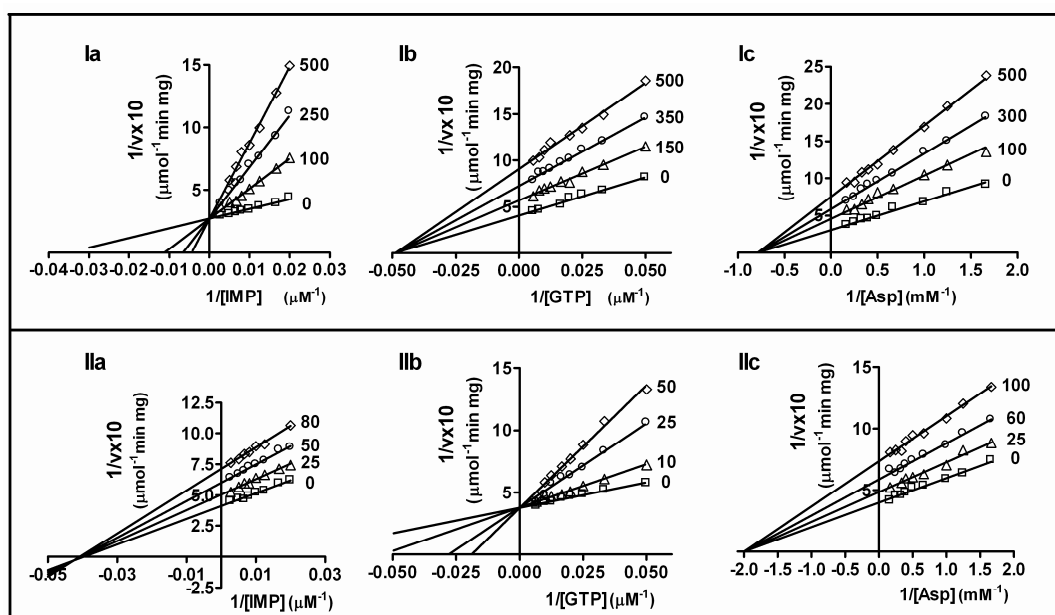


Figure 2.13: Lineweaver-Burk plots for inhibition of MjAdSS by I) AMP and II) GMP. Ia) Aspartate and GTP were held constant at 4.5 mM and 80 μM respectively, and IMP was varied from 50 μM to 350 μM ; Ib) Aspartate and IMP were held constant at 1.5 mM and 100 μM respectively, and GTP was varied from 20 μM to 175 μM ; Ic) IMP and GTP were held constant at 100 μM and 80 μM respectively, and aspartate was varied from 0.6 mM to 6 mM. Iia) Aspartate and GTP were held constant at 1.8 mM and 80 μM respectively, and IMP was varied from 50 μM to 375 μM ; Iib) Aspartate and IMP were held constant at 4.5 mM and 100 μM respectively, and GTP was varied from 20 μM to 150 μM ; Iic) IMP and GTP were held constant at 150 μM and 80 μM respectively, and aspartate was varied from 0.6 mM to 6.0 mM. Fixed concentration of inhibitor is indicated against each line.

The glycolytic intermediate, fructose 1,6 bisphosphate (F16BP) is a known modulator of AdSS activity (Borza *et al.*, 2003; Markham & Reed, 1977; Matsuda *et al.*, 1980; Ogawa *et al.*, 1976). F16BP was found to inhibit MjAdSS (Figure 2.14a). Inhibition patterns from Dixon plots indicated competitive inhibition with respect to IMP and noncompetitive inhibition with GTP (Figure 2.14 b,c). The data were fit to equations 10 and 11 to determine the K_i value. Apparent K_i values of 1.5 ± 0.1 mM and 4.8 ± 0.2 mM were obtained for IMP and GTP, respectively, which are significantly higher than those reported for mouse acidic AdSS (Borza *et al.*, 2003).

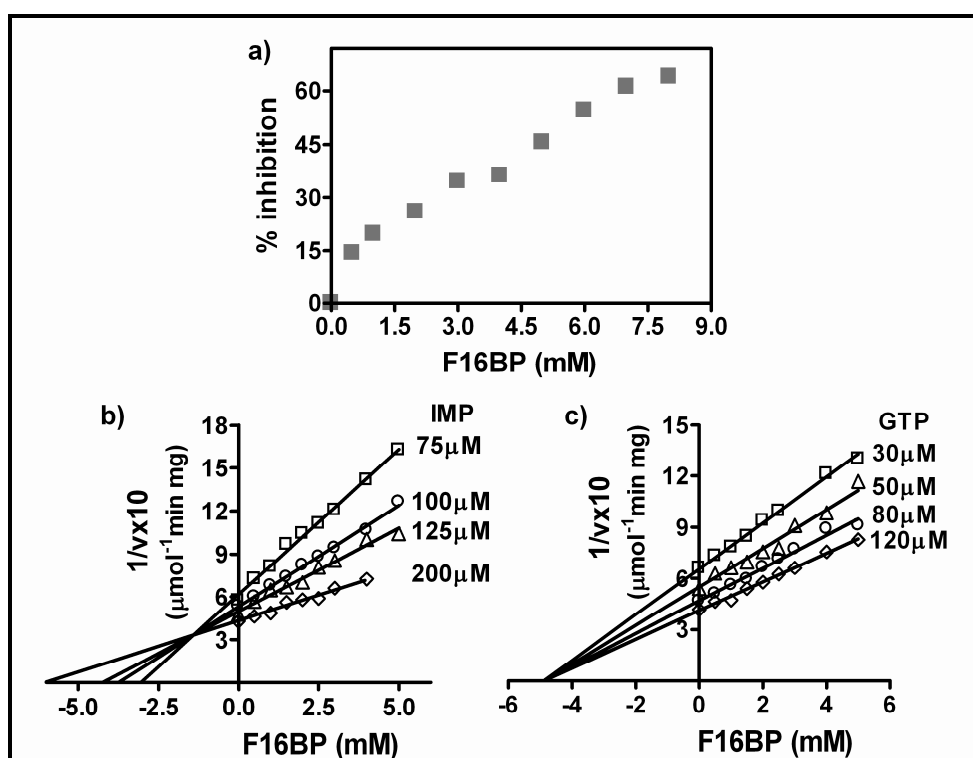


Figure 2.14: Regulation of MjAdSS activity by the glycolytic intermediate F16BP. a) Inhibition of MjAdSS activity by increasing F16BP concentration. b,c) Dixon analysis of effect of F16BP on enzyme activity. b) Aspartate and GTP were kept constant at 2 mM and 80 μM , respectively. The fixed concentrations of IMP appear against each line. c) Aspartate and IMP were held constant at 2 mM and 150 μM , respectively. The fixed concentration of GTP is indicated against each plot.

Table 2.4: Summary of MjAdSS inhibition kinetics using different metabolites.

Inhibitor	Substrate		
	IMP	GTP	Aspartate
AMP^a	Competitive $K_{iapp} = 58.2 \pm 6.7$	Noncompetitive $K_{iapp} = 402.6 \pm 11.3$	Noncompetitive $K_{iapp} = 324.0 \pm 20.1$
GMP^a	Noncompetitive $K_{iapp} = 110.6 \pm 2.1$	Competitive $K_{iapp} = 13.7 \pm 1.4$	Noncompetitive $K_{iapp} = 120.8 \pm 3.3$
F16BP^b	Competitive $K_{iapp} = 1.5 \pm 0.1$	Noncompetitive $K_{iapp} = 4.8 \pm 0.2$	ND

K_{iapp} is the apparent inhibition constant; ^a K_{iapp} values in μM ; ^b K_{iapp} values in mM; ND- not determined.

2.4 Discussion

Adenylosuccinate synthetase from the thermophilic archaea *M. jannaschii*, is 90-120 amino acids shorter than the biochemically and structurally well characterized counterparts from the mesophiles, *E. coli*, mouse and *P. falciparum*. Studies aimed at characterization of a thermophilic AdSS highlight certain unique kinetic and regulatory features of this enzyme. IMP and GTP K_m values for MjAdSS are higher than those reported for other AdSS in literature (Table 2.1) while the aspartate K_m value is similar to that for the mouse acidic isozyme. The catalytic efficiency of MjAdSS at 70°C is comparable to mouse acidic AdSS at ambient temperature whereas, at 25°C *P. falciparum* and *E. coli* AdSS exhibit lower k_{cat} values of 1.1 and 1.4 sec⁻¹, respectively (Raman *et al.*, 2004; Wang *et al.*, 1997a).

Crystallography and mutation analysis have shown that AdSS function as homodimers with both subunits contributing to the two active sites. The side chain of Arg143 (*E. coli* numbering) from one subunit penetrates the active site cleft of the symmetry related subunit and hydrogen bonds the 5' phosphate group of IMP. A complete active site thus requires structural elements from both subunits of the dimer (Kang *et al.*, 1996; Wang *et al.*, 1997a; Poland *et al.*, 1996a). *E. coli*, *P. falciparum* and yeast AdSS exhibit monomer-dimer equilibrium in solution, while mouse acidic and basic isozymes are predominantly dimers (Wang *et al.*, 1997a; Jayalakshmi *et al.*, 2002; Lipps & Krauss, 1999; Borza *et al.*, 2003). It is interesting to note that the *M. jannaschii* enzyme in solution exhibits dimer-tetramer equilibrium and this subunit association was found to be essential for enzyme activity (Figure 2.6 and 2.7). The extremely tight MjAdSS dimer may be a prerequisite for thermostability of the enzyme.

Variation in kinetic mechanism of AdSS from different species has been reported. Initial velocity kinetics and product inhibition studies have established a rapid equilibrium random sequential mechanism for *E. coli* AdSS (Rudolph & Fromm, 1969). Similar studies with human, *Schizosaccharomyces pombe* and *Dictyostelium discoideum* AdSS indicate a random sequential mechanism for the forward reaction (Van der Weyden & Kelly, 1974; Nagy *et al.*, 1973; Jahngen & Rossomando, 1984). AdSS catalyzes a reversible reaction and elucidation of steady-

state kinetic mechanism of *Azotobacter vinelandii* AdSS in both directions, highlighted random sequential binding for forward and reverse reactions (Markham & Reed, 1977). While similar results were obtained for rat muscle AdSS by equilibrium isotope exchange, these studies highlighted a preferred binding path in the forward reaction with the quaternary complex being formed by aspartate binding to E.IMP.GTP complex (Cooper *et al.*, 1986). This indicates that substrate induced conformational changes in the enzyme may be important in achieving a proper disposition of the active site for catalysis. In contrast, an ordered binding of substrates to the *P. falciparum* enzyme (Raman *et al.*, 2004) was observed by product inhibition studies, with IMP binding first followed by GTP and then aspartate. Initial velocity kinetics and product inhibition studies with MjAdSS are consistent with rapid equilibrium random binding of IMP and GTP followed by steady-state ordered binding of aspartate to E.IMP.GTP complex. This work is the second report of an enzyme exhibiting random AB ordered C kinetic mechanism with the first being that of guanylate cyclase (Garbers *et al.*, 1974).

Adenylosuccinate synthetase is an integral part of both de novo and salvage pathways for purine nucleotide biosynthesis, both of which proceed through the common intermediate, IMP. This is the first enzyme that commits IMP to formation of AMP and hence, it is implicated in maintaining AMP/GMP ratios in the cell (Stayton *et al.*, 1983). Studies in literature have highlighted different aspects of regulation of the enzyme by components of purine biosynthesis pathway and intermediates from the glycolytic pathway (Stayton *et al.*, 1983). Vertebrates have acidic and basic isozymes of AdSS which have been implicated in de novo biosynthesis of AMP and purine nucleotide cycle, respectively. These isozymes differ in kinetic properties and response to inhibitors, thereby indicating different modes of regulation of the two enzymes. Like the mouse acidic isozyme and *P. falciparum* AdSS (Borza *et al.*, 2003; Raman *et al.*, 2004), MjAdSS shows inhibition by IMP when GTP is limiting. In contrast, mouse basic isozyme is inhibited by high concentrations of IMP even at saturating concentrations of GTP (Borza *et al.*, 2003). Substrate inhibition pattern of MjAdSS is consistent with E-(IMP)₂ dead end complex formation indicating IMP binding to GTP site at subsaturating concentrations of GTP. This alternate binding mode of IMP is also evident in the crystal structure of an IMP

complex of mouse basic AdSS (Iancu *et al.*, 2002). Products of the reaction, sAMP, GDP and P_i , were also found to be effective regulators of enzyme activity. Studies with rabbit skeletal muscle AdSS suggest noncompetitive phosphate inhibition with all three substrates albeit with high K_i values (Muirhead & Bishop, 1974). Noncompetitive P_i inhibition with respect to GTP has been reported for *E. coli* AdSS. However, significantly high concentration of P_i (>10 mM) was required for detection of inhibition (Rudolph & Fromm, 1969). The biphasic inhibition curve at varying phosphate concentration implies two binding sites on MjAdSS, with one being the IMP binding site. The identity of the second site could not be established from these studies.

The acidic and basic isozymes of mammalian AdSS have been assigned to separate metabolic pathways based on susceptibility to inhibition by nucleotides and F16BP. The mouse basic isozyme exhibits greater sensitivity to inhibition by F16BP with the K_i value being 8 fold lower than that for the acidic isozyme (Borza *et al.*, 2003). Noncompetitive inhibition of F16BP with respect to all substrates has been reported in rat skeletal muscle AdSS and mouse isozymes (Ogawa *et al.*, 1976; Borza *et al.*, 2003). This inhibition pattern invokes an inhibitory site distinct from the active site. However, a preliminary crystallographic study by Borza *et al.* suggests that F16BP occupies 6-phosphoryl IMP binding site. Thus, these studies indicate that at low concentrations of IMP, F16BP competes for IMP binding site but when the concentration of substrate is high it binds to a site, still unidentified (Borza *et al.*, 2003). This feature is reflected in MjAdSS also, where a competitive inhibition pattern with respect to IMP was seen when the substrates were nonsaturating. As described in Chapter 4 of this thesis, *P. falciparum* AdSS is the only enzyme that exhibits activation with F16BP when assays are initiated with aspartate (Raman *et al.*, 2004).

These results highlight that in different organisms and different tissue types modulation of AdSS activity by certain ligands is conserved while other metabolites exhibit marked variation. These differences in turn reflect dissimilarities in metabolic flux and in modes of regulation across organisms.

2.4.1 Structural implications for the observed kinetic mechanism of MjAdSS

Examination of the NCBI database shows that short AdSS sequences do not segregate solely to thermophilic organisms. The structure of *Pyrococcus horikoshii* adenylosuccinate synthetase (PhAdSS), also a short AdSS, has been recently solved by the RIKEN Structural Genomics/Proteomics Initiative (RSGI) (PDB ID: 2D7U, Xie, Y., Kishishita, S., Muarayama, K., Shirouzu, M., Yokoyama, S., Crystal structure of hypothetical adenylosuccinate synthetase, PH0438 from *Pyrococcus horioshii* OT3). The 68% sequence identity between the AdSS sequences of *M. jannaschii* and *P. horikoshii* permits structure-function correlations to be made using the available structure of Pyrococcus AdSS. Though the deleted segments in MjAdSS form a part of subdomains that are associated with ligand binding and interface contacts in PfAdSS, the residues within these segments do not contribute significantly to either ligand or intersubunit contacts (Eaazhisai *et al.*, 2004). The superposition of the *E. coli* and Pyrococcus structures shows that the two ends of the deleted segments get connected by loops. Interestingly, no gross structural reorganization is evident in the core of the protein as a consequence of the deletions.

A comparison of various liganded and unliganded structures of AdSS reveals that there are five loops that respond to substrate binding namely, the Switch loop, IMP loop, GTP loop, Asp loop and Val loop (Iancu *et al.*, 2001; Poland *et al.*, 1996a). IMP bound structures of *E. coli* and mouse AdSS indicate that IMP binding is sufficient to organize all loops except the Asp loop that responds to hadacidin binding (Iancu *et al.*, 2002; Hou *et al.*, 2002). The structure of the unliganded *P. horikoshii* AdSS (PDB ID: 2D7U) has four loops in the closed conformation with IMP loop not mapped. This is the first structure of AdSS with a loop-closed conformation in the absence of ligands. Absence of contacts between the loop residues shows that such interactions cannot contribute to the stability of the closed state. The loop closed conformation in the Pyrococcus AdSS structure may be stabilized due to energy contributions from interactions of loop residues with amino acids in other segments of the protein.

Comparison of the fully liganded PfAdSS structure with mouse and *E. coli* structures highlights differences that could be contributing to the ordered substrate

binding in PfAdSS. Hydrogen bonding of Ser57 and Asp60 in the Switch loop with Asn429 in GTP loop results in inward movement of Switch loop into the ligand binding pocket. As a result, nonconserved Lys62 in the Switch loop hydrogen bonds with ribose hydroxyls of GDP (Eaazhisai *et al.*, 2004). These residues are not conserved in mouse, *E. coli* and Methanococcus AdSS which show random binding of IMP and GTP. In the liganded PfAdSS structure GDP hydrogen bonds with the side chain hydroxyl of Thr307 on Asp loop indicating that GTP binding brings about loop movements that prepare the cavity for aspartate binding (Eaazhisai *et al.*, 2004). Thr307, not conserved in mouse and *E. coli* AdSS, while being conserved in MjAdSS could possibly dictate ordered binding of aspartate in a manner analogous to that observed in the parasite enzyme. The orientation of the two catalytic residues, Asp13 and His43 in the unliganded Pyrococcus structure is comparable to liganded crystal structures of *E. coli*, mouse and *P. falciparum* AdSS, whereas comparison with unliganded mouse or *E. coli* structures shows good overlap of Asp13 but His43 is flipped by 180°. Therefore, this indicates that the Pyrococcus enzyme is fully poised for catalysis and the loop movements are driven even in the absence of ligands. Availability of liganded structure of MjAdSS should provide the structural implication for the observed random AB ordered C kinetic mechanism.

Chapter 3

Studies on Temperature Dependence of Catalytic Activity and Structural Stability of *M. jannaschii* Adenylosuccinate Synthetase

Two important attributes of enzymes produced by thermophilic organisms are thermophilicity and structural stability. This chapter discusses the characterization of these two aspects in adenylosuccinate synthetase from the thermophilic archaea, Methanocaldococcus jannaschii. Temperature dependence of MjAdSS catalysis exhibited a biphasic Arrhenius Plot with a transition at 40°C. A combination of steady-state and transient kinetics showed that thermophilicity in MjAdSS arises due to slow product release from the enzyme active site at ambient temperatures. Stability of MjAdSS assessed by equilibrium unfolding revealed the robustness of the secondary and tertiary structure of the enzyme which remained intact even at 8 M concentration of urea. Guanidinium chloride induced unfolding profiles of MjAdSS could be described as a composite of at least two distinct transitions, with a stable intermediate in the unfolding pathway.

3.1 Introduction

A tradeoff between stability, catalytic activity and conformational flexibility governs an enzyme's function and its structural integrity under different

environmental conditions. With life flourishing over a wide range of temperature, pressure and pH, proteins have evolved to maintain a balance between structural rigidity, permitting appropriate three dimensional conformation to be maintained under extreme conditions, and local flexibility or dynamics necessary for protein function. Protein function thus relies on a delicate balance between macromolecular stability and micromolecular flexibility. Proteins from psychrophiles, which are residents of cold habitats, are thought to display high catalytic efficiency at low temperatures due to increased conformational flexibility; a feature which compromises protein stability (Fields, 2001; Georlette *et al.*, 2003). In contrast, enzymes from hyperthermophilic organisms are adapted to function and maintain native structure at temperatures greater than 80°C where the three dimensional structure of the mesophilic counterparts often collapse. The structural similarity of the active site and conservation of catalytic residues between homologous mesophilic and thermophilic enzymes leads one to expect similar catalytic rates at a given temperature. However, enzymes from thermophiles are barely active at ambient temperatures where the mesophilic enzymes exhibiting similar function are optimally active. The increased conformational rigidity which serves to stabilize thermophilic proteins at extreme temperatures results in differences in their temperature optima from that of the mesophilic counterparts (Fields, 2001; Georlette *et al.*, 2003; Jaenicke, 1991; Vihinen, 1987; Wrba *et al.*, 1990; Zavodszky *et al.*, 1998; Merz *et al.*, 2000; Wolf-Watz *et al.*, 2004; Jaenicke & Bohm, 1998). However, a “corresponding state” with respect to flexibility and hence, catalytic activity is achieved at the respective temperature optimum of the two enzymes (Georlette *et al.*, 2003; Jaenicke, 1991; Vihinen, 1987; Wrba *et al.*, 1990; Zavodszky *et al.*, 1998; Jaenicke & Bohm, 1998).

Search for structural basis of thermostability has not led to a unifying set of rules applicable in general, to a variety of thermostable proteins. High sequence and structural similarity between homologous mesophilic-thermophilic enzyme pairs make the identification of determinants of thermostability difficult. Infact, thermostability as discussed in Chapter 1, seems to be an intrinsic property of the protein molecule contributed by a combination of factors like increased intra and

intermolecular interactions (which include hydrogen bonds, salt bridges, hydrophobic interactions and disulphide bonds), compactness of structure, increased rigidity, reduced surface area and higher oligomeric states (Jaenicke, 1991; Wrba *et al.*, 1990; Jaenicke & Bohm, 1998; Vieille & Zeikus, 2001; Petsko, 2001). Native structure of a protein, held by non-covalent interactions, weakens under extreme conditions of temperature or pH, finally resulting in protein unfolding. Stability of protein structures can be ascertained by equilibrium unfolding studies. Thermal unfolding studies on proteins, when the process is reversible, permit estimation of thermodynamic parameters that allows evaluation of their stability (Pace, 1975; Pace, 1990; Privalov, 1979). However, the process of thermal unfolding is often irreversible as a consequence of formation of insoluble aggregates due to the sticky, hydrophobic nature of the exposed surfaces of the unfolded protein (Vermeer & Norde, 2000; Benjwal *et al.*, 2006). Hence, the literature is replete with detailed studies on chemical denaturation of proteins with established methodologies for the determination of stability parameters (Pace, 1975; Privalov, 1979; Kauzmann, 1959; Tanford, 1968; Aune & Tanford, 1969; Tanford, 1970). Small globular proteins often unfold by a cooperative transition where only folded and unfolded conformational states are present at equilibrium (Pace, 1975; Privalov, 1979; Tanford, 1968; Pace, 1986). Intermediates, if present in the unfolding pathway, are either transient or at low concentrations making their detection by conventional spectroscopic techniques difficult. Unlike the monomeric counterparts where only intramolecular interactions dictate the unfolding process, in multidomain and oligomeric proteins this process is more complicated with the folding and unfolding being dictated by both intra and intersubunit interactions. Stable intermediates in the unfolding pathway have been shown to exist for many proteins including small, single domain proteins (Kim & Baldwin, 1990; Privalov, 1996). These intermediates may be partially denatured or may retain appreciable amount of secondary structure with loss of oligomerization. Both qualitative and quantitative characterization of stable intermediates has been attempted by various groups (Privalov, 1996; Ptitsyn, 1995; Englander, 2000). Thermostable proteins often show presence of stable intermediates in the unfolding pathway enabling both qualitative and quantitative estimation of their stability and

structure (Schultes & Jaenicke, 1991; MacBeath *et al.*, 1998; Bonvin *et al.*, 2006). Thermozyms thus serve as model systems to understand aspects of thermostability and thermophilicity.

This chapter discusses the studies carried out on adenylosuccinate synthetase from the thermophilic archaea, *M. jannaschii* (MjAdSS) with an aim to understand structural stability and catalytic function under thermophilic conditions. Unlike the mesophilic counterparts from mouse, *E. coli* and *P. falciparum*, MjAdSS showed a continuous increase in activity till 85°C. An Arrhenius plot revealed a temperature dependent change in activation energy around 40°C. A combination of steady-state and pre-steady-state kinetics has been used to gain insight into aspects of thermophilicity of MjAdSS. Quaternary, tertiary and secondary structural stability of MjAdSS was assessed by equilibrium unfolding measurements using chemical chaotropes. Guanidinium chloride (GdmCl) induced denaturation of MjAdSS permitted estimation of thermodynamic parameters. The unfolding profiles could be described as a composite of atleast two distinct transitions, with a stable intermediate in the unfolding pathway.

3.2 Materials and Methods

All media components were purchased from HiMedia Laboratories (Mumbai, India). Substrates used for enzyme assays, buffer components, protein markers, urea and guanidinium chloride were purchased from Sigma Chemical Company (St.Louis, MO, USA). All reagents were of analytical grade. Hadacidin was a kind gift from Developmental Therapeutics Program, National Cancer Institute, NIH, Bethesda, MD. Akta Basic HPLC, Superdex 200 and Sephasil C18 column were from Amersham Pharmacia (Uppsala, Sweden). All assays were done using Hitachi U2010 (Hitachi High-Technologies Corporation, Tokyo, Japan) spectrophotometer fitted with a water circulated cell holder. MALDI-MS spectra were recorded on Ultraflex II TOF/TOF mass spectrometer (Bruker Daltonics, Bremen, Germany).

3.2.1 Protein Purification

The protein was purified as described in Chapter 2, Section 2.2.1. The protein samples were greater than 95% pure as judged by SDS-PAGE (Laemmli, 1970).

3.2.2 Temperature dependence of MjAdSS activity

To monitor the effect of temperature on MjAdSS catalyzed reaction, reaction rates were monitored at different temperatures. Assays were done using Hitachi U-2010 spectrophotometer fitted with a water circulated cell holder. The temperature was maintained using Julabo F25 (JULABO Labortechnik GmbH, Seelbach, Germany) circulating water bath. The reaction mix consisted of 30 mM MES, pH 6.5, 15 mM magnesium acetate, 500 μ M IMP, 250 μ M GTP and 10 mM aspartate. 0.65 μ g of protein was used in 300 μ l reaction volume. sAMP formation was monitored as an increase in absorbance at 290 nm and a $\Delta\epsilon$ of 3390 $\text{M}^{-1}\text{cm}^{-1}$ was used to calculate the amount of product formed (Kang & Fromm, 1995). No change in substrate K_m values was observed with change in temperature. The activation energy, E_a , was calculated using the linear form of Arrhenius equation (Gray & Barker, 1970; Segel, 1975).

$$\log k = -E_a/2.3RT + \log A \quad \text{Equation 1}$$

where, k is the reaction rate constant determined at each temperature, T is the absolute temperature and R the ideal gas constant ($1.98 \text{ cal mol}^{-1} \text{ degree}^{-1}$). E_a was determined by plotting $\log k_{\text{cat}}$ vs $1/T$ where the slope corresponds to $-E_a/2.3R$. Thermodynamic activation parameters ΔH and ΔS , were determined by least square analysis of the data collected from 20-85°C using equation 2

$$k = (k_B T/h) e^{-[(\Delta H/RT)-(\Delta S/R)]} \quad \text{Equation 2}$$

where, h is Planck's constant and k_B is Boltzmann constant.

3.2.3 Reverse Phase HPLC

Separation of IMP, GTP and GDP was carried out on an Akta Basic HPLC system using a Sephasil C18 column (5 μ m particle size, 4.6 x 250 mm). The mobile

phase consisted of Buffer A (Water + 2 mM tetrabutylammonium hydrogen sulphate used as ion pairing agent) and Buffer B (Methanol + 2 mM tetrabutylammonium hydrogen sulphate). The elution condition used to obtain separation of nucleotides consisted of the following sequential steps, 100% buffer A for 6 minutes, upto 20% buffer B in 15 minutes, 20 to 50% buffer B in 20 minutes and finally 50 to 100% buffer B in 25 minutes. The flow rate was kept at 0.5 ml/min and the elution monitored at 254 nm. 100 μ M protein samples were incubated with 100 μ M IMP, 100 μ M GTP and 2 mM magnesium acetate with/without hadacidin at 25°C or 70°C for different time periods after which the reaction was quenched by adding EDTA to a final concentration of 3 mM. The protein was then precipitated using 2% TCA, the solution neutralized with NaOH and 100 μ l of the reaction mixture was injected into C18 reverse phase column. The peak identities were confirmed by MALDI mass spectrometry and by comparison with the elution profiles of standard samples of IMP, GTP and GDP. Area under the peaks was used to quantitate the amount of product formed.

For MALDI measurements, 1 μ l of the reaction mix or the sample collected from reverse phase column was allowed to crystallize with 1.5 μ l of 2,5-dihydroxybenzoic acid (DHB) on the MALDI target plate. The spectra were recorded in the positive ion mode on Ultraflex II TOF/TOF mass spectrometer.

3.2.4 Transient kinetics

Pre-steady-state kinetic experiments were performed at 25°C using a SFM-400 stopped flow apparatus (dead time, 14.8 ms; flow rate, 5 ml/sec) attached to a spectrophotometer (Bio-Logic, Grenoble, France) in a quartz cuvette of 0.2 mm path length. Four syringes were filled with enzyme, substrates, magnesium acetate and buffer. To monitor multiple turnovers, the substrates were kept in excess over the enzyme. The contents of the syringes were mixed to achieve a final concentration of 150 μ M GTP, 250 μ M IMP, 10 mM aspartate, 15 mM magnesium acetate and 8.7 μ M MjAdSS in the flow cell. Product formation was monitored at 280 nm. Due to slow catalytic rates at low temperatures, transient kinetics between 18-37°C could be monitored on U-2010 spectrophotometer fitted with a water circulated cell holder. To

monitor multiple turnovers, 1.5 μM enzyme was preincubated with 70 μM IMP, 70 μM GTP and 15 mM magnesium acetate at the desired temperature. The reactions were initiated with 6 mM aspartate and monitored at 290 nm.

3.2.5 Thermostability of MjAdSS

Thermostability of MjAdSS was investigated by preincubating the enzyme at 65, 70, 75, 80, 85 and 90°C in the storage buffer (20 mM Tris HCl, pH 7.4, 10% glycerol, 1 mM EDTA, 0.1 mM PMSF and 2 mM DTT). Samples were taken at different time intervals and the residual activity checked at 70°C. The assay conditions were as described in Section 3.2.2. Changes in secondary structure of the protein on thermal denaturation were monitored on Jasco J-810 spectropolarimeter at 220 nm and at a protein concentration of 5 μM . Temperature was ramped at 1°C min⁻¹.

3.2.6 Size exclusion chromatography

Gel filtration experiments were carried out on a Superdex 200 (1cm * 30cm) column attached to an Akta Basic HPLC using 20 mM Tris HCl, pH 7.4 containing the required concentration of GdmCl as the solvent system. The runs were performed at a flow rate of 0.5 ml/min and protein elution monitored simultaneously at 280 and 220 nm. The column was calibrated with β -amylase (200 kDa), alcohol dehydrogenase (150 kDa), bovine serum albumin (66 kDa), carbonic anhydrase (29 kDa) and cytochrome c (12.4 kDa). 20 μM protein was incubated for 45 minutes with the required GdmCl concentration in 20 mM Tris HCl, pH 7.4 and injected onto the column pre-equilibrated with the same buffer.

3.2.7 Equilibrium unfolding measurements

A) *Fluorescence spectroscopy.* Fluorescence measurements were performed on a Hitachi F-2500 spectrofluorimeter (Hitachi High-Technologies Corporation, Tokyo, Japan). Preliminary studies confirmed that equilibrium was reached within 20 minutes of incubation with the chaotrope. Unfolding by GdmCl was monitored at a protein concentration of 2 μM in 20 mM Tris HCl, pH 7.4 at varying chaotrope concentrations. Protein samples after incubation for 45 minutes with the chaotrope,

were excited at 290 nm with emission monitored from 292-400 nm. Excitation and emission bandwidths were set to 2.5 and 10 nm, respectively. Baseline corrections were done by subtraction of buffer spectrum.

B) Circular dichroism spectroscopy. Circular dichroism measurements were performed on a Jasco J-810 spectropolarimeter (JASCO Corporation, Tokyo, Japan) equipped with a Peltier heating system. For denaturation studies, 5 μM protein was preincubated for 45 minutes with the required concentration of GdmCl in 20 mM Tris HCl, pH 7.4. Ellipticity changes at 220 nm were monitored to follow far-UV unfolding transition in a cuvette of 0.1 cm path length. Each spectrum represented the average of three accumulations and all spectra were corrected for background by subtraction of the spectrum of the buffer with appropriate additives.

3.2.8 Analysis of equilibrium unfolding data

Three conformational states, native (N), intermediate (I) and unfolded (U) were observed by both fluorescence and circular dichroism spectroscopy on denaturation with GdmCl. The transition from one conformational state to another can be represented by a three state model



The amplitude of the spectroscopic signal, Y , determined at each GdmCl concentration can be assumed to be sum of the contribution from each of the three species (equation 3)

$$Y = Y_{\text{N}}f_{\text{N}} + Y_{\text{I}}f_{\text{I}} + Y_{\text{U}}f_{\text{U}} \quad \text{Equation 3}$$

$$f_{\text{N}} + f_{\text{I}} + f_{\text{U}} = 1 \quad \text{Equation 4}$$

where, Y_{N} , Y_{I} and Y_{U} are the amplitude of signals for the respective species and f_{N} , f_{I} and f_{U} is the fraction of each species. The $[\theta]_{220}$ measured as a function of GdmCl concentration were fit to equation 5 and a Y_{I} value of 0.27 determined.

$$Y = Y_U + [Y_N - Y_U (Y_I / \{1 + 10^{X - C_m1}\})] + [Y_N - Y_U (\{1 - Y_I\} / \{1 + 10^{X - C_m2}\})] \quad \text{Equation 5}$$

where, C_m is the denaturant concentration at midpoint of each transition. Using the Y_N , Y_U and Y_I values obtained from the global fit, the equilibrium constant, K_{eq} , and ΔG at each GdmCl concentration were calculated using the relationship

$$\Delta G = -RT \ln K_{eq} \quad \text{Equation 6}$$

where, R is the gas constant and T is the temperature in degrees Kelvin. Assuming that the free energy change for each transition is linearly dependent on denaturant concentration (Thompson *et al.*, 1989), the free energy change in the absence of denaturant can be calculated using the following equation

$$\Delta G_1 = \Delta G_1^0 - m_1[C] \quad \text{Equation 7}$$

$$\Delta G_2 = \Delta G_2^0 - m_2[C] \quad \text{Equation 8}$$

where, ΔG^0 is the free energy change in the absence of denaturant, C is the denaturant concentration and m is a measure of co-operativity of GdmCl induced denaturation.

3.3 Results

3.3.1 Temperature dependence of MjAdSS catalytic activity

AdSS catalyzes the Mg^{2+} dependent formation of succinyl-AMP (sAMP) from IMP and aspartate in a reaction accompanied by the conversion of GTP to GDP. Figure 3.1a shows the temperature dependence of the MjAdSS activity.

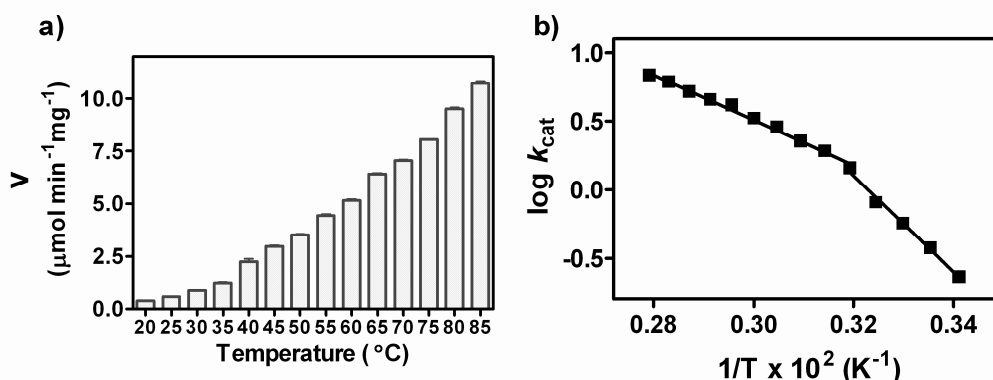


Figure 3.1: a) Temperature dependence of MjAdSS catalyzed reaction. b) Arrhenius plot of the data to determine the activation parameters for the catalytic process.

Variation of enzyme activity with temperature when plotted as $\log k_{\text{cat}}$ vs $1/T$ (Arrhenius plot) enabled the calculation of activation parameters for the reaction. A discontinuity in the slope of the Arrhenius plot was found at 40°C (Figure 3.1b). The activation energy, E_a , calculated using equation 1, is 16.1 kcal mol⁻¹ between 20 and 40°C and 7.6 kcal mol⁻¹ in the temperature range 40 to 85°C (Table 3.1). From the data in Figure 3.1b, the enthalpy and entropy of activation were determined using equation 2. The values for these parameters are listed in Table 3.1.

Table 3.1: Activation parameters for MjAdSS catalyzed reaction.

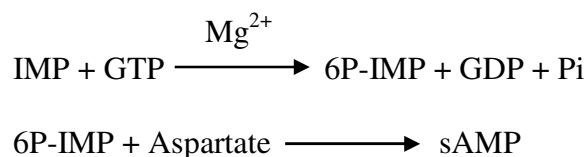
Temperature	E_a (kcal mol ⁻¹)	ΔH (kcal mol ⁻¹)	ΔS (cal mol ⁻¹ K ⁻¹)
293 K – 333 K	16.1 ± 1.4	15.5 ± 1.5	0.48
333 K- 358 K	7.6 ± 0.4	6.9 ± 0.3	-26.6 ± 1.1

I) Thermophilicity of MjAdSS

MjAdSS exhibited high reaction rates at elevated temperatures but at 25°C it showed only 10% of its activity at 70°C. To gain insight into the aspect of thermophilicity of MjAdSS the effect of temperature on the following two processes was examined; 1) formation of the reaction intermediate, 6-phosphoryl IMP, and 2) pre-steady-state kinetics of MjAdSS catalyzed reaction.

3.3.2 Effect of temperature on 6-phosphoryl IMP formation

AdSS catalyzed conversion of IMP to sAMP proceeds via a concerted two step process as shown below



The first step involves the phosphorylation of IMP by the transfer of a phosphate group from GTP. This is followed by nucleophilic attack by aspartate leading to the formation of sAMP (Lieberman, 1956). Isotope scrambling experiments with *E. coli* AdSS indicated that the reaction intermediates, 6P-IMP and GDP, do not fall off from the enzyme before the formation of sAMP (Bass *et al.*, 1984).

The first step of catalysis leading to the formation of 6P-IMP and GDP was monitored at 25 and 70°C by reverse phase HPLC (RP-HPLC) and MALDI mass spectrometry (Figure 3.2 a,b and Figure 3.4). Equimolar concentrations (100 µM) of enzyme, IMP and GTP were used to ensure complete complex formation and absence of turnover. The mix was incubated at the two temperatures for different time intervals, after which the GDP bound to the enzyme was liberated by TCA precipitation of the protein and detected by RP-HPLC. Water-methanol solvent system containing the ion pairing agent tetrabutylammonium hydrogen sulphate allowed separation of IMP, GDP and GTP on a C18 reverse phase column. Appearance of GDP peak and decrease in intensity of GTP peak was an indication of the formation of 6P-IMP by transfer of γ -phosphoryl group from GTP. Control experiments with GTP alone or enzyme and GTP at both 25 and 70°C over the time period of the study showed no detectable appearance of GDP. A separate 6P-IMP peak could not be detected probably due to the instability of 6P-IMP which reverts back to IMP upon TCA precipitation of the protein. As shown in Figure 3.2, GDP formation is evident at both 25 and 70°C and the amount of GDP formed over 5 minutes is similar at both the temperatures (Figure 3.3). The identity of the GDP peak

from reverse phase column was further confirmed by MALDI mass spectrometry in the positive ion mode (Figure 3.4, panel B). Though equivalent amounts of enzyme, GTP and IMP were used in the reactions, GDP concentration built over time at both 25 and 70°C indicating that the first step of intermediate formation was not instantaneous in the absence of aspartate.

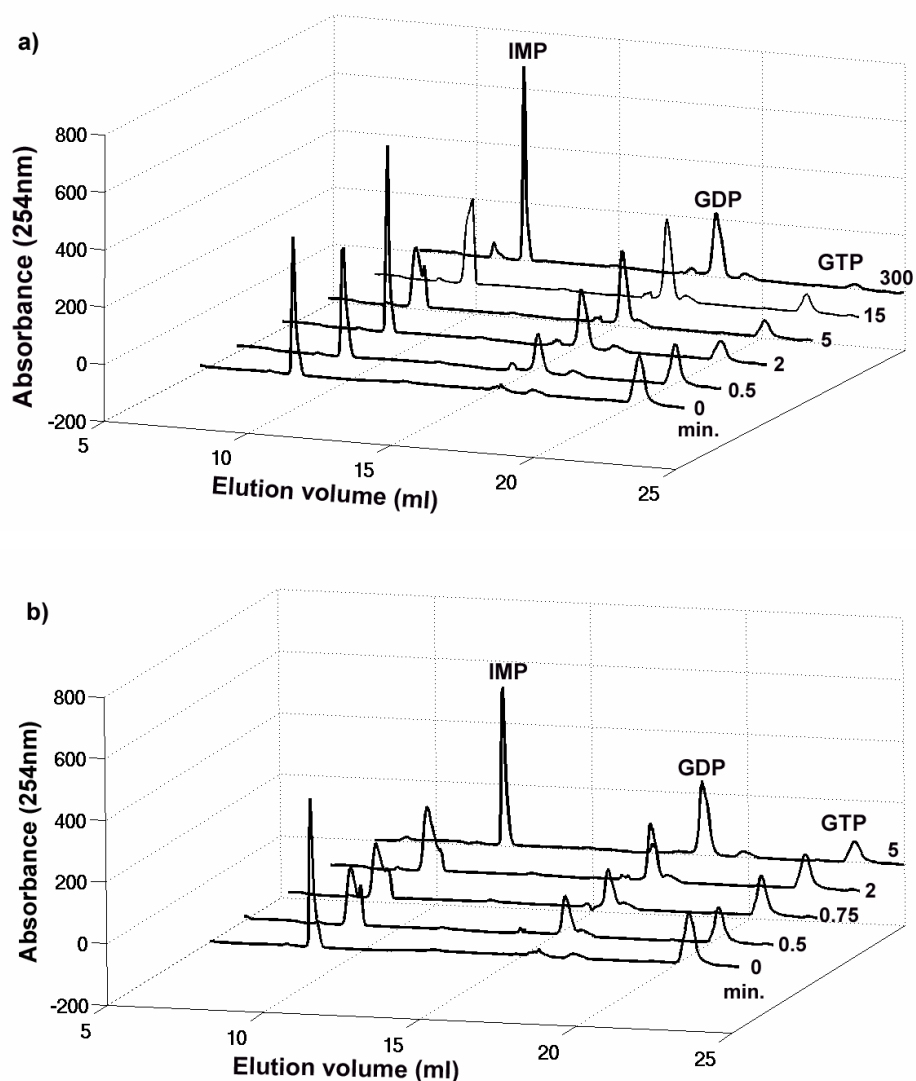


Figure 3.2: MjAdSS catalyzed formation of GDP monitored by ion pair RP-HPLC. a) RP-HPLC profiles of MjAdSS reaction carried out at 25 and b) 70°C monitored as a function of time. 100 μ M MjAdSS was incubated with 100 μ M each of IMP and GTP in the presence of 2 mM magnesium acetate for different time periods after which GDP bound to the enzyme was liberated by TCA precipitation of the protein. The time over which the reaction was allowed to progress is indicated against each trace.

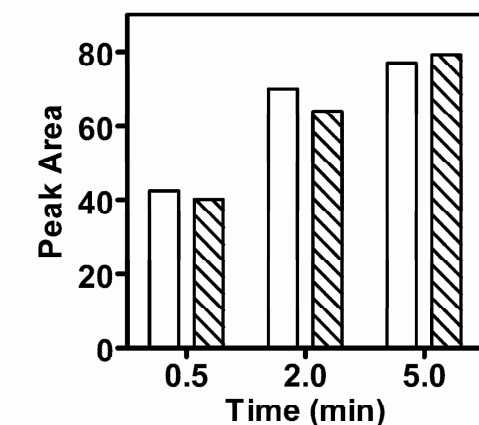


Figure 3.3: GDP formation at 25°C (open bars) and 70°C (hashed bars) as a function of time. Amount of GDP formed is represented as area under the peaks in the HPLC profiles.

To mimic the fully liganded catalytic state of MjAdSS, hadacidin, an aspartic acid analog was added to the reaction mixture containing enzyme, IMP and GTP. Under these conditions almost complete utilization of GTP was observed within 30 seconds, at both 25 and 70°C. The increase in the amount of GDP formed in the presence of hadacidin is an indication of its (and hence, aspartate) binding to the enzyme at ambient temperatures. This observation also indicates that the low activity of MjAdSS at 25°C is not due to the inability of aspartate to bind to E.IMP.GTP complex. Thus, the similarity in the amounts of GDP formed at both 25 and 70°C is in contrast to the different steady state k_{cat} s for sAMP formation at the two temperatures.

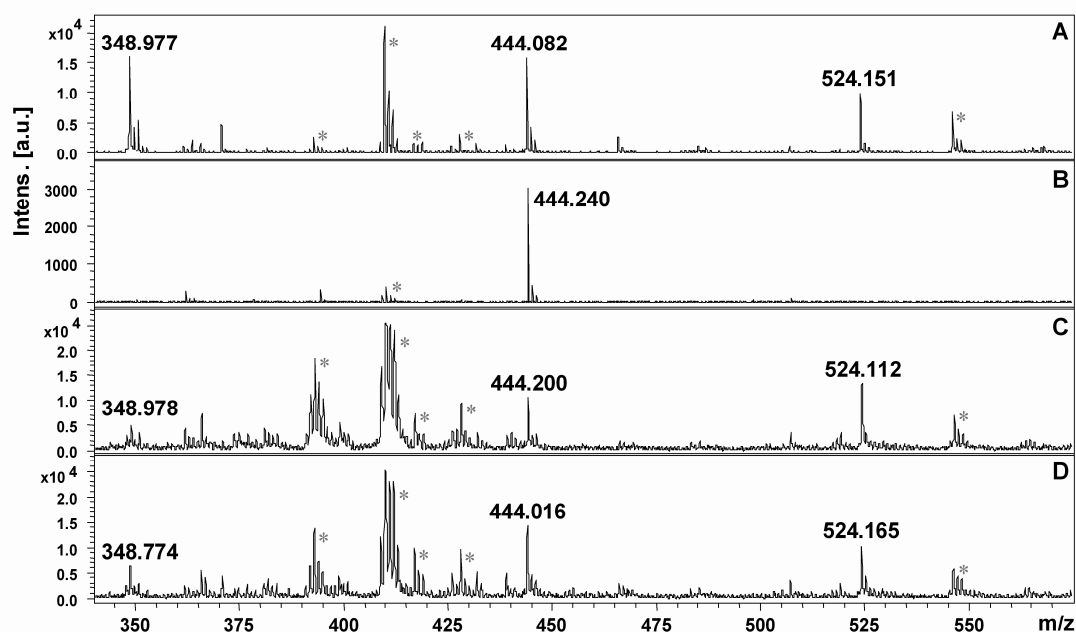


Figure 3.4: MALDI-MS detection of GDP formation catalyzed by MjAdSS. (A) Spectra of IMP, GTP and GDP spotted in 2,5 dihydroxybenzoic acid (2,5 DHB) matrix, (B) GDP peak collected from RP-HPLC column confirmed by MALDI mass spectrometry. 100 μ M protein was incubated with 100 μ M each of IMP and GTP and 2 mM magnesium acetate for 5 minutes at 25 (C) and 70°C (D). The protein was precipitated using 2% TCA and the mix spotted on MALDI target plate. Spectra were recorded in positive ion mode and * indicates peaks coming from the matrix. Expected molecular mass of IMP, GDP and GTP are 348.13, 443.1 and 523.05, respectively.

3.3.3 Effect of temperature on pre-steady-state kinetics

Transient kinetics was performed at different temperatures between 18-37°C. In a multiple turnover experiment where substrates were in excess of the enzyme, a biphasic time course was obtained between 18-32°C, which consisted of a rapid ‘burst’ of product formation followed by steady-state turnover (Figure 3.5). The presence of the burst is an indication of product release or a step subsequent to chemical conversion being rate limiting at ambient temperatures (Johnson, 1995). However, at higher temperatures of 35 and 37°C, which are close to the transition temperature in the Arrhenius Plot, the plot of turnover versus time was linear indicating that the rate limiting step is either the catalytic step or a step preceding chemical conversion (Johnson, 1995). Thus transient kinetics provides evidence for

the product release to be rate limiting in the catalytic activity of MjAdSS at ambient temperatures.

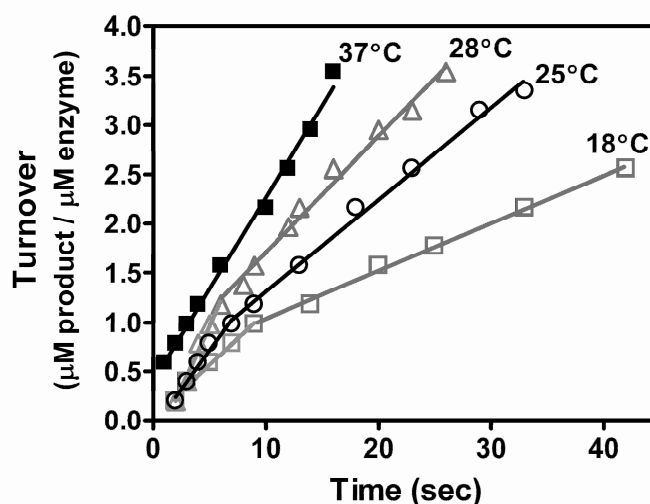


Figure 3.5: Multiple turnover transient kinetics of MjAdSS catalyzed reaction monitored at different temperatures. 1.5 μM MjAdSS was used in a 300 μl reaction volume where IMP and GTP concentrations were 70 μM each and aspartate concentration was 6 mM. Each time course shown is an average of 3-6 traces. Pre-steady-state burst of product formation is evident between 18-28°C, whereas at 37°C a linear time course is obtained indicating a switch in rate determining step of the reaction with change in temperature.

II) Structural stability of MjAdSS

3.3.4 Thermal stability

The structural stability of the enzyme to thermal denaturation was examined using far-UV circular dichroism spectroscopy and activity measurements. Figure 3.6 shows the effect of preincubation of MjAdSS at different temperatures on its activity measured at 70°C. The half life of inactivation was 340 minutes, 150 minutes, 110 minutes, 60 minutes, 30 minutes and 15 minutes at 65, 70, 75, 80, 85 and 90°C, respectively.

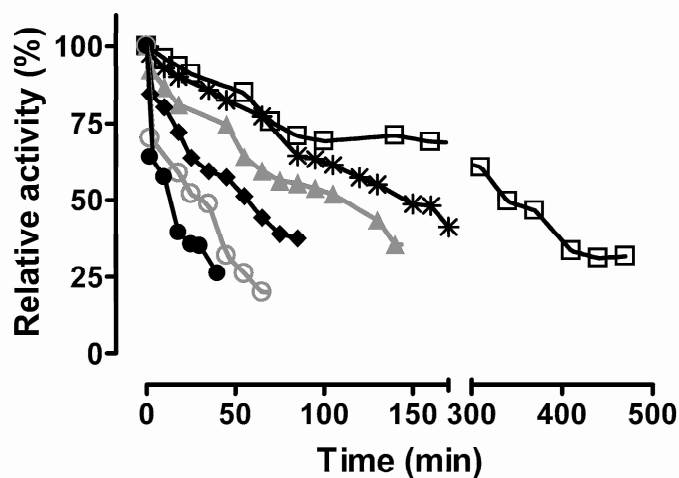


Figure 3.6: Thermal inactivation profile of MjAdSS. Enzyme was incubated at (□) 65 °C, (*) 70 °C, (▲) 75 °C, (◆) 80 °C, (○) 85 °C and (●) 90°C for different time intervals, aliquots drawn and the remaining activity assayed at 70°C under standard assay conditions.

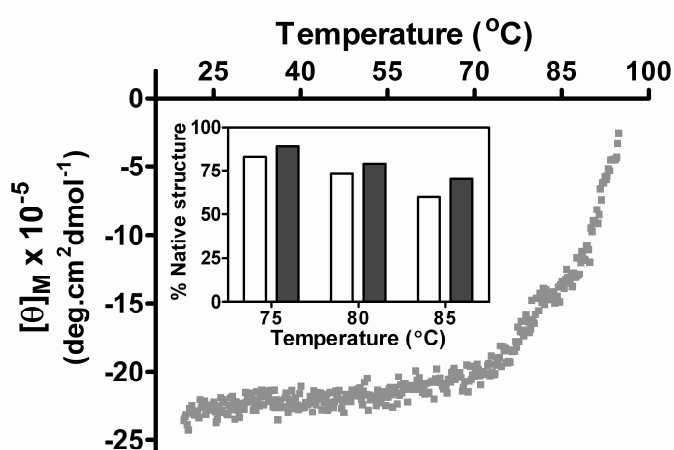


Figure 3.7: Stability of secondary structure of MjAdSS to thermal denaturation monitored as change in molar ellipticity at 220 nm. The inset shows % native structure retained (open bars) after heating to different temperatures and the % native structure regained after cooling (filled bars) to 20°C. The temperature was ramped at the rate of 1°C min⁻¹.

The stability of secondary structure to temperature was monitored using circular dichroism spectroscopy at 220 nm (Figure 3.7). CD showed 13% decrease in ellipticity at 70°C, beyond which there was a dramatic loss in ellipticity. Time dependent loss in activity seen at 70°C is probably due to local unfolding while the

global structure of the protein is largely retained. Cooling of the unfolded protein heated to 80, 75 and 70°C, did not result in complete recovery of the native structure indicating that the thermal unfolding process is only partially reversible (Figure 3.7, inset).

These results indicate that MjAdSS is not hyperthermostable under in vitro conditions. However, the enzyme may be stabilized by extrinsic factors in vivo to enable protein structure and function to be retained under extreme growth conditions of *M. jannaschii*. The effect of substrates, enzyme concentration etc., in increasing temperature stability of MjAdSS cannot be ruled out.

3.3.5 Equilibrium unfolding using chemical chaotropes

Both far-UV CD measurements and tryptophan fluorescence indicated that the protein was stable to denaturation by urea (Figure 3.8).

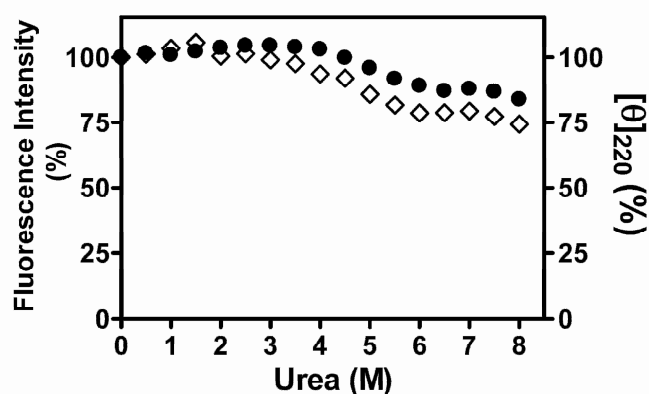


Figure 3.8: Urea induced unfolding of MjAdSS monitored by fluorescence (●) and CD (◇) spectroscopy. The fluorescence intensity at 320.5 nm and ellipticity values at 220 nm in the absence of denaturant were taken as 100%.

Emission maximum on excitation at 290 nm, shifted from 320.5 nm to 322.5 nm at 8 M urea concentration. However, minor changes in fluorescence intensity with increasing urea concentration, indicated changes in tryptophan environment due to

structural fluctuations. The same was evident in CD measurements, where small perturbations in secondary structure were evident with increasing urea concentration. Hence, urea did not serve as a useful probe to monitor the equilibrium unfolding of MjAdSS.

3.3.6 Unfolding in guanidinium chloride

(i) Size exclusion chromatography

To characterize changes in quaternary structure of MjAdSS in guanidinium chloride (GdmCl) solution, size exclusion chromatography was performed (Figure 3.9). In the absence of denaturant, MjAdSS eluted as a single peak corresponding to a molecular mass of 109 kDa, which is indicative of dimer-tetramer equilibrium. The equilibrium shifted to a dimer on adding 0.5 M GdmCl, and beyond this concentration of the chaotrope the dimer started to unfold. A fully unfolded monomer would have a larger Stoke's radius than a compact folded dimer and hence, elute at a lower elution volume. Unfolded monomeric species first appeared at 2.5 M GdmCl concentration though, significant amount of dimeric form was retained till 4 M concentration of the chaotrope. Fully solvated, unfolded monomeric species were detected at 6 M GdmCl concentration. These profiles indicate that the process of unfolding brought about by GdmCl first involves dissociation of tetramer to dimers at very low concentration of GdmCl, followed by the dimer unfolding and subsequent dissociation to monomers at 4 M concentration of chaotrope. The presence of two peaks between 2.5 and 4 M GdmCl concentration is indicative of a slow equilibrium between unfolded dimeric and unfolded monomeric species.

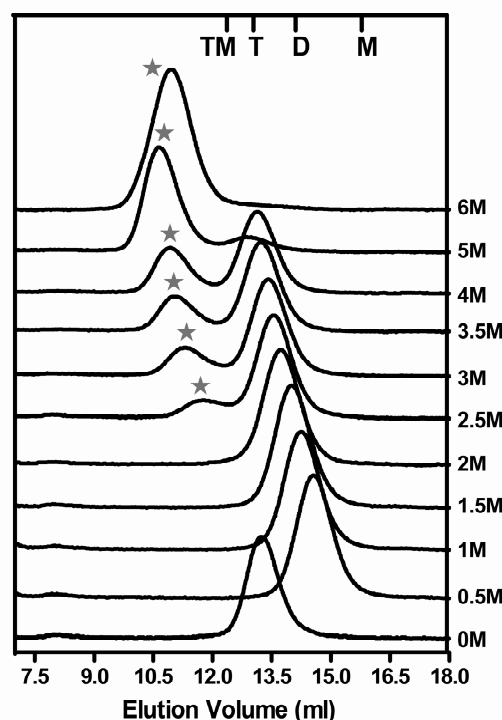


Figure 3.9: Size exclusion chromatography profile of MjAdSS at different GdmCl concentrations, to monitor changes in quaternary structure of the protein with increasing GdmCl concentration. The expected elution volumes (deduced from calibration curve using protein markers) for the different oligomeric forms of MjAdSS are indicated at the top of the panel. Grey stars mark the unfolded monomeric species. TM, tetramer; T, trimer; D, dimer and M, monomer.

(ii) Intrinsic tryptophan fluorescence

Changes in tertiary/quaternary structure of MjAdSS as a function of GdmCl concentration were monitored as change in intensity and emission maximum of tryptophan fluorescence. The protein contains two tryptophans per monomer at positions 11 and 19. Excitation at 290 nm resulted in an emission spectrum with maximum at 320 nm, suggesting that both the tryptophans are in relatively hydrophobic environment. Very small wavelength shift was observed between 0-4 M GdmCl concentration, with the emission maximum shifting from 320 to 321.5 nm. Further increase in chaotrope concentration to 5 M lead to a sharp shift in the emission maximum to 345 nm (Figure 3.10). Fully exposed tryptophan residues red shift to 348-356 nm and the observed emission maximum of 345 nm in 6 M GdmCl

solution is indicative of one or both tryptophans still remaining in partially hydrophobic environment. Fluorescence intensity at 320 nm when plotted as a function of GdmCl concentration indicated the presence of a stable intermediate in the unfolding pathway (Figure 3.10).

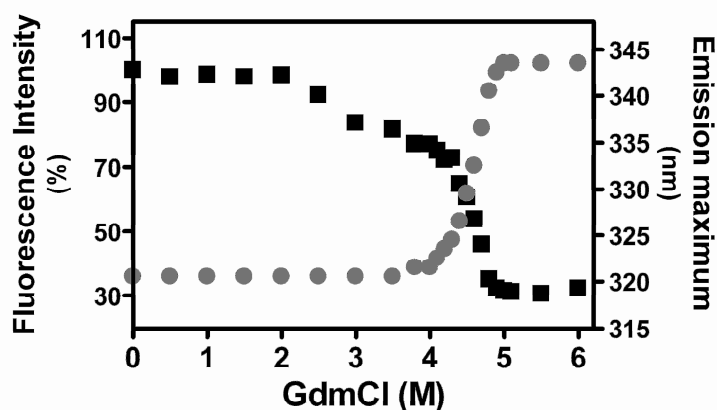


Figure 3.10: GdmCl induced unfolding of MjAdSS monitored by tryptophan fluorescence. Change in fluorescence intensity (■) at 320 nm and emission maxima (●) with increasing denaturant concentration. The fluorescence intensity was normalized by taking the intensity in the absence of denaturant as 100%.

Intrinsic tryptophan fluorescence, however, did not report on the tetramer dissociation of MjAdSS. GdmCl induced transition of MjAdSS involved at least two steps consisting of three stable conformational states; N (native), I (intermediate) and D (denatured). The midpoints (C_m) for the first and second transitions were 2.8 M and 4.6 M GdmCl, respectively. The intermediate state, I, was obtained near 3.75 M GdmCl.

(iii) Circular Dichroism

The far-UV CD spectrum of MjAdSS recorded in Tris HCl, pH 7.4 showed two minima, at 220 nm and 209 nm, characteristic of α -helical proteins (Saxena & Wetlaufer, 1971). CD spectra were recorded at 25°C as a function of GdmCl concentration to assess the effect of the chaotrope on the stability of the secondary

structure of MjAdSS. With increasing denaturant concentration there was loss in ellipticity without significant change in shape of spectrum till 3.75 M GdmCl concentration (Figure 3.11b). The far-UV CD spectrum showed major changes in the region of the second transition (4-5 M GdmCl) indicative of a dramatic loss in secondary structure above 4 M GdmCl concentration, with complete loss in secondary structure seen at 5 M GdmCl.

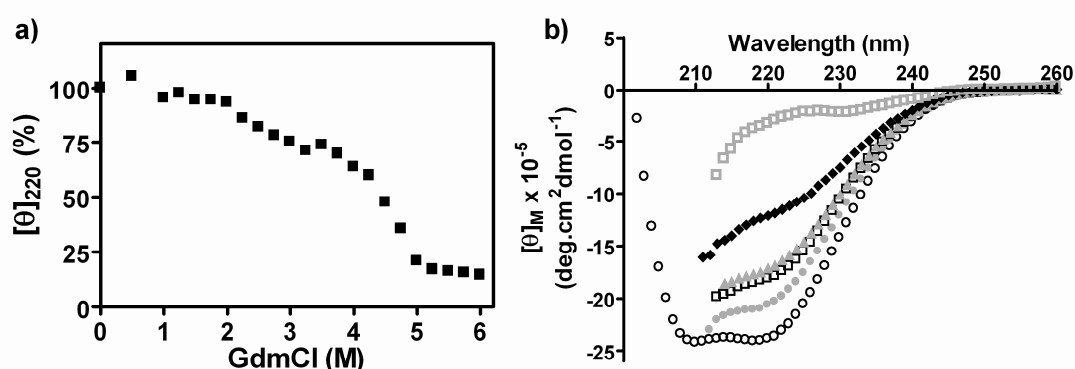


Figure 3.11: GdmCl induced unfolding of MjAdSS monitored by far-UV CD spectroscopy. a) Molar ellipticity of MjAdSS at 220 nm as a function of GdmCl concentration. The ellipticity of the protein at 0 M denaturant concentration was taken as 100%. b) CD spectra of MjAdSS at the following GdmCl concentrations: (o) 0 M, (●) 2.5 M, (□) 3.5 M, (▲) 3.75 M, (◆) 4.5 M and (◻) 6 M GdmCl. Rise in high tension prevented the recording of full spectra.

Figure 3.11a shows ellipticity at 220 nm plotted as a function of GdmCl concentration. The protein resisted change in secondary structure till 2 M GdmCl after which there was gradual unfolding till 3.25 M GdmCl concentration. An intermediate was seen between 3.25-3.75 M GdmCl concentration, after which the protein underwent a sharp unfolding transition between 4-5 M GdmCl. The CD spectrum of the intermediate was characteristic of α -helical protein (Figure 3.11b, MjAdSS spectrum at 3.5 and 3.75 M GdmCl). Like fluorescence, CD measurements also displayed two transitions with the midpoints of the transitions (C_m) being 2.1 M and 4.6 M GdmCl. The data were fit to equations 3-8 to determine the free energy change, ΔG^0 , and the cooperativity index, m , for the two transitions. The free energy changes for the first step of unfolding and for dissociation of dimeric unfolded intermediate to

unfolded monomers were determined to be 4.89 ± 0.38 and 8.47 ± 0.36 kcal mol⁻¹, respectively (Table 3.2).

Table 3.2: Thermodynamic parameters for GdmCl induced unfolding of MjAdSS at pH 7.4 and 25°C.

	N ↔ I	I ↔ D	N ↔ D
<u>Circular Dichroism</u>			
C_m (M)	2.08	4.58	
m (kcal mol ⁻¹ M ⁻¹)	2.19 ± 0.15	1.84 ± 0.08	4.03
ΔG (kcal mol ⁻¹)	4.89 ± 0.38	8.47 ± 0.36	13.36

3.4 Discussion

Two important properties of proteins that enable thermophilic organisms to carry out metabolic processes at high temperatures are, structural stability (includes kinetic and thermodynamic stability) and thermophilicity (exhibit optimum activity between 60-125°C). We have examined these two aspects in adenylosuccinate synthetase from a thermophilic archaea, *M. jannaschii*.

Enzyme activity, in general, increases with temperature which beyond a maximum exhibits a decline due to denaturation of the protein. Arrhenius plots of log k versus $1/T$ permit determination of the activation energy of a reaction. Studies on temperature dependence of catalysis of thermophilic enzymes have often yielded biphasic Arrhenius plots indicating increased activation energies at temperatures below the transition point (Wrba *et al.*, 1990; Lakatos *et al.*, 1978; Witzmann & Bisswanger, 1998; Kohen *et al.*, 1999). Biphasic Arrhenius plots can arise from irreversible enzyme inactivation due to denaturation at high temperatures, subsaturating substrate concentration due to increase in K_m value with temperature, presence of two competing enzyme forms with each dominating in a different temperature range and finally as a consequence of a change in the rate determining step across two temperature ranges (Segel, 1975; Lehrer & Barker, 1970; Levy *et al.*, 1959; Massey *et al.*, 1966; Londesborough, 1980).

AdSS reaction, which results in the formation of sAMP, proceeds through the intermediate 6P-IMP. AdSS from the thermophile, *M. jannaschii*, shows very low level of sAMP formation at mesophilic temperatures. Systematic analysis of MjAdSS catalyzed reaction provides evidence for the reaction intermediate (6P-IMP) formation not being impeded at ambient temperatures under steady-state conditions. Temperature dependence of MjAdSS catalysis exhibited a nonlinear Arrhenius plot, with an inflection at 40°C (Figure 3.1b). This discontinuity was accompanied by a change in the thermodynamic activation parameters ΔH and ΔS around the transition temperature (Table 3.1). Transient kinetics as a function of temperature indicated two distinct rate limiting steps on either side of the transition temperature. At lower temperatures an initial ‘burst’ of product formation implied that product release was rate limiting. Absence of a burst at temperatures close to the transition point in the Arrhenius plot indicates that either catalysis or a preceding step is rate limiting. Infact, at 70°C MjAdSS exhibits rapid equilibrium random AB steady-state ordered C kinetic mechanism implying that E.IMP.GTP.Asp complex formation from E.IMP.GTP is the rate limiting step (Mehrotra & Balaram, 2007).

The presence of burst in rapid kinetics is taken to indicate slow release of products with rapid rates of chemical conversion. In MjAdSS catalyzed reaction the burst corresponds to rapid sAMP formation followed by slow release of product/s. However, the burst could also arise due to rapid formation of 6P-IMP followed by slow aspartate attack. This possibility was ruled out because the burst was fully evident even in reactions where the enzyme was briefly preincubated with IMP and GTP followed by initiation of the reaction with aspartate. The RP-HPLC studies also show the formation of 6P-IMP and GDP in the absence of aspartate even at short time points of 30 seconds. Therefore, the burst in MjAdSS reaction at low temperatures is indicative of slow release of products from the enzyme active site.

Protein dynamics has been implicated to play a key role in substrate binding, product release and even in the process of chemical conversion (Wrba *et al.*, 1990; Zavodszky *et al.*, 1998; Merz *et al.*, 2000; Wolf-Watz *et al.*, 2004; Kohen *et al.*, 1999; Eisenmesser *et al.*, 2005; Hammes-Schiffer & Benkovic, 2006). Crystal structures of liganded and unliganded AdSS from various sources show that there are five loops

which get organised and closed during catalysis (Poland *et al.*, 1996a). The structure of first thermophilic AdSS from *Pyrococcus horikoshii* (PhAdSS), which shares 68% identity with MjAdSS, has the five loops in closed conformation in the absence of substrates (PDB ID: 2D7U, Xie, Y., Kishisita, S., Murayama, K., Shirouzu, M., Yokoyama, S., RIKEN Structural Genomics/Proteomics Initiative (RSGI), Crystal structure of hypothetical adenylosuccinate synthetase, PH0438 from *Pyrococcus horikoshii* OT3) (Figure 3.12). The enzyme at any temperature would be an equilibrium mixture of open and closed conformations, with one or more specific forms favoured at different temperatures. Catalysis requires loop closure that is triggered by substrate binding. Presence of products in the active site pocket leads to stabilization of loop closed conformation of the protein by two sets of interaction, one being interactions of the loops with other segments of the protein and the second involving interactions with the bound products. The reduced rate of catalysis of MjAdSS at low temperatures could arise from the hindered loop movements that prevent product release from the active site and hence hamper subsequent rounds of catalysis. However, with increasing temperature conformational flexibility increases leading to increased catalytic rates. Examination of the sequence and structure of the ligand binding loops in *M. jannaschii* and *P. horikoshii* AdSS did not show any gross changes from that of mesophilic enzymes. The high temperature optima for catalysis must arise from increased dynamics in other regions of the protein influencing the movement of ligand binding loops. Studies on indoleglycerol phosphate synthase from the hyperthermophile, *Sulfolobus solfataricus* and adenylate kinase from *Aquifex aeolicus* highlighted similar mechanisms modulating the temperature dependence of activity in these enzymes (Merz *et al.*, 2000; Wolf-Watz *et al.*, 2004). NMR relaxation experiments on thermophilic adenylate kinase, demonstrated the opening of nucleotide-binding lids, to be rate limiting at ambient temperatures (Wolf-Watz *et al.*, 2004). Further, in an attempt to convert indoleglycerol phosphate synthase from *S. solfataricus* to an enzyme with high activity at mesophilic temperatures, random mutagenesis was used to produce active protein variants. The mutations mapped to sites which resulted in increased flexibility of the loops that

otherwise obstructed the active site or loosened the phosphate binding site thereby facilitating product release (Merz *et al.*, 2000).

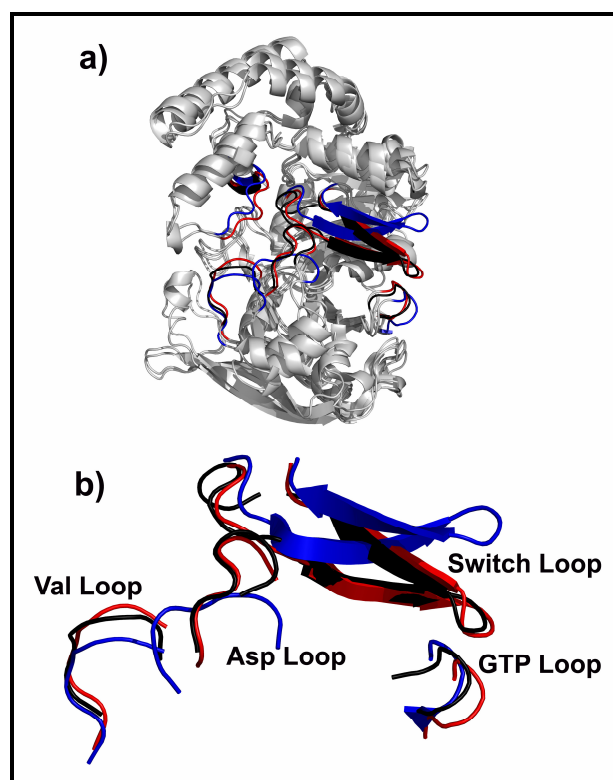


Figure 3.12: a) Superposition of *E. coli* unliganded (PDB ID: 1ADE), fully liganded (6P-IMP, GDP, hadacidin, Mg^{2+} complex, PDB ID: 1CG0) and *P. horikoshii* unliganded (PDB ID: 2D7U) AdSS structures. Loops that respond to substrate binding are highlighted in blue (*E. coli* unliganded AdSS), red (*E. coli* liganded AdSS) and black (*P. horikoshii* unliganded AdSS). b) Closer view of the catalytic loops. *E. coli* liganded and *P. horikoshii* unliganded AdSS exhibit better superposition when compared to *E. coli* unliganded structure. The figure was generated using PyMOL (DeLano, 2002).

Another vital property of thermophilic proteins is their ability to maintain native folded structure in extreme environments. Enhanced stability of protein molecules involves only a marginal increase in free energy, equivalent to a small number of interactions which include a few hydrogen bonds, hydrophobic interactions or ion pairs (Jaenicke, 1991; Jaenicke & Bohm, 1998). The conformational stability of proteins can be studied by thermal melting and equilibrium unfolding in urea and GdmCl solutions. The thermal unfolding of MjAdSS was only partially reversible and hence, did not permit determination of thermodynamic parameters. The tertiary and

secondary structure of MjAdSS does not collapse even in 8 M urea solution. Although the tetramer of MjAdSS dissociates at 0.5 M GdmCl, changes in the dimer and overall secondary structure become evident only at 2 M denaturant concentration. The unfolding probed by both intrinsic tryptophan fluorescence and circular dichroism spectroscopy indicates that the denaturation profile is biphasic with a stable intermediate detected around 3.75 M GdmCl. The denaturation profile of MjAdSS can be schematically represented as shown in Figure 3.13.

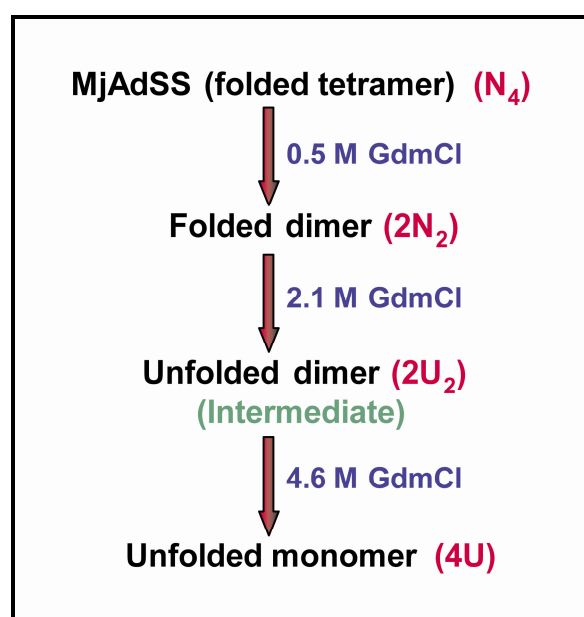


Figure 3.13: Schematic representation of MjAdSS unfolding pathway in GdmCl solution.

Ignoring the tetramer dissociation which occurs at very low GdmCl concentration, the scheme implies a coupled equilibria between natively folded (N), intermediate (I) and unfolded (U) species. Taken together, the size exclusion chromatography, fluorescence and far-UV CD measurements show that the first transition corresponds to dimer unfolding, with the second transition corresponding to dimer dissociation resulting in unfolded monomers. However, both CD and fluorescence were insensitive to tetramer dissociation. Thermodynamic parameters associated with GdmCl induced unfolding of MjAdSS monitored by CD spectroscopy, are listed in Table 3.2. Native MjAdSS is $4.9 \text{ kcal mol}^{-1}$ more stable than the intermediate which in turn is $8.5 \text{ kcal mol}^{-1}$ more stable than the unfolded protein.

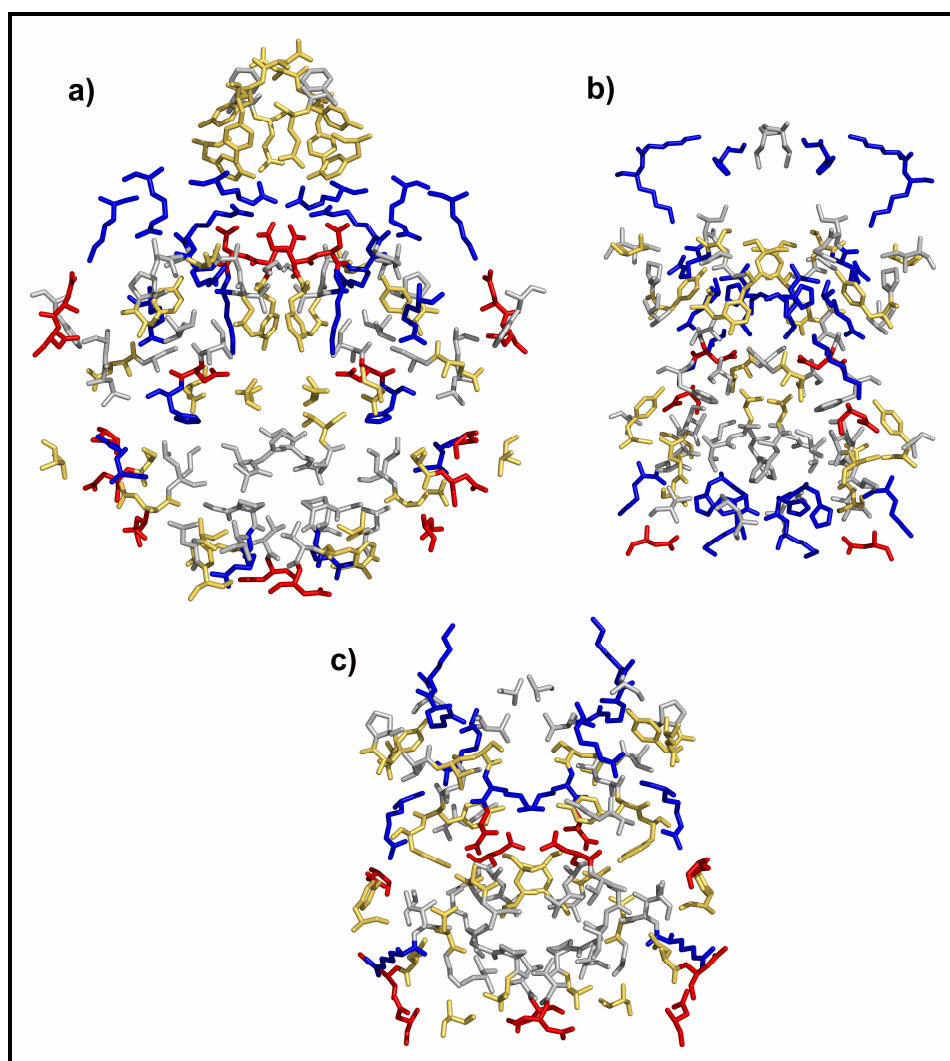


Figure 3.14: Residues at the dimer interface of a) *E. coli* (PDB ID: 1CG0), b) *P. falciparum* (PDB ID: 1P9B) and *P. horikoshii* (PDB ID: 2d7U) AdSS. Blue, red, yellow and grey represent positive, negative, polar and uncharged residues, respectively. The figure was generated using PyMOL (DeLano, 2002).

To elucidate the structural features contributing to enhanced stability of MjAdSS dimer, the dimer interface in MjAdSS was examined. The conservation of interface residues across *P. horikoshii* and MjAdSS enabled conclusions to be drawn based on the available structure of *P. horikoshii* AdSS (PhAdSS). The interface in MjAdSS is largely polar showing absence of large hydrophobic patches. *P. falciparum* and mouse AdSS have a more extensive dimer interface compared to MjAdSS, although regions contributing to the interface remain largely conserved

(Figure 3.14). However, a significantly larger number of hydrogen bonds, salt bridges and π -cation interactions stand out in MjAdSS when compared to the mouse, *E. coli* or *P. falciparum* enzymes. These interactions could be playing a key role in the remarkable stability of MjAdSS dimer and such interactions have been implicated in the stability of other thermophilic proteins too (Wrba *et al.*, 1990; Vieille & Zeikus, 2001; Vogt *et al.*, 1997; Karshikoff & Ladenstein, 2001). The presence of a stable dimeric intermediate on the unfolding pathway indicates that the subunit interactions that hold the MjAdSS dimer are particularly strong and remain intact even when peripheral portions of the protein begin to unfold.

In summary, this is the first report on the biochemical characterization of a small thermostable AdSS. This enzyme is useful for studying the interdependence of structural stability and dynamics, and their influence on catalysis. The increased thermostability of MjAdSS cannot be attributed to its smaller size as compared to Clade 1 AdSS because certain thermophiles also have full length AdSS. However, it would be interesting to examine the role of the deletions in the context of the non-enzymatic function of AdSS associated with the binding of autonomously replicating DNA sequences, as seen in yeast AdSS (Zeidler *et al.*, 1993).

Chapter 4

Studies on Active Site Mutants of *P. falciparum* Adenylosuccinate Synthetase: Insights into Enzyme Kinetics and Activation

*This chapter discusses the biochemical characterization of *P. falciparum* AdSS mutants with an aim to understand two unique features of the parasite enzyme, namely, ordered kinetic mechanism and activation by the glycolytic intermediate, fructose 1,6 bisphosphate. Two conserved (Arg155 and Thr309) and three nonconserved residues (Asn429, Lys62 and Thr307) were mutated and the impact on enzyme structure and function examined. Biochemical and biophysical characterization of the mutants resulted in the elucidation of the role of these residues in modulating structural stability, catalysis and substrate affinity of PfAdSS. Molecular docking studies along with activation kinetics of the mutants, provide insight into the possible mode of activation of PfAdSS by fructose 1,6 bisphosphate.*

4.1 Introduction

Adenylosuccinate synthetase catalyzes the condensation of IMP with aspartate to form adenylosuccinate (sAMP), in a reaction that is Mg^{2+} dependent and involves the conversion of one molecule of GTP to GDP. This is the first reaction that commits IMP to the formation of AMP and hence plays an important role in purine nucleotide biosynthesis.

<i>S. citri</i>	QWGDEGKGGKITDYFAQQADLIVRWAG..GDNAGHTIV
<i>H. pylori</i>	QWGDEGKGGKIVDRIAKDYDFVVRVYQG..GHNAGHTIV
<i>S. cerevisiae</i>	QWGDEGKGGKLVDLLVGKYDIVARCAG..GNNAGHTIV
<i>C. albicans</i>	QWGDEGKGGKLVDLLCDDIDVCARCQG..GNNAGHTIV
<i>Mus musculus</i>	QWGDEGKGGKVVDLLATDADIVSRCQG..GNNAGHTVV
<i>Homo sapiens</i>	QWGDEGKGGKVVDLLAQDADIVCRCQG..GNNAGHTVV
<i>A. niger</i>	QWGDEGKGGKITDMLAQQATLCCRAAG..GHNAGHTIV
<i>A. thaliana</i>	QWGDEGKGGKLVDDILAQHFDIVARCQG..GANAGHTIY
<i>Zea mays</i>	QWGDEGKGGKLVVDLAPRFDIVARCQG..GANAGHTIY
<i>D. discoideum</i>	QWGDEGKGGKLVDDILSQQFDVVARCQG..GANAGHTIV
<i>P. falciparum</i>	QWGDEGKGGKIIDMLSEYSDITCRFNG..GANAGHTIS
<i>E. coli</i>	QWGDEGKGGKIVDLLTERAKYVVRVYQG..GHNAGHTLV
<i>H. influenzae</i>	QWGDEGKGGKIVDLLTDRVKYVVRVYQG..GHNAGHTLI
<i>V. cholerae</i>	QWGDEGKGGKIVDLLTEDAKYVVRVYQG..GHNAGHTLV
<i>A. vinelandii</i>	QWGDEGKGGKIVDLLTDQAAAVVRVYQG..GHNAGHTLV
<i>L. pneumophila</i>	QWGDEGKGGKIVDLLTQDAQVVRVYQG..GHNAGHTLK
<i>B. subtilis</i>	QWGDEGKGGKITDFLSENAEVIARYQG..GNNAGHTIK
<i>B. licheniformis</i>	QWGDEGKGGKITDFLSENAEVIARYQG..GNNAGHTIK
<i>C. botulinum</i>	QWGDEGKGGKMTDYLAENADVVRVRFQG..GNNAGHTVV
<i>M. leprae</i>	QWGDEGKGGKVTDLLGGRAQVVRVYQG..GNNAGHTVV
<i>Methanosarcina</i>	QFGDEGKGGKIVDLLAKDYDIVARFQG..GNNAGHTVR
<i>M. mazei</i>	QFGDEGKGGKIVDLLAKDYDVVRVRFQG..GNNAGHTVK
<i>A. fulgidus</i>	FWGDEGKGGKIVAHVAHSDKPVIIARGGVGPNAGHTVE
<i>M. jannaschii</i>	QWGDEGKGGKIIISYICDKDKPSIIARGGVGPNAGHTVN
<i>P. furiosus</i>	QWGDEGKGSIIAYLALHDEPEIIARGGVGTNAGHSVV

Figure 4.1: Conservation of catalytic base (aspartic acid) and catalytic acid (histidine), highlighted in yellow, across AdSS from different organisms. Other conserved residues in the vicinity are boxed in blue. The alignment was generated using CLUSTAL W (Thompson *et al.*, 1994) and represented using ESPRIPT (Gouet *et al.*, 1999).

Adenylosuccinate synthetase mediated conversion of IMP to sAMP occurs by a two step process involving acid base catalysis. The catalytic base (Asp13, in *E. coli* AdSS) abstracts a proton from the N1 atom of IMP, resulting in the formation of 6-oxyanion of IMP, which then displaces GDP from the γ -phosphate of bound GTP to form 6-phosphoryl IMP (6P-IMP). Mg^{2+} and the catalytic acid (His41, in *E. coli* AdSS) play an important role in stabilizing the charge developed on the β and γ phosphates of GTP in the transition state. Mg^{2+} does this by coordinating to the bridging oxygen atom between the β - γ phosphoryl groups and histidine, by protonating the β -phosphoryl group of GDP. After formation of 6-phosphoryl IMP, Asp13 moves into the co-ordination sphere of the catalytic Mg^{2+} . As a consequence Asp13 becomes a catalytic acid and reprotonates the N1 position of 6-phosphoryl

IMP, thereby generating the C6 cation of the intermediate. Binding of aspartate initiates the next step of catalysis. Nucleophilic attack by the α -amino group of aspartate on C6 of 6-phosphoryl IMP displaces the phosphate group leading to the formation of adenylosuccinate. The catalytic histidine stabilizes the charge on the leaving group by transferring a proton to the 6-phosphoryl group (Poland *et al.*, 1996a; Poland *et al.*, 1997). The catalytic acid and base in AdSS are absolutely conserved (Figure 4.1) and mutation of Asp13 to Ala and His41 to Asn in *E. coli* AdSS leads to complete inactivation of the enzyme (Kang *et al.*, 1997).

4.1.1 Ligand binding pockets: A comparison of *E. coli* and *P. falciparum* enzymes

The interactions of the ligands with the protein are largely conserved across similarly liganded structures of *P. falciparum* and *E. coli* AdSS (6P-IMP, Mg²⁺, GDP and hadacidin complex). Residues that lie within 3.5Å of the ligands are shown in Figures 4.2, 4.3 and 4.4. The active site in AdSS is located at the dimer interface and is comprised of residues from both subunits.

6P-IMP makes extensive contacts with the protein including an arginine residue from the symmetry related subunit (Figure 4.2). The minor differences seen in the contacts of this ligand across *P. falciparum* and *E. coli* enzymes disappear if the distance cut off is set at 4 Å, implying that 6P-IMP contacts are conserved across the bacterial and parasite AdSS.

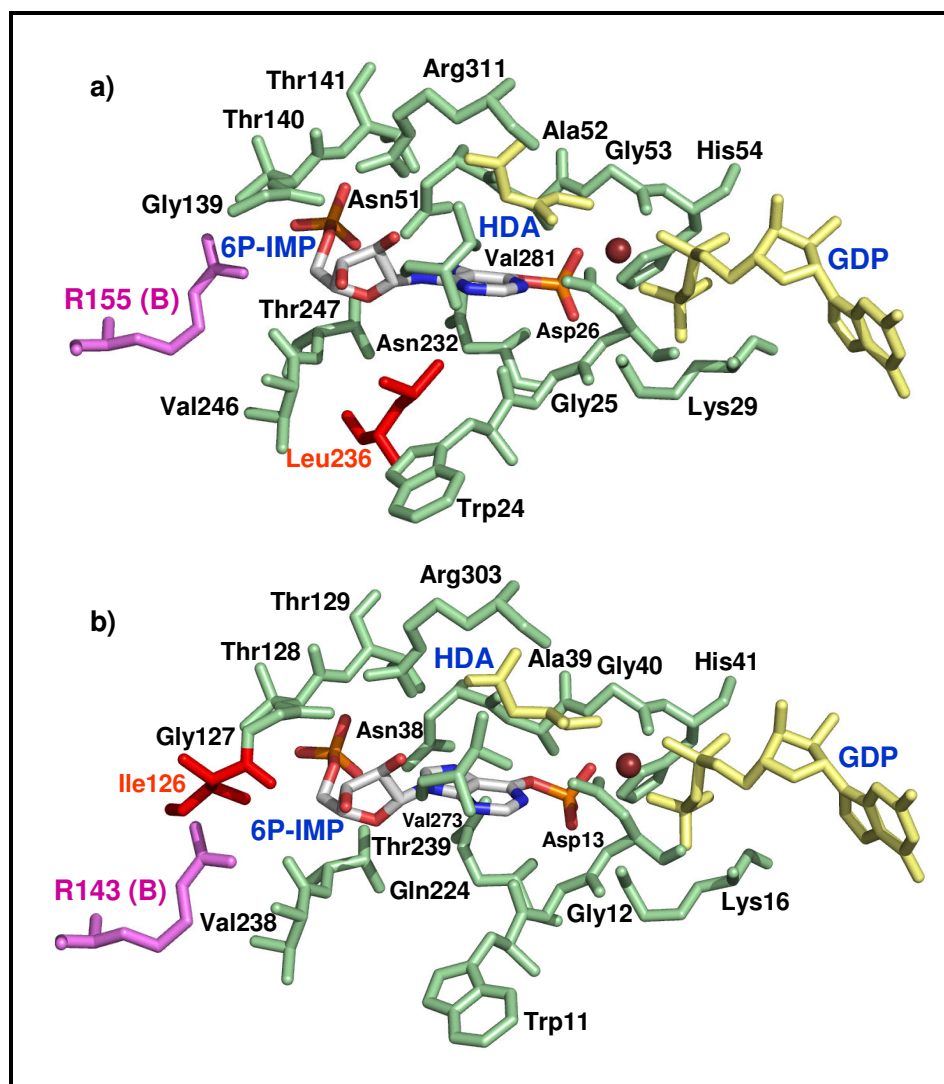


Figure 4.2: 6P-IMP contacts in a) *P. falciparum* (PDB ID: 1P9B) and b) *E. coli* (PDB ID: 1CG0) AdSS. Residues within 3.5Å of the ligand are shown. 6P-IMP is represented in CPK and the other ligands are shown in yellow. The red sphere denotes Mg²⁺. The residues common to both the structures are shown in green while the residues unique to either enzyme are shown in red. Arginine residue from the symmetry related subunit is shown in pink. The figure was generated using PyMOL (DeLano, 2002).

Unlike IMP, significant variations are seen in the interactions of GDP with the polypeptide in *E. coli* and *P. falciparum* structures (Figure 4.3). Gly425 in PfAdSS is a serine (Ser414) in the *E. coli* enzyme. The side chain hydroxyl group of Ser414 interacts with 6-oxo group of the guanine base in *E. coli* AdSS (Poland *et al.*, 1996a). The cavity created by serine to glycine substitution in PfAdSS is occupied by a water

molecule which hydrogen bonds to both N7 and O6 of GDP and hence mimics OG of Ser414 (Eaazhisai *et al.*, 2004). Further, Val246 which is a threonine in *E. coli* AdSS and Pro428 and Lys31 in PfAdSS which correspond to Pro417 and Lys18 in *E. coli* AdSS, respectively, lie within 4Å from GDP.

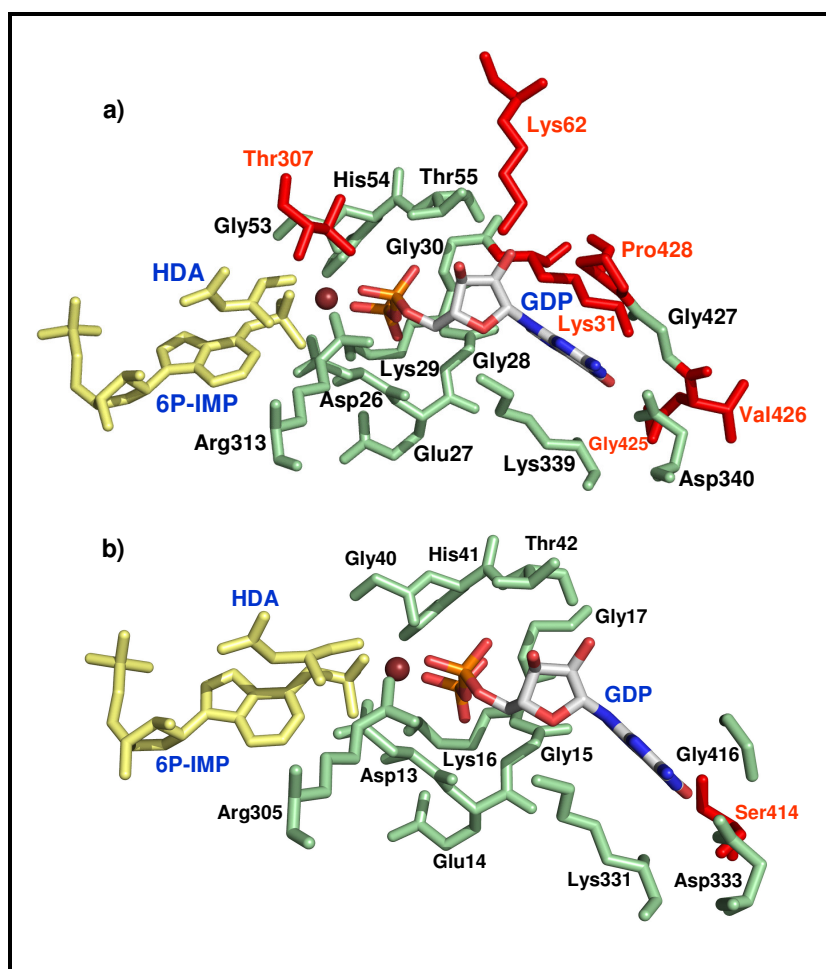


Figure 4.3: GDP contacts in a) *P. falciparum* (PDB ID: 1P9B) and b) *E. coli* (PDB ID: 1CG0) AdSS. Residues within 3.5Å of the ligand are shown. GDP is represented in CPK and the other ligands are shown in yellow. The red sphere denotes Mg^{2+} . The residues common to both the structures are shown in green while the residues unique to either enzyme are shown in red. The figure was generated using PyMOL (DeLano, 2002).

However, there are two unique hydrogen bonds that GDP makes in PfAdSS which are absent in *E. coli* and mouse AdSS structures. OG of Thr307 forms a hydrogen bond with O2A of GDP. The corresponding residues in mouse and *E. coli* AdSS are valine and alanine, respectively. Similarly, Lys62 forms hydrogen bonds

with ribose hydroxyls of GDP, an interaction that is absent in other AdSS. The corresponding residues in mouse and *E. coli* AdSS are Glu79 and Lys49, respectively. Lys49 in the *E. coli* enzyme lies at a distance greater than 5Å from ribose hydroxyls of GDP.

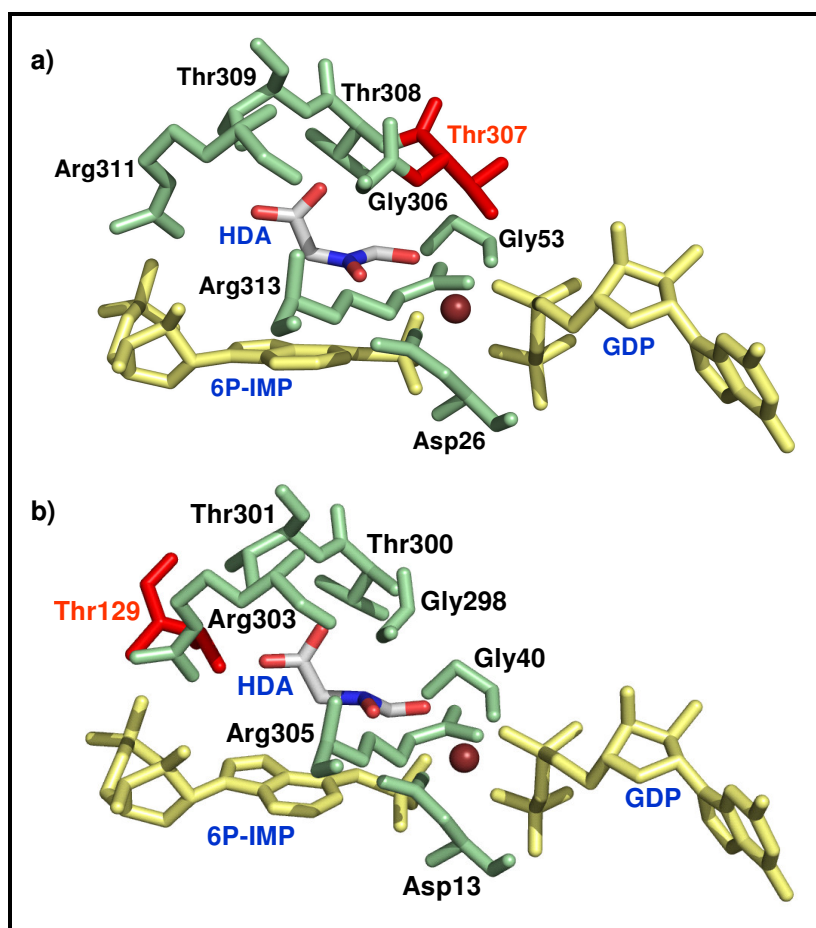


Figure 4.4: Hadacidin (HDA) contacts in a) *P. falciparum* (PDB ID: 1P9B) and b) *E. coli* (PDB ID: 1CG0) AdSS. Residues within 3.5Å of the ligand are shown. Hadacidin is represented in CPK and the other ligands are shown in yellow. The red sphere denotes Mg²⁺. The residues common to both the structures are shown in green while the residues unique to either enzyme are shown in red. The figure was generated using PyMOL (DeLano, 2002).

Hadacidin, which is an aspartic acid analog, mainly interacts with Asp26, which is the catalytic base in PfAdSS, and the residues in the aspartate loop (residues 306-312), which is one of the dynamic loops in AdSS that gets organized in response to aspartate binding to the enzyme (Figure 4.4). OG of Thr307 interacts with an

oxygen atom of hadacidin. This interaction is absent in both mouse and *E. coli* AdSS where Thr307 is replaced by valine and alanine, respectively. Thr307 also hydrogen bonds to Arg313, which lies at the hinge of the aspartate loop. These interactions of Thr307 with hadacidin and Arg313 may aid in substrate binding and proper orientation of the aspartate loop.

4.1.2 Dynamic loops in adenylosuccinate synthetase

Adenylosuccinate synthetase employs dynamic loops in catalysis. The first crystal structure of unliganded *E. coli* AdSS showed regions of structural disorder which clustered around the putative active site cavity. These regions included stretches of residues from 42-49, 121-129, 298-304 and 355-363. These residues were speculated to lie in segments that undergo a conformational change on substrate binding (Poland *et al.*, 1993). The structure of *E. coli* AdSS complexed with GDP, IMP, hadacidin, NO³⁻ and Mg²⁺, indeed showed that the above mentioned segments get ordered as a consequence of substrate binding to the enzyme (Poland *et al.*, 1996a).

```

P.falciparum  . . . . .MNIFDHQIK
Mousebasic   . . . . .MSGTRASNDRPPGTGGVKGRLQQEA
A.thaliana   MSLSSLTLDSNPRFAVGGPYHRRYPPLHHPRSFVSCSAKRPAVSASLSVAADSAATESLGR
E.coli       . . . . .
P.horikoshii . . . . .

```

```

                                A (P-loop)                                Switch Loop
P.falciparum  NVDKGNVVAILGAQWGDEGKGIIIDMLSEY..SDITCRFNGGANAGHTISVN.DKKYALHL
Mousebasic   AATGSRVTVVLGAQWGDEGKGVVVDLLATD..ADIVSRCQGGNNAGHTVVVD.GKEYDFHL
A.thaliana   IGSLSQVSGVLGCQWGDEGKGLVLDILAQH..FDIVARCQGGANAGHTIYNSEGKKFALHL
E.coli       ...MGNNVVVLGTQWGDEGKGIIVDLLTER..AKYVVRYQGGHNAGHTLVIN.GEKTVLHL
P.horikoshii ...MPSVIVVGGQWGDEGKGSIVAYLSLHDEPEIIARGGVGTNAGHSVVIN.GKKYAVRQ
                * * * * * * * * * * * * * * * * * * * * * * * * * * * *

```

```

P.falciparum  LPCGVLYDNNISVLGNGMVIHVKSLMEEIESVGGKLLD...RLYLSNKAHILFDIHQIID
Mousebasic   LPSGIINTKAVSFIGNGVVIHLPGLFEEAEKNEKKGLKDWEKRLIISDRAHLVDFHQAVD
A.thaliana   VPSGILNEDTTCVINGVVVHLPGLFKEIDGLESNGVSCGK.RILVSDRAHLLVDFHQEVD
E.coli       IPSGILRENVTSIINGVVLSPAALMKEMKELEDRGIPVR.ERLLLSEACPLILDYHVALD
P.horikoshii IPTGFMQTKARLLIGAGVLVDPEVFFHELEQLKDFNVKDR...VGIDYRCAIIEEKHKQLD
                * * * * * * * * * * * * * * * * * * * * * * * * * * * *

```

```

                                IMP Loop
P.falciparum  SIQETKKLK.EGKQIGTTKRGIGPCYSTKASRIGIRLG.TLKNFENFKNMYSKLIDHLMDL
Mousebasic   GLQEVQRQAQEGKNIGTTKKGIGPTYSSKAARTGLRICDLLSDFDEFSARFKNLAHQHQS
A.thaliana   GIRESELAK...SFIGTTKRGIGPAYSSKVIIRNGIRVG.DLRHMDTLPQKLDLLSDAAR
E.coli       NAREKARGA...KAIGTTGRGIGPAYEDKVARRGLRVGDLFDKETFAEKLKEVMEYHNFQL
P.horikoshii RTNGYLHGK...IGTTGSGCGPANADRVMRK.....
                * * * * * * * * * * * * * * * * * * * * * * * * * * * *

```


does not organize the loops in mouse and *E. coli* AdSS (Poland *et al.*, 1996c; Iancu *et al.*, 2002).

Figure 4.5, shows the segments that constitute the dynamic loops in AdSS (highlighted in yellow). The nomenclature proposed by Iancu *et al.* has been followed (Iancu *et al.*, 2002). As evident from the alignment, the loop residues are not absolutely conserved across different organisms. These variations, may indeed account for the observed differences in kinetic mechanism, substrate affinity and modes of regulation of the enzyme from different sources.

4.1.3 Mutational analysis

Extensive mutational analysis by Fromm and co-workers has enabled mapping of functionally important residues in *E. coli* adenylosuccinate synthetase (Table 4.1). These include residues involved in catalysis, ligand binding and also those involved in stabilizing the transition state. The following section discusses the role of certain conserved residues in modulating the substrate affinity and catalytic activity of *E. coli* AdSS, as inferred by site directed mutagenesis. The residue numbering in the following discussion corresponds to the *E. coli* AdSS sequence.

Adenylosuccinate synthetase contains stretches of residues in its GTP binding domain that are homologous to other guanine nucleotide binding proteins belonging to the GTPase superfamily. These include a glycine-rich phosphate binding loop, GXXXXGK, near the N-terminus of the protein, a nucleotide-phosphate binding region (D/E)XX(G/A) and a guanine-specific binding motif (N/T/Q)KXD (Dever *et al.*, 1987; Bourne *et al.*, 1991) (Figure 4.5). Apart from the above sequences, very little sequence similarity exists between AdSS and other G-proteins. The N-terminal glycine rich sequence, GDEGKGK (P-loop, Residue 12-18), in *E. coli* AdSS is homologous to the conserved sequence, GXXXXGK, found in many guanine nucleotide binding proteins. This sequence has been implicated in GTP binding in many proteins which use GTP as a substrate (Saraste *et al.*, 1990). To study the structural and functional role of the residues in P-loop of adenylosuccinate synthetase from *E. coli* the following five mutants were constructed; G12V, G15V, G17V, K18R

and I19T. Kinetic characterization of the glycine and K18R mutants showed that these mutations result in dramatic drop in k_{cat} value of the enzyme, with no significant affect on GTP K_m value, indicating that in AdSS these residues play a more important role in catalysis than in substrate binding (Liu *et al.*, 1992). Further studies with Gly15 mutant showed that the phosphate binding loop (P-loop) in AdSS may be involved in conformational changes that accompany the binding of the nucleotide substrates (Kang & Fromm, 1994). This is quite unlike the role proposed for this loop in other GTP utilizing proteins. In other G-proteins, a threonine or serine residue follows the conserved lysine in the sequence GXXXXGK. However, in AdSS this residue is a valine, isoleucine or leucine. Mutation of Ile18 to threonine, resulted in a 160-fold increase in GTP K_m value, implying that a hydrophobic residue that this position may play a critical role in GTP binding to AdSS (Liu *et al.*, 1992). Further, mutation of Lys16 to glutamine resulted in a reduction in catalytic efficiency of the enzyme with no significant change in substrate affinity (Kang *et al.*, 1997). The NZ atom of Lys16 interacts with the β - and /or γ -phosphoryl groups of GTP. The corresponding mutation in p21^{ras} (K16N) drastically reduced the affinity for guanine nucleotides and the corresponding mutant of *E. coli* adenylate kinase (K13Q) exhibited significantly lower catalytic activity with only modest effect on substrate affinity (Saraste *et al.*, 1990). Mutation of Lys331, found in guanine specific binding region (N/T/Q)KXD), to leucine and arginine, resulted in an increase in GTP K_m value implicating the role of this residue in GTP binding (Kang & Fromm, 1994). Mutation of the conserved aspartic acid residue (Asp333) in the above consensus sequence to asparagine, glutamate and glutamine, resulted in decreased k_{cat} value and increased K_m values for GTP. The mutants exhibited higher affinity for XTP and ITP when compared to the wild type protein. This suggested the role of Asp333 in catalysis as well as a determinant of nucleoside triphosphate specificity in *E. coli* AdSS (Kang *et al.*, 1994).

Aspartate binding to *E. coli* AdSS was found to be sensitive to mutations at position 303, 304 and 305. Mutation of arginine residues at these positions to leucine resulted in 10-100 fold drop in k_{cat} value and a 50-300 fold increase in the aspartate K_m values, implicating the role of these residues in catalysis as well as aspartate

binding (Wang *et al.*, 1995). Mutation of Arg131 to leucine also resulted in reduction in affinity for aspartate probably as a consequence of its role in stabilizing the closed conformation of the aspartate loop in *E. coli* AdSS (Kang *et al.*, 1997). Though Val273 and Thr300 do not hydrogen bond with aspartate, mutation of these residues also resulted in an increase in K_m value for aspartate (Gorrell *et al.*, 2002). Another important residue involved in aspartate binding is Thr301, which forms hydrogen bonds with the carboxyl group of hadacidin. Mutation of Thr301 to alanine completely abolished catalysis with L-aspartate. However, the kinetic parameters of this mutant were comparable to the wild type enzyme when hydroxylamine was used in place of aspartate (Gorrell *et al.*, 2002).

Mutation of two conserved threonines, Thr128 and Thr129, which interact with 5'-phosphoryl group of IMP, resulted in increase in IMP K_m value for the mutants (Gorrell *et al.*, 2002). Chemical modification studies with phenylglyoxal followed by site directed mutagenesis suggested a critical role for Arg147 in catalysis. Mutation of Arg147 to leucine resulted in increased Michaelis constants for the nucleotide substrates (4-6 fold) and a dramatic reduction in k_{cat} value (1.3×10^4 fold) (Dong *et al.*, 1991). Similar modification studies using pyridoxal 5'-phosphate followed by site directed mutagenesis suggested an important role for Lys140 in enzyme activity (Dong & Fromm, 1990).

Since AdSS undergoes large conformational changes on ligand binding, the effect of a mutation cannot be easily anticipated on the basis of available structural information. This feature was highlighted in several site directed mutagenesis studies with *E. coli* AdSS. Asp21, Asn38, Thr42 and Arg419, though not involved in the chemical mechanism of adenylosuccinate synthetase, are well conserved across different organisms. Mutation of Thr42, which forms hydrogen bonds with α -phosphoryl group of guanine nucleotide, to Ala resulted in significant increase in K_m value for all substrates. Mutation of Asn38 which interacts with 5'-phosphoryl group of IMP, to alanine and glutamate, had no effect on K_m value for the substrates but resulted in 200 and 30-fold drop in k_{cat} value of the mutant enzymes, respectively. The interaction between IMP and Asn38 has been implicated in enabling a conformational change in the switch loop on ligand binding. Mutation of Asp21 to Ala and Arg419 to

Leu resulted in 20 and 10 fold drop in k_{cat} values, respectively. These results implicate the role of Asp21 and Arg419 in stabilization of the transition state (Wang *et al.*, 1998). Gln34, Gln224, Leu228 and Ser240 are conserved residues that lie in the vicinity of bound IMP in the crystal structure of *E. coli* AdSS. Mutational analysis revealed that neither Leu228 nor Ser240 play essential roles in catalysis or substrate binding. Gln224 forms hydrogen bonds with N7 and O6 of IMP. In addition to an increase in K_m value for IMP in Q224M mutant, the dramatic drop in catalytic efficiency of Q224M, Q224E and Q34E mutants implicates the role of Q224 and Q34 in catalysis (Wang *et al.*, 1997b).

Glu14 in *E. coli* AdSS makes hydrogen bonds with backbone amides of residues 10 and 12 of the P-loop and Lys16 side chain and in turn stabilizes the P-loop conformation. Mutation of Glu14 to alanine resulted in dramatic loss in enzyme activity probably as a consequence of perturbation of P-loop conformation which in turn leads to conformational perturbation of the catalytic aspartic acid that lies in the P-loop (Kang *et al.*, 1997).

A study involving mutation of two interface residues, Asp231 and Arg143, showed that the dimer is the catalytically active form of AdSS and that the enzyme dimerizes in response to the active site ligands. Asp231 by hydrogen bonding to Arg147 and Lys140 of the 2-fold related subunit and Arg143 by hydrogen bonding to IMP in the active site of the symmetry related subunit help in holding the subunits in close contact. Mutation of Arg143 to leucine and lysine and Asp231 to alanine resulted in increase in K_m values for IMP and GTP, while the k_{cat} and K_m values for aspartate were similar to the wild type protein. The mutants, like the wild type enzyme, existed predominantly in the monomeric state in the absence of ligands. In the presence of active site ligands the wild type enzyme shifted completely to a dimer with the mutants showing only slight reduction in dissociation constant for dimerization (Wang *et al.*, 1997a).

Table 4.1: Elucidation of the functional role of residues in *E. coli* AdSS by site-directed mutagenesis. The corresponding residues in *P. falciparum* and mouse AdSS are also listed. The non-conserved residues are highlighted in bold.

Residue mutated in <i>E. coli</i> AdSS	Corresponding residue in PfAdSS	Corresponding residue in mouse enzyme
Gly12	Gly25	Gly42
Asp13	Asp26	Asp43
Glu14	Glu27	Glu44
Gly15	Gly28	Gly45
Lys16	Lys29	Lys46
Gly17	Gly30	Gly47
Lys18	Lys31	Lys48
Ile19	Ile32	Val49
Asp21	Asp34	Asp51
Gln34	Asn47	Gln64
Asn38	Asn51	Asn68
Thr42	Thr55	Thr72
Thr128	Thr140	Thr162
Thr129	Thr141	Thr163
Arg131	Arg143	Lys165
Arg143	Arg155	Arg177
Arg147	Arg159	Arg181
Gln224	Asn232	Asn256
Leu228	Leu236	Leu260
Asp231	Asp239	Asp263
Ser240	Ser248	Ser272
Val273	Val281	Val305
Thr300	Thr308	Thr332
Thr301	Thr309	Thr333
Arg303	Arg311	Arg335
Arg304	Pro312	Lys336
Arg305	Arg313	Arg337
Lys331	Lys339	Lys363
Asp333	Asp341	Asp365
Arg419	Arg430	Arg450

4.1.4 Kinetic mechanism of adenylosuccinate synthetase

Variation in kinetic mechanism of AdSS from different organisms has been reported. Initial velocity kinetics and product inhibition studies have been extensively used to elucidate the kinetic mechanism of AdSS from various sources. Based on these studies a rapid equilibrium random sequential mechanism has been proposed for *E. coli*, *Azotobacter vinelandii*, rat muscle, human and yeast AdSS (Rudolph & Fromm, 1969; Markham & Reed, 1977; Cooper *et al.*, 1986; Van der Weyden & Kelly, 1974; Nagy *et al.*, 1973). However, kinetic isotope exchange studies with rat muscle AdSS showed preferred binding of aspartate to E.IMP.GTP complex (Cooper *et al.*, 1986). Initial velocity kinetics and product inhibition studies, discussed in Chapter 2, were consistent with a rapid equilibrium random AB steady-state ordered C kinetic mechanism for AdSS from the thermophilic archaea, *M. jannaschii* (Mehrotra & Balaram, 2007). Product inhibition studies showed that substrate binding in PfAdSS is ordered with IMP binding first to the enzyme, followed by GTP and then aspartate (Raman *et al.*, 2004).

4.1.5 Effect of glycolytic intermediates on the activity of adenylosuccinate synthetase

The effect of glycolytic intermediates, glucose, glucose-6-phosphate, fructose-6-phosphate, fructose 1,6 bisphosphate, dihydroxyacetone phosphate, glyceraldehyde-3-phosphate, 2,3 diphosphoglycerate, 3-phosphoglycerate, 2-phosphoglycerate, phosphoenolpyruvate, pyruvate and lactate was tested on rat skeletal muscle adenylosuccinate synthetase. While 15-20% inhibition of enzyme activity was observed at 2 mM concentration of 2,3-diphosphoglycerate, 3-phosphoglycerate, 2-phosphoglycerate and phosphoenolpyruvate, 2 mM fructose 1,6 bisphosphate resulted in 80% inhibition of enzyme activity. Noncompetitive inhibition with respect to all three substrates was observed (Ogawa *et al.*, 1976).

Infact, the two isozymes of AdSS, have been assigned to different pathways based on inhibition by fructose 1,6 bisphosphate (F16BP). The basic isozyme exhibits

a higher K_m value for IMP and a lower K_m value for aspartate when compared to the acidic isozyme. While the basic isozyme is more susceptible to inhibition by F16BP, the acidic isozyme is sensitive to inhibition by nucleotides. On the basis of these findings, the basic isozyme was assigned to the purine nucleotide cycle and the acidic isozyme to AMP biosynthesis pathway (Matsuda *et al.*, 1977).

F16BP also inhibited AdSS isolated from Yoshida Sarcoma ascites tumor cells with an IC_{50} value of 0.92 mM (Matsuda *et al.*, 1980). K_i values of 130 μ M and 50-100 μ M were reported for the basic isozyme from rat and rabbit, respectively (Stayton *et al.*, 1983). Noncompetitive inhibition with respect to all substrates has been reported for both the isozymes of mouse AdSS. However, a preliminary crystallographic study by Borza *et al.* showed that F16BP binds to 6P-IMP binding site. Thus, they speculated that at low concentration of IMP, F16BP exhibits competitive inhibition with respect to IMP, but it binds to another site on the enzyme when IMP is saturating (Borza *et al.*, 2003).

Another glycolytic intermediate, phosphoenolpyruvate, was found to be a competitive inhibitor of aspartate in case of *Leishmania donovani* and *Azotobacter vinelandii* AdSS, exhibiting K_i values of 5 and 0.2 mM, respectively (Spector *et al.*, 1979; Markham & Reed, 1977).

This chapter presents results of studies carried out on various mutants of *P. falciparum* adenylosuccinate synthetase to understand two important properties of the parasite enzyme, namely ordered substrate binding and modulation of enzyme activity by the glycolytic intermediate, fructose 1,6 bisphosphate.

4.2 Materials and Methods

All media components were purchased from HiMedia Laboratories (Mumbai, India). Taq DNA polymerase, restriction enzymes and T4 DNA ligase were from Bangalore Genei Pvt. Ltd., (Bangalore, India) and oligonucleotides from Microsynth AG (Balgach, Switzerland). IPTG, substrates and inhibitors used in kinetic studies and protein molecular weight markers were from Sigma Chemical Company

(St.Louis, MO). Akta Basic HPLC, Sephadex G25, Q-sepharose, Sephacryl 200 and Superdex 200 were from Amersham Pharmacia (Uppsala, Sweden). All assays were done using Hitachi U2010 (Hitachi High-Technologies Corporation, Tokyo, Japan) spectrophotometer fitted with a water circulated cell holder. Circular dichroism measurements were performed on a Jasco J-810 spectropolarimeter (JASCO Corporation, Tokyo, Japan) equipped with a Peltier heating system. Fluorescence spectra were recorded on a Hitachi F-2500 spectrofluorimeter (Hitachi High-Technologies Corporation, Tokyo, Japan).

4.2.1 Site-directed mutagenesis

Site-directed mutagenesis was carried out by the megaprimer PCR method (Sarkar & Sommer, 1990). The mutagenic primers used were:

N429V: 5' GGTGTAGGGCCCGTTAGAAAAAATATGATAG 3'

K62L: 5' GTAAAGCATAAAGCTTATCATTACTGATATC 3'

T307V: 5' CATGAATATGGAGGTGACTACTAAGAGACCAAGAAGG 3'

T309V: 5' CATGAATATGGTACCACTGTCAAGAGACCAAGAAGGTG 3'

R155L: 5' CTTATACCTATTAAGGAGGCTTTAGTAG 3'

R155A: 5' CTTATACCTATTGCGGAGGCTTTAGTAG 3'

R155K: 5' CTTATACCTATTTTGCTAGCTTTAGTAG 3'

G146R: 5' AGAATAACATGGTCGAATTCCCTCTTTTTG 3'

These primers along with the end primers (AdSSfl: 5' ACACCATGGCCATATTTGATCATCAAATAAAAAAT 3' and AdSSc: 5' CCAGGTACCCTCGAGTTAGTTTGGTTAAAATTCTT 3') were used to generate the mutants. The mutated codon is shown in bold and underlined in the primer sequence. In addition to the desired mutation the primers also contained a restriction site incorporated by silent mutagenesis, which allowed for selection of the positive clones from the transformants. The sites incorporated were *Apa*I in N429V, *Kpn*I in T309V, *Hind* III in K62L, *Dde*I in T307V, *Nhe*I in R155K and *Eco*R1 in G146R, indicated in bold and italics. In the mutants, R155L and R155A, the *Hind* III

restriction site present in the wild type gene was eliminated by silent mutagenesis. The loss of this restriction site allowed for selection of positive clones. The wild type PfAdSS gene in pET23d vector was used as the template for generating the mutants. Briefly, the mutagenic primer along with the appropriate end primer was used to generate the megaprimer. The PCR mix contained 200 ng of each primer, 20 ng of the template, 200 μ M of each dNTP and 5 units of *Taq* DNA polymerase in a 50 μ l reaction. The PCR cycle was separately optimized for each mutant. The product obtained after 30 cycles was purified by gel elution and then used along with the other end primer to amplify the full gene. The PCR product was purified, digested with *Nco*1 and *Xho*1 and ligated into pET23d vector digested with the same enzymes. Recombinants were selected after transformation into DH5 α strain of *E. coli* cells on the basis of supercoiled plasmid mobility. The presence of the right insert was confirmed by restriction digestion with the enzyme whose site was incorporated in the mutagenic primer by silent mutagenesis.

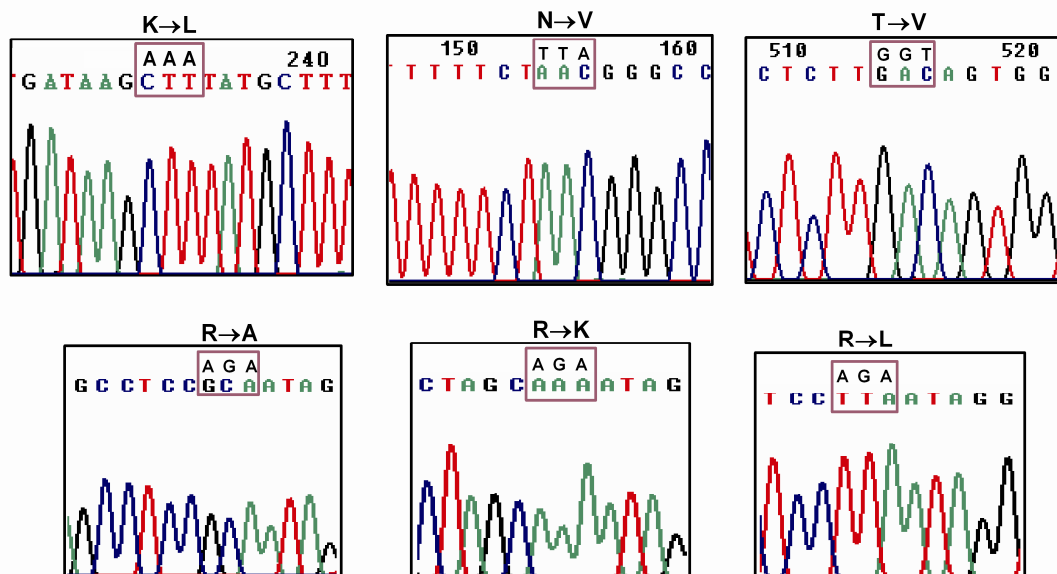


Figure 4.6: Sections of sequencing chromatograms confirming the incorporation of the desired mutation. The mutated codon and the same codon in the parent wildtype are boxed.

The R155A-G146R double mutant was constructed using R155A gene in pET23d vector as the template. To facilitate purification, R155A-G146R mutant was subcloned into pET28b expression vector. The gene in pET23d vector was PCR amplified using the primers

DMHis (5' GGCGCTAGCGCCATATTTGATCATCAAATAAAAAATGTG 3') and AdSSc, digested with *Nhe1* and *Xho1* and ligated into the vector resulting in a N-terminal 6xHis-tag fusion. All the mutants were confirmed by sequencing (Figure 4.6).

4.2.2 Protein expression and purification

For protein expression, wild type PfAdSS and the mutants were transformed in BL21(DE3) strain of *E. coli* cells. The freshly transformed cells were inoculated into 200 ml of terrific broth and allowed to grow for 5-6 hours at 37°C with constant shaking. This culture was used as an inoculum for 3-4 liters of terrific broth. The cultures were allowed to grow to an OD₆₀₀ of 0.6 at 37°C, cooled to 20°C and induced by adding 200 µM IPTG. Induction was carried out at 20°C for 12 hours. Induced cultures were pelleted by centrifugation and then resuspended in lysis buffer containing 50 mM Tris HCl, pH 7.4, 10% glycerol, 1 mM DTT and 0.1 µM PMSF. Cells were lysed using french press and cellular debris removed by centrifugation at 16,000 rpm for 20 minutes. The supernatant was treated with 0.2% PEI to precipitate nucleotides, followed by 40% and 65% ammonium sulphate fractionation. The resultant pellet was dissolved in 20 mM Tris HCl, pH 8.0, 10% glycerol and 1 mM DTT and desalted on a Sephadex G-25 column equilibrated with the same buffer. The fractions containing the protein were loaded onto an anion exchange column connected to an AKTA Basic HPLC. Protein was eluted with a linear gradient of 0 to 1 M NaCl in the same buffer. Fractions were analyzed by SDS-PAGE and the fractions containing the protein pooled and concentrated. The concentrated protein was loaded onto a Sephacryl 200 column equilibrated with 20 mM Tris HCl, pH 6.9, 10% glycerol, 2 mM DTT and 1 mM EDTA. The fractions containing the protein were concentrated and stored at -20°C. The protein concentration was estimated by method of Bradfords using BSA as standard (Bradford, 1976).

R155A mutant failed to purify by the above mentioned procedure. This mutant was lysed in a buffer containing 50 mM Tris HCl, pH 7.4, 10% glycerol, 1 mM DTT, 0.1 mM PMSF and 100 mM NaCl. After 40 and 65% ammonium sulphate precipitation the pellet was resuspended in buffer containing 20 mM Tris HCl, pH 7.4,

10% glycerol, 2 mM DTT, 1 mM EDTA and 100 mM NaCl and then injected into Sephacryl 200 column equilibrated with the same buffer. The fractions containing the protein were concentrated and then diluted to a final NaCl concentration of 20 mM. This was followed by DEAE sepharose anion exchange chromatography. The protein containing 20 mM NaCl was injected into the column equilibrated with 20 mM Tris pH 6.9, 10% glycerol and 1 mM DTT. The protein did not bind to the column and eluted in the flowthrough. The purified protein was concentrated and stored at -20°C.

Repeated attempts to purify the double mutant cloned in pET23d vector by the above mentioned procedures yielded impure protein. To facilitate purification, the double mutant (R155A-G146R) was cloned in pET28b vector and expressed as a N-terminal His-tagged fusion protein in BL21(DE3) cells. After induction at 20°C for 10 hours, the cells were pelleted, resuspended in lysis buffer containing 50 mM Tris HCl, pH 7.4, 10% glycerol, 100 mM NaCl, 2 mM DTT and 0.2 mM PMSF and lysed using french press. After removal of cellular debris the supernatant was incubated for 6 hrs at 4°C with Ni-NTA beads (Novagen, Madison, USA) pre-equilibrated with Buffer A (20 mM Tris HCl, pH 7.4, 10% glycerol, 100 mM NaCl, 2 mM DTT and 0.2 mM PMSF). The beads were washed with two bed volumes of Buffer A followed by 20 volumes of Buffer B (Buffer A + 15 mM imidazole). Protein was eluted with 100, 250 and 500 mM imidazole. The different fractions were checked on SDS-PAGE. The fractions containing the protein were pooled, concentrated and injected into Sephacryl 200 gel filtration column equilibrated with 20 mM Tris HCl, pH 6.9, 10% glycerol, 100 mM NaCl, 2 mM DTT and 1 mM EDTA. The fractions containing pure protein were concentrated and stored at -20°C.

4.2.3 Circular dichroism and fluorescence spectroscopy

Fluorescence spectra of wild type and mutant proteins were recorded on a Hitachi F-2500 spectrofluorimeter. Spectra were recorded in 10 mM sodium phosphate, pH 7.4 at 2 and 4 μ M protein concentrations. Protein samples were excited at 280 nm and emission monitored from 282 to 400 nm. Excitation and emission bandwidths were set to 2.5 and 10 nm, respectively. Baseline corrections were done by subtraction of the buffer spectrum.

Circular dichroism measurements were performed on a Jasco J-810 spectropolarimeter equipped with a Peltier heating system. Spectra were recorded from 300 to 200 nm in 10 mM sodium phosphate, pH 7.4 at 3 and 5 μ M protein concentrations in a cuvette of 1 mm path length. Appropriate blank spectra were subtracted and each spectrum represents an average of three scans.

4.2.4 Analytical size-exclusion chromatography

Superdex 200 column (30*1cm) calibrated with β -amylase (200 kDa), alcohol dehydrogenase (150 kDa), bovine serum albumin (66 kDa), carbonic anhydrase (29 kDa) and cytochrome c (12.5 kDa) was used for analytical gel filtration studies. The oligomeric status of the proteins was checked at two different concentrations, 1 and 15 μ M. 100 μ l of the protein was injected into the column equilibrated with 10 mM sodium phosphate, pH 7.4, 5% glycerol, 1 mM EDTA and 1 mM DTT. The flow rate was maintained at 0.5 ml/min and elution monitored simultaneously at 280 and 220 nm. 50 and 100 mM NaCl was included in the running buffer for R155A and R155A-G146R mutants, respectively.

4.2.5 Enzyme assays and kinetics

Enzyme assays for the mutants, N429V, K62L, T307V and T309V, were performed at 37°C using the water circulated cell holder fitted to Hitachi U-2010 spectrophotometer. The temperature was maintained with Julabo F25 (JULABO Labortechnik GmbH, Seelbach, Germany) circulating water bath. Kinetic parameters for Arg155 mutants were determined at 25°C. For comparison with the mutants, the kinetic constants for the wild type enzyme were determined at both 25 and 37°C. Assays were performed in 30 mM Hepes, pH 7.0 and 5 mM magnesium acetate. Depending on the mutant, 1.5-10 μ g of enzyme was used in a reaction volume of 300 μ l. Reactions were initiated with the enzyme and the reaction rates monitored as an increase in absorbance at 290 nm. A $\Delta\epsilon$ value of 3390 $\text{M}^{-1}\text{cm}^{-1}$ (Carey & Mandel, 1961; Kang & Fromm, 1995) was used to calculate the amount of product (sAMP) formed. For determination of kinetic constants, concentration of one substrate was varied at fixed saturating concentration (10 times the $10 K_m$) of the other two

substrates. The data were analyzed by fits to Michaelis Menten equation (equation 1) using GraphPad Prism, version 4 (GraphPad Software, Inc., San Diego, CA).

$$v = V_{\max}[S] / K_m + [S] \quad \text{Equation 1}$$

where, v and V_{\max} are the initial velocity and maximum velocity respectively, K_m is the Michaelis constant and S is the variable substrate concentration. All measurements were repeated twice with two independently purified batches of proteins.

4.2.6 Initial velocity measurements and inhibition studies

For the determination of initial velocity patterns for the wild type enzyme, concentration of one substrate was varied maintaining the concentration of the other two substrates in a fixed ratio at different levels in the range of their Michaelis constant.

Phosphate inhibition of wild type AdSS was studied by the method of Dixon (Dixon, 1953), where the inhibitor concentration was varied at different fixed concentrations of one substrate with the other two substrates maintained at thrice their K_m values.

Inhibition patterns with GDP and the aspartate analog, hadacidin, for the mutants were determined by measuring the reaction rates at variable concentrations of one substrate, fixed subsaturating concentrations of the other two substrates and at different fixed concentrations of the inhibitor.

4.2.7 Fructose 1,6 bisphosphate activation

The effect of F16BP on the activity of the wild type protein was monitored in 30 mM HEPES, pH 7.0 at 37°C and 30 mM sodium phosphate, pH 7.4 at 25°C. Activation kinetics of the mutants, N429V, K62L and T307V was performed in 30 mM HEPES, pH 7.0 at 37°C. The IMP, GTP and aspartate concentrations were fixed at 5, 2 and 5 times their K_m values for each enzyme, respectively and the reactions initiated with aspartate.

4.3 Results and Discussion

4.3.1 Initial velocity kinetics to elucidate the kinetic mechanism of *P. falciparum* adenylosuccinate synthetase

As for MjAdSS, initial velocity kinetics and product inhibition studies have been used to characterize the kinetic mechanism of *P. falciparum* AdSS. Initial velocity kinetics was done by the method proposed by Fromm (Rudolph & Fromm, 1969; Rudolph & Fromm, 1979). IMP, GTP and aspartate concentrations were varied in separate experiments, where the concentration of the other two substrates was varied simultaneously in a fixed ratio around their respective K_m values. The results are summarized in Figure 4.7.

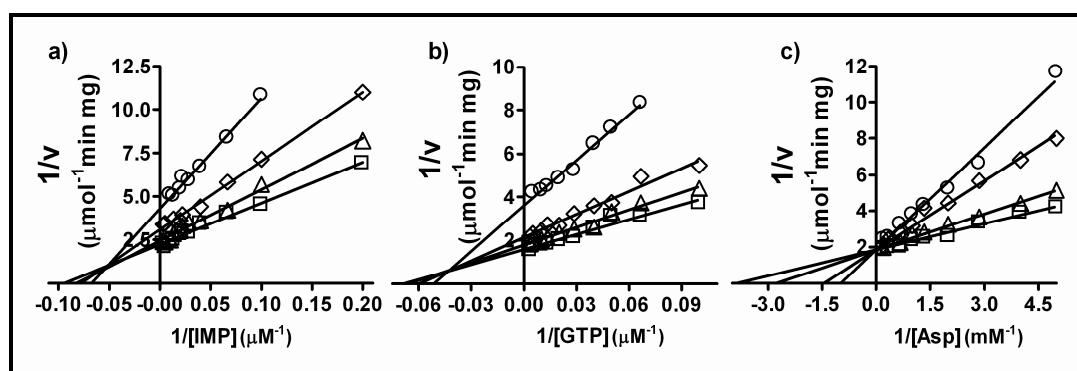


Figure 4.7: Plots of reciprocal of initial velocity (v) with respect to reciprocal of substrate concentration. Each substrate was varied at different fixed concentration of the other two substrates. The ratio of the fixed substrate was maintained constant across each line in a particular experiment. a) IMP concentration was varied from 5-300 μM and the respective concentrations of aspartate and GTP were, 0.3 mM and 20 μM (O); 0.6 mM and 40 μM (\diamond); 0.9 mM and 60 μM (Δ) and 1.2 mM and 80 μM (\square). b) GTP concentration was varied from 10 to 300 μM . The respective concentrations of aspartate and IMP were, 0.3 mM and 20 μM (O); 0.6 mM and 40 μM (\diamond); 0.9 mM and 60 μM (Δ) and 1.2 mM and 80 μM (\square). c) Aspartate concentration was varied from 0.2 mM to 5 mM. The respective concentrations of IMP and GTP were, 20 μM each (O); 40 μM each (\diamond); 60 μM each (Δ) and 80 μM each (\square).

Absence of parallel lines in any of the plots rules out a ping pong mechanism. Convergence of lines in each of the plots in Figure 4.7 denotes a sequential mechanism. The line patterns are indicative of the following two mechanisms,

- a) Random AB ordered C mechanism, where all enzyme forms or E, EA, EB and EAB are in rapid equilibrium and EABC in steady-state.
- b) Completely ordered mechanism where all enzyme forms or E-EA-EAB are in rapid equilibrium with EABC in steady-state. Here, A, B and C denote IMP, GTP and aspartate, respectively. Infact, if both A and B are at equilibrium with E, EA and EAB, the system behaves as a full rapid equilibrium system even though the reaction $EAB+C \rightarrow EABC$ is in steady state (Segel , 1975).

Inhibition studies using products and substrate analogs indicated ordered substrate binding in PfAdSS (Raman *et al.*, 2004), thereby ruling out a random AB ordered C kinetic mechanism for PfAdSS. The equation defining a completely rapid equilibrium or partial rapid equilibrium ordered trisubstrate system (equation 2) has three unknown variables and hence, getting numerical values for the kinetic constants that define the reaction scheme proved difficult.

$$v/V_{\max} = [A][B][C] / (K_A K_B K_C + K_B K_C [A] + K_C [A][B] + [A][B][C]) \quad \text{Equation 2}$$

where, v is the initial velocity, V_{\max} is the maximum velocity, A, B and C indicate IMP, GTP and aspartate, respectively and K_A , K_B and K_C are the dissociation constants for the substrates IMP, GTP and aspartate, respectively.

4.3.2 Structural basis for ordered substrate binding in PfAdSS

A comparison of liganded and ligand-free crystal structures of mouse and *E. coli* AdSS shows that there are five loops in adenylosuccinate synthetase that get organized on substrate binding (Figure 4.8). The most pronounced conformational change is exhibited by the switch loop which undergoes a 9Å movement on ligand binding (Iancu *et al.*, 2002; Poland *et al.*, 1996a). Comparison of the structures of

various complexes of *E. coli* and mouse AdSS with that of fully liganded PfAdSS, throw light on the structural basis for the unique kinetic mechanism of PfAdSS.

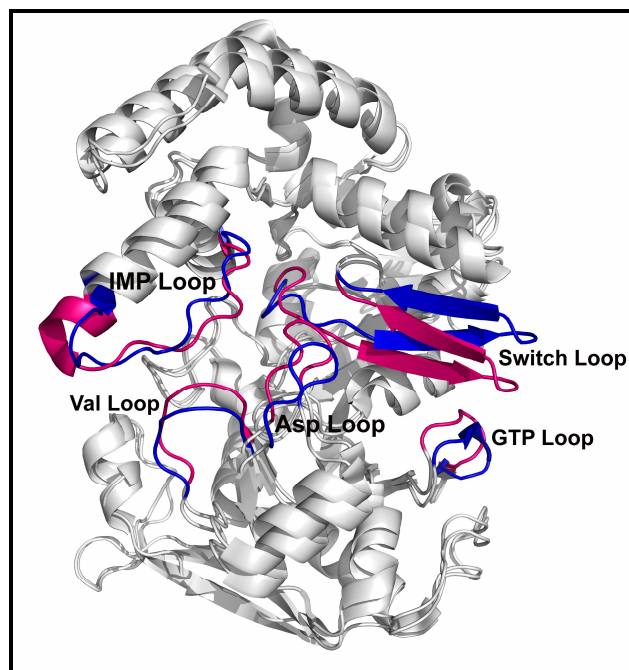


Figure 4.8: Superposition of fully liganded (PDB ID: 1LON) and unliganded mouse AdSS (PDB ID: 1J4B) structures. The loops that undergo conformational change on ligand binding are shown in color. The loops in the unliganded structure are shown in blue and in pink are the loop positions in the liganded mouse AdSS structure. The figure was generated using PyMOL (DeLano, 2002).

Superposition of fully liganded *P. falciparum* AdSS structure (PDB ID: 1P9B) with similarly liganded counterparts from mouse and *E. coli* (PDB ID: 1LON and 1CG0) shows that the switch loop is positioned further inwards towards GDP, in the *P. falciparum* structure (Figure 4.9). This conformation of the switch loop seems to be enforced by unique H-bonding interactions between residues Ser57 and Asp60, positioned at the closed end of the loop, and Asn429 in the GTP loop. As a consequence of the inward movement of the tip of the switch loop, Lys62 comes within H-bonding distance of GDP ribose hydroxyls. The importance of this interaction in modulating the affinity of the enzyme for GTP, may result in ordered binding of GTP after IMP has bound to the active site. GDP in PfAdSS also H-bonds to T307 which is in the aspartate loop that gets organized in response to aspartate binding at the active site (Hou *et al.*, 2002; Iancu *et al.*, 2002). This indicates that GTP binding to the active site of PfAdSS probably aids in organizing this loop.

Thr307 interacts with hadacidin in the crystal structure and also co-ordinates Mg^{2+} . These factors together could lead to the ordered binding of aspartate subsequent to GTP binding to the enzyme (Eaazhisai *et al.*, 2004; Raman *et al.*, 2004). As discussed in Section 4.1.1, counterparts of Lys62 and Thr307 in *E. coli* and mouse AdSS do not come in the vicinity of the ligands and the interactions of these residues with GDP and hadacidin are unique to the parasite enzyme.

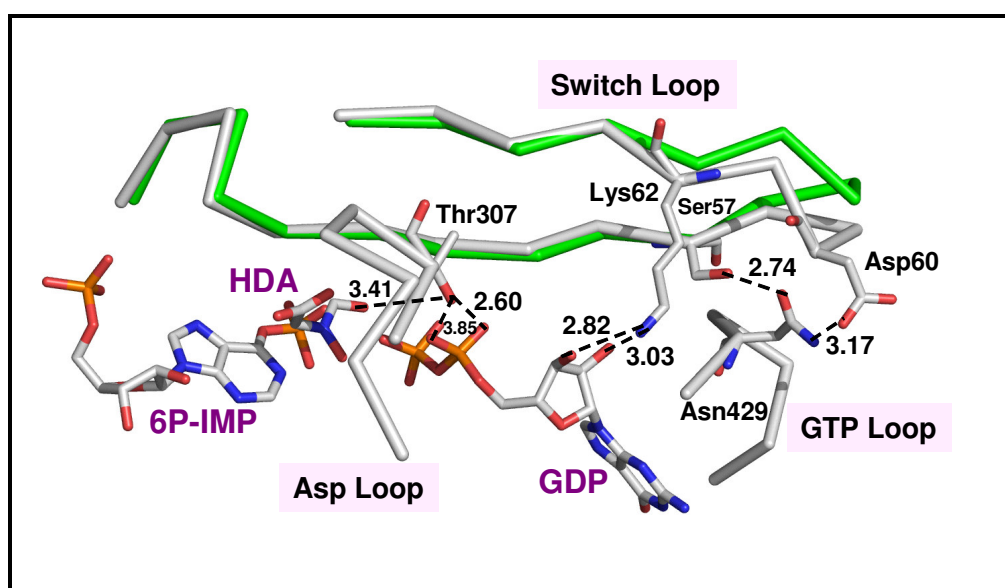


Figure 4.9: Superposition of switch loop from *P. falciparum* (PDB ID: 1P9B, grey) and mouse (PDB ID: 1LON, green) AdSS. Also shown are GTP and aspartate loops of PfAdSS. The residue numbering corresponds to the *P. falciparum* sequence. The ligands in the active site are shown in CPK. Dashed lines represent hydrogen bonds and the numbers indicate the distance in Å. The figure was generated using PyMOL (DeLano, 2002).

To evaluate the role of these interactions in modulating the affinity of PfAdSS for the ligands, site-directed mutagenesis has been used. The following mutants, N429V, K62L and T307V were constructed and kinetically characterized.

In addition, two conserved residues, Arg155 (involved in dimer crosstalk) and Thr309 (which interacts with carboxyl group of hadacidin) were also mutated. Kinetic characterization of the arginine mutants highlights features that are again unique to the parasite enzyme. In addition, studies on a double mutant, R155A-G146R are also summarized.

4.3.3 Conservation of Asn429, Lys62 and Thr307 in adenylosuccinate synthetase

As seen in Figure 4.10, Asn429 and the two residues, Ser57 and Asp60, with which it forms H-bonds, are not conserved across AdSS for which kinetic and/or structural information is available. While Thr307 is a valine or alanine in mouse, yeast and *E. coli* AdSS, Arabidopsis and Dictyostelium enzymes have a Thr residue at the corresponding position. Except for mouse AdSS, the lysine residue occurring at position 62 in PfAdSS is conserved. However, as will be discussed later, this residue in other proteins does not come within H-bonding distance of GDP.

	429			
A. thaliana	ELVGVP	IHYIGIGPGRDALIYK		
D. discoideum	ELVGVP	IVYIGVGERKNLIERKELI . .		
Mouseacidic	DELQIP	VKWIGVGKSRESMIQLF		
Mousebasic	NHMGVA	VKWVGVGKSRESMIQLF		
S. cerevisiae	DFVGVP	VEWVGTGPARESMLHKEIK . . .		
P. falciparum	KYLKTP	IVWIGVGNRKNMIVKKNFNLN		
E. coli	ELTGVP	IDIIISTGPDRTETMILRDPFDA		
	57 60 62			
A. thaliana	GANAGHTIY	NSEGGKKFALHLP	SGILNE	
D. discoideum	GANAGHTIV	VVD.GKKIALHLP	SGILNE	
Mouseacidic	GNNAGHTV	VVD.SVEYDFHLLP	SGIINP	
Mousebasic	GNNAGHTV	VVD.GKEYDFHLLP	SGIINT	
S. cerevisiae	GNNAGHTIV	VVD.GVKYDFHMLP	SGLVNP	
P. falciparum	GANAGHTIS	VN.DKKYALHLLP	CGVLYD	
E. coli	GHNAGHTLV	IN.GEKTVLHLP	SGILRE	
	307			
A. thaliana	LAGQEF	GT	TTGRPRRCGWLD	IVALKFSC
D. discoideum	KAGSEF	GT	TTGRPRRIGWLD	AVVLRYS
Mouseacidic	TRGREF	GV	TTGRKRRCGWLD	LVSLKYAH
Mousebasic	NRGHEW	GV	TTGRKRRCGWLD	LMILRYAH
S. cerevisiae	TIGAEF	GV	TTGRKRRCGWLD	LVVLKYST
P. falciparum	EKGHEY	GT	TTKRPRRCGWLD	IPMLLYVK
E. coli	KQGNEF	GA	TTGRRRRTGWLD	TVAVRRAV

Figure 4.10: Alignment of segments of AdSS sequences for which biochemical and/or structure data is available. The conserved residues are highlighted in cyan. The nonconserved residues that were subjected to site-directed mutagenesis in PfAdSS are colored in yellow. The numbers displayed on the sequence correspond to PfAdSS. The alignment was generated using CLUSTAL W (Thompson *et al.*, 1994) and represented using ESPRIPT (Gouet *et al.*, 1999).

4.3.4 Protein expression and purification of PfAdSS mutants

The mutants were generated by megaprimer PCR method (Sarkar and Sommer, 1990) and cloned into pET23d expression vector, except for the double mutant which was cloned into pET28b vector. The recombinant proteins were expressed in BL21(DE3) strain of *E. coli* cells. The proteins were purified as described in section 4.2.2. All proteins were >95% pure as judged by SDS-PAGE (Figure 4.11). The proteins were also confirmed by western blot using PfAdSS specific antibodies.

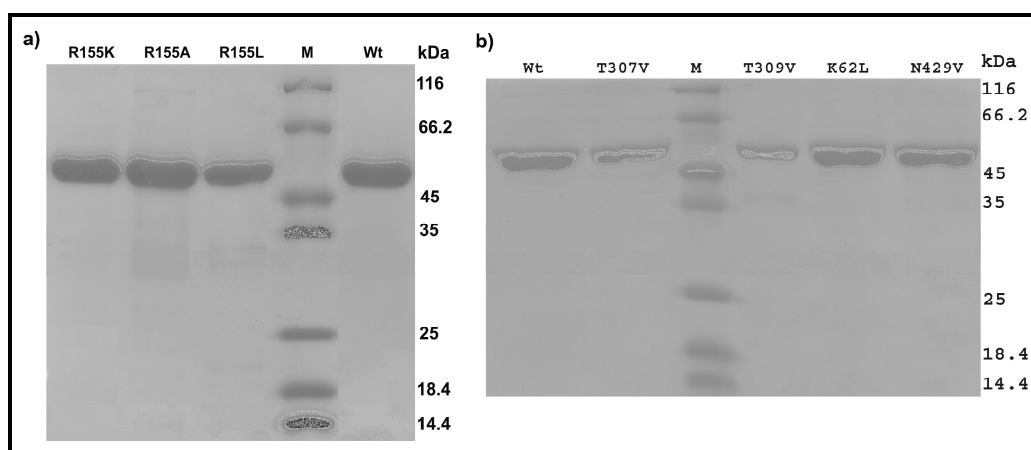


Figure 4.11: SDS-PAGE profile of AdSS mutants. a) purified recombinant wild type protein along with the Arg155 mutants and b) PfAdSS active site mutants along with wild type AdSS.

4.3.5 Structural integrity of the active site mutants

AdSS exhibits monomer-dimer equilibrium with the dimer being implicated in catalysis (Kang *et al.*, 1996; Wang *et al.*, 1997a). Therefore, the quaternary structure of the mutants was checked on a calibrated Superdex 200 column. Two different protein concentrations, 15 and 1 μ M (concentration at half peak height is 1.25 and 0.08 μ M, respectively) were used and the results are summarized in Table 4.2. The wild type protein eluted at a retention volume which corresponds to a molecular mass of 92 kDa. The subunit mass predicted from the amino acid sequence of the protein is 50 kDa. Thus, the profile is indicative of monomer-dimer equilibrium with the dimer

being the predominant form. No change in the elution profile was observed when the protein concentration was decreased to 1 μM . N429V and K62L mutants exhibited profiles similar to the wild type protein. T307V and T309V mutants eluted at a volume corresponding to a molecular mass of 92 kDa. However, on reducing the protein concentration to 1 μM , the peak shifted to a retention volume corresponding to 83 and 75 kDa for T307V and T309V mutants, respectively, indicating that at lower protein concentration there is a shift in monomer-dimer equilibrium of these mutants.

Table 4.2: Summary of analytical gel filtration and fluorescence measurements to evaluate the structural integrity of the mutants. 1 and 15 μM denote protein stock concentrations, with the concentration at half peak height being about 0.08 and 1.25 μM , respectively. Fluorescence spectra of the mutants were recorded at 2 μM protein concentration after excitation at 280 nm.

Protein	Size exclusion Chromatography		Fluorescence
	Molecular mass (15 μM)	Molecular mass (1.0 μM)	Emission max (nm)
Wild type	92 kDa	89 kDa	325
N429V	91 kDa	89 kDa	325
K62L	92 kDa	92 kDa	325
T307V	92 kDa	83 kDa	326
T309V	92 kDa	75 kDa	325
R155L	95 kDa	95 kDa	327
R155K	89 kDa	89 kDa	327
R155A	Spreads on column		331
R155A-G146R*	48 kDa, 89 kDa	48 kDa, 89 kDa	327

*The proportion of the monomeric peak was much greater than the dimeric peak.

Arg155 is an interface residue which holds the two subunits of the dimer through its interaction with IMP and other residues of the symmetry related subunit. The quaternary structural features of R155L and R155K mutants were similar to the wild type protein. However, R155A mutant was highly destabilized. No clear peak was

observed on an analytical gel filtration column even in the presence of salt in the running buffer, indicating that mutation of Arg155 to alanine results in loss of stable quaternary structure. The double mutant (R155A-G146R) showed two peaks corresponding to molecular mass of 89 and 48 kDa. However, the mutant was predominantly monomeric in nature as judged by the area under the two peaks.

PfAdSS has four tryptophans per monomer and exhibits an emission maximum of 325 nm on excitation at 280 nm. The fluorescence spectra for all the mutants (recorded at 2 and 4 μ M protein concentration) except R155A, were largely similar to that of the wild type protein with not more than 2 nm shift in the emission maximum (Table 4.2). The R155A mutant, which failed to show a clear peak in size exclusion chromatography, showed a 6 nm red shift exhibiting an emission maximum of 331 nm.

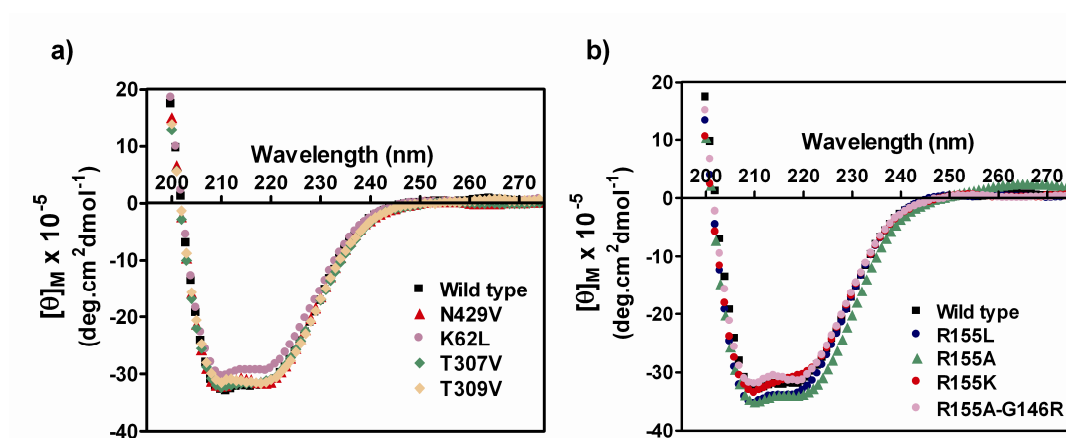


Figure 4.12: Circular dichroism spectra of wild type and mutant proteins.

The secondary structural integrity of the mutants was analyzed by circular dichroism spectroscopy. The CD spectra of the wild type protein and the mutants were largely similar in the wavelength range 260–210 nm (Figure 4.12). The spectra were characteristic of a largely helical protein. Thus, mutation of residues in the active site and interface of PfAdSS did not grossly perturb the quaternary, tertiary and secondary structural characteristics of the protein, except for the R155A mutant which retained secondary structural features of the wild type protein but exhibited altered tertiary and quaternary structure.

4.3.6 Kinetic Characterization of Wild type and mutant adenylosuccinate synthetase

To examine the effect of mutations on enzyme activity and substrate affinity, initial rate kinetic studies with the AdSS mutants were carried out and compared with those of the wild type enzyme. The activity of the mutants was checked in different buffers like Tris HCl, Hepes and phosphate in the pH range 7-8.5. Most mutants showed lower activity in phosphate buffer when compared to Tris HCl and Hepes. Maximum activity was observed in the pH range 7-7.5 with the activity dropping at higher pH. Hence, Hepes at pH 7.0 was chosen for the kinetic characterization of the mutants.

Kinetic parameters for wild type PfAdSS were earlier reported in sodium phosphate, pH 7.4 and at 25°C (Raman *et al.*, 2004). For comparison with the mutants, the k_{cat} value and substrate affinities of the wild type enzyme were determined in Hepes, pH 7.0 and 37°C (Table 4.3). Though the IMP and GTP K_m values were comparable to the earlier reports, the aspartate K_m value showed a 6- fold drop when compared to the reported value of 1.8 mM (Jayalakshmi *et al.*, 2002; Raman *et al.*, 2004). However, no significant variation with respect to the k_{cat} value was observed. As there was a difference in temperature across the two studies, the Michaelis constant for aspartate was determined in Hepes, pH 7.0 and at 25°C to rule out the effect of temperature on the observed decrease in the aspartate K_m value. Only a minor variation in the K_m value was seen with change in temperature (0.31 ± 0.03 mM at 37°C to 0.34 ± 0.04 mM at 25°C). This observation was indicative of phosphate being a true competitive inhibitor of aspartate. Dixon analysis indeed revealed that phosphate is a competitive inhibitor of aspartate exhibiting a K_i value of 28 ± 2.5 mM (Figure 4.13). Therefore, in the presence of phosphate an apparent increase in the aspartate K_m value was observed.

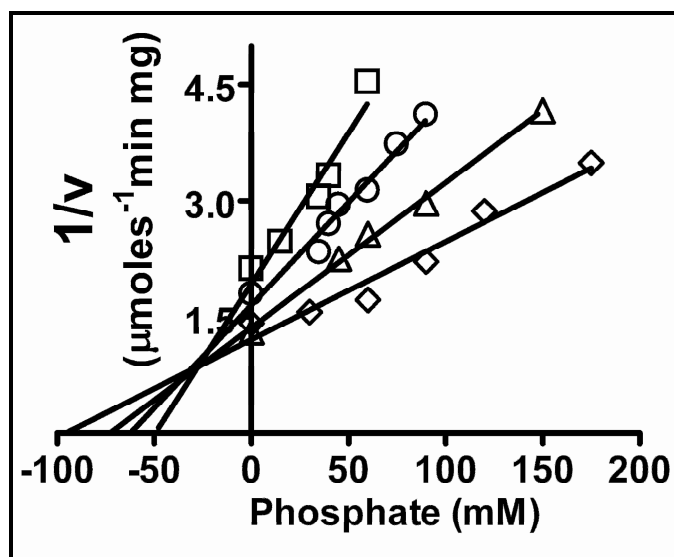


Figure 4.13: Dixon analysis of the inhibition of PfAdSS by phosphate. IMP and GTP were held constant at 60 μM each. The fixed concentrations of aspartate were, 0.5mM (\square), 1 (o), 2 (Δ) and 3 mM (\diamond).

Table 4.3: Kinetic parameters for the wild type and mutant adenylosuccinate synthetase from *P. falciparum* measured in Hepes, pH 7.0 and at 37°C.

Protein	k_{cat} (s^{-1})	K_m		
		IMP (μM)	GTP (μM)	Aspartate (mM)
Wild type	1.44 ± 0.11	16.77 ± 1.97	24.77 ± 2.34	0.31 ± 0.03
N429V	0.32 ± 0.02	49.66 ± 2.39	27.05 ± 2.52	0.57 ± 0.03
K62L	1.09 ± 0.12	21.61 ± 2.7	46.46 ± 4.68	0.78 ± 0.09
T307V	1.72 ± 0.02	28.49 ± 2.15	34.74 ± 4.81	1.10 ± 0.07
T309V	Inactive			

The kinetic parameters for the wild type and mutant enzymes in Hepes, pH 7.0 and at 37°C are summarized in Table 4.3. The kinetic parameters were determined twice for each mutant on two independently purified batches of protein. The results across experiments were found to be fully reproducible. Since there was no significant

variation in the k_{cat} value whether IMP, GTP or aspartate was the variable substrate, an averaged k_{cat} value is represented.

4.3.7 Characterization of N429V mutant

Asn429 lies in the GTP loop. The side chain of this residue makes hydrogen bonds with Ser57 and Asp60 which lie at the closed end of the switch loop in PfAdSS (Figure 4.14). These H-bonds are probably responsible for the further inward movement of the switch loop in the active site of PfAdSS, when compared to the *E. coli* and mouse enzymes (Figure 4.9). Asn429 was mutated to valine to abolish the hydrogen bonding interactions involving the side chain of this residue. While the GTP K_m value of the mutant was comparable to the wild type protein, it showed two and three fold increase in aspartate and IMP K_m values, respectively. Surprisingly, the mutant exhibited a 5 fold drop in k_{cat} value when compared to the wild type enzyme. These results implicate the role of Asn429 in both catalysis as well as ligand binding.

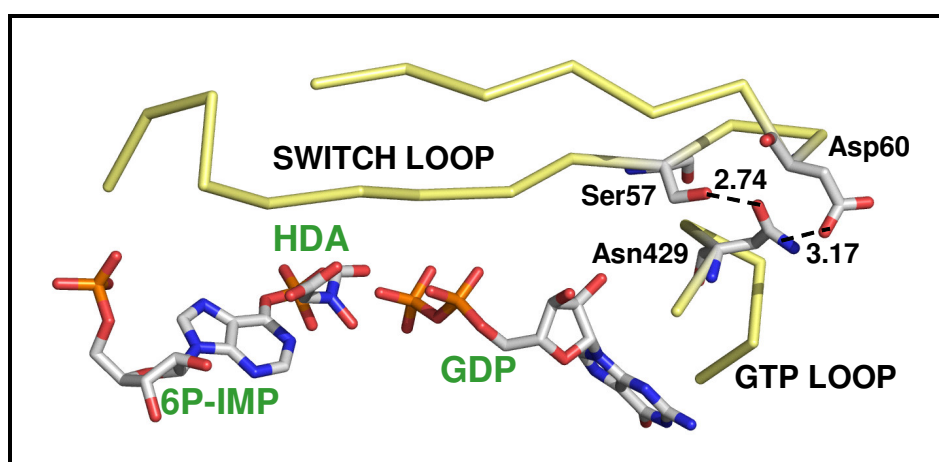


Figure 4.14: Interactions involving the side chain of Asn429 with the residues Ser57 and Asp60 located at the tip of the switch loop. The ligands, 6P-IMP, GDP and HDA (hadacidin) are shown in CPK. The figure was generated using PyMOL (DeLano, 2002).

Asn429 makes no direct contacts with either the ligands or the catalytic residues, Asp26 and His54. Mutation of Asn429 to valine abolishes all the contacts made by the Asn side chain groups, OD1 and ND2. These groups interact extensively

with residues at the tip of the switch loop, especially Ser57, Val58, Asn59 and Asp60. OD1 of Asn429 makes a bifurcated H-bond with side chain hydroxyl group of Ser57 and backbone nitrogen of Asp60, while ND2 makes a hydrogen bond with the side chain of Asp60. Thus, mutation of Asn429 to valine could probably lead to improper orientation of the switch loop in PfAdSS. The switch loop harbors the catalytic acid, His54 while the catalytic base, Asp26 lies in the P-loop (Residues 25-31). A network of H-bonds exists between residues in the switch loop, GTP loop and the residues that lie between the P-loop and switch loop (Figure 4.15). These interactions probably dictate the proper orientation of the loops that harbor residues involved in catalysis and ligand binding. The mutation of N429 may perturb the conformation of the loops and in turn the orientation of the catalytic acid and base, leading to the observed drop in k_{cat} value of the mutant. The differences between the kinetic properties of this mutant and the wild type enzyme, with respect to k_{cat} and aspartate and IMP K_m values, highlights the role of the switch loop in modulating ligand binding and conformation of other loops in PfAdSS.

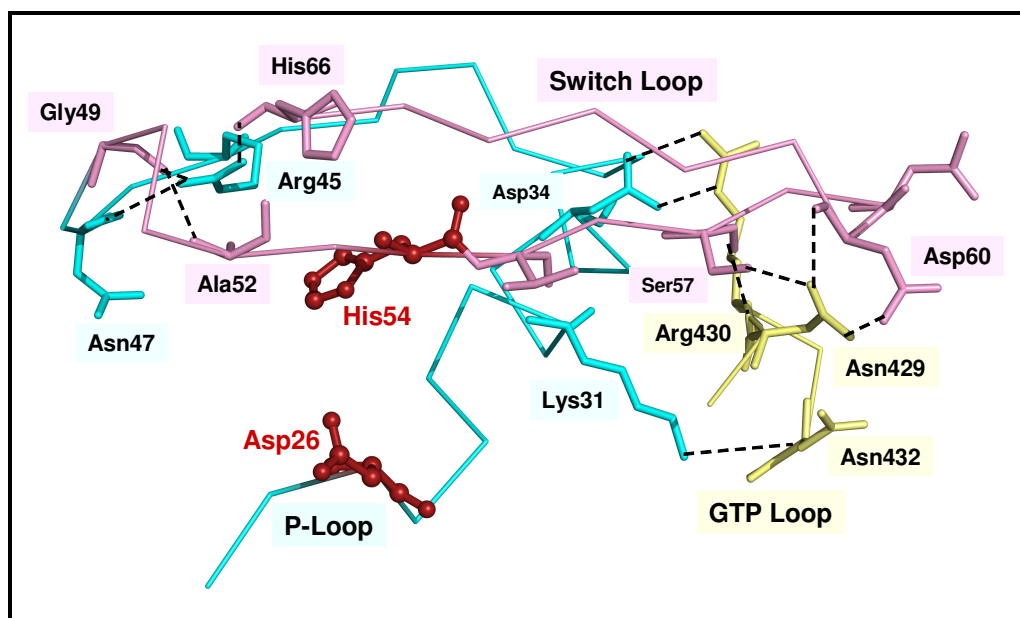


Figure 4.15: H-bonding interactions between loops in liganded PfAdSS which lead to proper orientation of the catalytic residues, His54 and Asp26, shown in ball and stick. The ligands have been removed from the active site for clarity. The black dashed lines show the hydrogen bonds between residues that lie in different loops. The figure was generated using PyMOL (DeLano, 2002).

4.3.8 Characterization of K62L mutant

Lys62 in *P. falciparum* AdSS makes a bifurcated hydrogen bond with ribose hydroxyls of GDP (Figure 4.16). Mutation of Lys62 to leucine resulted in an increase in GTP and aspartate K_m values by 2 and 2.5 fold, respectively while the k_{cat} and IMP K_m values were largely similar to the wild type protein (Table 4.3).

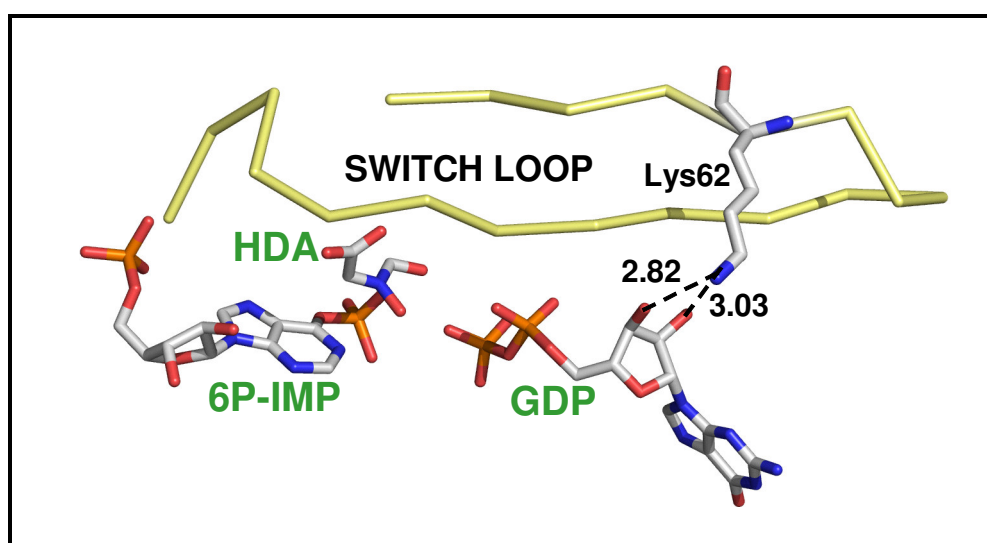


Figure 4.16: Bifurcated H-bond made by NZ group of Lys62 with ribose hydroxyls of GDP in PfAdSS. Shown in CPK are the ligands, 6P-IMP, GDP and hadacidin (HDA). The numbers denote distance in Å. The figure was generated using PyMOL (DeLano, 2002).

Lys62 in *P. falciparum* AdSS moves close to GDP ribose as a consequence of the inward movement of the switch loop due to the unique H-bonding interactions between residues at the tip of the switch loop and the GTP loop. Though the H-bonds involving the side chain of Lys62 are lost on mutation of this residue, only a two fold increase in GTP K_m value of the mutant was observed. This indicates the dominant role of other interactions in holding GTP in the enzyme active site. The 2.5 fold increase in aspartate K_m value of the mutant is probably a consequence of aspartate binding being conditional to GTP binding.

Lys62 though not conserved in mouse AdSS, is present in *E. coli*, Arabidopsis and *S. cerevisiae* AdSS (Figure 4.10). In *E. coli* AdSS, the NZ group of the corresponding lysine (Lys49) is 5.2 and 5.9 Å away from the ribose hydroxyls. In

Arabidopsis also, the corresponding lysine residue is at a distance of 8.0 and 6.6 Å from the ribose hydroxyls, indicating that the hydrogen bonding interactions observed between Lys62 and GDP in *P. falciparum* AdSS are unique to the parasite enzyme.

4.3.9 Characterization of T307V mutant

Thr307 lies in the aspartate loop, which is the only loop that does not get organized by IMP binding to the active site of AdSS (Hou *et al.*, 2002; Iancu *et al.*, 2002). Initial velocity and product inhibition studies with *P. falciparum* AdSS showed that aspartate is the last substrate to bind to the enzyme during catalysis. Mutation of Thr307 to valine resulted in a marginal increase in k_{cat} and IMP and GTP K_{m} values of the enzyme. However, the mutant exhibited a four fold increase in aspartate K_{m} value (Table 4.3).

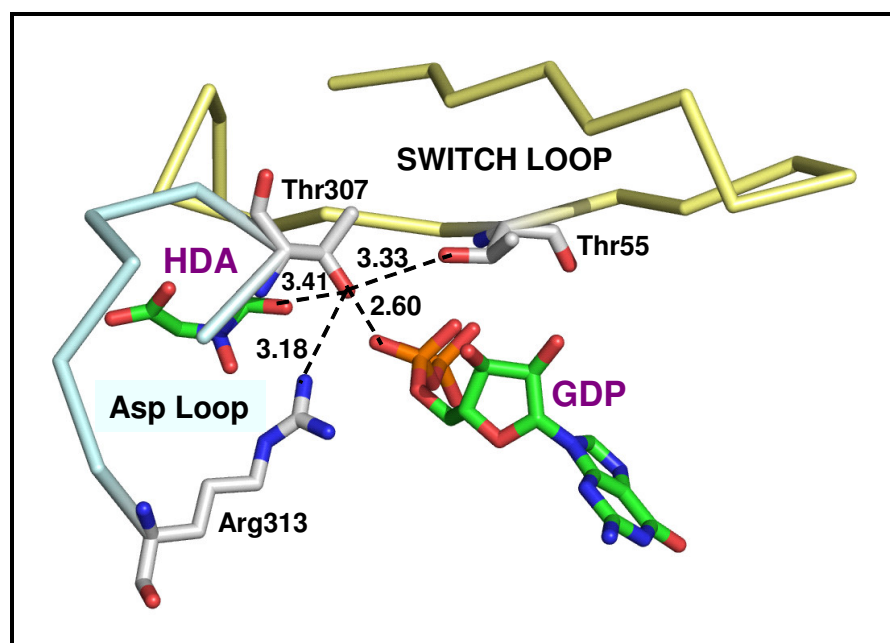


Figure 4.17: H-bonds (black dotted lines) made by Thr307 with the ligands and other loop residues. Shown in green are the ligands, GDP and hadacidin (HDA), in the active site. The numbers denote bond length in Å. The figure was generated using PyMOL (DeLano, 2002).

Thr307 in *P. falciparum* AdSS interacts with GDP and hadacidin through its side chain hydroxyl group (Figure 4.17). OG of Thr307 also makes a hydrogen bond

with the side chain of Arg313. Arginine 313 is a conserved residue whose mutation in *E. coli* AdSS resulted in about 40 fold increase in the aspartate K_m value along with a 100 fold reduction in k_{cat} value. This effect was attributed to its direct interaction with aspartate and its role in dictating the precise alignment of the substrates in the quaternary complex of the enzyme, GTP, IMP and aspartate, the breakdown of which is the rate limiting step in *E. coli* AdSS reaction (Wang *et al.*, 1995).

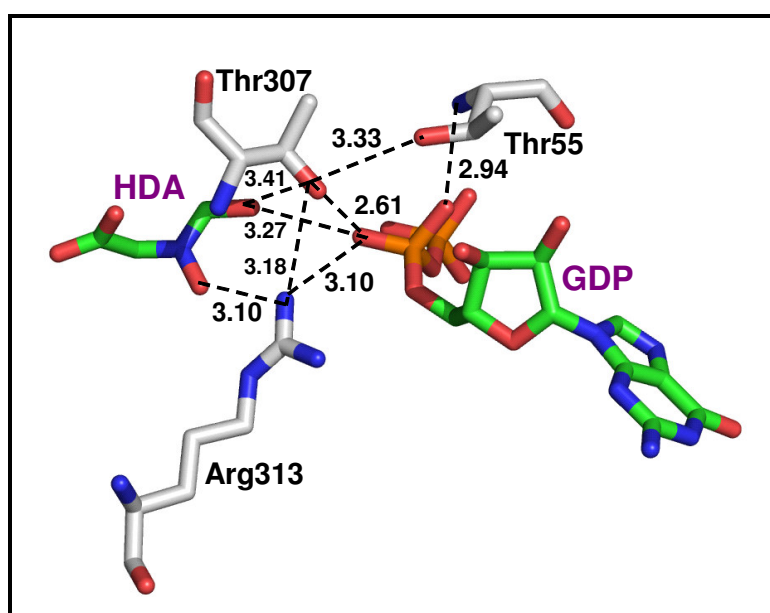


Figure 4.18: Network of hydrogen bonds involving the amino acids Thr307 (Asp Loop), Thr55 (Switch Loop) and Arg313 (Asp Loop) and the ligands, GDP and hadacidin (HDA). The figure was generated using PyMOL (DeLano, 2002).

Arg313 in PfAdSS makes close range interactions with both hadacidin and GDP (Figure 4.18). Arg313 lies at the hinge of the aspartate loop and its interaction with Thr307 may be necessary for proper orientation of the aspartate loop. Thus this network of hydrogen bonds between GDP and residues in aspartate loop may dictate the ordered binding of aspartate after GTP has bound to the active site.

Mutation of Thr307 to valine abolishes the interactions of threonine with GDP, hadacidin and Arg313. The observed increase in aspartate K_m value of Thr307 mutant may arise in part due to loss of hydrogen bonds involving the threonine side chain and hadacidin and also due to improper orientation of aspartate loop, which is implicated in recognizing the carboxyl group of aspartate.

The corresponding residues in *E. coli* and mouse AdSS are Ala299 and Val331. Thr307 corresponds to Thr364 in the Arabidopsis enzyme, which does not lie within 5 Å of bound GDP. However, in the absence of hadacidin bound structure of the plant enzyme, its role in aspartate binding cannot be commented.

4.3.10 Product inhibition studies with PfAdSS mutants

Inhibition studies with dead-end competitive inhibitors may be used to determine the kinetic mechanism of a reaction. The kinetics of inhibition of wild type PfAdSS by sAMP, AMP, GDP, GMP and the aspartate analog, hadacidin were earlier examined to elucidate the kinetic mechanism of PfAdSS (Raman *et al.*, 2004). sAMP and AMP, competitive inhibitors of IMP, showed noncompetitive inhibition with GTP and aspartate. GMP and GDP, competitive inhibitors of GTP showed noncompetitive inhibition with aspartate and uncompetitive inhibition with IMP. Parallel line patterns in double reciprocal plots of 1/velocity versus 1/[substrate] at different fixed concentrations of hadacidin indicated uncompetitive inhibition with respect to both IMP and GTP (Raman *et al.*, 2004). These inhibition patterns are indicative of an ordered kinetic mechanism for PfAdSS, with GTP binding to the enzyme being conditional to the catalytic pocket being occupied by IMP and aspartate binding only to E.IMP.GTP complex.

The plots for wild type AdSS showing parallel line patterns, namely, hadacidin versus IMP, hadacidin versus GTP and GDP versus IMP, were analyzed for the mutants, N429V, K62L and T307V. The results are summarized in Table 4.4. No change in line patterns was observed indicating that though the residues selected for mutagenesis modulated the affinity of the enzyme for the ligands, these mutations in isolation did not alter the kinetic mechanism of the enzyme.

Table 4.4: Line patterns in double reciprocal plots of $1/v$ versus $1/[\text{substrate}]$ in the presence of the inhibitors, hadacidin and GDP.

Inhibitor	GDP	Hadacidin	
	Substrate	IMP	GTP
Wild type	Parallel	Parallel	Parallel
N429V	Parallel	Parallel	Parallel
K62L	Parallel	Parallel	Parallel
T307V	Parallel	Parallel	Parallel

4.3.11 Arg155 and Thr309 mutants: Sequence comparison

Arg155 is an absolutely conserved residue as shown in Figure 4.19, whereas Thr309 is replaced by serine in *Spiroplasma citri*. While Thr309 interacts with β -carboxyl group of aspartate, Arg155 moves into the active site of the symmetry related subunit and interacts with IMP (Eaazhisai *et al.*, 2004).

S. citri	KKGIGPCYQDKAE R IGIRLGDLEF
H. pylori	KKGIGPCYEDKMAR S GIRMGDLLD
S. cerevisiae	GKGIGPTYSTKAS R SGLRVHHLVN
C. albicans	GKGIGPTYSTKAS R SGLRVHHLVN
Mus musculus	KKGIGPTYSSKAAR T GLRICDLLS
Homo sapiens	KKGIGPVYSSKAAR S GLRMCDLVS
A. niger	GKGIGPCYSDKAAR R GVVGEILD
A. thaliana	KRGIGPAYSSKVI R NGIRVGDLRH
Zea mays	KRGIGPCYSSKV T RNGLRVCDLRH
D. discoideum	KRGIGPCYSSKAS R GGLRVCDLYS
P. falciparum	KRGIGPCYSTKAS R IGIRLGTLN
E. coli	GRGIGPAYEDKVARR R GLRVGDLEF
H. influenzae	GRGIGPAYEDKVARR R GLRVGDLEF
V. cholerae	GRGIGPAYEDKVARR R GLRVGDLEF
A. vinelandii	GRGIGPAYEDKVARR R GLRIGDLEF
L. pneumophila	GRGIGPAYEDKVARR R ALRVGDLEF
B. subtilis	KKGIGPAYMDKAAR I GIRIADLLD
B. licheniformis	KKGIGPAYMDKAAR V GIRIADLLD
C. botulinum	GKGIGPSYTDKMERS G IRVCDLIH
M. leprae	GRGIGPCYQDKIAR M GIRVADVLE
Methanosarcina	KRGIGYAYIDKVAR D EFRMAELVD
M. mazei	KRGIGYAYIDKVAR D EIRMAELVD
A. fulgidus	GTGCGPANVDRV N RVAKQAKDIPE
M. jannaschii	GSGCGPANVDRV L RILKQAKDIEE
P. furiosus	GSGCGPANADRV M RVAKQAKDIKE

S. citri	ETYIREAGHEYGT V SGRARWIGWFDG
H. pylori	GDHLRTKGA E FGTTTKRPRRCGWLDL
S. cerevisiae	GEKLQ T IGAEFGVTTGRKRRCGWLDL
C. albicans	GETLQ D VGA E YGVTTGRKRRCGWLDL
Mus musculus	GDLLQ N RGHEWGVTTGRKRRCGWLDL
Homo sapiens	GELLQ T RGREFGVTTGRKRRCGWLDL
A. niger	GDKLQ G VGKEFGVTTGRRRRCGWFDL
A. thaliana	GDLLR L AGQ E FGTTTGRPRRCGWLDI
Zea mays	GDRLR K AGMEFGTTTGRPRRCGWLDI
D. discoideum	GDSL R KAGSEFGTTTGRPRRIGWLDL
P. falciparum	GOYL R EKGHEFGVTTTKRPRRCGWLDI
E. coli	GEFLC K QGN E FGATTGRRRRTGWLDL
H. influenzae	GAEI A RKGNEFGAVTGRPRRCGWFDA
V. cholerae	GDHLG T KGHEFGATTGRKRRCGWFDA
A. vinelandii	GAHL A SKGHEFGSTTGRARRCGWFDA
L. pneumophila	GKRIA E RGOEFGAVTGRPRRCGWFDA
B. subtilis	GDQI R EVGREYGVTTGRPRRVGWFDL
B. licheniformis	GDQI R EVGREYGVTTGRPRRVGWFDL
C. botulinum	GDWV R EKGHEFGVTTGRARRCGWLDL
M. leprae	GEYL A KTGSEIGVTTGRRRRCGWFDA
Methanosarcina	GERLQ K AGGEFGTTTGRGRRRCGWFDL
M. mazei	GERIQ K AGGEFGTTTGRGRRRCGWFDL
A. fulgidus	AEK L G . IVEYGT V TGRRRRIGYWDG
M. jannaschii	AES L G . IVEYGT V TGRRRRVGYFDF
P. furiosus	ADRL G . LIEYGT V TGRRRRVWGFDF

Figure 4.19: Conservation of Arg155 and Thr309 across AdSS sequences from different organisms. Boxed in blue are the conserved residues in the vicinity of Arg155 and Thr309, which are highlighted in yellow. The alignment was generated using CLUSTAL W (Thompson *et al.*, 1994) and represented using ESPRIPT (Gouet *et al.*, 1999)

4.3.12 Characterization of Arg155 mutants

Arg155 is involved in cross-talk across the two subunits of PfAdSS dimer through its interaction with 5'-phosphoryl group of IMP in the active site of the symmetry related subunit (Figure 4.20).

To dissect the role of Arg155 in modulating activity, substrate affinity and dimer stability in PfAdSS, arginine mutants were constructed. Arg155 was replaced with leucine to remove the guanidinium group while maintaining the long alkyl side chain, with lysine to retain the positive charge but reduce the hydrogen bonding capacity of the side chain and with alanine to create a cavity and hence abolish side chain interactions at position 155.

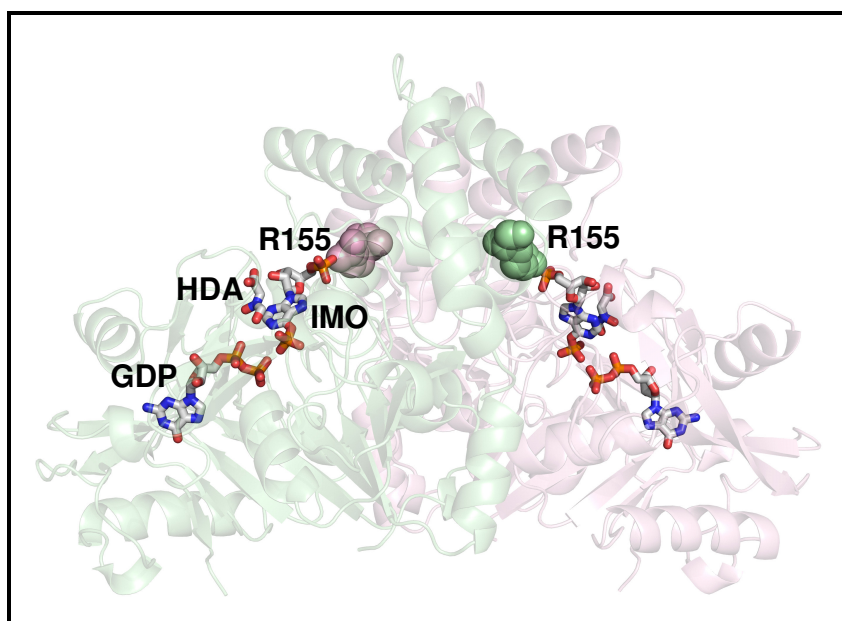


Figure 4.20: Interaction of Arg155 with IMP in the active site of the symmetry related subunit. The two subunits are colored in pink and green and the spheres denote Arg155 residues from the two subunits. The ligands in the active site are shown in sticks. IMO and HDA denote 6-phosphoryl IMP and hadacidin, respectively. The figure was generated using PyMOL (DeLano, 2002).

The kinetic parameters for the Arg155 mutants were determined in 30 mM Hepes, pH 7.0 and at 25°C because the spectra at 37°C were noisy, probably as a consequence of protein aggregation at higher temperature. For comparison with the

mutants, the substrate affinities and k_{cat} value for the wild type enzyme were also determined under identical conditions. The Michaelis constants for the wild type enzyme and Arg155 mutants are summarized in Table 4.5. The k_{cat} value for the mutants, R155K, R155L and R155A showed 9, 100 and 160 fold decrease, respectively, when compared to the wild type enzyme. Due to the low activity exhibited by R155A mutant, the substrate affinities of this mutant could not be determined. While the GTP K_m values of the mutants were largely comparable to the wild type enzyme, changes in IMP and aspartate K_m values were clearly evident. R155K and R155L mutants showed 27 and 125 fold increase in IMP K_m values, respectively, when compared to the wild type enzyme. While R155K mutant showed only a marginal increase in aspartate K_m value, the R155L mutant showed a 4 fold increase in aspartate K_m value when compared to wild type PfAdSS. Due to extremely high IMP K_m value of R155L mutant, its concentration could not be kept saturating, while determining the K_m value for the other two substrates. Hence, the K_m values for GTP and aspartate reported for the R155L mutant are apparent values.

Table 4.5: Kinetic parameters for wild type and Arg155 mutants of adenylosuccinate synthetase from *P. falciparum* measured in Hepes, pH 7.0 and at 25°C.

Protein	k_{cat} (min^{-1})	K_m		
		IMP (μM)	GTP (μM)	Aspartate (mM)
Wild Type	59.92 ± 4.5	20.5 ± 2.1	27.14 ± 4.3	0.37 ± 0.03
R155K	6.97 ± 0.49	557.4 ± 0.1	38.57 ± 4.6	0.48 ± 0.02
R155L	0.62 ± 0.07	2554 ± 260	$27.85 \pm 4.8^{\text{a}}$	$1.32 \pm 0.03^{\text{a}}$
R155A	0.38 ± 0.01	ND	ND	ND
T309V		Inactive		

^a apparent K_m values.

These results show that Arg155 contributes significantly to the binding of IMP by stabilizing the dimer through hydrogen bonding interactions with IMP in the active

site of the symmetry related subunit. In addition, a dramatic drop in catalytic efficiency of the arginine mutants was observed. This was not unexpected for the R155A mutant where the loss in stable quaternary structure probably resulted in extremely low activity of the mutant. However, R155L and R155K mutants exhibited secondary, tertiary and quaternary structural features which were largely similar to that of the wild type protein (Section 4.3.5). In *E. coli* AdSS, mutation of the corresponding arginine residue (Arg143) to leucine and lysine did not alter the catalytic efficiency and aspartate K_m value of the enzyme. Differences were observed in the binding affinities of the mutants for IMP and GTP. While the GTP K_m value showed 2 and 10 fold increase for R155K and R155L mutants, respectively, increase in IMP K_m value was about 100 fold for both mutants (Wang *et al.*, 1997a). Replacement of Arg155 with lysine, that carries a positive charge in the side chain, did not restore wild type characteristics in PfAdSS, thereby suggesting that not only the positive charge, but specific side chain length and orientation of the guanidinium group of arginine is necessary for optimum catalysis and substrate binding. Replacement of arginine with lysine leaves a void at the interface which is probably filled by a water molecule. This gives conformational flexibility to the side chain of the residue at position 155, thereby allowing more than one possible conformational arrangement of the side chain. Of these only one particular arrangement of the lysine residue would be conducive for substrate binding, thereby resulting in reduced substrate affinity of the mutant. A similar reasoning has been put forth to explain the kinetic properties of Arg143 mutants in *E. coli* AdSS (Wang *et al.*, 1997a).

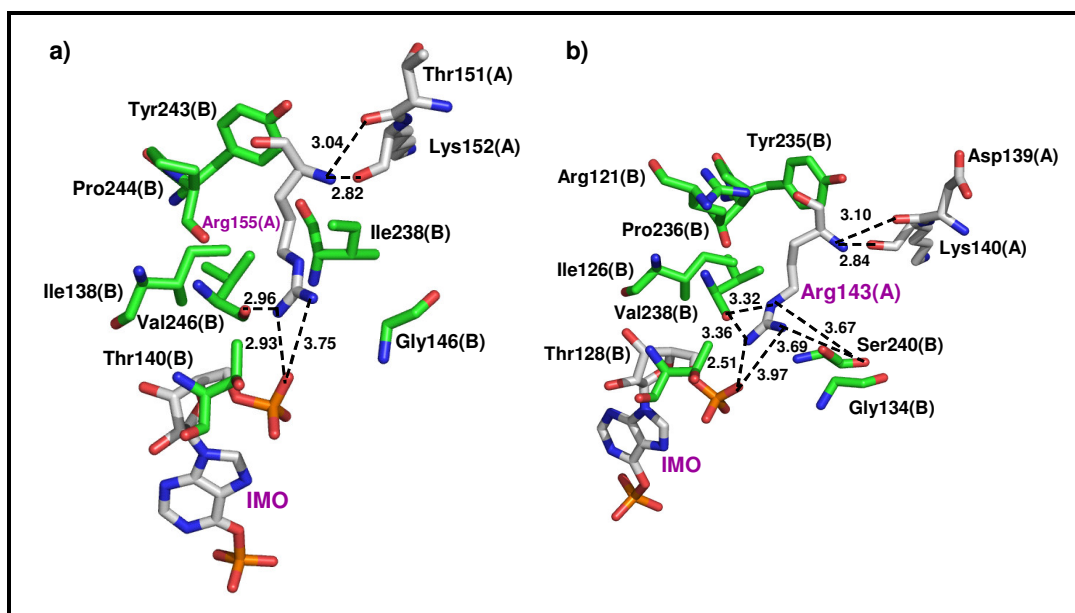


Figure 4.21: Environment of a) Arg155 in PfAdSS and b) Arg143 in *E. coli* AdSS. The hydrogen bonds made by the guanidinium group of arginine are shown by dashed lines. The numbers represent bond length in Å. Residues from the symmetry related subunit is shown in green. An additional serine comes in the vicinity of Arg143 in *E. coli* AdSS. IMO denotes 6-phosphoryl IMP. The figure was generated using PyMOL (DeLano, 2002).

In addition to IMP of the symmetry related subunit, Arg155 contacts other residues that lie at the dimer interface and also residues that constitute the IMP loop (residues 131-143), which is one of the loop that undergoes a conformational change on ligand binding. Thus, mutation of arginine may disrupt the organization of the IMP loop which in turn may also lead to suboptimal organization of the other dynamic loops in PfAdSS. Impaired catalysis may therefore result from improper orientation of the loops which carry the catalytic residues and other residues involved in ligand binding and stabilization of the transition state. Arginine contacts are largely conserved across *E. coli* and *P. falciparum* AdSS (Figure 4.21), except for a serine residue that comes in the vicinity of Arg143 in *E. coli* AdSS. This indicates that the observed differences in *P. falciparum* and *E. coli* AdSS with respect to the arginine mutants may be species specific.

As discussed in Section 4.3.5 of this chapter, Arg155 to alanine mutation destabilizes the quaternary structure of the protein. The replacement of arginine with alanine at the interface leaves a void and results in loss in interface contacts involving

the Arg155 side chain. Filling the void by a second mutation may restore structural stability and improve activity of the protein. Examination of the environment around Arg155 highlighted the presence of a glycine residue at position 146. Model building showed that mutation of Gly146 to arginine could fill the cavity created at the interface. Hence, R155A-G146R double mutant was constructed and purified as a his-tagged fusion protein. Analytical gel filtration chromatography of the double mutant showed that the protein elutes as two peaks with retention volumes corresponding to molecular mass of 47 kDa (monomer) and 94 kDa (dimer). Integration of the area under the peak indicated that the mutant was predominantly monomeric. Unlike the R155A mutant, the R155A-G146R double mutant exhibited secondary and tertiary structural characteristics similar to the wild type protein. Though, structural stability was achieved by introducing a second mutation, the k_{cat} value did not exhibit any improvement over the R155A mutant. This highlights the need for precise orientation of Arg155 side chain both for IMP binding and catalysis, which if impaired leads to dramatic drop in catalytic activity.

4.3.13 Characterization of T309V mutant

The side chain of Thr309 hydrogen bonds with the carboxyl group of hadacidin. OG of Thr309 also makes a hydrogen bond with Arg311 which lies at one end of the aspartate loop (Residues 306-312, Figure 4.22). Arg311 is a conserved residue and its mutation (Arg303) in *E. coli* AdSS resulted in dramatic increase in aspartate K_m value as well as a 10-fold reduction in k_{cat} value. Destabilization of the conformation of IMP and Aspartate loop as a consequence of Arg303 mutation was proposed to be responsible for reduction in activity and substrate affinity of the mutant (Wang *et al.*, 1995). Arg311 in PfAdSS interacts with Thr309 and also with residues in Val Loop, IMP Loop and with 6P-IMP in the active site of the enzyme.

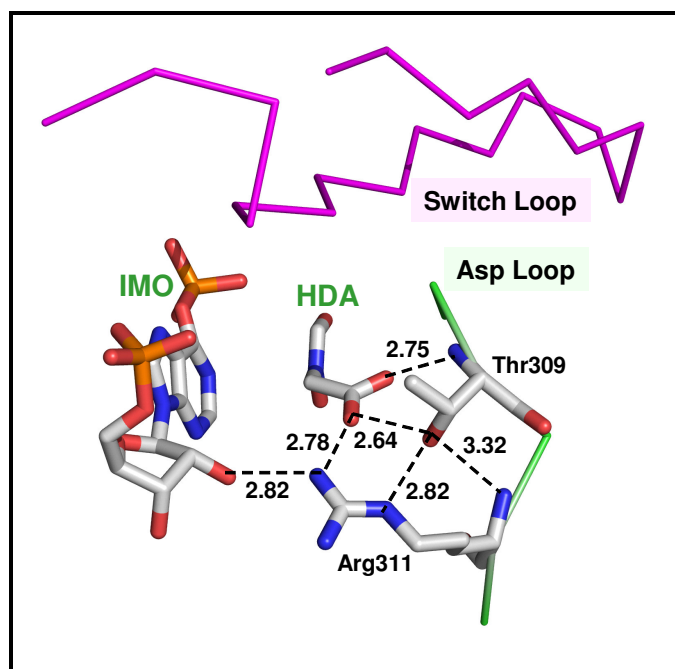


Figure 4.22: Hydrogen bonding interactions involving Thr309 in PfAdSS. The numbers indicate the distance in Å. IMO denotes 6-phosphoryl IMP and HDA denotes hadacidin. The figure was generated using PyMOL (DeLano, 2002).

Mutation of Thr309 to valine completely abolished activity in PfAdSS. No product formation could be detected even at high enzyme or high aspartate concentration. The loss in activity is not a consequence of loss of structural stability of the mutant, as evident from size-exclusion chromatography, fluorescence and circular dichroism spectroscopy measurements (Table 4.2, Figure 4.12). Hence, the absence of catalytic activity could be a consequence of either decrease in affinity for the substrate or a direct effect of the mutation on the k_{cat} value. Mutation of Thr309 to valine would result in complete loss of all interactions contributed by the side chain hydroxyl group, including those with carboxyl group of hadacidin. The observed loss in activity of the mutant could be an indirect effect seen as a consequence of the loss of interaction of Thr309 with residues such as Arg311, which in turn contact residues in other catalytic loops. Loss of these interactions may result in the improper orientation of loops that bind ligands and harbor the catalytic residues.

Mutation of the corresponding threonine (Thr301) in *E. coli* AdSS also lead to a similar observation when L-aspartate was used as a substrate. However, the kinetic parameters for the Thr301 to alanine mutant were similar to the wild type enzyme

when hydroxylamine was used as a substrate, thereby indicating that the threonine residue makes critical hydrogen bonds with the β -carboxyl group of L-aspartate which are necessary for aspartate recognition (Gorrell *et al.*, 2002). A similar feature may be true for the Thr309 mutant in PfAdSS.

4.3.14 Activation of PfAdSS by fructose 1,6 biphosphate (F16BP)

In contrast to other AdSS, PfAdSS was not inhibited by F16BP even at a concentration of 2 mM. Remarkably, a significant enhancement in activity was observed when GTP was limiting in reactions initiated with aspartate (Figure 4.23). No activation was evident when IMP and GTP were kept saturating or when the reaction was initiated with the nucleotide substrates or the enzyme. The activation seen on initiation with aspartate is indicative of F16BP binding to a site that is probably made inaccessible in the presence of aspartate.

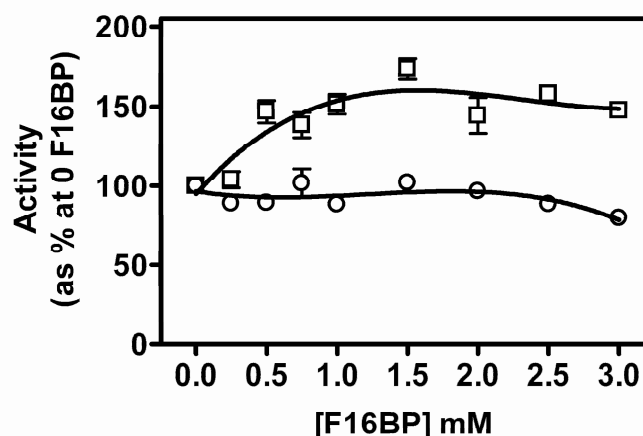


Figure 4.23: Effect of F16BP on the activity of PfAdSS at saturating (250 μ M IMP and 150 μ M GTP, circles) and subsaturating (150 μ M IMP and 50 μ M GTP, squares) substrates. Activity in the absence of F16BP is taken as 100%. Activity is plotted as a percentage of the activity in the absence of F16BP. Reactions were carried out in 30 mM sodium phosphate, pH 7.4 and at 25°C and initiated with 5 mM aspartate. The lines in the figure are the best fit of the data points and do not represent a fit to any kinetic model.

4.3.15 Molecular docking

In the absence of a crystal structure of PfAdSS bound to F16BP, docking was used to predict a binding site for the molecule on the enzyme. Biochemical studies showed that the activation of PfAdSS by F16BP was evident only when the reaction was initiated with aspartate. AdSS has five loops that respond to substrate binding. IMP alone organizes all the loops except for the aspartate loop that gets organized after aspartate binds to the active site cavity. Thus, the biochemical observations imply that the interactions of F16BP with the enzyme facilitate aspartate binding, thereby, resulting in activation. The fully liganded structure of *P. falciparum* AdSS, having 6-phosphoryl IMP, GDP, Mg²⁺ and hadacidin bound at the active site, was used for the docking studies. Nine sites involving the aspartate loop were examined to find a probable binding site for the metabolite (Figure 4.24). F16BP was docked and scored at each of the 9 sites using the Flexidock program. Infact, F16BP was docked twice at each site – once with hadacidin being present and once with hadacidin being left out of the enzyme active site. During docking at each site, the terminal side-chain torsion angles of Arg, Lys, His, Gln, Asn, Glu and Asp residues occurring at the site were allowed to rotate. By allowing only the terminal bonds to rotate it was ensured that the conformation of the protein backbone and most of the side-chains was not drastically altered and also the side-chain functional group had some freedom to reorient themselves and form H-bonds with F16BP. All single bonds in the ligand were allowed to rotate, allowing the ligand to change conformation. The program, Flexidock, uses genetic algorithms to find and score the best orientation. The score is an energy value and more negative the score, more favorable is the docking.

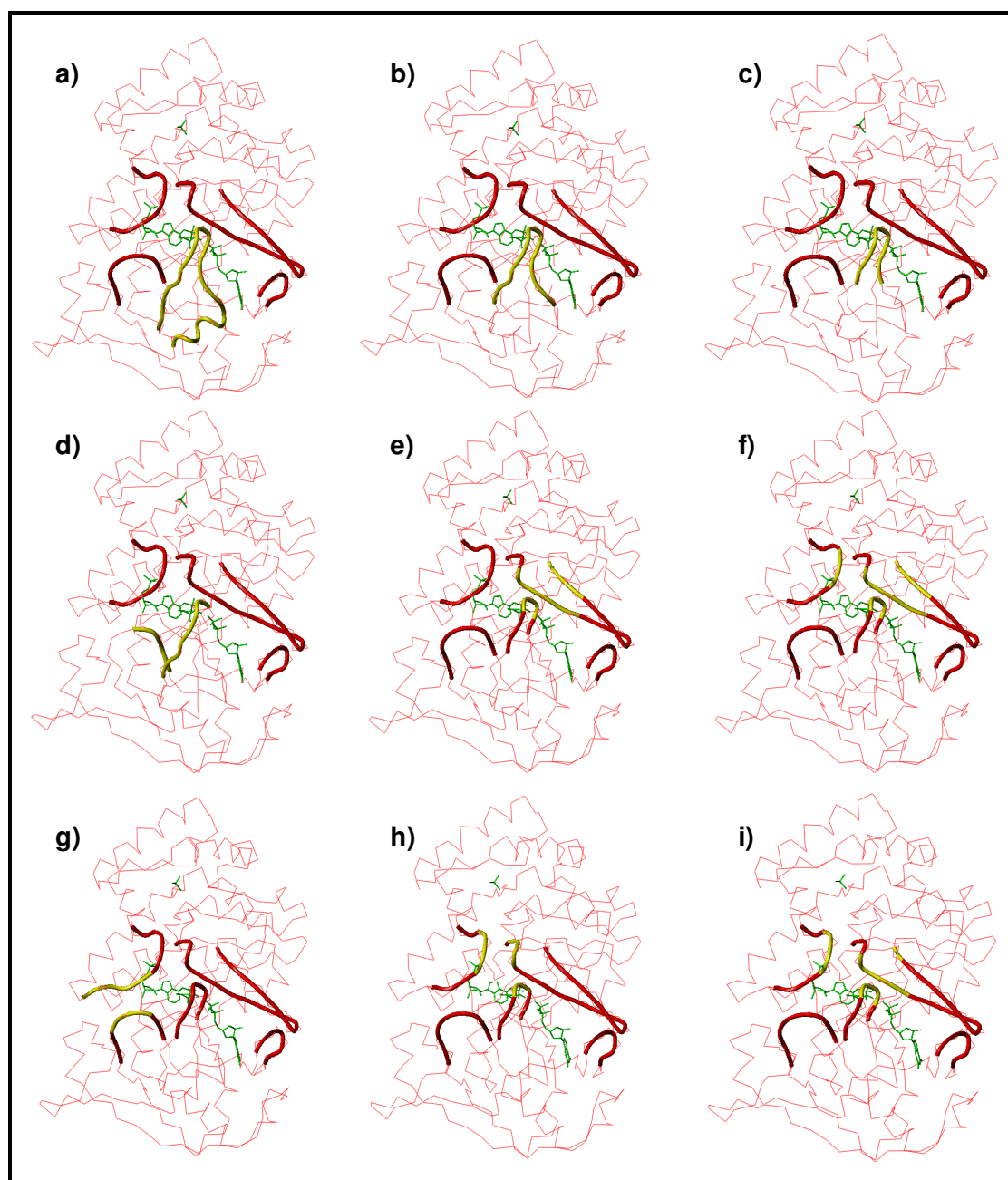


Figure 4.24: The nine sites selected for F16BP docking. Shown in green sticks are the ligands in the active site. Marked in yellow are the sites used for docking. The residues comprising each site are a) Gly295-Gly316, b) His303-Arg314, c) Tyr305-Pro312, d) Thr308-Arg314 and Thr279-Gly282, e) Thr307-Thr309, Asn51-Thr55 and Ala64-His66, f) Thr307-Thr309, Asn51-Thr55, Ala64-His66 and Thr141-Arg143, g) Gly282-Gly284 and Lys136-Thr140, h) Thr141-Gly144, Gly49-Asn51 and Thr308-Thr309 and i) Thr307-Thr309, Asn51-His54 and Thr141-Gly144.

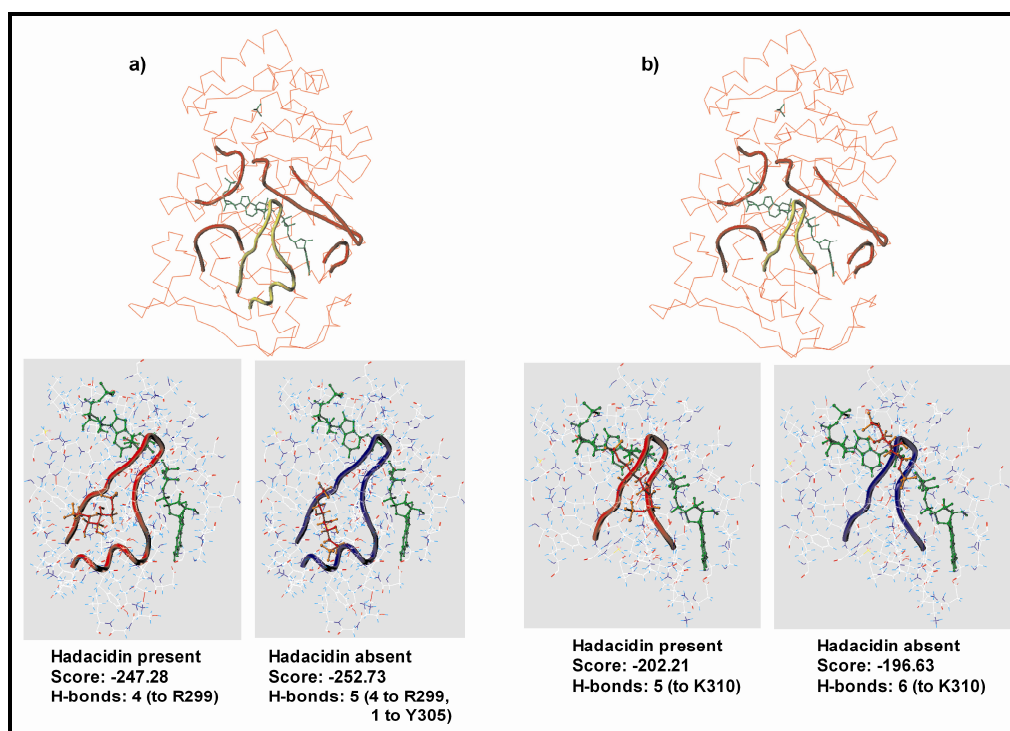


Figure 4.25: The favorable sites for F16BP docking. The active site loops in the top panel are shown as red tubes. Region selected for docking are shown in yellow in the top panels and in red and blue in the lower panels. The ligands are shown in green and F16BP molecule is shown in red sticks.

The docking scores were found to be most favorable for the sites marked as (a) and (b) in Figure 4.24. At the first site, the F16BP docking score without hadacidin (-252.7) was marginally more favorable than the docking score with hadacidin (-247.3) (Figure 4.25). Kinetics also indicated that F16BP interacts more favorably with the enzyme in the absence of aspartate resulting in a change in the active site, thereby leading to enzyme activation. Further, F16BP in the absence of hadacidin made 5 H-bonds with the enzyme as compared to 4 H-bonds in the presence of hadacidin. The residues predicted to be involved in making H-bonds with F16BP (Arg299 and Tyr305), are not conserved across Plasmodium, *E. coli* and mouse AdSS. An examination of Figure 4.25, suggests that F16BP binding at the first site might push the hairpin end of the aspartate loop outwards, resulting in easy access of the ligand to the active site of the enzyme.

4.3.16 Fructose 1,6 bisphosphate activation of the mutants

The activation by fructose 1,6 bisphosphate was monitored for the wild type enzyme, N429V, K62L and T307V mutants in Hepes, pH 7.0 and 37°C. PfAdSS showed a 35% increase in activity at 1.5 mM F16BP when the reaction was initiated with aspartate at subsaturating GTP concentration (Figure 4.26a). With further increase in F16BP concentration there was a decrease in the level of activation with inhibition setting in at F16BP concentration >4mM. The activation was found to be sensitive to aspartate concentration with maximum enhancement in activity being observed when aspartate was maintained at 5-6 times the K_m value.

Effect of F16BP on the activity of the mutants was checked. N429V and K62L mutants exhibited features similar to the wild type enzyme, showing 45% and 39% activation at 1.5 mM F16BP concentration, respectively (Figure 4.26 b,c). With increase in F16BP concentration, there was a gradual decrease in activation and at concentrations greater than 4 mM, inhibition in activity was observed. Like in wild type enzyme, no activation was seen when the reaction was initiated with either enzyme, IMP or GTP. Saturating levels of GTP also resulted in loss of activation of the mutants. Interestingly, activation was completely abolished in T307V mutant with a 50% drop in activity of the mutant seen at 7 mM F16BP (Figure 4.26 d).

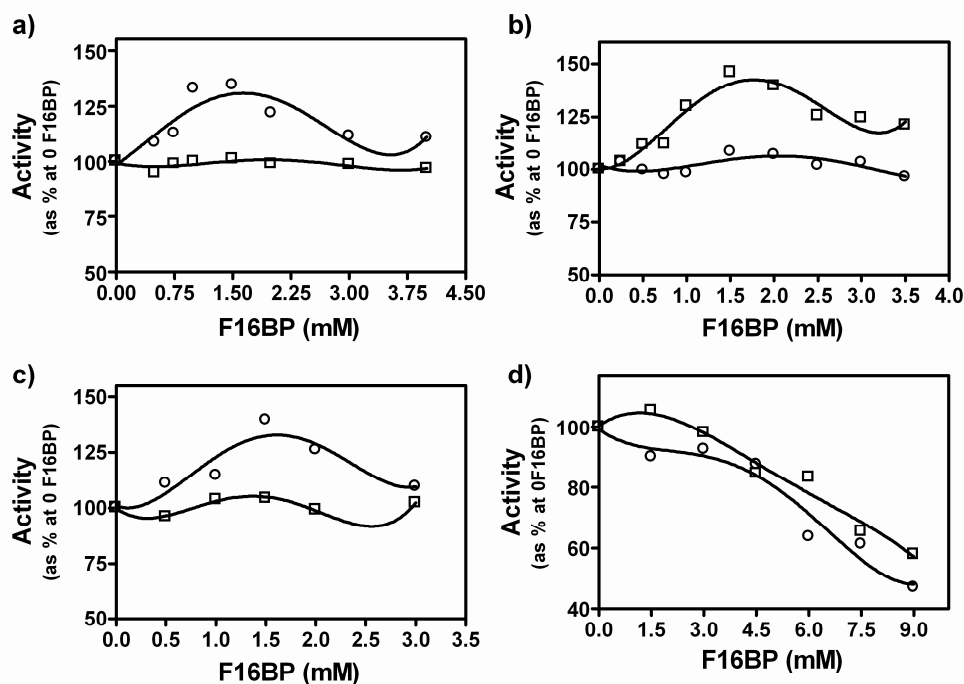


Figure 4.26: Effect of fructose 1,6 bisphosphate on the activity of a) wild type, b) K62L, c) N429V and d) T307V mutants in Hepes, pH 7.0 and at 37°C. IMP, GTP and aspartate were maintained at 5, 2 and 5 times their respective K_m s for each enzyme. The reactions were initiated with aspartate. Activity in the absence of F16BP is taken as 100%. The lines in the figure are best fit of the data points and do not represent a fit to a kinetic model.

This observation provides biochemical support for the docking studies which showed that F16BP interacts with the Aspartate loop and facilitates aspartate binding to the enzyme. Mutation of Thr307 to valine resulted in an increase in aspartate K_m value probably as a consequence of the loss of interaction of Thr307 with hadacidin and residues in the aspartate loop which in turn maintain proper conformation of the Aspartate loop (Section 4.3.9). Perturbation in orientation of the Aspartate loop may result in loss of F16BP binding site which according to docking data binds across the loop and stitches the two ends of the loop. Inhibition of activity of the wild type enzyme as well as the mutants at high F16BP concentrations, implicates a second binding site for this molecule on the enzyme. A preliminary crystallographic analysis by Borza *et al.* showed that F16BP bound as an analog of 6P-IMP. On the basis of this observation and other biochemical evidences they proposed that F16BP binds to the IMP binding site, when IMP is subsaturating. However, at saturating

concentration of IMP it binds to another unidentified site (Borza *et al.*, 2003). Indeed F16BP was found to be competitive inhibitor of IMP and a noncompetitive inhibitor of GTP in MjAdSS exhibiting a K_i value of 1.5 mM (Mehrotra & Balaram, 2007).

4.3.17 Physiological implications of the activation of PfAdSS by fructose 1,6 bisphosphate

Higher metabolic rate in a rapidly dividing system like *P. falciparum* imposes higher demand for ATP in the cell. As *P. falciparum* derives its entire ATP pool from glycolysis alone (Sherman, 1979), flux through this pathway would be high, potentially leading to high intracellular intermediate concentrations. Though absence of inhibition of PfAdSS by F16BP is significant, the physiological relevance of the activation is not obvious. F16BP concentrations as high as 3.2 mM and 2.5 mM have been reported for *E. coli* and yeast, respectively (Buchholz *et al.*, 2001; Albers *et al.*, 2002). Oscillations in glycolytic intermediates have been shown to correlate with oscillations in the levels of adenine nucleotides in rat muscle (Tornheim & Lowenstein, 1974). The activation by F16BP seen with PfAdSS may be important for the co-ordinated regulation of these two primary pathways in the parasite, especially since it occurs at low concentrations of GTP, a nucleotide that may be limiting due to the low GC content of the *P. falciparum* genome.

4.4 Conclusion

In summary, studies described in this chapter elucidate the role of Asn429, Lys62 and Thr307 in modulating substrate affinity and catalysis in the parasite adenylosuccinate synthetase. AdSS employs dynamic loops in catalysis which undergo large conformational changes on ligand binding. The effect of the mutations on enzyme activity and substrate affinity can be understood on the basis of direct influence of the target residues in ligand binding or by their influence on ligand induced organization of the enzyme active site. Although mutation of these residues

did not alter the ordered substrate binding, the effect on Michaelis constants for the nucleotide substrates and aspartate was evident. Mutation of a conserved threonine, Thr309 completely abolished activity, an effect similar to that observed in *E. coli* enzyme. Mutation of Arg155 lead to an increase in IMP K_m value along with a dramatic reduction in k_{cat} value of the mutants, implicating the role of this residue in not only modulating the affinity of the enzyme for IMP but also in catalysis probably through its interactions with residues in other dynamic loops. Interestingly the double mutant, R155A-G146 was predominantly monomeric in nature. Studies with these mutants also helped in understanding the probable mode of activation of the parasite enzyme by the glycolytic intermediate, F16BP. Docking studies predicted a binding site for the metabolite on the Aspartate loop. Complete loss of activation in Thr307 mutant, which also exhibits reduced affinity for aspartate, provides biochemical support for the docking studies.

Chapter 5

Studies on Interface Cysteine Mutants of *P. falciparum* Adenylosuccinate Synthetase

This chapter discusses the role of interface cysteines in maintaining dimer integrity and stability of P. falciparum adenylosuccinate synthetase. Site-directed mutagenesis of two non-conserved interface cysteine residues in PfAdSS highlights the possible role of negatively charged cysteines in maintaining structural stability of the P. falciparum enzyme. This is further supported by the crystal structure of PfAdSS which shows additional electron density around the interface cysteines, Cys328 and Cys368.

5.1 Introduction

5.1.1 Cysteines

Cysteine by virtue of its thiol group endows proteins with unique biochemical properties. Its nucleophilicity, redox activity and metal binding property makes cysteine a key catalytic component of enzyme function and enables proteins containing cysteine to act as “redox switches” and provide “storage facility” for excess metal ions, to control the activity of metalloproteins and to take part in important regulatory and signaling pathways (Giles *et al.*, 2003a; Giles *et al.*, 2003b). Cysteine thiols in proteins can be divided into four broad categories, those that form

permanent disulfide bonds, those that coordinate metals, those that are permanently in the reduced state and those that are reversibly oxidized. The last category of protein thiols are of interest from the perspective of redox regulation.

Reactive oxygen species (ROS) including superoxide anion (O_2^-), hydrogen peroxide (H_2O_2) and hydroxyl radical (OH^\cdot) and reactive nitrogen species (RNS) including nitric oxide (NO) and peroxynitrite ($ONOO^-$) are involved in many physiological as well as pathological conditions. The antioxidant defense mechanisms operating in a living cell tightly regulate the level of ROS/RNS. However, aging and disease result in excessive generation of ROS/RNS which cannot be taken care of by the antioxidant defense mechanisms, and this condition is known as oxidative stress. Excess oxidants affect cellular components like membrane lipids, proteins and nucleic acids. The reaction of oxidants with biomolecules is the basis of sensing perturbation in the redox status of the cell. The translation of the oxidant signal into a biological response can be mediated in several ways, one of which involves oxidation of cysteine thiols in proteins, which results in either activation or inactivation of the target protein. Not all cysteine thiols are capable of functioning as redox sensors. The pKa of most protein thiols is approximately 8.5 and hence, are less reactive at intracellular pH. However, some thiols ionize to thiolate anion more readily because their surrounding environment lowers their pKa and such cysteines have higher reactivity for oxidants. The oxidation susceptibility of cysteines in proteins depends on their solvent accessibility and the identity and distance of atoms surrounding the thiol. Proximity to basic amino acids that stabilize the negative charge on the thiolate anion promotes ionization of the cysteine residue (Poole, 2003a; Claiborne *et al.*, 2001). Cysteine thiol oxidation often results in the formation of intramolecular disulfide bonds, but in the absence of a nearby cysteine residue, thiol oxidation typically results in the formation of sulfenic acid, sulfinic acid, sulfonic acid, S-nitrosothiol and S-nitrothiol (Eaton, 2006). There is increasing evidence to implicate the role of cysteine modification in regulation of protein activity (Barford 2004; Claiborne *et al.*, 1999; Giles *et al.*, 2003a; Poole *et al.*, 2004). Further, modification of reactive cysteines in receptors, phosphatases and kinases modulates the cell signaling

cascades (Cross & Templeton, 2006; Salmeen & Barford, 2005; den Hertog *et al.*, 2005).

A) *Cysteine oxyacids*

Cysteine thiol oxidation by molecular oxygen or peroxide compounds gives rise to several oxidized species including sulfenic (–SOH), sulfinic (–SO₂H), and sulfonic (–SO₃H) acid derivatives. The sulfonate state is irreversible and leads to protein dysfunction and eventually its cellular degradation. Cysteine sulfenic acids are generally regarded as highly unstable, short lived intermediates that are in most situations rapidly converted back to the reduced state as part of a catalytic cycle or are alternatively oxidized to a more stable state. Depending on the reaction conditions and presence of other redox active components, sulfenation may be an intermediate step in sulfination, sulfonation, disulfide bond formation and sulfenyl-amide bond formation (Poole *et al.*, 2004). Protein sulfenation has been recognized as an important post-translational modification with potential for regulation of protein function.

B) *Cysteine labeling*

There are many methods available to identify changes in the protein thiol status of cells and tissues, and also to identify the modification on the cysteine thiol. Oxidized thiols can be identified directly by using agents that react with specific oxidized species of cysteines or indirectly by the inability of thiol reactive agents to react with modified thiols. Mass spectrometry combined with labeling techniques is a powerful tool to identify cysteine oxidation states. A major limitation, however, is the high reactivity of the thiol derivatives which tend to get reduced as soon as they are removed from native protein environment.

i) *Free thiol labeling methods*

There are a wide range of thiol labeling agents that can be used to quantify free protein thiols. These include p-chloromercuribenzoate (PCMB), 5,5'-dithiobis (2-

nitrobenzoic acid) (DTNB), *N*-ethylmaleimide (NEM), iodoacetamide (IAM) and iodoacetate (IAA). The reactions can be monitored spectrophotometrically or by mass spectrometry. PCMB and DTNB are most routinely used reagents to quantify free thiols in proteins. The reaction product of these reagents with protein thiols can be quantified spectrophotometrically and since both reagents react quantitatively with thiols, they can be used to determine the number of free thiols in purified proteins. NEM, IAM and IAA are also used extensively to detect free thiols and are available tagged with radioactivity, biotin or fluorophores. Biotin tag allows concentration of the labeled protein using streptavidin whereas fluorescent and radiolabel tags allow direct detection. NEM reacts with thiols over a wide pH range but is nonspecific and exhibits low reactivity towards lysine, methionine, histidine and tyrosine residues and hence, is often not a reagent of choice.

ii) Labeling cysteine oxidation states

Sulfenic acids (R-SOH) are the simplest oxy-acids of sulfur, and unlike sulfenic (R-SO₂H) and sulfonic acid (RSO₃H) they are highly reactive and unstable. Sulfenic acid is formed upon mild oxidation of thiols and is a central intermediate in the redox modulation of a large number of proteins. One of the most important factors in sulfenic acid stabilization is the absence of proximal thiols. Other factors include proximity of suitable hydrogen-bonding and/or basic side chains to stabilize the protonated or deprotonated sulfenic acid and restricted solvent accessibility. Direct identification of sulfenic acids in proteins has been achieved by crystallography and NMR approaches. ESI-MS has also been used to detect sulfenic acid derivatives (Fungthong & Helmann, 2002). Chemical reagents that can be used to identify cysteine sulfenic acids are, 7-chloro-4-nitrobenzo-2-oxa-1,3-diazole (NBD chloride) or 4-fluoro-7-nitrobenzo-2-oxa-1,3-diazole (NBD fluoride), 2-nitro-5-thiobenzoic acid (TNB) and 5,5-dimethyl-1,3-cyclohexanedione (dimedone). NBD chloride reacts with both thiol groups and sulfenic acids in proteins at pH 7.0, resulting in adducts that can be distinguished spectroscopically and by mass. Thiol-NBD adduct absorbs at 420 nm and adds a mass of 164 Da for each modified thiol whereas sulfenic acid-NBD adduct absorbs at 347 nm and has an additional mass of 16 Da coming from

oxygen (Ellis & Poole, 1997). TNB reacts with sulfenic acids and the adduct formation can be monitored as a decrease in absorbance at 412 nm. Dimedone reacts specifically and irreversibly with cysteine sulfenic acid and not thiol and the reaction can be monitored by ESI-MS or radioactivity (Poole, 2003a). Readily detectable fluorescent and affinity probes to identify sulfenic acid modifications in proteins are available which can be combined with mass spectrometric analysis to confirm covalent attachment of the conjugates and directly determine the site of modification (Poole *et al.*, 2007; Poole *et al.*, 2005).

Direct detection by ESI-MS

ESI-MS under gentle conditions (e.g. ammonium bicarbonate buffer) can be used for direct detection of cysteine oxidation states and the resolution of the technique permits differentiation of various states of cysteines (Fuangthong & Helmann, 2002). However, overoxidation of sulfenic acid to sulfonic acid is observed when acetonitrile and formic acid are used as solvents.

C) Cysteine oxidation in proteins: Link to function

By virtue of the reversible nature of sulfenic acids and disulfide bonds, cysteines are suitable as catalytic redox centers or as redox-sensitive regulatory components within enzymes and transcription factors. Antioxidant enzymes such as NADH peroxidase, NADH oxidase and peroxiredoxins function via a Cys-SH/Cys-SOH redox couple (Claiborne *et al.*, 1999). Many enzymes utilize a catalytic cysteine residue in the form of a thiolate anion as a nucleophile. These include cysteine proteases like human apoptosis protease caspase-3, cathepsin F, cathepsin B and calpains (Giles *et al.*, 2003b). The oxidative inhibition of caspase activity has in vivo implication as these are important players in the apoptotic pathways. Several dehydrogenases are regulated by the redox status of an active site cysteine residue. In glyceraldehyde-3-phosphate dehydrogenase (GAPDH) from *Bacillus stearothermophilus*, Cys149 in its thiol form catalyzes the production of 1,3-bisphosphoglycerate. On oxidation to sulfenic acid, the enzyme does not catalyze the

dehydrogenase reaction, instead it participates in the direct hydrolytic decomposition of D-glyceraldehyde-3-phosphate (Schmalhausen *et al.*, 1999). Several metalloproteases and mammalian liver alcohol dehydrogenase (ADH) contain an active site zinc/sulfur complex that is under redox control. In ADH cysteine thiolate binds zinc ion that is essential for catalytic activity. Nitrosothiolation of the cysteine at the catalytic site releases zinc and hence results in loss of activity. However, in matrix metalloprotease family of proteases, cysteine thiolate occupies a coordination site on the metal that is essential for substrate binding (Massova *et al.*, 1998). In these proteins, upon oxidation of the thiolate, the binding site for the substrate becomes available which in turn results in activation of the protein (Gu *et al.*, 2002). Cysteine oxidation also influences signal transduction events in the cell. ROS mediate cell-signaling responses especially those that signal via receptor tyrosine kinases (Salmeen & Braford, 2005). Increased level of tyrosine phosphorylation mediated by ROS is via inactivation of protein tyrosine phosphatase (PTP) which in turn results in increase in protein tyrosine kinase (PTK) activity. PTPs are susceptible to oxidation owing to the catalytic site cysteine thiolate which acts as a nucleophile (Denu & Tanner, 1998). The chaperone, Hsp33 from *E. coli* responds to oxidative stress with the activation of chaperone activity (Jakob *et al.*, 1999). The redox sensitive cysteine residues in Hsp33 are located in a cluster that forms a high affinity Zn^{2+} binding motif. Under oxidizing conditions the Zn^{2+} ion is released and two intramolecular disulfide bonds are formed accompanied by dimerization of the oxidized monomers (Graf *et al.*, 2004). Zn^{2+} release and intramolecular disulfide bond formation exposes the substrate binding site and dimerization interface which in turn results in exposure of hydrophobic surfaces required for chaperone activity (Raman *et al.*, 2001). Transcriptional factors such as Fos, Jun (activator protein 1) and bovine papillomavirus-1 E2 protein sense changes in redox status through oxidation of Cys-SH to Cys-SOH which regulates their DNA binding activity (Xanthoudakis & Curran, 1996). Sulfenic acid dependent redox regulation of transcriptional regulators, OxyR, OhrR and NF- κ B, has been well studied. Cysteine sulfenic acid and intramolecular disulfide bond formation in response to oxidative stress have been implicated in modulating the DNA binding ability of OxyR and OhrR (Poole, 2003).

5.1.2 Protein association and interfaces

Protein subunit interactions play an important role in catalysis as well as regulation. Transient association between proteins forms the basis of a number of biological processes, such as, action of antibody against antigen, hormone-receptor binding, signal transduction cascades and enzyme allostery. Subunit associations that are permanent in nature are essential for proteins whose function and stability is dependent on multimerization. Thus in a multisubunit protein, it is important to understand the factors that drive subunit association and dissociation. Permanent interfaces between subunits are generally large, very often involving several peptide stretches which are sequentially separated but come close together to interact in the three dimensional protein structure and are stabilized by both hydrophobic and charge interactions. Transient interfaces on the other hand are less extensive and have a higher proportion of charged and polar groups, which in turn indicates the dominant role of hydrogen bonds and salt bridges in stabilizing these associations (Zhanzua *et al.*, 2005; Bahadur *et al.*, 2003; Conte *et al.*, 1999; Korn & Burnett, 1991). However, both types of interfaces are close-packed and exhibit geometric as well as electrostatic complementarity (Lawrence & Colman, 1993; McCoy *et al.*, 1997)

Subunit interfaces are very diverse, both in size and chemical composition. These interfaces have a core of hydrophobic residues containing atoms that are fully buried in the dimer. The core is surrounded by a rim, containing residues that have residual accessibility to the solvent and has a composition similar to that of the protein surface (Bahadur *et al.*, 2003). Interfaces are largely neutral with charged residues being neutralized by oppositely charged residues which belong to the same or the neighboring chain (Brinda *et al.*, 2002; Jones & Thornton, 1996). Interface residues in proteins are generally conserved and this highlights their importance in maintaining the stability of the oligomer (Hu *et al.*, 2000; Valder & Thornton, 2001; Brinda *et al.*, 2002). Several studies have indicated the preference for polar and hydrophobic residues at protein interfaces. Leucine, valine, arginine, histidine, phenylalanine and tyrosine are enriched at the interfaces. There is a significant contribution from methionine and tryptophan also. However, the interfaces are depleted in aspartic acid,

glutamic acid and lysine when compared to solvent accessible protein surface (Bahadur *et al.*, 2003; Zhanhua *et al.*, 2005; Brinda *et al.*, 2002; Lijnzaad & Argos, 1997; Jones & Thornton, 1996).

5.1.3 Dimerization in adenylosuccinate synthetase

As stated in Chapter 1, adenylosuccinate synthetase in solution is an equilibrium mixture of dimers and monomers. The dissociation constant for *E. coli* AdSS dimer in the absence of active site ligands was found to be 10 μ M and this reduced to a number indistinguishable from zero in the presence of substrates (Wang *et al.*, 1997a).

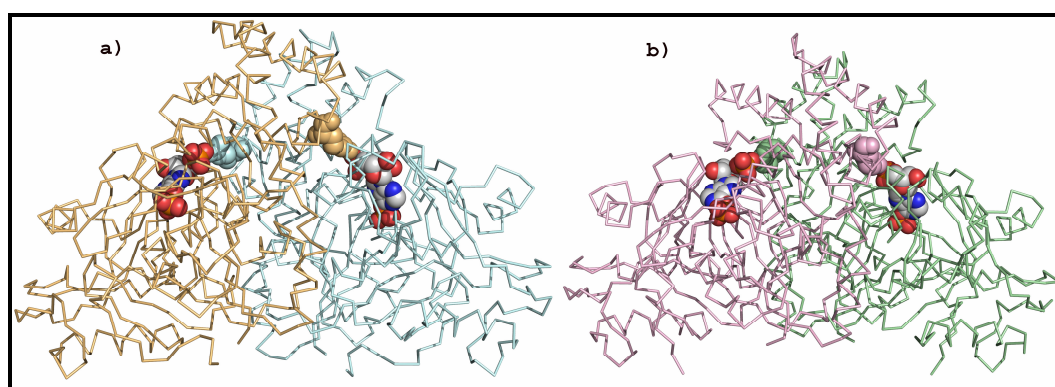


Figure 5.1: Ribbon representation of a) *E. coli* (PDB ID: 1CG0) and b) PfAdSS (PDB ID: 1P9B) dimer. Shown in spheres are IMP (CPK) and Arg 143 in blue and orange spheres (a) and Arg155 in green and pink spheres (b). The figure was generated using PyMOL (DeLano, 2002).

Crystal structures of AdSS provide a structural basis for the ligand induced stabilization of the AdSS dimer (Silva *et al.*, 1995; Poland *et al.*, 1996a; Poland *et al.*, 1996b; Eaazhisai *et al.*, 2004). In *E. coli* AdSS, the side chain of Arg143 from one subunit penetrates into the active site of the symmetry related subunit and hydrogen bonds with 5'-phosphoryl group of IMP (Figure 5.1). This arginine residue is absolutely conserved in all AdSS. Though not directly involved in catalysis, its interaction with IMP is essential for substrate binding (Wang *et al.*, 1997a). A complete active site of AdSS thus, requires structural elements from both subunits. The corresponding arginine in PfAdSS is Arg155 and studies on Arg155 mutants have

been described in Chapter 4 of the thesis. Essentiality of the dimer for catalysis in AdSS has been demonstrated by site-directed mutagenesis and subunit complementation studies in *E. coli* AdSS (Wang *et al.*, 1997a; Kang *et al.*, 1996).

Dimerization in AdSS buries a large surface area with both hydrophobic and hydrophilic interactions contributing to subunit association. The subunit interface in the mouse enzyme has fewer salt links, more hydrophobic contacts and an equal number of hydrogen bonds when compared to the *E. coli* enzyme. Segments contributing to the dimer interface in *P. falciparum* and *E. coli* AdSS are largely similar (Figure 5.2). Stretches of residues that contribute to the interface in PfAdSS are 149-159, 243-270 and 325-333. Both hydrophobic and hydrophilic interactions, including four salt bridges and 18 hydrogen bonds (cut off value 3.5 Å), stabilize the dimer (Eaazhisai *et al.*, 2004). Other unique features of the dimer interface in PfAdSS are discussed later in the chapter.

An examination of the sequence alignment of mouse, *E. coli* and *P. falciparum* AdSS shows that the mouse and *E. coli* enzymes have 5 and 4 cysteines, respectively, 2 of which are at the interface of the mouse enzyme. None of the 4 cysteines in *E. coli* AdSS occur at the interface. PfAdSS has 10 cysteines per monomer, out of which three lie at the interface. These are Cys250, Cys328 and Cys368 and are not conserved across mouse or *E. coli* AdSS (Figure 5.2).

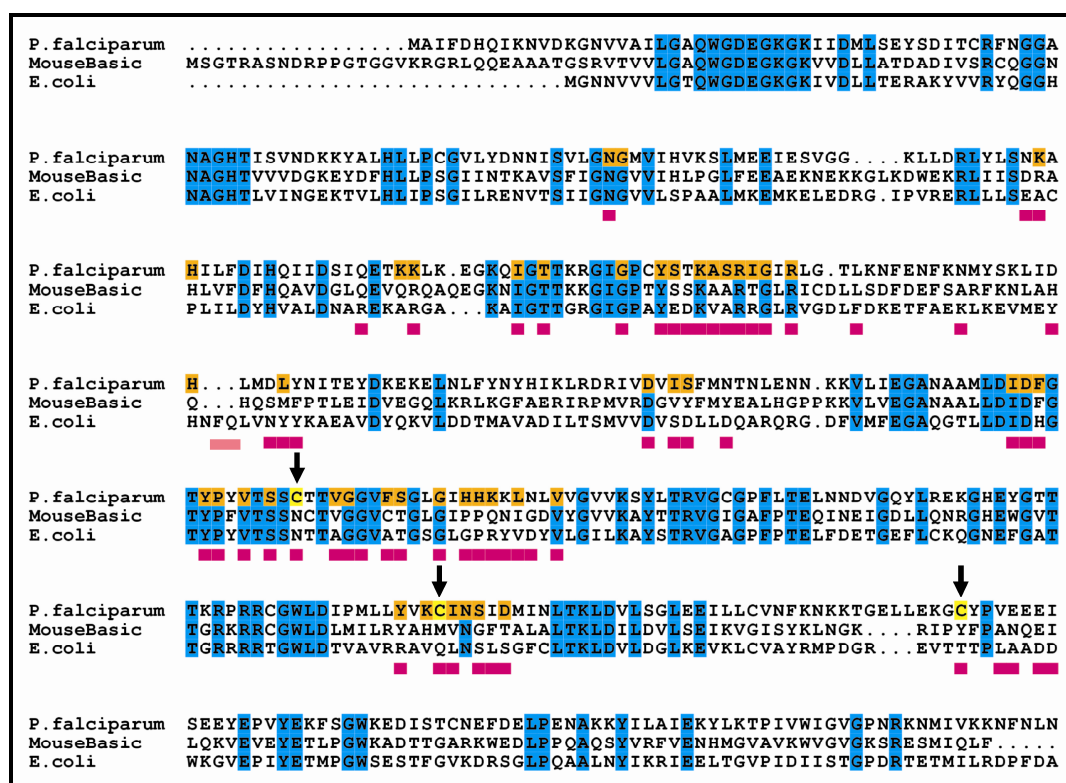


Figure 5.2: Sequence alignment of *P. falciparum*, *E. coli* and mouse AdSS. Conserved residues are shaded in blue, residues at the interface of PfAdSS are shaded in orange and the pink bars show the residues that constitute the interface of *E. coli* AdSS. The arrows show the three interface cysteines, Cys250, Cys328 and Cys368 in PfAdSS. The alignment was generated using CLUSTAL W (Thompson *et al.*, 1994) and represented using ESPRIPT (Gouet *et al.*, 1999).

Cysteine modification studies with *E. coli* AdSS suggested that free cysteines are not essential for catalysis. The cysteines were divided into three classes based on their reactivity. The highly reactive Cys291 was classified in Class 1, Cys344 which gets modified only in presence of 3.5 M urea formed the second class, and class 3 comprised of Cys103 and Cys328 which became accessible to thiol modifying agents only in presence of 8 M urea (Dong *et al.*, 1990). AdSS from Yoshida sarcoma ascites tumor cells was found to be inactivated by very low concentrations of Hg^{2+} , with the activity being restored on treatment with excess of DTT. Treatment with the thiol modifying agent, PCMB, also resulted in complete loss of activity (Matsuda *et al.*, 1980). The rabbit skeletal muscle enzyme was completely inactivated on incubation with the thiol modifying agent, DTNB (Muirhead & Bishop, 1974).

5.1.4 Structural and functional role of cysteines in *P. falciparum* AdSS

Earlier studies on PfAdSS showed that in the absence of DTT in the purification buffers, protein elution was spread over a wide range of salt concentration on an anion exchange column. All protein fractions collected were inactive and addition of DTT after purification did not restore the activity. However, when the purification was carried out in the presence of 1 mM DTT, the protein eluted as a sharp peak at about 100 mM NaCl. The protein was active but on storage in 20 mM Tris HCl, pH 8.0, 1 mM DTT, 10% glycerol and 100 mM NaCl showed loss of activity with time. Stabilization of activity could be achieved by lowering the pH and introduction of 1 mM EDTA in the storage buffer. Under these conditions the enzyme activity was stable for atleast three months at 4°C (Jayalakshmi *et al.*, 2002). These observations hinted towards the role of contaminating metal ions and cysteines in the inactivation of PfAdSS. The effect of two metal ions, Cu²⁺ and Mn²⁺, on enzyme activity was examined. Presence of 5 mM MnCl₂ did not alter the activity of the protein. However, addition of 5 mM CuCl₂, which is a redox active metal, resulted in protein precipitation. Addition of only 0.5 mM CuCl₂ resulted in rapid loss of enzyme activity with complete inactivation observed in 48 hours. This was surprising, as the concentration of EDTA during the inactivation was 1 mM which was 2 fold in excess of Cu²⁺ added. Presence of IMP alone or in combination with GTP protected the enzyme from inactivation. Non-reducing SDS-PAGE showed that the inactivation was accompanied by the formation of disulfide bonded species (R. Jayalakshmi, Thesis).

Effect of cysteine modifying agents on activity and stability of PfAdSS

In the absence of substrates, treatment with iodoacetate (IAA) for 15 minutes at 4°C lead to almost complete loss of activity of PfAdSS and this inactivation was prevented in the presence of IMP. Size exclusion chromatography of the IAA modified samples showed that iodoacetate modification was accompanied by a shift in elution profile of the protein towards a larger retention volume. Iodoacetamide

(IAM) treatment also lead to loss of activity and the modified protein failed to give a defined peak on a Superdex 200 column (R. Jayalakshmi, Thesis).

These observations indicate that cysteine modification results in dimer dissociation and implicate the role of interface cysteines in maintaining dimer integrity and stability of PfAdSS. They also raise the possibility of the role of negatively charged cysteine/cysteines at the interface of PfAdSS in maintaining dimer stability. Iodoacetate modification of cysteine results in the formation of a negatively charged adduct, whereas modification with iodoacetamide results in the formation of a neutral species. The fact that iodoacetate modification resulted in shift in equilibrium towards a monomer, whereas, iodoacetamide modification lead to the distribution of the protein over different oligomeric states, hinted at the possible involvement of negatively charged cysteines in maintaining dimer stability in PfAdSS.

The crystal structure of PfAdSS complexed with 6-phosphoryl IMP, GDP and hadacidin, was solved to 2 Å resolution (Eaazhisai *et al.*, 2004). The structure highlights unique features of the dimer interface of PfAdSS which will be discussed later in the chapter. In the structure two of the interface cysteines, Cys328 and Cys368, show additional electron density, although the precise nature of the modification could not be deduced from the electron density map.

This chapter describes the results of studies carried out to identify the nature of interface cysteines in PfAdSS and to establish their role in maintaining dimer stability.

5.2 Material and Methods

Restriction enzymes, *Taq* DNA polymerase, T4 DNA ligase were from Bangalore Genei Pvt. Ltd. (Bangalore, India) and oligonucleotides from Microsynth AG (Balgach, Switzerland). Media components were from Hi Media (Mumbai, India). IMP, GTP, aspartate, protein markers for gel filtration, cysteine modifying agents and other reagents were from the Sigma Chemical Company (St. Louis, MO). Column

materials and Akta Basic HPLC were from Amersham Pharmacia (Uppsala, Sweden). UV spectrophotometer and spectrofluorimeter were from Hitachi High-Technologies Corporation, Tokyo, Japan.

5.2.1 Site-directed mutagenesis

Interface cysteine to serine mutants, C328S, C368S and C328S-C368S, were already available in the laboratory at the time of initiation of these experiments. To construct the interface cysteine to aspartic acid mutants, site-directed mutagenesis was carried out by the megaprimer PCR method. The primers used were:

Asfl: 5' ACACCATGGCCATATTTGATCATCAAATAAAAAATG 3'
AdSSc: 5' CCAGGTACCCTCGAGTTAGTTTAGGTTAAAATTCTT 3'
C328D: 5' ACCAATGTTATTATATGTTAAG**GATAT**CAATAGTATTGA
TATGATAAACTT 3'
C368D: 5' CTGCTTGAAAAGGGT**GACTACCCGGT**TGAAGAAG 3'.

Asfl and AdSSc are the end primers of the PfAdSS gene. In addition to the desired mutation, primers C328D and C368D also contained restriction sites (indicated in bold and italics) incorporated by silent mutagenesis, in order to aid the selection of recombinants. The sites incorporated were *EcoRV* in C328D and *NciI* in C368D. The mutated codons are shown in bold and underlined. The wildtype PfAdSS gene in pET23d vector was used as a template for the construction of the single mutant, C328D. Briefly, the mutagenic primer along with the C-terminal primer (AdSSc) was used to generate the megaprimer containing the mutation. The PCR mix contained 200 ng of each primer, 20 ng of the template, 200 μ M of each dNTP and 5 units of *Pfu* polymerase for a 50 μ l reaction. Hot start PCR was used with an initial denaturation at 98°C for 5 minutes, followed by 30 cycles of denaturation at 94°C for 40 seconds, annealing at 55°C for 30 seconds and extension at 72°C for 90 seconds. The product obtained after 30 cycles of PCR was purified by elution from agarose gel and used as the megaprimer in a second round of PCR. The other primer used in the second PCR was Asfl and the PCR conditions used were as described above with the

extension time increased to 3 minutes. The full-length amplified product containing the desired mutation was purified, digested with the enzymes *Nco*I and *Xho*I and ligated into pET23d vector digested with the same enzymes. Recombinants were selected after transformation into the *E. coli* strain DH5 α on the basis of supercoiled plasmid mobility. The presence of the right insert was confirmed by restriction digestion with the enzyme, the site for which was incorporated in the design of the mutagenic primer. The double mutant, C328D-C368D, was constructed using the C328D mutant in pET23d vector as the template. The presence of the mutations was confirmed by DNA sequencing. The mutants were found to be free of PCR introduced errors (Figure 5.3).

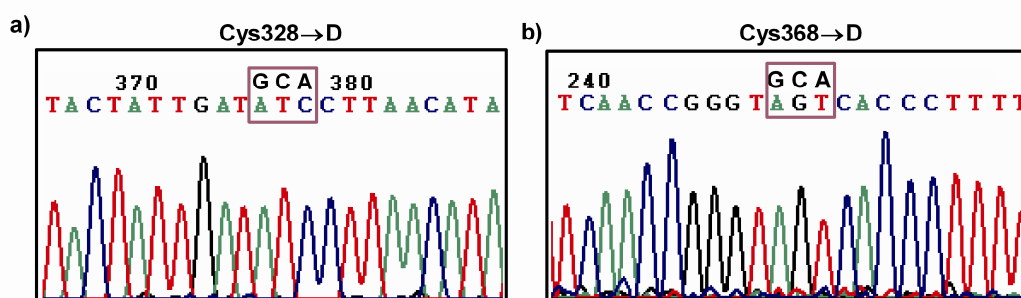


Figure 5.3: Sections of sequencing chromatograms confirming the incorporation of a) C328D and b) C368D mutations. The mutated codon and the same codon in the parent wildtype are boxed.

5.2.2 Protein expression and purification

Recombinant PfAdSS and the mutants were expressed in BL21(DE3) strain of *E. coli*. Protein purification protocol was identical to that used for wild type AdSS (WtAdSS). The purification involved 40 and 70% ammonium sulphate fraction of the crude lysate followed by anion exchange chromatography. The fractions containing the protein were concentrated and injected into Sephacryl 200 column. The purified protein fractions were pooled, concentrated and stored in a buffer containing 20 mM Tris HCl, pH 6.9, 10% glycerol, 1 mM EDTA and 2 mM DTT.

5.2.3 Enzyme assays and kinetics

Enzyme assays were performed in 30 mM sodium phosphate, pH 7.4 containing 5 mM magnesium acetate at 25°C on a Hitachi U2010 spectrophotometer

fitted with water circulated cell holder. Reaction rates were monitored as an increase in absorbance at 290 nm and a $\Delta\epsilon$ value of $3390 \text{ M}^{-1}\text{cm}^{-1}$ was used to calculate the reaction velocities (Kang & Fromm, 1995). For the determination of kinetic constants, concentration of one substrate was varied with the concentration of the other two substrates held constant at 10 times their K_m value. Substrate concentrations when held saturating were, 250 μM IMP, 300 μM GTP and 15 mM aspartate.

5.2.4 Size exclusion chromatography

Superdex 200 (30*1 cm) gel filtration column calibrated with β -amylase (200 kDa), alcohol dehydrogenase (150 kDa), bovine serum albumin (66 kDa), carbonic anhydrase (29 kDa) and cytochrome c (12.4 kDa) was used for analytical gel filtration studies. 100 μl of 12.5 μM protein was injected into Superdex 200 column pre-equilibrated with varying concentration of sodium phosphate, pH 7.4 containing 5 mM MgCl_2 with or without salt. Elution was monitored simultaneously at 220 and 280 nm and the runs were performed at a flow rate of 0.5 ml min^{-1} .

5.2.5 Cysteine modification

Wild type AdSS (WtAdSS) at a concentration of 1.5 mg ml^{-1} was dialyzed extensively against 10 mM Tris HCl, pH 8.0 and 5% glycerol followed by treatment with iodoacetate/iodoacetamide (IAA/IAM) at 25°C for varying time periods. The ratio of protein to IAA/IAM was maintained at 1:5. Reactions were quenched by adding excess cysteine. Unreacted IAA/IAM and cysteine were removed by dialysis against 10 mM Tris HCl, pH 8.0 containing 5% glycerol. The samples were digested with trypsin (trypsin:protein ratio kept at 1:100) for 15 minutes at 37°C . The controls were also subjected to the same treatment except that IAA/IAM was excluded from the reaction mixtures.

For 7-chloro-4-nitrobenzo-2-oxa-1,3-diazole (NBD chloride) treatment, protein samples were dialyzed against 25 mM potassium phosphate, pH 7.0 and 5% glycerol, followed by treatment with NBD chloride at 1:10 ratio at room temperature for varying time periods. After modification, protein samples were dialyzed against

10 mM potassium phosphate, pH 7.0 containing 5% glycerol. The samples were digested with trypsin (trypsin:AdSS ratio kept at 1:50) at 37°C for 15 minutes.

The mass spectra were recorded on Ultraflex II TOF/TOF mass spectrometer (Bruker Daltonics, Bremen, Germany). 1 μ l of the digested sample was mixed with 1 μ l of 2,5-dihydroxybenzoic acid (DHB) prior to spotting on the target plate. Spectra were acquired in the positive ion mode. For identification of the modified cysteines, theoretical masses for peptides resulting from tryptic digestion of PfAdSS were generated using the Bruker Daltonics sequence editor 3.0. Incremented peptide masses were calculated for all cysteine containing peptides based on their cross-linking with iodoacetate or iodoacetamide, both of which add a mass of 58 Da for every cysteine modified. The modified cysteine containing peptides were identified by comparison of the MS spectra of the IAA/IAM modified protein with the control protein spectra followed by examination of correspondence to the theoretical mass lists. A similar strategy for data analysis was used for NBD chloride modification studies, where reaction of NBD chloride with cysteine thiol and sulfenic acid adds a mass of 164 or 180 Da, respectively, to the cysteine containing peptide.

5.2.6 Equilibrium unfolding

Fluorescence spectroscopy. Fluorescence measurements were done on a Hitachi F-2500 spectrofluorimeter. The excitation and emission band widths were set to 2.5 and 10 nm, respectively. Protein samples were excited at 280 nm and emission recorded from 282-400 nm at a scan speed of 300 nm min⁻¹. Preliminary experiments suggested that unfolding equilibrium was reached within 20 minutes of incubation with the denaturant. Therefore, equilibrium unfolding was measured after incubating 2 μ M protein samples in 30 mM sodium phosphate, pH 7.4 and 2 mM magnesium acetate with the desired concentration of urea at 25°C for 30 minutes. Substrate induced protein stabilization was monitored by preincubating the protein samples on ice with IMP and/or GTP along with magnesium acetate for 30 minutes, followed by incubation with urea at 25°C for 30 minutes. The final concentrations of IMP or GTP and magnesium acetate were maintained at 75 μ M and 2 mM, respectively. Baseline corrections were done by subtraction of appropriate buffer spectra.

Circular dichroism spectroscopy. Far UV-CD measurements were performed on a JASCO J-810 spectropolarimeter. For denaturation studies, 5 μM protein samples were incubated with the desired urea concentration in 30 mM sodium phosphate, pH 7.4 and 2 mM magnesium acetate for 30 minutes at 25°C. To monitor the effect of IMP and/or GTP on the urea induced denaturation of PfAdSS, protein samples were preincubated with IMP and/or GTP on ice for 30 minutes followed by incubation with urea. Final concentrations of IMP or GTP and magnesium acetate were 75 μM and 2 mM, respectively. Ellipticity changes at 220 nm were monitored in a cuvette of 1 mm pathlength. Each spectrum represented an average of three different scans and appropriate blank spectra were subtracted.

Size exclusion chromatography. Changes in protein quaternary structure as a consequence of urea denaturation were monitored by size exclusion chromatography using Superdex 200 (1*30 cm) column attached to Akta Basic HPLC system. Proteins samples at 6 μM concentration were incubated with the desired urea concentration for 30 minutes at 25°C in 30 mM sodium phosphate, pH 7.4. To monitor the effect of substrates on the urea induced unfolding of the wild type protein, the samples were preincubated with 2 mM magnesium acetate and 100 μM IMP and/or GTP. 500 μl of the protein sample was injected into the column pre-equilibrated with 30 mM sodium phosphate, pH 7.4, 2 mM magnesium acetate and the required urea concentration. 100 μM IMP was introduced in the running buffer when the effect of IMP was being evaluated. The runs were performed at a flow rate of 0.5 ml min⁻¹ and protein elution monitored simultaneously at 280 and 220 nm.

5.3 Results

To identify the nature of interface cysteines in PfAdSS, to examine their role in structural stability of the enzyme and to evaluate their accessibility and reactivity to cysteine modifying agents following two approaches were used,

- 1) **Mass spectrometry.** This involves the use of specific reagents which covalently react with different oxidized species of cysteines. After modification, these species can be identified by changes in mass of the peptides carrying the modified cysteines in the tryptic digest of the protein.
- 2) **Site directed mutagenesis** leading to mutation of interface cysteines to amino acids that are isosteric but do not ionize at ambient pH or to amino acids that constitutively express a charge. Activity and stability studies on these mutants provide insight into the nature of cysteines at the interface. Hence, interface cysteine to serine and cysteine to aspartic acid mutants of PfAdSS were generated for further studies.

5.3.1 Mass spectrometry

PfAdSS has 20 cysteines per dimer whose spatial location on the dimer is shown in Figure 5.4. The solvent accessible surface area of the cysteines in the monomer and dimer of PfAdSS are listed in Table 5.1.

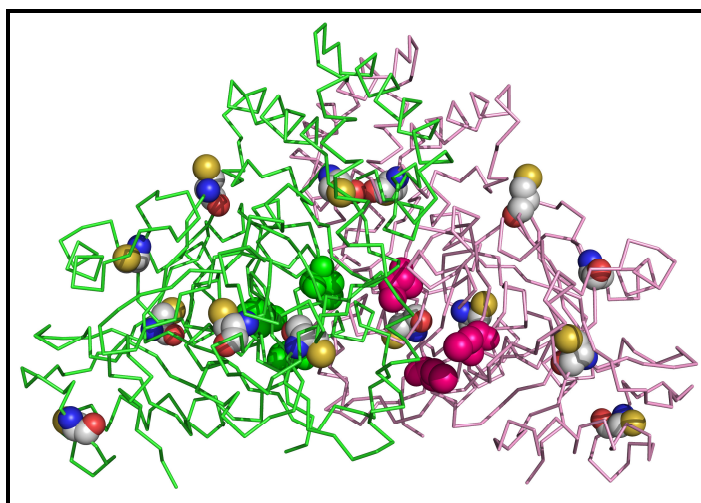


Figure 5.4: Ribbon representation is the PfAdSS dimer with the two subunits colored in green and pink. Spheres represent the cysteine residues in the two subunits. The three interface cysteines in each monomer are colored in pink and green. The figure was generated using PyMOL (DeLano, 2002)

Table 5.1: Solvent accessible surface area of cysteines in the monomer and dimer of PfAdSS.

The values were calculated using CCP4 Package (The CCP4 Suite: Programs for Protein Crystallography Acta Cryst. D) with solvent/probe radius set to 1.4 Å.

Cysteine	Solvent Accessible surface area	
	Monomer	Dimer
44	0.00	0.00
70	0.00	0.00
148	0.2	0.2
250	41.70	25.40
283	39.90	39.90
315	1.10	1.10
328	99.20	19.00
352	0.00	0.00
368	55.00	16.20
396	18.30	18.30

To assess the reactivity and to identify the oxidation state of cysteines, molecular weight mapping of the proteolytic digest of unmodified and modified PfAdSS was done by means of MALDI mass spectrometry. Iodoacetate and iodoacetamide were used to assess cysteine reactivity and NBD chloride, which reacts with both cysteine thiol and sulfenic acid, was used to identify these species in PfAdSS. The protein samples were treated with the above reagents as described in Section 5.2.5, followed by limited proteolysis with trypsin. Control samples were similarly treated except that the cysteine modifying agent was omitted from the reaction mixture. Peptides representing ~95% of the protein were identified in the tryptic digest of unmodified PfAdSS (Figure 5.5) with peptides corresponding to the 10 cysteines mapped with high accuracy (less than 2 Da error, Table 5.2).

MAIFDHQIKNVDKGNVAILGAQWGDEGKGKIIDMLSEYSDITCRFNG
GANAGHTISVNDKKYALHLLPCGVLYDNNISVLGNGMVIHVKSLMEEI
ESVGGKLLDR LYLSNKAHILFDIHQIIDSQETKK LKEGKQIGTTKRGIG
PCYSTKASR IGIRLGTLK NFENFKNMYSK LIDHLMDLYNITEYDKEKEL
NLFYNYHIKLRDRIVDVISFMNTNLENNKKVLIEGANAAMLDFGTYP
YVTSSCTTVGGVFSGLGIHHKK LNLVVGVVK SYLTR VGCGPFLTELNN
DVGQYLREKGHEYGTTTKRPRRCGWLDIPMLLYVKCINSIDMINLTKL
DVLSGLEEILLCVNFKNKKT **GELLEK** GCYPVEEEISEEYEPVYEKFSGW
KEDISTCNEFDELPENAK KYILAIEKYLKTPIVWIGVGPNRKNMIVKKN
FNLN

Figure 5.5: Sequence coverage in a partial tryptic digest of PfAdSS. The grey boxed regions represent the two stretches of amino acids that are not represented in the mass spectrum of the digest. The grey lines show the sequence stretch of the peptides in the partial digest of PfAdSS.

Table 5.2: Cysteine containing peptides found in the partial tryptic digest of *P. falciparum* AdSS.

Each cysteine was represented by more than one peptide.

Cysteine	Peptide	MH ⁺ mass (Da)	
		Expected	Observed
44	[10- 45]	3894.9	3895.3
44	[32- 45]	1658.8	1658.9
70	[46- 90]	4763.4	4764.0
70	[63- 90]	3052.6	3052.8
148	[143-152]	1081.5	1081.6
148	[144-152]	925.4	925.5
250	[225-265]	4269.1	4269.4
250	[226-265]	4141.1	4141.4
283	[267-301]	3894.1	3895.3
283	[281-299]	2095.0	2095.2
315	[314-327]	1706.9	1707.0
315/328	[314-339]	3052.6	3052.8
328	[328-339]	1364.7	1365.1
352	[340-356]	1905.0	1904.1
368	[360-385]	3062.4	3062.7
368	[367-385]	2291.9	2292.3
396	[391-430]	4606.4	4609.0

Modification of PfAdSS with IAA and IAM yielded similar results. A total of five modified cysteines were identified within 2 minutes of treatment with iodoacetate or iodoacetamide. These were cysteine 44, 148, 250, 283 and 368. In addition, a peptide containing Cys328 and Cys315 was observed in which only one cysteine was modified (Table 5.3). However, in all cases peaks corresponding to the unmodified cysteine containing peptide were present. The masses determined experimentally for the modified cysteine containing peptides corresponded well to the theoretical masses with a maximum of ± 2 Da error. Treatment of PfAdSS with IAA/IAM for 20 minutes resulted in no new cysteine getting modified. This shows that though the solvent accessibility of the cysteines in PfAdSS dimer is low (Table 5.1), they are highly reactive.

Table 5.3: Iodoacetate modified cysteine containing peptides of PfAdSS.

Peptide	Sequence	Modified Cysteine	Mass (MH ⁺)	
			Theoretical*	Observed
Treatment with IAA/IAM for 2minutes				
32-45	IIDMLSEYSDITCR	44	1716.8	1717.7
143-152	RGIGPCYSTK	148	1139.5	1140.1
144-152	GIGPCYSTK	148	983.4	983.9
226-265	VLIEGANAAMLDIDFGTYPYVTS SCTTVGGVFSGLGIHHK	250	4199.1	4201.2
281-299	VGCGPFLTELNDVGQYLR	283	2153.0	2154.1
281-301	VGCGPFLTELNDVGQYLREK	283	2410.2	2411.4
357-385	NKKTGELLEKGCYPVEEEEISEEY EPVYEK	368	3490.6	3488.3
314-339	RCGWLDIPMLLYVKCINSIDMINL TK	315/328	3110.6	3112.2

*corresponds to the peptide mass with 58 Da added to it to account for iodoacetate/iodoacetamide modification of the cysteine present in the peptide.

To identify the oxidation state of cysteines in PfAdSS, the protein was treated with NBD chloride for 15, 30, 60 and 120 minutes at 22°C. The earliest cysteine to get

modified was Cys352. Modification with NBD chloride for 30 minutes resulted in an additional peptide having a mass of 2457.4 Da being identified. This could either correspond to the peptide spanning amino acids 367-385 with cysteine 368 forming a thiol adduct with NBD, or to Cys352 in the peptide 340-359 forming NBD-sulfenate adduct. In the absence of MS/MS data however, the two could not be differentiated. Further, extension of incubation time to 1 hour resulted in the modification of cysteines 148, 396, 315 and 328. In addition, a peptide having a mass of 3226.7 which could correspond to a peptide (340-366) having Cys368 thiol adduct or a peptide (360-385) carrying Cys352 sulfenate adduct with NBD was observed (Table 5.4).

Surprisingly, NBD chloride failed to modify Cys44, Cys250 and Cys283 which get labeled with IAA/IAM at the earliest time point. Variation in pH across the two experiments probably contributes to the observed differences in the reactivity of the cysteines. Unlike the NBD modification studies which were carried out at pH 7.0, IAA/IAM treatments were done at pH 8.0 which is close to the pKa of cysteine side chain and hence the reactivity of cysteines could be expected to be higher under these conditions. However, this data does not provide unambiguous results on the oxidation state of the interface cysteines. High intensity peptide peaks corresponding to unmodified Cys328 and Cys368 could be identified even after one hour of treatment with NBD chloride. Hence, we resorted to site-directed mutagenesis to evaluate the charge status and the role of interface cysteines in the stability of PfAdSS.

Table 5.4: NBD modified peptides of PfAdSS after cleavage with trypsin.

Peptide	Sequence	Mass (MH ⁺)				Cysteine/ State
		Thiol Adduct		Sulfenate adduct		
		Theoretical ^a	Observed	Theoretical ^b	Observed	
Treatment for 15 minutes at RT						
340-359	LDVLSGLEEILLCVN FKNKK	2439.3	2441.9			352/ Cys-SH
Treatment for 30 minutes at RT (in addition to above peptide)						
367-385	GCYPVEEEEISEEYE PVYEK	2455.9	2457.4			368/ Cys-SH
340-359	LDVLSGLEEILLCVN FKNKK			2455.3	2457.4	352/ Cys-SOH
Treatment for one hour at RT (in addition to above peptides)						
131-155	KLKEGKQIGTTKRG GPCYSTKASR	2871.5	2871.5			148/ Cys-SH
131-159	KLKEGKQIGTTKRG GPCYSTKASRIGIR	3310.8	3309.9			148/ Cys-SH
386-408	FSGWKEDISTCNEF DELPENAKK	2851.2	2854.4			396/ Cys-SH
314-339	RCGWLDIPMLLYVK CINSIDMINLTK	3216.6	3219.8			315,328/ Cys-SH
340-366	LDVLSGLEEILLCVN FKNKKTGELLEK			3225.7	3226.7	352/ Cys-SOH
360-385	TGELLEKGCYPVEE EISEEYEPVYEK	3226.4	3226.7			368/ Cys-SH

^a peptide mass + 164 Da; ^b peptide mass + 180 Da.

5.3.2 Interface cysteine mutants

Three interface cysteine to serine mutants, C328S, C368S and C328S-C368S, were earlier made in the laboratory and characterized with respect to activity and oligomeric status (R. Jayalakshmi, Thesis). The activity of the interface mutants was comparable to the wild type (Wt) protein. The elution profile of C368S mutant on an analytical Superdex 200 column was identical to that of the Wt protein, with the retention volume being indicative of a monomer-dimer equilibrium with the dimer

predominating. Surprisingly, C328S mutant eluted as a broad peak indicating a shift in the equilibrium towards the monomer. The oligomerization of the double mutant was drastically affected with a small peak corresponding to monomer species appearing (Figure 5.6). These observations along with the effect of IAA/IAM on subunit association of PfAdSS (Section 5.1.4), implicate the probable role of negatively charged interface cysteine/cysteines in modulating the quaternary structural stability of PfAdSS.

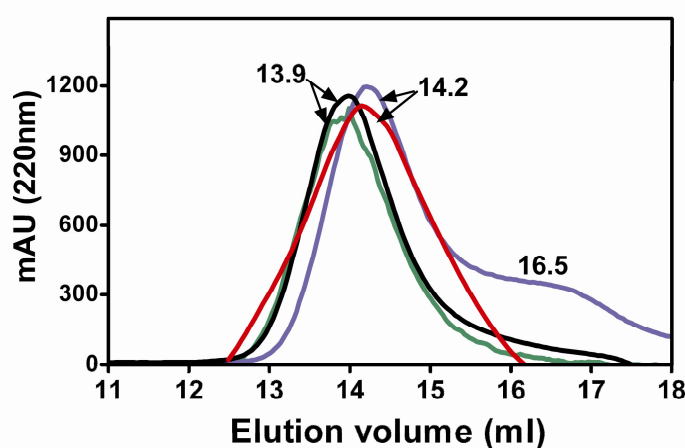


Figure 5.6: Gel filtration profile of wild type and PfAdSS mutants. Wild type (green), C368S (black), C328S (red) and C328S-C368S (blue). Elution volumes in ml are indicated (Figure taken from R. Jayalakshmi, thesis)

5.3.3 Kinetic characterization of C328D and C328D-C368D mutants of PfAdSS

The aspartic acid mutants were constructed using the megaprimer PCR method (Sarkar & Sommer, 1990) and cloned in pET23d expression vector. The recombinant proteins were expressed in *E. coli* BL21(DE3) cells and purified using a combination of anion exchange and gel filtration chromatography. The proteins were >90% pure as judged by SDS-PAGE (Figure 5.7). The purified C328D mutant was fully soluble and stable to storage for many months. This was unlike the Wt protein

and serine mutants which precipitated on storage, with the serine mutants precipitating more rapidly than the wildtype protein.

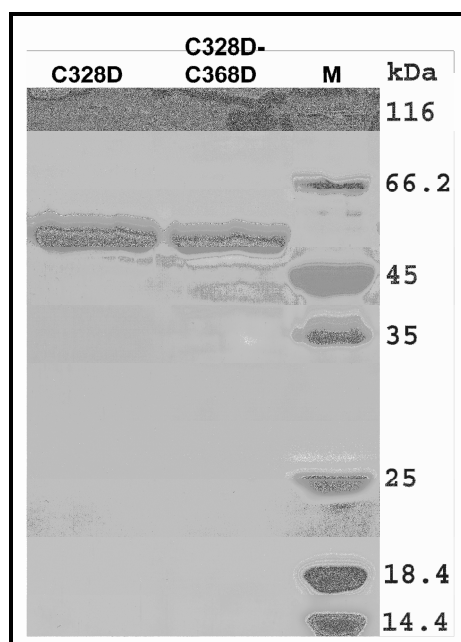


Figure 5.7: SDS-PAGE profile of purified interface aspartic acid mutants.

Table 5.5: Kinetic parameters of wild type protein and interface cysteine to aspartic acid mutants in 30 mM sodium phosphate, pH 7.4 and at 25°C.

Protein	k_{cat} (sec^{-1})	K_m		
		IMP (μM)	GTP (μM)	Aspartate (mM)
Wild type	1.1 ± 0.2	16.77 ± 2.0	24.77 ± 2.3	1.96 ± 0.2
C328D	1.72 ± 0.12	27.59 ± 3.5	25.14 ± 2.1	1.44 ± 0.2
C328D-C368D	0.72 ± 0.03	29.19 ± 2.7	35.81 ± 2.8	1.73 ± 0.2

The kinetic parameters for the aspartic acid mutants determined in 30 mM sodium phosphate, pH 7.4, are listed in Table 5.5. The k_{cat} value of C328D mutant was 1.6 fold higher and that of C328D-C368D mutant was 1.5 fold lower than the Wt protein. The K_m values for the nucleotide substrates, IMP and GTP, were marginally

elevated in the mutants with the aspartate K_m value being marginally lower for the C328D mutant. These values were measured on 3 independently purified batches of protein.

5.3.4 Oligomeric status

C328D mutant

Oligomerization of wild type PfAdSS was found to be sensitive to the ionic strength of the buffer used (Figure 5.8a). With increase in phosphate concentration from 10 to 50 mM, the protein showed a shift from dimer (105 kDa) to a species having a molecular mass of 82 kDa, which is indicative of monomer-dimer equilibrium. A small peak corresponding to monomeric species appeared when the phosphate concentration was increased to 200 mM or 500 mM NaCl was added to 10 mM sodium phosphate (Jayalakshmi *et al.*, 2002). On a calibrated Superdex 200 column equilibrated with 10 mM sodium phosphate, pH 7.4, C328D mutant eluted as a single peak at a retention volume corresponding to a molecular mass of 97 kDa. On increasing the phosphate concentration to 50 mM, the peak shifted to a retention volume corresponding to a molecular mass of 82 kDa, which is indicative of monomer-dimer equilibrium with the dimer predominating. No further change in elution pattern was observed on further increase in phosphate concentration to 200 mM or introduction of 1.5 M NaCl in the running buffer (Figure 5.8b). Unlike the wild type protein, a distinct peak corresponding to a monomer did not appear in C328D mutant.

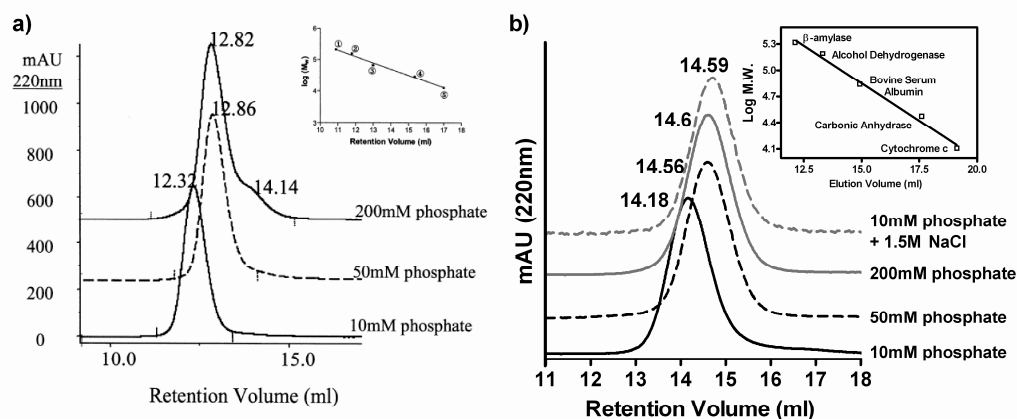


Figure 5.8: Analytical gel filtration of a) recombinant PfAdSS (taken from Jayalakshmi *et al.*, 2002) and b) C328D mutant on a calibrated Superdex 200 column under different buffer conditions. Buffers were of indicated phosphate concentration, pH 7.4. The insets show the calibration curve of Log MW of standard proteins versus elution volume. Protein molecular weight markers used in panel (a) are same as in panel (b).

C328D-C368D mutant

The elution profile of C328D-C368D mutant was dramatically different from that of the single mutant and the wild type protein. In 10 mM sodium phosphate, pH 7.4 the profile showed the presence of two species corresponding to 92 and 55 kDa. On increase in phosphate concentration to 50 mM, the peaks shifted to a region corresponding to 82 and 51 kDa with no further change in elution volume observed on increasing the phosphate concentration to 200 mM or in the presence of 1.5 M NaCl in 10 mM sodium phosphate, pH 7.4 (Figure 5.9). Though there was no change in retention volume with increase in phosphate or salt concentration, there was a clear shift in monomer-dimer equilibrium with the population of monomeric species increasing at high phosphate concentrations and in the presence of salt. Addition of the substrate IMP, which binds at the dimer interface, did not shift the equilibrium towards the dimer. Thus, the mutation of two interface cysteines to aspartic acid perturbs the rate of monomer-dimer equilibrium in PfAdSS allowing simultaneous detection of both the species.

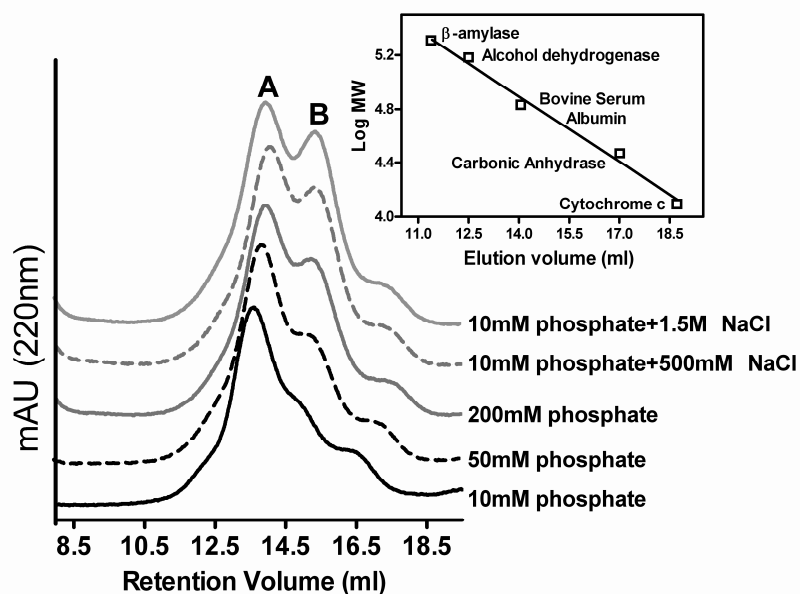


Figure 5.9: Analytical gel filtration profile of C328D-C368D mutant on a calibrated Superdex 200 column under different buffer conditions. Buffers were of indicated phosphate concentration, pH 7.4. A and B denote the dimer and monomer of C328D-C368D mutant. Inset shows the calibration curve of Log MW of standard proteins versus elution volume.

5.3.5 Stability of wildtype and mutants to urea induced denaturation

The relative stabilities of wild type AdSS (WtAdSS) and the mutants were evaluated under unfolding conditions. Urea induced unfolding of the proteins was monitored by far-UV circular dichroism spectroscopy, fluorescence spectroscopy and size exclusion chromatography which report on changes in secondary, tertiary and quaternary structure of the protein. The far UV-CD spectra of the interface mutants were identical to that of the wild type protein, with the spectral patterns being characteristic of proteins containing helices. PfAdSS has four tryptophans in each monomer with tryptophan 24 and 317 being proximal to the ligand binding site. All tryptophans are buried and the emission maximum of PfAdSS at 325 nm is indicative of this nature. Emission profile of the wildtype protein and mutants measured at 2 μ M protein concentration showed only a minor shift of about ± 1 nm across different samples and less than 10% variation in emission intensity. Similarity in fluorescence

and CD spectra of the wildtype and mutant proteins indicates the absence of gross secondary and tertiary structural changes as a consequence of mutagenesis.

The proteins selected for comparative equilibrium unfolding studies were:

- a) Wild type PfAdSS
- b) C328S mutant which showed a minor shift in the monomer-dimer equilibrium.
- c) C328D mutant which exhibited a stable quaternary structure and unlike the wild type protein, it did not dissociate to form monomeric species in the presence of salt and at high phosphate concentrations.
- d) C328D-C368D which was highly destabilized and showed monomeric species even at low phosphate concentrations.

5.3.6 Urea induced unfolding of PfAdSS and the mutants monitored by size exclusion chromatography

Size exclusion chromatography permits evaluation of the association state of the protein during the process of urea denaturation. Similar studies with mutants enable comparative analysis of stability and subunit association across different proteins.

Wildtype PfAdSS in 30 mM phosphate, pH 7.4 eluted at a retention volume corresponding to a molecular mass of 89 kDa, which is indicative of monomer-dimer equilibrium. Presence of 1 M concentration of urea shifted the equilibrium towards a monomer with a small shoulder corresponding to dimeric population being retained (Figure 5.11a). However, at 1.5 M urea concentration, the enzyme completely shifted towards a monomer with further increase in urea concentration causing unfolding of this species. Monomer unfolding was accompanied by aggregation and protein precipitation evident at 3 M urea concentration, where both unfolded monomers and high molecular weight aggregates were present. With further increase in urea concentration to 4 and 5 M, the aggregates solubilized and eluted in the void volume of the column (Figure 5.10a).

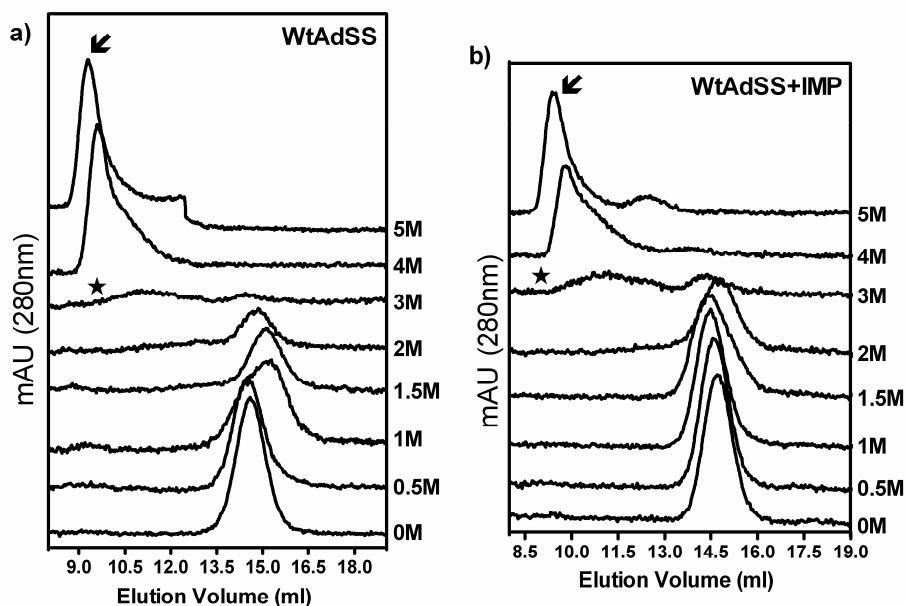


Figure 5.10: Urea induced changes in the quaternary structure of a) WtAdSS and b) WtAdSS liganded with IMP, monitored by size exclusion chromatography. * indicates protein precipitation and the arrow indicates the unfolded soluble protein aggregates formed at high urea concentration.

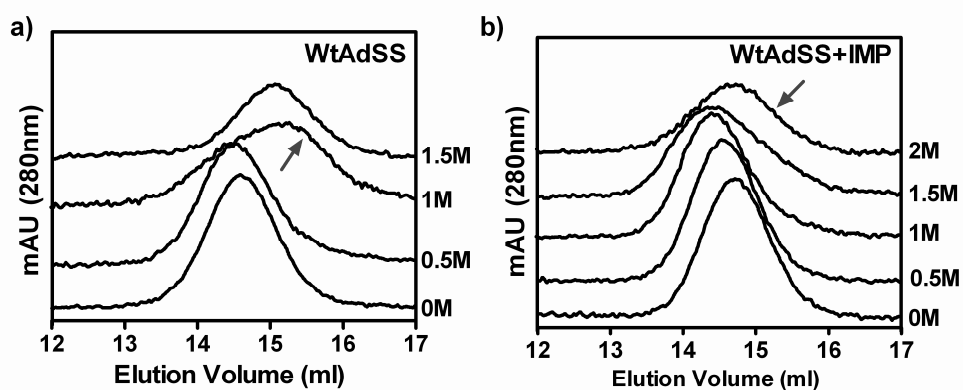


Figure 5.11: An enlarged view of the panels above. The arrows indicate the monomeric species formed as a consequence of dimer dissociation. Liganding with IMP stabilizes the dimer till 1.5 M urea concentration.

Liganding with IMP prior to urea denaturation stabilized the PfAdSS dimer. Urea at 0.5, 1 and 1.5 M concentrations resulted in a minor decrease in the retention volume of the protein which is indicative of dimer unfolding prior to its dissociation to monomers. At 2 M urea concentration the peak shifted to larger elution volume and

this was suggestive of a shift in monomer-dimer equilibrium towards the monomer (Figure 5.11b). Profiles at 3, 4 and 5 M urea concentrations were similar to the unliganded protein samples, with the monomer unfolding resulting in the formation of soluble aggregates (Figure 5.10b). Liganding with GTP produced profiles that were similar to the unliganded protein whereas IMP and GTP in combination resulted in profiles similar to the IMP bound protein.

The effect of urea on the quaternary structure of C328S mutant was largely similar to the wildtype protein. Here again dimer dissociation was followed by monomer unfolding with high molecular weight aggregated species appearing at 4 M urea concentration (Figure 5.12a). The precipitation seen at 3 M urea concentration in case of Wt protein, was absent in C328S mutant. Liganding with IMP stabilized the C328S dimer to urea induced dissociation (Figure 5.12b).

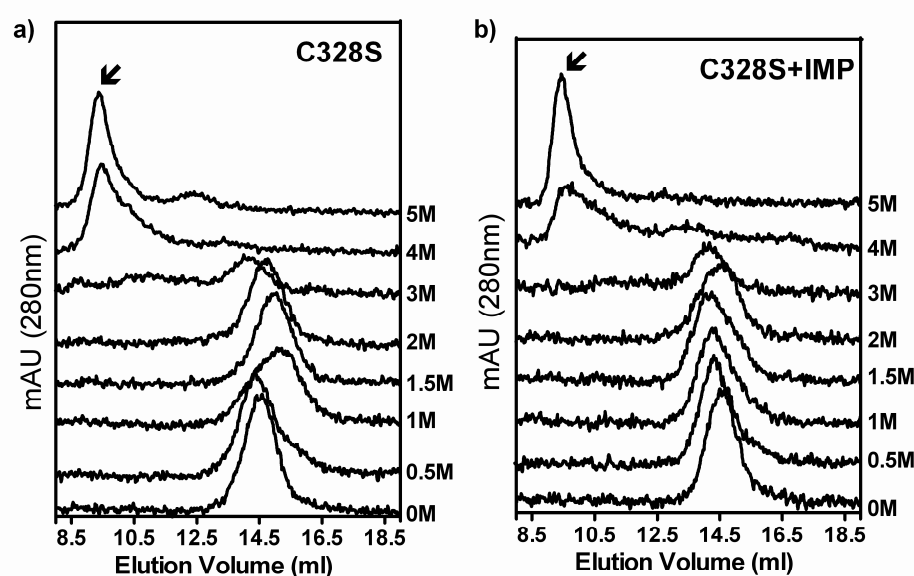


Figure 5.12: Urea induced changes in the quaternary structure of a) C328S mutant and b) C328S mutant liganded with IMP, monitored by size exclusion chromatography. The elution profile of the mutant was largely similar to the wild type protein. The arrows indicate the unfolded soluble protein aggregates formed at high urea concentrations.

Introduction of an aspartic acid residue at the interface of PfAdSS stabilized the dimer, as evident in the urea titration of C328D mutant. Unlike the Wt protein, significant dimeric population was retained in the C328D mutant at 1 M urea concentration, with complete shift to monomeric species seen only at 1.5 M urea concentration (Figure 5.14b). Further increase in urea concentration resulted in monomer unfolding and formation of soluble aggregates. Unlike the wild type protein which completely eluted in the void volume of the column at 4 and 5 M urea, in addition to soluble aggregates significant amount of unfolded solvated monomeric population was seen in the C328D mutant at similar urea concentrations (Figure 5.13a). Liganding with IMP stabilized the dimer till 2 M urea concentration (Figure 5.14b) and here again solvated unfolded monomers were evident even at 5 M urea (Figure 5.13b).

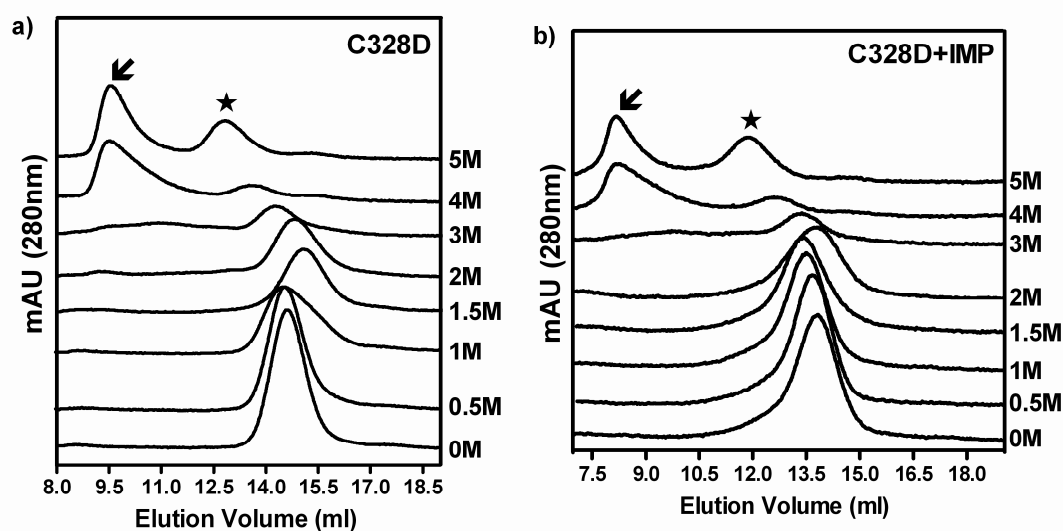


Figure 5.13: Changes in the quaternary structure of a) C328D mutant and b) C328D mutant preincubated with IMP at different urea concentrations, monitored by size exclusion chromatography. The arrows indicate unfolded soluble protein aggregates and stars denote the unfolded solvated monomer.

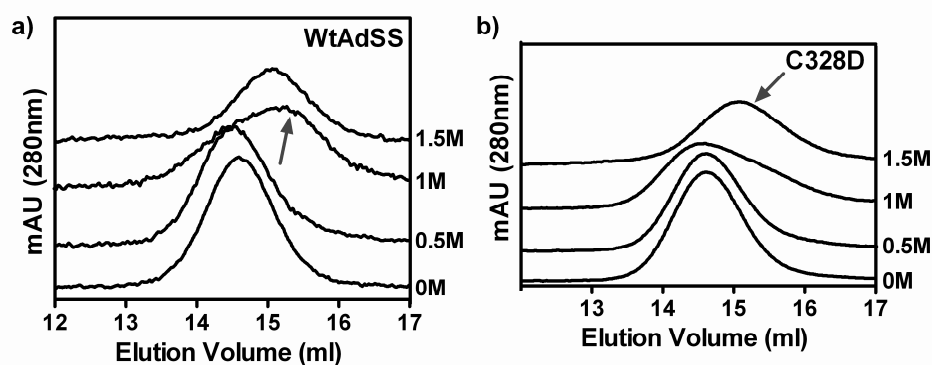


Figure 5.14: Elution profiles of a) WtAdSS and b) C328D mutant showing changes in subunit association of the proteins at low urea concentrations. The arrows indicate the appearance of monomeric species.

C328D-C368D mutant though predominantly dimeric, showed the presence of a peak corresponding to monomeric species even in the absence of urea. 0.5 M urea dramatically increased the concentration of the monomeric population with almost complete shift to monomer seen at 1 M urea concentration (Figure 5.16b). At 1.5 and 2 M urea concentrations, monomer unfolding occurred with the simultaneous appearance of aggregated species eluting in the void volume. At 3 and 4 M urea concentration, the unfolded monomeric species continued to be present in equilibrium with an intermediate species which may correspond to unfolded solvated monomers (Figure 5.15a). IMP binding significantly stabilized the C328D-C368D dimer. The protein predominantly existed in the dimeric form till 1 M urea concentration with a dramatic increase in monomeric population seen only at 1.5 M urea concentration. In the liganded state the monomeric species of C328D-C368D did not unfold significantly. At 3 and 4 M urea concentration, unfolded monomers and an intermediate similar to that seen in unliganded protein was evident. Presence of IMP also significantly reduced the formation of high molecular weight aggregates in C328D-C368D mutant (Figure 5.15b).

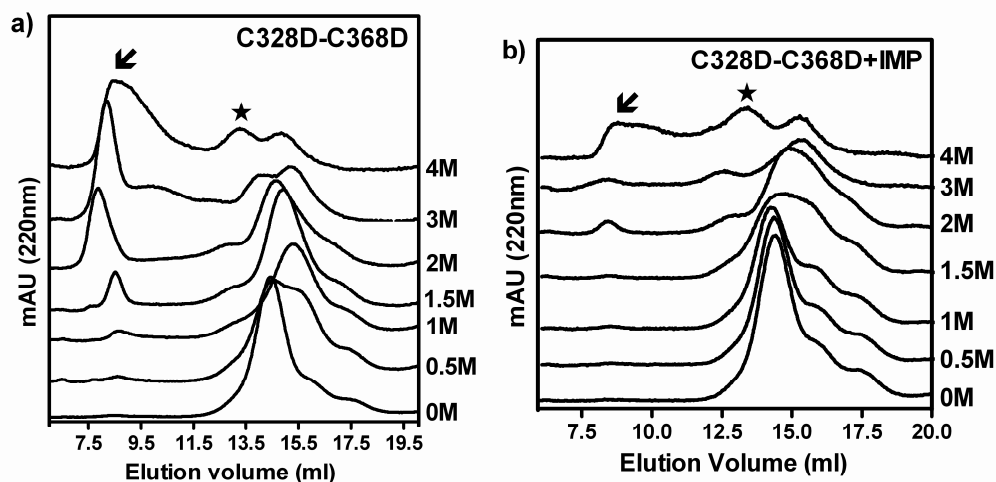


Figure 5.15: Size exclusion chromatography profiles of a) C328D-C368D mutant and b) C328D-C368D mutant liganded with IMP, at different urea concentrations. The arrows indicate the unfolded soluble protein aggregates and stars mark the unfolded solvated monomers.

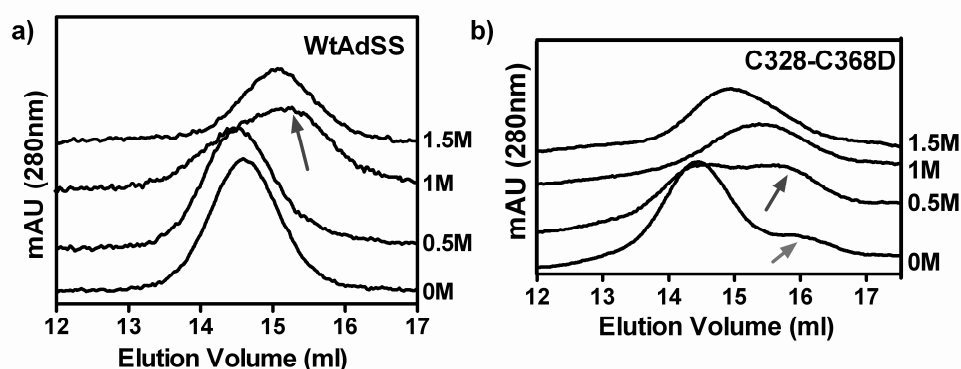


Figure 5.16: Comparison of urea induced changes in subunit association of a) WtAdSS and b) C328D-C368D mutant. The arrow in grey shows the monomeric species seen in C328D-C368D mutant even in absence of urea. The black arrows show the urea induced shift in oligomeric status of Wt and mutant AdSS towards a monomer.

5.3.7 Urea induced unfolding of PfAdSS and the mutants monitored by tryptophan fluorescence

PfAdSS has four tryptophans per monomer at positions 24, 317, 389 and 423 (Figure 5.17).

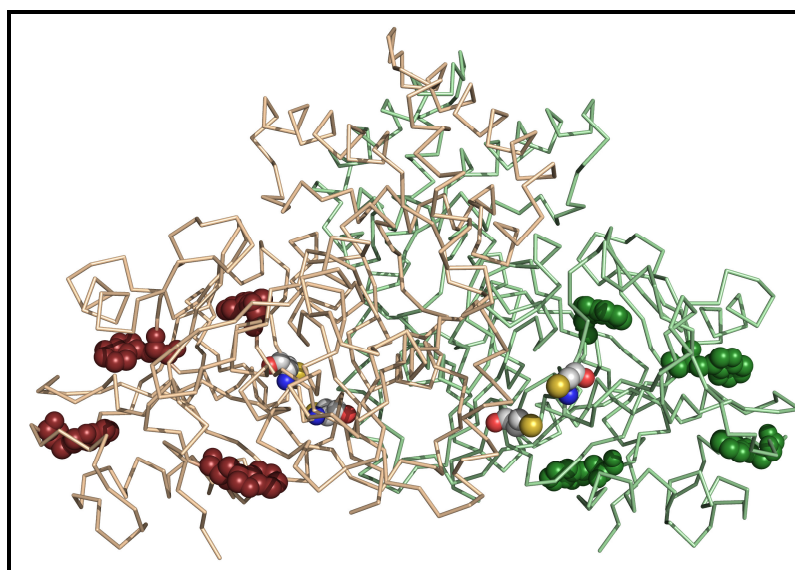


Figure 5.17: Tryptophans in PfAdSS. Green and red spheres represent the tryptophan residues in the two subunits of PfAdSS. The two interface cysteines, Cys328 and Cys368 are shown in CPK.

The emission maximum of PfAdSS in 30 mM sodium phosphate, pH 7.4 is 325 nm which shifts to 342.5 nm in 8 M urea concentration. Exposed tryptophan residues in proteins yield emission maxima between 348–356 nm. The 342.5 nm emission maximum observed at 8 M urea concentration suggests that even at this denaturant concentration, one or more tryptophans in PfAdSS are in a largely hydrophobic environment. Figure 5.18a shows the changes in intrinsic tryptophan fluorescence of WtAdSS monitored as a function of urea concentration and the fraction folded (f_a/f_b ie. fluorescence intensity at 325 nm/fluorescence intensity at 342.5 nm) calculated from the raw data. The weak association of PfAdSS dimer was highlighted by the shift in emission maximum of the protein even at a very low urea concentration of 0.5 M. Thereafter, wild type PfAdSS exhibited a largely continuous multistate transition in both plots of emission maximum and f_a/f_b resulting in complete unfolding of the protein at 6.5 M urea concentration (Figure 5.18a). Liganding with IMP stabilized the protein till 1.0 M urea concentration (Figure 5.18 b,d). This was followed by a sharp unfolding transition between 1-3.5 M urea concentration leading to a shift in emission maximum from 325 to 335 nm. A clear stabilization of an intermediate over the urea concentration range 3.5 to 5.0 M was

evident in the presence of IMP. With further increase in urea concentration, the protein unfolded exhibiting an emission maximum of 342.5 nm at 6.5 M urea concentration. The plot of f_a/f_b as a function of urea concentration also exhibited a similar profile (Figure 5.18b). The two transitions in presence of IMP were centered at 1.8 and 5.5 M urea. The unfolding profiles in the presence of GTP were similar to the unliganded protein and complexing with both IMP and GTP resulted in profiles that were identical to the IMP liganded samples, exhibiting similar C_m values (Figure 5.18c).

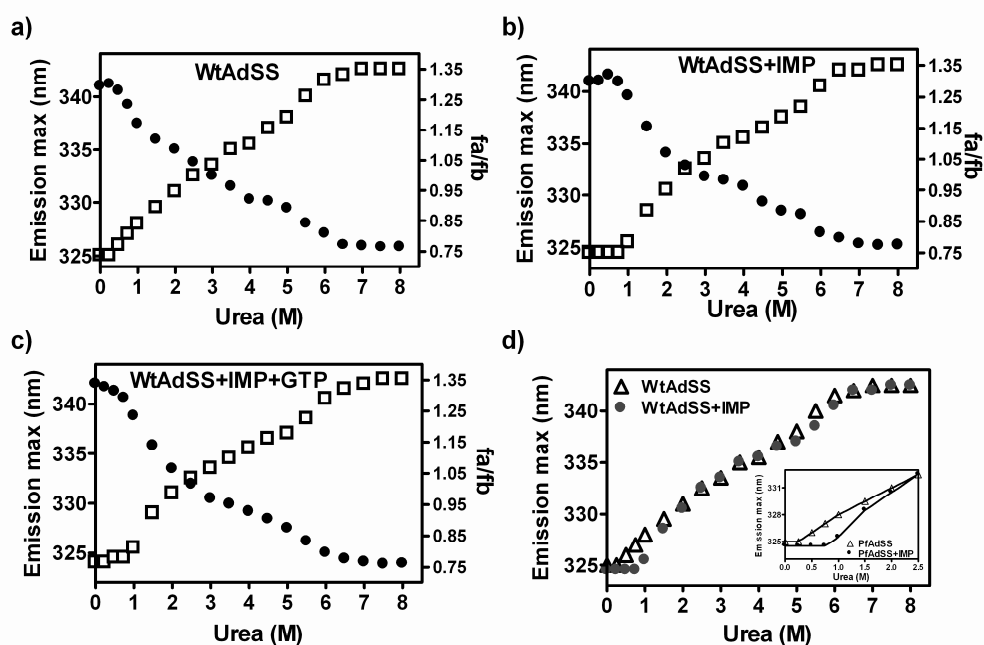


Figure 5.18: Unfolding of WtAdSS in urea solution monitored by intrinsic tryptophan fluorescence. Changes in emission maximum (□) and f_a/f_b (●) as a function of urea concentration for a) WtAdSS, b) WtAdSS liganded with IMP and c) WtAdSS liganded with IMP and GTP in the presence of Mg^{2+} . f_a is the fluorescence intensity at the emission maximum of the native protein and f_b is the fluorescence intensity at the emission maximum of the protein in 8 M urea solution. Panel (d) shows a comparison of the changes in emission maximum of unliganded WtAdSS (Δ) and IMP liganded WtAdSS (●). The inset shows the IMP induced stabilization of PfAdSS dimer till 1M urea concentration.

Unlike the Wt protein, both liganded and unliganded C328S samples showed a continuous multistate transition (Figure 5.19). Like in unliganded Wt protein, changes in tryptophan environment of the unliganded C328S protein were evident at 0.5 M

urea concentration. A sharp unfolding transition was observed between 0.5-1.5 M urea concentration with the emission maximum shifting from 325 to 330 nm. This was followed by a gradual change in emission maximum from 330-342 nm between 1.5-6 M urea concentration resulting in complete unfolding of the protein (Figure 5.19a). Liganding with IMP stabilized the mutant till 1 M urea concentration, after which it exhibited a continuous multistate transition (Figure 5.19b). Here too, liganding with GTP alone and with IMP and GTP in combination yielded profiles that were largely similar to unliganded and IMP liganded protein samples, respectively.

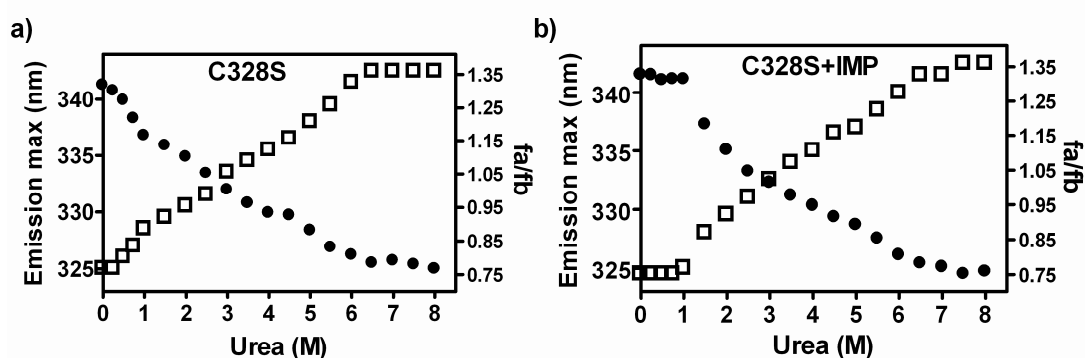


Figure 5.19: Urea induced unfolding of C328S mutant monitored by fluorescence spectroscopy. Changes in emission maximum (\square) and fraction folded (\bullet) of a) protein alone and b) C328S mutant liganded with IMP.

Both unliganded and liganded C328D protein showed initial stabilization till about 1 M urea concentration (Figure 5.20). The initial plateau seen at low urea concentrations in the unliganded sample of C328D mutant is indicative of a marginal stabilization of the mutant dimer over the wildtype protein (Figure 5.20c). Two unfolding transitions were evident in plots of emission maximum and f_a/f_b plotted as a function of urea concentration, for both liganded and unliganded protein (Figure 5.20 a,b). An intermediate was observed between 2.5-4 M urea concentration. The C_m values for the two transitions correspond to 1.3 and 5.0 M for the unliganded protein and 2.0 and 5.5 for IMP liganded protein. Thus, IMP binding at the interface of the protein stabilized the dimer, as evident from the increase in the C_m values.

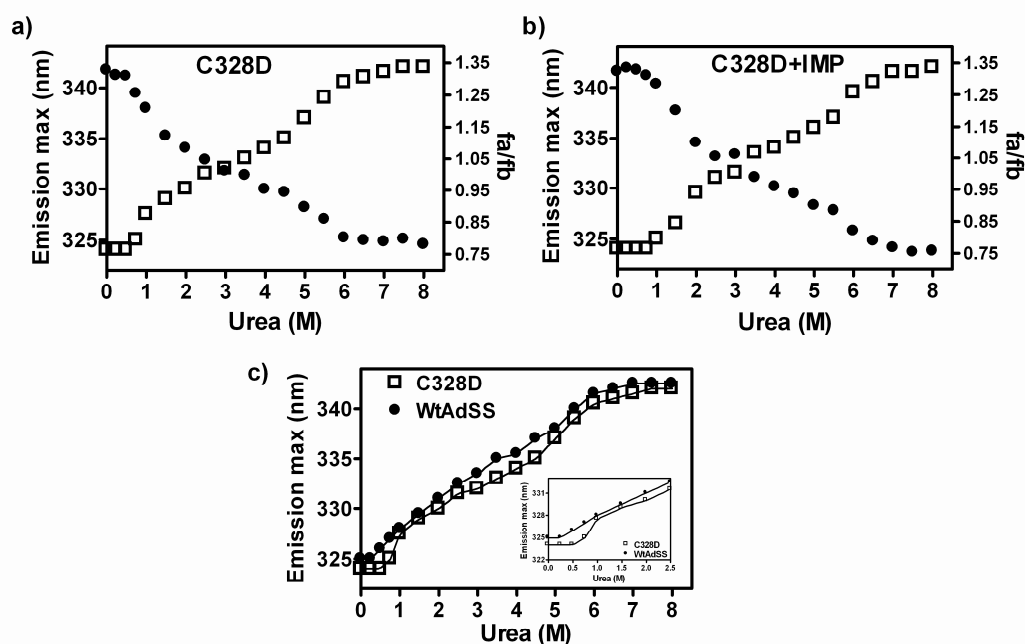


Figure 5.20: Unfolding of a) unliganded C328D mutant and b) IMP liganded C328D protein in urea solution monitored by intrinsic tryptophan fluorescence. Changes in emission maximum (□) and fa/fb (●) as a function of urea concentration are plotted. fa , is the fluorescence intensity at the emission maximum of the native protein and fb , is the fluorescence intensity at the emission maximum of the protein in 8 M urea solution. c) Comparison of unfolding profiles of Wt (●) and C328D mutant (□). The inset shows the initial stabilization of C328D mutant till 0.5 M urea concentration even in absence of IMP.

Unliganded C328D-C368D mutant showed a steep unfolding transition between 0-1 M urea concentration with the emission maximum shifting from 325 to 329 nm. This was followed by a gradual multistate transition leading to complete unfolding of the mutant protein at 6 M urea concentration (Figure 5.21a). Unlike the Wt protein and the other mutants, changes in emission maximum and fa/fb of C328D-C368D mutant were evident even at 0.25 M urea concentration (Figure 5.22 a,b). Unlike other proteins, liganding with IMP did not stabilize the mutant. The liganded protein showed a continuous multistate transition starting from 0.25 M urea concentration (Figure 5.21b and Figure 5.22 c,d). A similar feature was reflected in plots of fa/fb .

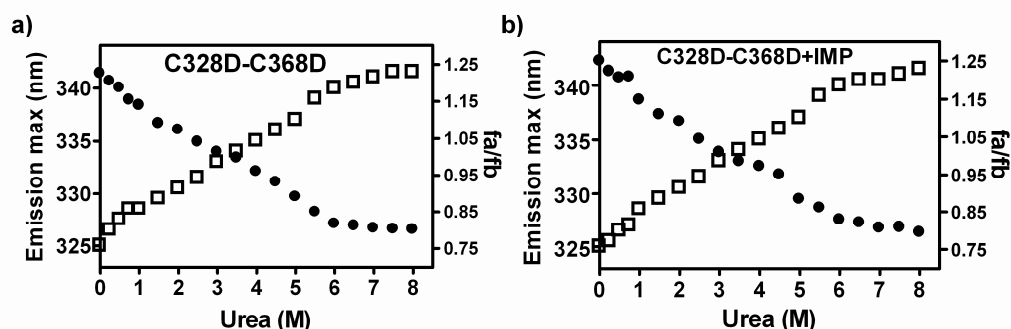


Figure 5.21: Unfolding of C328D-C368D mutant in urea solution monitored by intrinsic tryptophan fluorescence. Changes in emission maximum (\square) and fa/fb (\bullet) of the a) unliganded and b) IMP liganded protein samples as a function of urea concentration.

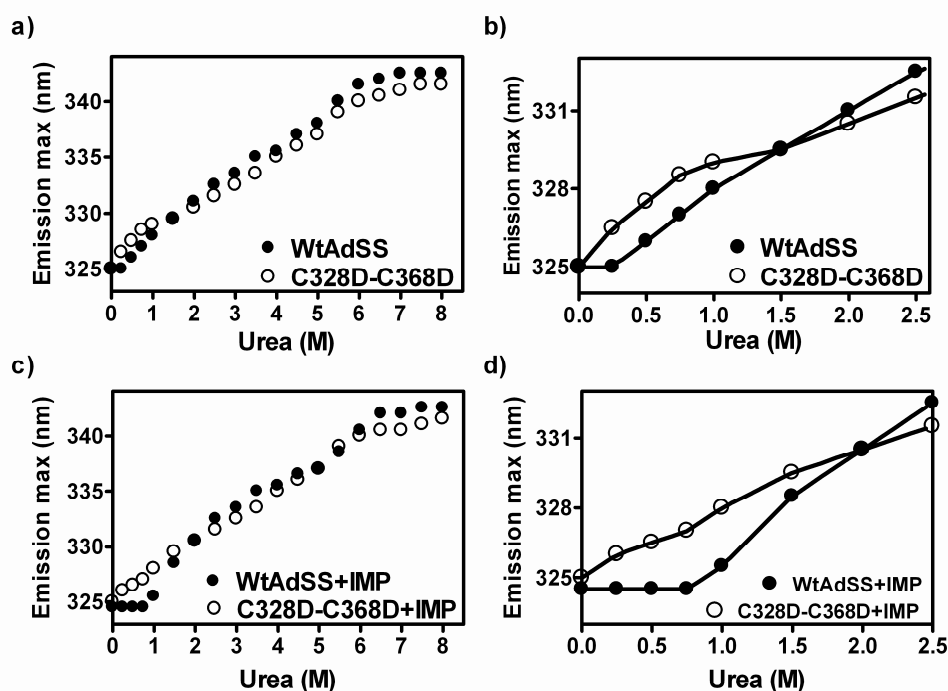


Figure 5.22: Comparison of urea induced unfolding transitions in unliganded (panels a and b) and IMP liganded (panels c and d) samples of WtAdSS (\bullet) and C328D-C368D mutant (\circ). Panel (b) and (d) show an enlarged view of the unfolding transitions at low urea concentrations. Unlike the Wt protein which is stabilized in the presence of IMP, liganding with IMP fails to stabilize the C328D-C368D mutant (panel d).

5.3.8 Unfolding of wild type PfAdSS and the mutants monitored by far UV-CD spectroscopy

Shown in Figure 5.23 are the unfolding profiles of unliganded and liganded Wt PfAdSS monitored by far UV-CD spectroscopy. Unlike fluorescence measurements, the unfolding profiles showed two clear transitions, which when compared to size exclusion chromatography profiles, correspond to dimer dissociation and monomer unfolding. Presence of an intermediate between 2.5-5 M urea was evident in all the traces.

As shown in 5.23a, molar ellipticity of PfAdSS remained unchanged till 1 M urea concentration. With further increase in urea concentration there was loss in ellipticity with no significant change in the shape of the spectrum. At intermediate urea concentrations of 2-3 M, there was dramatic loss in ellipticity due to protein precipitation. This indicates that dissociation of PfAdSS dimer to monomers exposes patches which are sticky resulting in protein aggregation and precipitation at the higher protein concentration used in CD measurements (protein concentration used in fluorescence and CD measurements are 2 and 5 μ M, respectively). A similar feature was observed when the unfolding was monitored by size exclusion chromatography (Figure 5.10, trace at 3 M urea). With further increase in urea concentration, the aggregates solubilized and the second transition which occurred between 5-6.5 M urea concentration was accompanied by complete loss of secondary structure of the protein (Figure 5.23a). Preincubation with IMP stabilized the protein secondary structure till 1.5 M urea concentration (Figure 5.23b). Though the observed increase in stability of the liganded sample was not dramatic, the observation was reproducible over three independent experiments. Interestingly, protein precipitation seen at intermediate urea concentrations was negligible in the presence of IMP and the unfolding curves showed two transitions centered at 1.8 and 5.7 M urea, respectively. These values are largely similar to those observed in fluorescence measurements. Like in fluorescence and size exclusion chromatography, liganding with GTP alone yielded profiles that were similar to the unliganded protein while addition of IMP and GTP in combination yielded profiles similar to the IMP liganded samples (Figure 5.23 c,d).

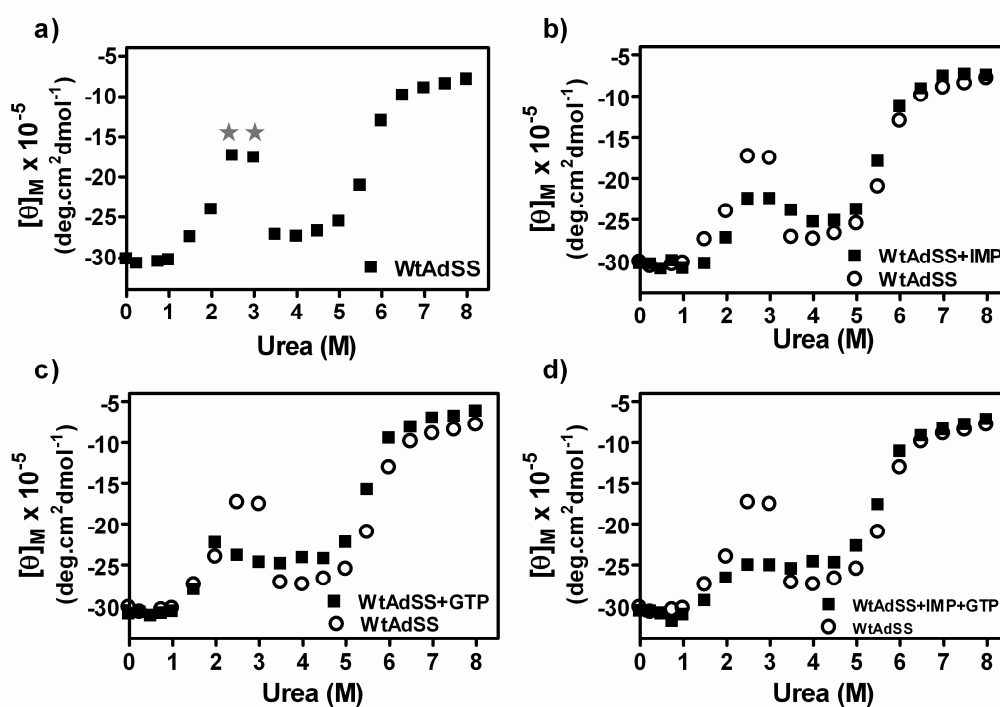


Figure 5.23: Changes in molar ellipticity of a) unliganded and b,c) liganded WtAdSS at 220 nm as a function of urea concentration. The stars in panel (a) mark the loss the ellipticity seen as a consequence of protein precipitation. d) Comparison of unfolding transitions in unliganded and IMP liganded WtAdSS.

Similar far UV-CD experiments were carried out with C328S (Figure 5.24) and C328D (Figure 5.25) mutants. Like Wt protein, the unfolding profiles of both mutants showed two transitions with the stabilization of an intermediate between 2.5-5 M urea concentration. However, unlike the unliganded wild type protein, C328S mutant exhibited full solubility at the intermediate urea concentrations of 2-3 M (Figure 5.24c). C328D mutant showed significantly reduced precipitation at similar urea concentrations (Figure 5.25c). The C_m values for the two transitions are largely similar for the two mutants. The two transitions in unliganded C328S mutant exhibited C_m values of 1.6 and 5.9 M urea and 2.0 and 5.9 M for the IMP liganded C328S protein. In C328D mutant the midtransition urea concentrations were 1.3 and 5.4 M for unliganded and 1.8 and 5.5 M for IMP liganded protein.

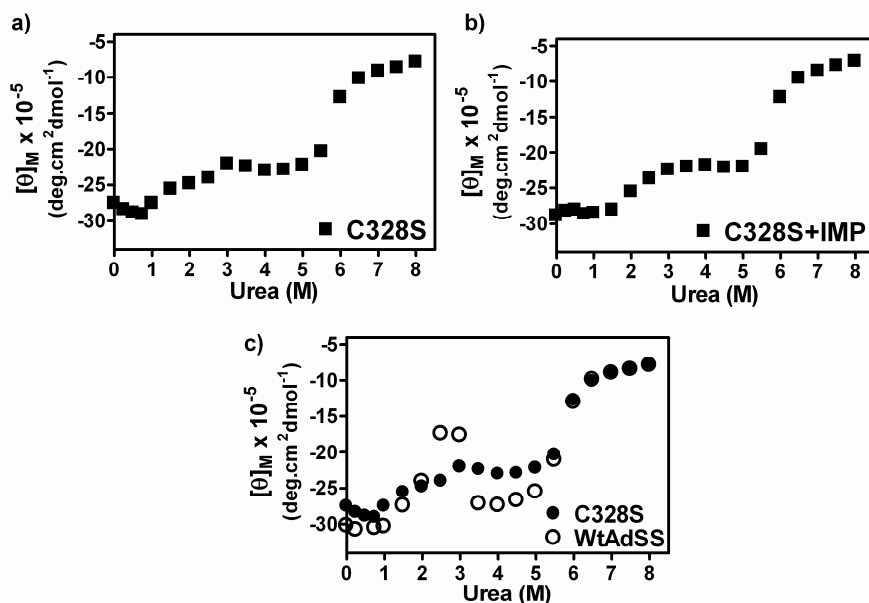


Figure 5.24: Urea induced unfolding of C328S mutant monitored by far UV-CD spectroscopy. Changes in molar ellipticity of a) C328S and b) IMP liganded C328S protein at 220 nm monitored as a function of urea concentration. c) Comparison of urea induced unfolding transitions of WtAdSS and C328S mutant.

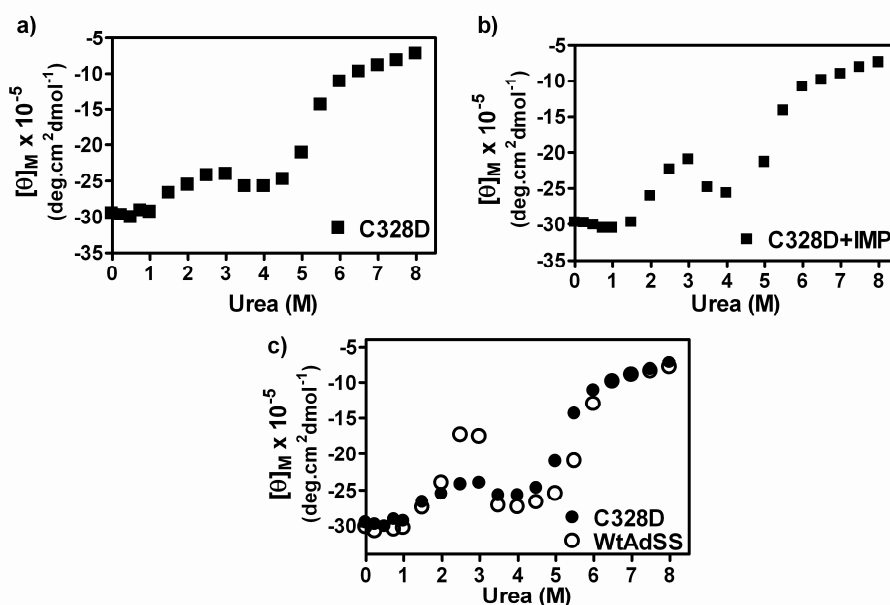


Figure 5.25: Changes in molar ellipticity of a) unliganded C328D and b) IMP liganded C328D protein at 220 nm monitored as a function of urea concentration. c) Comparison of urea induced unfolding profiles of WtAdSS (O) and C328D mutant (●).

5.3.9 Structural features of the unfolding intermediate

The urea induced unfolding of PfAdSS monitored by far UV-CD spectroscopy showed the presence of an intermediate on the unfolding pathway. The structural features of this intermediate seem to resemble those of a molten globule state. The structural characteristics of molten globule state are; presence of considerable amount of secondary structure, absence of precise tertiary structure, compactness of the molecule and presence of loosely packed hydrophobic core (Ptitsyn, 1995; Arai & Kuwajima, 2000; Kuwajima, 1996).

Urea induced denaturation of wild type and interface cysteine mutants monitored by far UV-CD spectroscopy, showed the presence of an intermediate between 2.5-5 M urea concentration. Gel filtration experiments indicate that the intermediate probably corresponds to unfolded monomeric AdSS. The CD spectra of the wild type protein and the mutants at the first C_m value and at 3.5, 4 and 5 M urea concentrations, which fall within the plateau region, are largely similar to that of the native protein with only 10-15% loss in ellipticity. This indicates that the intermediate exhibits secondary structural characteristics that are similar to the native protein. However, at these urea concentrations fluorescence measurements showed 8-10 nm shift in emission maximum over that in the absence of the chaotrope. These features are characteristics of a molten globule state which are found as intermediates in the unfolding pathway of a number of globular proteins.

5.4 Discussion

5.4.1 Importance of negatively charged cysteine/cysteines in maintaining dimer integrity of PfAdSS

Requirement of EDTA and DTT to maintain structural and functional integrity of PfAdSS implicates the role of metal ions and cysteines in the inactivation of the enzyme. Further, the inactivation of PfAdSS by Cu^{2+} and not Mn^{2+} ions indicates the involvement of a redox active system in the process. As stated in Section 5.1, cysteine

by virtue of possessing a thiol group is highly reactive and susceptible to oxidation. It is therefore, not surprising that PfAdSS, which has 10 cysteines per monomer, is inactivated in the presence of Cu^{2+} and forms disulfide linked oligomeric species. Infact, storage of the enzyme over time in presence of DTT but in the absence of EDTA yielded inactive disulfide bonded aggregates.

Several observations raise the possibility of the involvement of negatively charged cysteines in maintaining dimer stability of PfAdSS.

1. Iodoacetate treatment of the enzyme resulted in the destabilization of the PfAdSS dimer. However, the protein continued to exhibit monomer-dimer equilibrium. In contrast, treatment with iodoacetamide lead to the enzyme distributing over a wide range on a gel filtration column. Reaction of iodoacetate with cysteine results in the formation of an adduct that imparts a negative charge whereas iodoacetamide treatment leads to a neutral species. Thus, presence of a charge after modification helped to preserve the subunit association of PfAdSS.
2. Mutation of interface cysteines to serine did not lead to dimer stabilization. In proteins, where cysteine reactivity affects structural stability, cysteine to serine mutation often imparts stability. The two amino acids, cysteine and serine, are largely similar except for the ionization property of the side chain. Serine hydroxyl has a very high pKa and does not ionize easily, whereas the cysteine thiol has a pKa of 8.4 and hence can ionize to form a thiolate anion which is highly reactive and can undergo various oxidation reactions. The absence of stabilization in the single mutant (C328S) and destabilization of the double mutant (C328S-C368S) hints towards the possible involvement of a negatively charged species at one or both positions in maintaining the stability of PfAdSS.
3. Finally, the crystal structure of PfAdSS showed additional electron density around the two interface cysteines, 328 and 368. Although the exact modification could not be identified, there is probably more than one oxygen attached to the cysteines.

Attempts to identify the nature of interface cysteines by mass spectrometry did not provide unambiguous results. This could be a consequence of the instability of the oxidized species which reduce back to thiols once removed from the native protein environment or may get further oxidized to higher oxidation states. Using NBD chloride, which reacts with cysteine thiol and sulfenic acid, the interface cysteines, 328 and 368 were found to exist as thiols. However, a large proportion of unmodified parent peak corresponding to these cysteine containing peptides could be observed even after one hour of treatment with the reagent, which may imply the presence of the higher oxidation states, sulfinic or sulfonic acids at these positions. However, the significance of our observation of Cys352 probably existing as a sulfenic acid adduct, remains unclear.

To assess the possible role of negatively charged cysteines at the interface of PfAdSS, site-directed mutagenesis was used to replace Cys328 and Cys368 with aspartic acid. Aspartic acid side chain has a pKa of 3.9 and hence, would be ionized under the conditions in which the studies have been carried out. The quaternary structure of WtAdSS was found to be sensitive to the ionic strength of the buffer with a monomeric peak appearing at 200 mM phosphate or in the presence of 500 mM NaCl (Jayalakshmi *et al.*, 2002). In contrast, subunit association in C328D mutant was extremely stable with no evidence of dimer dissociation even in the presence of 1.5 M NaCl. Interestingly, the double mutant C328D-C368D, showed two peaks with one corresponding to a dimer and other to a monomer. Thus, introduction of two negative charges at the interface of PfAdSS perturbed the monomer-dimer equilibrium rate of the enzyme. The ability to capture two distinct species shows that the equilibrium rate in the mutant is slower than the time scale of the measurement. Although an increase in monomeric population was evident with increase in salt or ionic strength of the buffer, the dimeric species in C328D-C368D mutant was present under all conditions.

5.4.2 Urea unfolding

The conformational stability of multimeric proteins can be measured by equilibrium unfolding studies in urea and guanidine hydrochloride solution. The

structural stability of WtAdSS and the mutant proteins was assessed by urea unfolding. Changes in quaternary, tertiary and secondary structure of the proteins on treatment with urea were monitored by size exclusion chromatography, fluorescence and circular dichroism spectroscopy. The weak association of PfAdSS dimer was evident in size exclusion chromatography experiments, where a shift in equilibrium towards a monomer was seen even at a low urea concentration of 1 M (Figure 5.11). Further increase in urea concentration was accompanied by monomer unfolding and aggregation. Presence of IMP, which contacts Arg155 from the symmetry related subunit and thus holds the dimer, stabilized the protein dimer till 2 M urea concentration. The urea induced transitions of PfAdSS as measured by far UV-CD spectroscopy, involved atleast two transitions with three conformational states. When compared to size exclusion chromatography, the first transition corresponds to dimer dissociation and the second to monomer unfolding and aggregation. Protein precipitation seen between 2-3 M urea concentration (Figure 5.23), indicates that dimer dissociation leads to exposure of certain segments on the interface of the protein that result in protein aggregation and precipitation. The stabilization induced by IMP was evident here too, with a marked reduction in precipitation of the monomer in the presence of IMP. However, fluorescence measurements reflected a different pattern. Changes in tertiary structure of the protein set in at 0.5 M urea concentration where secondary structural changes were not evident. The unliganded protein showed a continuous multistate transition whereas liganding with IMP changed the pattern to a three-state process with an intermediate being stabilized between 3-5 M urea concentration (Figure 5.18). Such non-coincidence of denaturation profiles using different probes is indicative of the presence of intermediates on the unfolding pathway.

Similar studies with the mutants highlighted certain interesting features. Though the urea induced quaternary structural changes of C328S mutant were largely similar to the wild type protein, differences in the far UV-CD profiles were evident. Unlike the wild type protein which showed precipitation on dimer dissociation, dimer dissociation in C328S mutant resulted in the formation of fully soluble monomers (Figure 5.24). This shows that the interfaces exposed in the two proteins are different.

In C328D mutant, dimer stabilization was evident in both fluorescence and gel filtration studies. The minor loss in ellipticity around 2-3 M urea concentration seen in the case of C328D mutant highlights its similarity with the wild type protein, in terms of interfaces being exposed on dimer dissociation (Figure 5.25).

Interestingly, C328D-C368D mutant showed monomeric species even in the absence of urea (Figure 5.9). This is the first report of a mutation that results in perturbing the monomer-dimer equilibrium rate in AdSS and therefore, enables detection of a native monomer species. The unfolding of all the proteins was found to proceed through an intermediate that exhibits features of a “molten globule” state. It had intact secondary structure with the tertiary structural characteristics being different from the native protein.

5.4.3 Electrostatic complementarity at subunit interfaces

As stated in section 5.1.2, protein interfaces are neutral and the disruption of electrostatic balance at the interface leads to disruption of subunit association and modulation of catalysis in multisubunit proteins. ClpB is a member of multichaperon system of *E. coli* which reactivates aggregated proteins in an ATP dependent manner. In solution, ClpB undergoes reversible self association exhibiting a seven-fold symmetry and this association is enhanced in the presence of ATP. Mutation of positively charged interface residues, Lys212, Arg815 and Arg819 (K212T, R815A and R819A) inhibited the chaperon activity and self-association of ClpB monomers in the presence or absence of nucleotides (Barnett & Zolkiewski, 2002). These three residues participate in intersubunit salt bridges and stabilize the ClpB oligomer. Engineered soluble human calcium-activated nucleotidase (CAN) can exist both as dimer and monomer depending upon the protein and calcium ion concentration. The dimer interface of CAN consists of a central core of hydrophobic residues. Mutation of Ile170, which is located in the center of the hydrophobic core, to lysine or glutamic acid disrupted the calcium-dependent dimerization of CAN and in turn decreased its ADPase activity. Analysis of the crystal structure of soluble CAN suggested that several ionic interactions at the periphery of the central hydrophobic core were also

important for the stabilization of the dimer. To assess this, an aspartic acid residue (Asp228) was mutated to threonine. Asp228 is predicted to electrostatically interact with Lys224 on the other monomer in the dimer. Mutation of Asp228 to threonine (D228T) decreased both the tendency to form dimers and ADPase activity, while double mutation of D228T/K224N largely restored the ability to form dimers and the ADPase activity (Yang *et al.*, 2008). Alpha class glutathione S-transferase isozyme A1-1, is a dimer (51 kDa) of identical subunits. Using the crystal structure, two main areas of subunit interaction were predicted, (1) the hydrophobic ball and socket comprised of Phe52 from one subunit fitting into a socket formed on the other subunit by Met94, Phe136, and Val139 and (2) the Arg/Glu region consisting of Arg69 and Glu97 from both subunits. Mutation of residues in the socket region to alanine or substitution of Glu97 resulting in charge elimination had no appreciable effect on subunit association. In contrast, when Phe52 was replaced with alanine, the enzyme exhibited a molecular mass of 31.9 kDa, as determined by sedimentation equilibrium experiments. Eliminating the charge on Arg69 (as in R69Q) resulted in a dimeric enzyme; however, when the charge was reversed (as in R69E), the molecular mass of the protein shifted towards that of the monomer (33 kDa) (Vargo *et al.*, 2004). These examples show that perturbation of electrostatic and geometric balance at the interface leads to loss of oligomerization and function of multisubunit proteins.

In contrast, introduction of charged residues at appropriate locations in protein interfaces enhances structural stability of proteins. Asp421, which is a negatively charged residue at the dimer interface of human glucose-6-phosphate dehydrogenase, lies in an area which is rich in negatively charged residues. Mutation of D421 to neutral residues (alanine and asparagines) increased the thermostability of the protein. The stability was increased further when Asp421 was mutated to lysine or arginine, which are positively charged residues (Scopes *et al.*, 1998).

The fact that the negative charges introduced at the interface of PfAdSS by site-directed mutagenesis, are fully tolerated resulting in soluble and active enzyme, provides direct evidence for the existence of negatively charged cysteines at the dimer interface of PfAdSS.

5.4.4 Dimer interface in *P. falciparum* AdSS

An important question here is, what causes the ionization of interface cysteines in PfAdSS and stabilizes the negative charge on them? The most striking feature of PfAdSS dimer interface is the preponderance of positively charged residues (Figure 5.26). There are 22 positive residues with only 6 negatively charged residues (Eaazhisai *et al.*, 2004). In contrast, both *E. coli* and mouse AdSS exhibit a more balanced distribution of charges at the interface. Three cysteines, Cys250, Cys328 and Cys368, occur at the interface of PfAdSS.

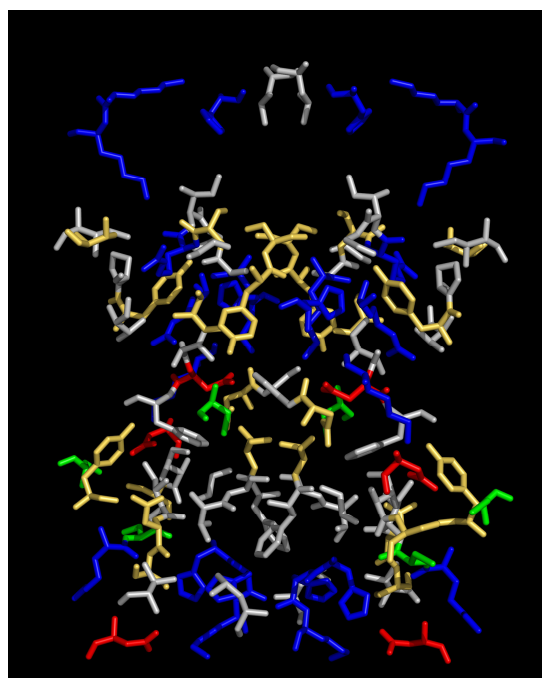


Figure 5.26: Residues at the dimer interface of *P. falciparum* AdSS. Blue, red, yellow and grey colors represent positive, negative, polar and hydrophobic residues, respectively. The figure was generated using PyMOL (DeLano, 2002).

The crystal structure of PfAdSS shows additional electron density around Cys328 and Cys368 (Eaazhisai *et al.*, 2004). Cys328 is surrounded by positively charged residues, lysine and histidine (Figure 5.27). Although the contact distances are large they may be relevant, as the additional electron density around Cys328 has not been modeled. Proximity with basic residues can lower the pKa of cysteine and

lead to its ionization. Once ionized the cysteine thiolate anion is highly reactive and can undergo oxidation to form sulfenic, sulfinic or sulfonic acid. Therefore, the positively charged interface of PfAdSS would provide the right environment for ionization and stabilization of the negative charge on the cysteines.

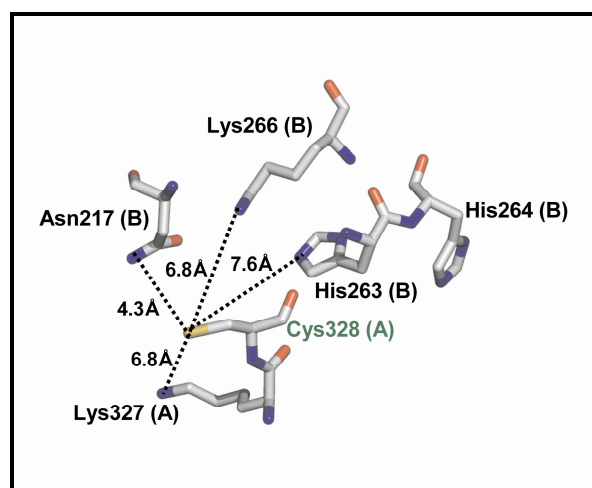


Figure 5.27: Environment around Cys328 in the crystal structure of PfAdSS. It is surrounded by positively charged residues. The contact distances are large but may be relevant because the additional electron density around Cys328 is not modeled. The figure was generated using PyMOL (DeLano, 2002)

To summarize, the studies described in this chapter support the role of negatively charged cysteines in maintaining dimer integrity and stability of PfAdSS. Redox sensitive cysteines in proteins flip between reduced and oxidized state in response to oxidative stress. However, any comment on the role of reactive cysteines in regulating PfAdSS activity *in vivo* and the link to redox regulation cannot be made at this stage.

Chapter 6

Molecular Dissection of the Purine Salvage Pathway in *P. falciparum*

Plasmodium falciparum lacks the *de novo* purine biosynthesis pathway and relies entirely on the salvage pathway to meet its purine nucleotide requirement. The entire flux for purine biosynthesis in the parasite is believed to be through the HGPRT pathway, with the enzymes, adenosine kinase and adenine phosphoribosyltransferase being unannotated in the *Plasmodium* genome database. This chapter outlines the studies carried out to dissect the purine salvage pathway of the parasite with an aim to find bypass mechanisms, if any, for AMP synthesis in the intraerythrocytic stages of the parasite life cycle.

6.1 Introduction

Nucleotides form the building blocks of DNA and RNA and their requirement is particularly demanding in cells undergoing rapid division. In addition, nucleotides either directly or as derivatives are important source of chemical energy (ATP, GTP), enzyme cofactors (FAD, NAD⁺), precursors of more complex molecules (e.g. conversion of GTP to pterins and folates), second messengers (cAMP) and signals involved in metabolic and gene regulation. Nucleotides can be obtained by a cell in various ways: *de novo* synthesis, salvage of preformed bases or salvage of precursors

followed by their enzymatic conversion to various purines and pyrimidines required for cellular processes.

6.1.1 Nucleotide metabolism in parasitic protozoa

Parasitic protozoa are generally capable of synthesizing pyrimidines *de novo* (Trager, 1970). One exception to this is *Cryptosporidium parvum* which lacks all the six genes encoding the enzymes necessary for pyrimidine synthesis (Striepen *et al.*, 2004) and hence, relies entirely on salvage mechanisms to fulfill its purine and pyrimidine nucleotide requirement. *de novo* pyrimidine biosynthesis involves a six step pathway where the pyrimidine ring is first synthesized from aspartic acid, glutamine and bicarbonate and then coupled to ribose-5-phosphate moiety. The first reaction of the pathway catalyzed by carbamoyl phosphate synthetase II, leads to the synthesis of carbamoyl phosphate from bicarbonate and amide nitrogen of glutamine. Aspartate transcarbamoylase (ATCase) catalyzes the condensation of carbamoyl phosphate with aspartate leading to the formation of carbamoyl aspartate which then undergoes intramolecular condensation catalyzed by dihydroorotase to form dihydroorotate. Dihydroorotate is irreversibly oxidized to orotate by dihydroorotate dehydrogenase which then reacts with PRPP to yield orotidine-5'-monophosphate (OMP). This reaction which leads to the acquisition of ribose phosphate moiety is catalyzed by orotate phosphoribosyltransferase. The final step in the pathway is the decarboxylation of OMP by OMP decarboxylase to form UMP. UMP gets converted to UTP by the sequential action of a nucleoside monophosphate and nucleoside diphosphate kinase. CTP is formed by the amination of UTP by CTP synthetase. The building blocks of DNA are deoxyribonucleotides. The conversion of ribonucleotides to deoxyribonucleotides takes place at the level of nucleoside diphosphates, catalyzed by ribonucleotide reductase. Formation of thymine nucleotide involves methylation of dUMP to produce dTMP in a reaction catalyzed by thymidylate synthase.

Unlike pyrimidine synthesis, almost all parasitic protozoa are incapable of synthesizing purines *de novo* (Fairlamb, 1989; Trager, 1970). Thus, parasites possess

mechanisms to uptake purines or their precursors from the host and convert them to the required nucleotides. The mechanisms by which protozoan parasites salvage purines are diverse. Salvage of purines can occur either by phosphoribosylation of adenine, guanine, hypoxanthine and xanthine or by phosphorylation of adenosine. These salvage activities are accounted for by the enzymes; PRTases, hypoxanthine guanine xanthine phosphoribosyltransferase (HGXPRT) and adenine phosphoribosyltransferase (APRT), and adenosine kinase. Adenosine kinase catalyzes the phosphorylation of adenosine leading to the formation of AMP. HGPRT, depending upon its specificity, catalyzes the phosphoribosylation of hypoxanthine and guanine to form IMP and GMP, respectively. IMP gets converted to AMP by a two step reaction catalyzed by the enzymes adenylosuccinate synthetase (AdSS) and adenylosuccinate lyase (ASL). APRT on the other hand catalyzes the direct conversion of adenine to AMP using PRPP as the phosphoribosyl group donor.

Parasites express a battery of purine transporters and salvage enzymes that enable purine acquisition from the host. Transport mechanisms and salvage pathways in a few parasitic protozoa are discussed in the following sections, with special emphasis on the available literature on *P. falciparum*.

6.1.2 Nucleoside/nucleobase transporters in parasitic protozoa

The first step in the synthesis of purines is the uptake of the required nucleobases and nucleosides from the host milieu and this is mediated by various nucleobase and nucleoside transporters located in the parasite plasma membrane. These transporters not only mediate the uptake of essential nutrients required by the parasite but are also capable of transporting a variety of toxic drugs (Wallace *et al.*, 2004; Al Safarjalani *et al.*, 2003; de Koning & Jarvis, 2001; Carter *et al.*, 1995). Though the enzymes involved in purine salvage have long been studied, the interest in molecular characterization of transporters is a more recent development. All purine transporters identified in parasitic protozoa are members of the equilibrative nucleoside transporter (ENT) family (de Koning *et al.*, 2005).

Leishmania donovani express two members of the equilibrative nucleoside transporter family; LdNT1 (which is encoded by two closely related and linked genes, LdNT1.1 and LdNT1.2) that transports adenosine and pyrimidine nucleosides and LdNT2 which transports inosine and guanosine (Iovannisci *et al.*, 1984; Vasudevan *et al.*, 1998; Aronow *et al.*, 1987; Carter *et al.*, 2000b). All three nucleoside transporters are electrogenic proton symporters (Stein *et al.*, 2003). To assess the role of LdNT1 and LdNT2 activity on the viability and infectivity of *L. donovani* parasites, Δ dnt1, Δ dnt2 and Δ dnt1/ Δ dnt2 knockouts were made. Mutants lacking LdNT1 could not transport adenosine but were capable of growing on other purine nucleosides and nucleobases. Δ dnt2 mutants failed to transport inosine and xanthosine but were capable of growing on inosine and guanosine but not xanthosine. All three knockout strains were capable of transforming into axenic amastigotes, establishing an infection and proliferating in murine macrophages. These studies established that nucleoside transport is not essential for the viability of either parasite life cycle stage and that the macrophages are capable of supplying nucleobases that are not ligands for LdNT1 or LdNT2, to meet the nutritional needs of the parasites (Liu *et al.*, 2006). In addition to the above nucleoside transporters, *Leishmania major* expresses two nucleobase transporters, LmaNT3 and LmaNT4. While LmaNT4 is a low affinity adenine transporter, LmaNT3 is a broad specificity purine nucleobase transporter, with K_m values for hypoxanthine, guanine, adenine and xanthine in the low micromolar range (Ortiz *et al.*, 2007; Sanchez *et al.*, 2004a). In addition, a high affinity uracil transporter ($K_m = 0.32 \mu\text{M}$), designated as LmU1 has been identified in *Leishmania*. The transporter is highly specific and has virtually no affinity for cytosine, thymine or purine nucleobases, nor does it transport pyrimidine nucleosides (Papageorgiou *et al.*, 2005).

The protozoan parasite, *Toxoplasma gondii*, expresses a high affinity nucleobase transporter, TgNBT1 that transports hypoxanthine and is inhibited by guanine and xanthine (de Koning *et al.*, 2003). It also expresses two nucleoside transporters; TgAT1 which is a low affinity transporter for adenosine and inosine (Schwab *et al.*, 1995; Chiang *et al.*, 1999) and TgAT2 which exhibits high affinity for a range of purine and pyrimidine nucleosides including adenosine, which is the main

purine source in *T. gondii*. Nucleobases such as adenine, cytosine and uracil have no effect on adenosine uptake by TgAT2 (de Koning *et al.*, 2003).

Two different adenosine transport systems have been characterized in *Trypanosoma brucei* cells (Carter & Fairlamb, 1993). The P1 system is a broad specificity purine nucleoside transport system (adenosine, inosine and guanosine) (Sanchez *et al.*, 1999; Sanchez *et al.*, 2002; de Koning & Jarvis, 1999) and P2 system mediates uptake of only adenosine and adenine along with certain anti-trypanosomal drugs (Maser *et al.*, 1999; Matovu *et al.*, 2003). While P1 is encoded by multiple genes of the TbNT family (TbNT2-TbNT11), P2 is encoded by a single gene, TbAT1. Expression in oocytes revealed that TbNT2, TbNT5, TbNT6 and TbNT7 are high affinity adenosine/inosine transporters while TbNT5, and to some extent TbNT6 and TbNT7 also mediate uptake of the nucleobase, hypoxanthine (Sanchez *et al.*, 2002). Four additional ENT family members, TbNT8, TbNT9, TbNT10 and TbNT11 have been identified in *T. brucei*. Characterization of NT10/AT-B revealed that it is a high affinity purine nucleoside transporter and is upregulated in the short stumpy form of the life cycle. The restricted expression of NT10/AT-B during the parasite life cycle suggests that the functional properties of this permease may be specialized to support development and growth of the differentiated short stumpy form or to promote the transformation of short stumpy to procyclic forms within the insect vector (Sanchez *et al.*, 2004b; Al-Salabi *et al.*, 2007). More recently, NT9/AT-D, another P1 transporter having exceptionally high affinity for adenosine ($K_m = 0.068 \mu\text{M}$) and 2'-deoxyadenosine, has been characterized. The affinity of the transporter for other purine nucleosides is in the low micromolar range (Al-Salabi *et al.*, 2007). A distinct transporter for uracil, designated as U1, has also been identified in the procyclic form of *T. brucei* (de Koning & Jarvis, 1998). In addition, four nucleobase transporters, H1, H2, H3 and H4, transporting hypoxanthine, guanine and adenine, have also been characterized (de Koning & Jarvis, 1997a; de Koning & Jarvis, 1997b; Burchmore *et al.*, 2003).

6.1.3 Purine transporters in *P. falciparum*

Plasmodium falciparum is auxotrophic for purines and hence, purine acquisition from the host is indispensable for parasite survival. The parasite residing in the human erythrocyte is separated from the external environment by three membranes, the erythrocyte plasma membrane, parasitophorous vacuolar membrane (PVM) and the parasite plasma membrane. Unlike the PVM, which is freely permeable to small molecules (Desai *et al.*, 1993), the plasma membrane employs transporters to import and export molecules (Kirk, 2001).

The first direct evidence for parasite encoded transporters came in the year 1998. Microinjection of *Xenopus laevis* oocytes with mRNA isolated from the asexual stages of *P. falciparum*, conferred the oocytes an ability to uptake nucleobase and nucleosides (Penny *et al.*, 1998). The *P. falciparum* genome has genes encoding for four members of the equilibrative nucleoside transporter (ENT) family, all of which are expressed in the intraerythrocytic stages of the parasite life cycle (Martin *et al.*, 2005). The first report on the isolation and functional characterization of a gene encoding a nucleoside transporter in *Plasmodium falciparum* appeared in year 2000. The gene product was named as PfNT1, and was found to encode a protein of 422 amino acids with 11 transmembrane domains, a feature homologous to members of equilibrative nucleoside transporter family. Northern analysis revealed that the gene was expressed throughout the asexual life cycle of the parasite with an increased expression at the early trophozoite stage. The transporter was found to have broad substrate specificity for purine and pyrimidine nucleosides and their L-stereoisomers. Expression of PfNT1 in *Xenopus laevis* oocytes increased their ability to uptake D-adenosine ($K_m = 13.2 \mu\text{M}$) and D-inosine ($K_m = 253 \mu\text{M}$). Unlike the mammalian counterpart, PfNT1 had the capacity to transport L-adenosine ($K_m > 500 \mu\text{M}$). PfNT1 exhibited low sensitivity towards NBMPR (6-[(4-nitrobenzyl)thio]-9- β -D-ribofuranosylpurine) which is a potent inhibitor of hENT1 (human transporter) but was inhibited by another hENT1 inhibitor, dipyrindamole (Carter *et al.*, 2000a). Simultaneously there was another report on the cloning and characterization of PfENT1 which differed from PfNT1 in having leucine instead of phenylalanine at

position 385. However, characterization of PfENT1 expressed in *Xenopus* oocyte showed that in addition to nucleosides, it was able to transport nucleobases and was insensitive to inhibition by dipyridamole. Also, the affinity of the transporter for adenosine reported in the two studies was significantly different. Parker *et al.* found that PfENT1 exhibited a higher affinity for adenosine ($K_m = 0.32 \pm 0.05$ mM) than for the pyrimidine nucleoside, uridine ($K_m = 3.5 \pm 1.1$ mM). The K_m values for the nucleobases, adenine and hypoxanthine were estimated to be 0.32 ± 0.1 mM and 0.41 ± 0.1 mM, respectively (Parker *et al.*, 2000). Using purified PfNT1 antibodies it has been shown that PfNT1 polypeptide is expressed in all intraerythrocytic stages of the parasite, with the expression increasing in the early trophozoite stage. Deconvolution and immunoelectron microscopy showed that PfNT1 localizes predominantly to the parasite plasma membrane indicating that the flux of nucleosides across the parasite plasma membrane is PfNT1 mediated (Rager *et al.*, 2001).

All the above mentioned studies that aimed at the functional characterization of PfNT1 used *Xenopus* oocytes to look at uptake of nucleosides and nucleobases with no direct evidence for the role of this transporter in *P. falciparum* intraerythrocytic stages. Downie *et al.* measured purine and pyrimidine uptake in saponin released parasites and showed that this transport had characteristics of PfNT1. The data were consistent with thymidine being transported into the parasite via a low affinity ($K_m = 1.1$ mM) equilibrative transporter which was slowed in the presence of adenosine and inosine, indicating that these nucleosides share the same transporter. The transporter was able to differentiate between thymidine and cytidine. The uptake of purine nucleosides, inosine and adenosine, comprised of three components; a fast relatively low-affinity component which was equilibrative, saturable, with an apparent K_m value of 1.45 mM for adenosine and was competed by thymidine and inosine but not cytidine, a second high-affinity fast component and a slow high-affinity component, both of which were ATP dependent (Downie *et al.*, 2006). To establish the importance of PfNT1 in the parasite purine salvage, the PfNT1 gene was genetically disrupted in *P. falciparum*. Unlike the wild type parasites that could use hypoxanthine, inosine or adenosine, the transgenic parasites lacking PfNT1 were incapable of using physiological concentrations of these purines. The growth of

*pfnt1*Δ parasites was restored, when hypoxanthine, inosine or adenosine were provided at very high, nonphysiological concentrations in the culture medium. Furthermore, transport studies with erythrocyte free *pfnt1*Δ parasites revealed a severe reduction in their ability to transport hypoxanthine, although adenosine and inosine uptake remained near the wild type levels. This indicated that the parasite plasma membrane harbors more permeases capable of transporting these nucleosides. Based on these observations, hypoxanthine was proposed to be the likely ligand for PfNT1 (El Bissati *et al.*, 2006). The hypothesis that PfNT1 serves as a major route for the uptake of purine nucleobases was further established by Downie *et al.* They measured the uptake of hypoxanthine and the related purine nucleobase, adenine, by mature blood stage parasites isolated from the host cells by saponin permeabilisation of the erythrocyte and parasitophorous vacuolar membrane and compared it to the transport characteristics of PfNT1 expressed in *Xenopus* oocytes. The uptake of both nucleobases comprised of two components, a low-affinity rapid equilibrative ATP-independent component and a higher affinity process which was ATP-dependent (Downie *et al.*, 2008)

In a recent report Quashie *et al.* proposed a comprehensive model for purine uptake by *P. falciparum* involving four purine nucleobase/nucleoside transporters. They reported on the characterization of a low affinity adenosine transporter (PfLAAT), a high affinity adenine transporter (PfADET1) and a low affinity uptake route for adenine (PfADET2). They generated PfNT1 knockout parasites which lost the high affinity adenosine and hypoxanthine uptake capacity, while the low affinity adenosine uptake and the high affinity adenine uptake was not dramatically altered thereby indicating that PfNT1 is a high affinity hypoxanthine/purine nucleoside transporter (Quashie *et al.*, 2008).

6.1.4 Purine salvage in parasitic protozoa

Parasitic protozoa are auxotrophic for purines and lack *de novo* purine biosynthesis pathway. They however differ in the choice of precursors and mechanisms by which the salvaged purines are interconverted. Two important

enzymes implicated in purine salvage in parasitic protozoa are adenosine kinase (AK) and hypoxanthine guanine xanthine phosphoribosyltransferase (HGXPRT).

Leishmania expresses adenosine kinase (AK) and three phosphoribosyltransferases, hypoxanthine guanine phosphoribosyltransferase, adenine phosphoribosyltransferase (APRT) and xanthine phosphoribosyltransferase (XPRT). Genetic studies have demonstrated that none of the four enzymes by themselves are essential for the viability of *L. donovani* promastigotes (Hwang & Ullman, 1997; Iovannisci & Ullman, 1984) and neither HGPRT, APRT or XPRT by themselves are important for amastigote proliferation (Boitz & Ullman, 2006a). This indicated that purine salvage in *L. donovani* occurs through multiple routes. The viability of $\Delta hgprt/\Delta aprt/ak^-$ and $\Delta xprt/\Delta aprt/ak^-$ *L. donovani* promastigotes indicated that the parasite could rely on a functional HGPRT or XPRT to meet its entire purine nucleotide requirement (Boitz & Ullman, 2006a). This was genetically validated by constructing a conditional $\Delta hgprt/\Delta xprt$ mutant strain which showed an absolute requirement for adenine or adenosine as a source of purines (Boitz & Ullman, 2006b). These studies demonstrated that either HGPRT or XPRT is absolutely essential for purine acquisition, parasite viability and parasite infectivity, and that all exogenous purines are funneled to hypoxanthine and/or xanthine by *L. donovani*.

Toxoplasma gondii uses only two pathways for purine salvage involving the enzymes hypoxanthine guanine xanthine phosphoribosyltransferase (HGXPRT) and adenosine kinase (AK). The genes encoding these enzymes have been cloned and characterized (Donald *et al.*, 1996; White *et al.*, 2000; Sullivan *et al.*, 1999; Darling *et al.*, 1999). Two isozymes of HGXPRT are expressed in *T. gondii*, as a result of differential splicing from a single HGXPRT gene. The two isozymes differ by 49 amino acids, form tetramers and the specific activity of HGXPRT-I is five times that of HGXPRT-II (White *et al.*, 2000). Fluorescent protein fusions when expressed in parasites lacking the endogenous HXGPRT gene, showed that HXGPRT-I (which lacks the 49 amino acid insertion) is found in the cytosol, whereas HXGPRT-II (which contains the insertion) localizes to the inner membrane complex (IMC) of the parasite. Simultaneous expression of both isoforms resulted in the formation of hetero-oligomers, which distributed between the cytosol and IMC (Chaudhary *et al.*,

2005). Like HGXPRT, *T. gondii* tachyzoites also show two inosine 5'-monophosphate dehydrogenase (IMPDH) transcripts. The larger transcript contains an open reading frame of 551 amino acids while, the shorter transcript is an alternative spliced product that generates a 371 amino acid protein that lacks the active-site flap (Sullivan *et al.*, 2005). Deletion of either HGXPRT or adenosine kinase in *T. gondii* did not abolish parasite viability, indicating that one of the activities was sufficient to meet the parasite's purine nucleotide requirement. Relative fitness measurements on the two knockout parasites showed that the salvage of adenosine was more important than salvage of hypoxanthine or other purine nucleobases. Simultaneous deletion of both HGXPRT and AK was not possible indicating that alternate routes of purine synthesis are not present in the parasite (Chaudhary *et al.*, 2004).

Trypanosoma has the full set of enzymes needed to salvage adenosine, hypoxanthine, adenine and inosine (Ogbunude & Ikediobi, 1983; Davies *et al.*, 1983). In addition, *Trypanosoma brucei* expresses high affinity adenosine transporters. Adenosine in the parasite can be salvaged by the cleavage-dependent pathway or by adenosine kinase. The cleavage-dependent pathway involves the conversion of adenosine to adenine by the enzyme inosine-adenosine-guanosine-nucleoside hydrolase (IAG-NH) which has low affinity for adenosine (Parkin, 1996; Pelle *et al.*, 1998). Adenine thus formed gets phosphoribosylated to form AMP, which then forms GMP via IMP and XMP. The trypanosoma genome contains two putative adenosine kinase genes. The products of the two genes differ in four amino acids. One of these genes has been cloned, expressed and characterized. The enzyme (TbAK) showed higher catalytic activity and affinity for adenosine when compared to IAG-NH. However, it was inhibited by high adenosine concentrations (Vodnala *et al.*, 2008). The role of TbAK in activation of nucleoside analogs to manifest cytotoxicity has also been demonstrated (Luscher *et al.*, 2007). Hence, adenosine kinase along with an efficient adenosine transport system enables survival of the parasite in environments having scarce purine supply. In purine rich environments, the cleavage-dependent pathway supplies purines needed for the parasite survival.

Cryptosporidium parvum lacks *de novo* purine as well as pyrimidine biosynthesis pathways and relies entirely on salvage mechanisms (Striepen *et al.*, 2004). Although hypoxanthine, guanine and xanthine phosphoribosyltransferase activities had been demonstrated in crude cell-free extracts of *Cryptosporidium* sporulated oocysts utilizing radiolabeled substrates (Doyle *et al.*, 1998), no evidence of a gene or genes encoding these activities has been found in the sequenced genome of the parasite (Abrahamsen *et al.*, 2004). Thus, salvage of adenosine is the sole source of purines in the parasite. Characterization of *Cryptosporidium* adenosine kinase revealed that it exhibits high specificity for adenosine but the specificity for the phosphodonor was relaxed and it could use all four nucleoside triphosphates. Adenosine kinase phosphorylates adenosine to form AMP, which is deaminated to IMP by the enzyme AMP deaminase. IMPDH and GMP synthetase then convert IMP to GMP. The two IMPDH inhibitors, mycophenolic acid and ribavirin inhibited parasite development and the block could not be overcome in the presence of excess guanine (Galazka *et al.*, 2006; Striepen *et al.*, 2004).

6.1.5 Purine salvage in *Plasmodium falciparum*

Hypoxanthine is regarded as the key source of all other purines in *P. falciparum* (Webster & Whaun, 1981). Evidence for this comes from the fact that depletion of hypoxanthine in parasitized erythrocytes by treatment with xanthine oxidase inhibited parasite growth and the inhibition could be reversed by excess hypoxanthine. This indicated that supply of host derived hypoxanthine is essential for parasite viability (Berman *et al.*, 1991). Further, nutritional supplementation of parasite culture medium with hypoxanthine enhances parasite growth (Zolg *et al.*, 1982) and labeled hypoxanthine incorporation in nucleic acids is used to monitor parasite growth (Desjardins *et al.*, 1979; Chulay *et al.*, 1983; Geary *et al.*, 1983). The source of hypoxanthine is believed to be the ATP present in the infected erythrocytes, which is catabolized to hypoxanthine via ADP, AMP, IMP and inosine (Webster & Whaun, 1981; Sherman, 1979). Parasite plasma membrane harbors high affinity transporters for both adenosine and hypoxanthine. Adenosine cannot be efficiently

salvaged by the parasite due to low levels of adenosine kinase activity (Reyes *et al.*, 1982; Ting *et al.*, 2005). Instead adenosine is converted to inosine by adenosine deaminase (Reyes *et al.*, 1982). *P. falciparum* adenosine deaminase (PfADA) unlike the mammalian enzyme is able to deaminate the L-nucleoside analogues, L-adenosine, 2,6-diamino-9-(L-ribofuranosyl)-purine and 4-amino-1-(L-ribofuranosyl)-pyrazolo[3,4-d]-pyrimidine but not L-thioinosine and L-thioguanosine. L-nucleoside structural analogues of 2'-deoxy-D-coformycin selectively inhibited *P. falciparum* adenosine deaminase in the picomolar range. Given the ability of PfNT1 to selectively transport L-adenosine and the ability of PfADA to deaminate the L-isomers of adenosine, makes it an attractive drug target (Brown *et al.*, 1999).

Inosine produced by adenosine deaminase is converted to hypoxanthine by purine nucleoside phosphorylase (PNP). *P. falciparum* PNP is able to utilize inosine, guanosine and deoxyguanosine but not adenosine or xanthosine (Daddona *et al.*, 1986; Kicska *et al.*, 2002a). In addition, it has the ability to use alternate substrates like 5'-methylthioinosine, which is a byproduct of polyamine biosynthesis pathway (Shi *et al.*, 2004). Thus, PfADA and PfPNP together have ability to use methylthiopurines and therefore to function in both purine salvage and methylthiopurine recycling pathways (Ting *et al.*, 2005). Use of immucilins, which are PNP transition-state analogs, in malaria therapy is hindered by the fact that the transition state conformation across human and parasite enzyme is highly conserved (Kicska *et al.*, 2002a; Kicska *et al.*, 2002b). However, the methylthio specificity of PfPNP has lead to the design of 5'-methylthio-immucilinH which shows higher specificity for the parasite PNP (Lewandowicz *et al.*, 2005; Shi *et al.*, 2004).

Hypoxanthine formed by parasite PNP, is the key precursor of other purines. A single protein in *P. falciparum* harbors hypoxanthine, guanine and xanthine phosphoribosyltransferase activities and is termed as HGXPRT (Queen *et al.*, 1988; Keough *et al.*, 1999). Phosphoribosylation of hypoxanthine results in the formation of IMP which is the common precursor of both AMP and GMP. GMP can also be formed directly from guanine by the action of HGXPRT or from XMP formed as a result of phosphoribosylation of xanthine by HGXPRT. Thus, HGXPRT is an essential enzyme in the purine salvage pathway of *P. falciparum* and can be targeted

for drug development. This involves the identification of purine base analogs which are poor or weak substrates for human HGPRT but have high affinity for the parasite enzyme (Shivashankar *et al.*, 2001). The ability of the human and *P. falciparum* HGPRT to use four groups of purine analogs bearing substitutions at 2-, 6-,7- and 8-position was tested. Three base analogs, 6-chloroguanine, 8-azaguanine and 8-azahypoxanthine were found to be selective and effective substrates for PfHGXPRT when compared to the human enzyme. These compounds also inhibited *in vitro* *P. falciparum* culture at micromolar concentrations (Keough *et al.*, 2006). In addition, immucilin-based compounds which were phosphorylated at the 5' position, immucilinGP and immucilinHP, showed potent inhibition of HGPRT activity and exhibited binding constants that were more than 1,000-fold higher than the binding constants of the nucleotide substrates. However, these molecules failed to discriminate between the human and parasite enzyme. These molecules thus serve as lead compounds which can be chemically modified to increase their affinity and selectivity for the parasite enzyme (Li *et al.*, 1999). Interestingly, recombinant *P. falciparum* HGPRT is inactive when purified and can be switched into an active state by the product, IMP (Raman *et al.*, 2005).

IMP formed as a result of HGPRT activity serves as a precursor for both AMP and GMP. All the enzymes involved in this process, adenylosuccinate synthetase, adenylosuccinate lyase, IMP dehydrogenase and GMP synthetase are expressed in the parasite. The *P. falciparum* genome has a strong AT (>70%AT) bias and hence, regulation of the activity of these enzymes is necessary to maintain its genome integrity. *P. falciparum* adenylosuccinate synthetase, GMP synthetase and adenylosuccinate lyase have been biochemically characterized and these studies have highlighted features unique to the *P. falciparum* enzyme both in terms of kinetic mechanism and regulation (Raman *et al.*, 2004; Jayalakshmi *et al.*, 2002; McConkey, 2000; Bhat *et al.*, 2008; adenylosuccinate lyase, unpublished results from this laboratory). In addition structural information exists for PfAdSS which enables a better understanding of the observed biochemical features (Eaazhisai *et al.*, 2004).

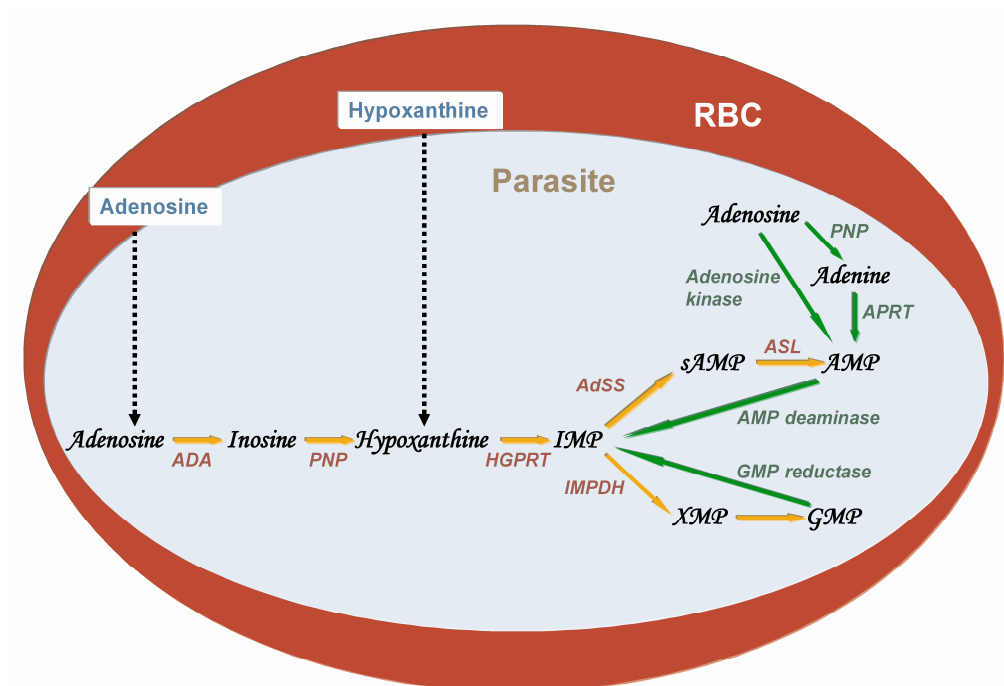


Figure 6.1: The purine salvage pathway. The arrows in orange show the flux through the HGPRT pathway, which is the main purine nucleotide source in the malaria parasite, *P. falciparum*. The arrows in green show possible bypass pathways for AMP and GMP synthesis. Annotations for APRT, adenosine kinase and GMP reductase are absent in the Plasmodium genome database (Bahl *et al.*, 2003). The abbreviations used are: ADA, adenosine deaminase; PNP, purine nucleoside phosphorylase; HGPRT, hypoxanthine guanine phosphoribosyltransferase; IMPDH, inosine 5'-monophosphate dehydrogenase; AdSS, adenylosuccinate synthetase; ASL, adenylosuccinate lyase; APRT, adenine phosphoribosyltransferase.

Bypass mechanisms of AMP/GMP formation include the conversion of adenosine directly to AMP by adenosine kinase and phosphoribosylation of adenine to AMP catalyzed by adenine phosphoribosyltransferase (Figure 6.1). Very weak adenosine kinase activity has been detected in *P. falciparum* culture lysates. However, a sequence with significant homology to known adenosine kinases from other species is not present in the parasite (Reyes *et al.*, 1982; Ting *et al.*, 2005). The other possible bypass to the HGPRT pathway, involves the conversion of adenine to AMP by APRT. Adenine levels in the parasite are low as adenosine is not a substrate for either host or parasite PNP and the high levels of adenosine deaminase keep the levels of adenosine in the parasite negligible. Weak APRT activity has been detected in the parasite lysate

using [³H]-adenine (Reyes *et al.*, 1982). The cloning of *P. falciparum* APRT by functional complementation in APRT deficient mouse cells has been reported (Pollack *et al.*, 1985). Another study reported on the kinetic characterization of APRT purified from the parasite and this highlighted certain unique features of the parasite enzyme. The protein exhibited a molecular weight of 18 kDa which is smaller than the host enzyme. Unlike the erythrocyte enzyme, parasite APRT was not inhibited by sulfhydryl reagents. 6-mercaptopurine and 2,6-diaminopurine which do not inhibit the human enzyme, were found to be competitive inhibitors of the parasite enzyme. The affinity of the parasite enzyme for the substrates (K_m for adenine = 0.80 μ M and K_m for 5-phosphoribosyl-1-pyrophosphate = 0.70 μ M) was significantly higher than the human enzyme (Queen *et al.*, 1989). However, no sequence information for this enzyme is available in the Plasmodium genome database (Bahl *et al.*, 2003). Thus, the existence of this enzyme in the parasite remains ambiguous. AMP deaminase, which converts AMP to IMP, though annotated in *P. falciparum*, has not been characterized. The last enzyme, GMP reductase, which catalyzes the NADPH-dependent reductive deamination of GMP to IMP, is also unannotated in the Plasmodium genome database (Bahl *et al.*, 2003).

This chapter describes results on studies carried out to dissect the purine salvage pathway in *P. falciparum*.

6.2 Materials and Methods

RPMI 1640, percoll, xanthine oxidase, hypoxanthine, AMP and adenine were from Sigma Chemical Company (St.Louis, MO). [³H]-hypoxanthine, [³H]-adenine and [³H]-isoleucine were purchased from PerkinElmer Life Sciences, Inc., Boston, MA. Human O⁺ serum and erythrocytes for culturing the parasites were collected from healthy volunteers. Combi-12 automated cell harvester (Molecular Devices, Sunnyvale, CA) and Wallac 1409 (Wallac OY, Turku, Finland) liquid scintillation counter were used for monitoring radiolabel incorporation. Hadacidin was a kind gift from Developmental Therapeutics Program, NIH, Bethesda, MD. MALDI-MS spectra

were recorded on Ultraflex II TOF/TOF mass spectrometer (Bruker Daltonics, Bremen, Germany).

6.2.1 In vitro *P. falciparum* culture

The *P. falciparum* strain 3D7 was cultivated in vitro using the method described by Trager and Jensen (Trager & Jensen, 1976). The parasites were maintained at 5% hematocrit in RPMI 1640-Hepes-HCO₃ medium supplemented with 10% heat inactivated human serum and O⁺ RBCs. The culture was maintained in a candle-jar at 37°C and the medium changed every 24 hours. Subculturing was done on attainment of 8-10% parasitemia.

6.2.2 Saponin Lysis

Parasites were isolated from the host erythrocytes by treating parasitized erythrocytes with saponin following procedure reported earlier (Hsiao *et al.*, 1991) with slight modification in the conditions. Treatment of parasitized erythrocytes with saponin, which is a mild detergent, renders the erythrocyte and parasitophorous vacuolar membrane permeable to macromolecules but leaves the parasite plasma membrane intact (Saliba *et al.*, 1998). Trophozoite rich *P. falciparum* culture at 9-10% parasitemia was pelleted by centrifugation at 2000 rpm for 4 minutes. The pellet was washed twice with 1xPBS and the pellet volume noted. Two volumes of 0.15% saponin dissolved in incomplete medium (RPMI-Hepes-HCO₃) were added to the parasite pellet followed by incubation at 25°C for 8 minutes with intermittent shaking. The reaction was stopped by adding 5 volumes of ice-cold incomplete medium, followed by centrifugation at 4000 rpm for 12 minutes. The parasite pellet was carefully washed with 1xPBS. Giemsa stained smears were made to assess the quality of the preparation. For all experiments involving erythrocyte free parasites, 40 ml of trophozoite rich *P. falciparum* culture at 9-10% parasitemia was lysed resulting in 60-80 µl of free parasites.

6.2.3 Separation of infected erythrocytes from uninfected erythrocytes using percoll gradient centrifugation

Red cells harboring different stages (ring, trophozoite and schizonts) of the parasite have different densities. The younger the parasite the greater is the density with uninfected cells having the highest density. Percoll, a colloidal silica medium coated with polyvinylpyrrolidone, was used for isolating trophozoite infected erythrocytes from in vitro *P. falciparum* culture. Nine parts of percoll (density 1.13 g/ml) were mixed with 1 part of 10xPBS (pH 7.4) to make a stock solution. From this stock solution the desired percentage of percoll was made by diluting with 1xPBS and the solution was filtered through a 0.45 µm filter. The culture with an initial parasitemia of 9-10% was harvested into a Falcon tube, centrifuged at 1300 rpm for 10 minutes and the medium discarded. The pellet was resuspended in incomplete medium to make a 10% suspension. The suspension was overlaid onto equal volume of 70% percoll and centrifuged at 1800 rpm for 20 minutes at room temperature. The trophozoites and schizonts at the interface were recovered and washed four times with incomplete medium to give a 90% enrichment of the late stages. Giemsa stained smears were examined to assess the quality of the preparation.

6.2.4 Antiplasmodial activity and IC₅₀ determination

The IC₅₀ values of compounds for inhibition of parasite growth in in vitro culture, were determined using previously reported methods (Desjardins *et al.*, 1979). Hadacidin, an aspartic acid analog was serially diluted 2-fold over the concentration range 10 mM to 4.88 µM. Each well contained 250 µl of the cell suspension at 2% parasitemia and 2% hematocrit. The plates were incubated at 37°C in a candle jar. After 24 hours, each well was pulsed with 10 µl PBS containing 1.0 µCi of [³H]-hypoxanthine, followed by incubation for another 12 hours. The contents of each well were then harvested onto glass fiber filters using a Combi-12 automated cell harvester, washed extensively with distilled water and dried. The radioactivity incorporated into the parasite nucleic acid pool was measured as disintegrations per minute using a Wallac 1409 liquid scintillation counter. Each experiment was repeated at least thrice in duplicate. For drug treated cultures, percent radioactivity

incorporated with respect to the control was plotted against the logarithm of the drug concentration. The concentration causing 50% inhibition of radioisotope incorporation (IC_{50}) was determined by interpolation. A parallel experiment by microscopy, using Giemsa-stained smears, was also conducted. All experiments incorporated three kinds of controls. These were, a) parasitized erythrocytes not treated with the drug, b) parasitized erythrocytes treated with the solvent in which the drug was dissolved and c) non-parasitized erythrocytes incubated with [3H]-hypoxanthine. The drug solvent did not significantly affect the [3H]-hypoxanthine incorporation in the parasites and the counts in non-parasitized erythrocytes were very low.

The antiplasmodial effect of hadacidin on percoll enriched parasites was monitored by treating the parasites with 5 mM hadacidin for 12 hours followed by 12 hours of incubation with 1 μ Ci of [3H]-hypoxanthine and on saponin released parasites by treating with 2.5 mM hadacidin for 2 hours followed by incubation with the label for 8 hours. The parasites were harvested and radiolabel incorporated into the nucleic acid pool measured using liquid scintillation counter.

Effect of xanthine oxidase on saponin released and whole parasite cultures (mix of parasitized and non-parasitized erythrocytes) was monitored by measuring [3H]-isoleucine incorporation and microscopy, respectively. In vitro *P. falciparum* culture at 2% hematocrit and 2% parasitemia was incubated with different concentrations of xanthine oxidase in complete media at 37°C for 24, 36 and 48 hours. The parasitemia at the end of each time-point was estimated by counting giemsa stained smears of the control and xanthine oxidase treated cultures. To evaluate the effect of xanthine oxidase on saponin released parasites, the culture medium was pretreated with xanthine oxidase for 3 hours at 37°C. Saponin released parasites were cultured in the xanthine oxidase treated medium for 12 hours in the presence of 3 μ Ci [3H]-isoleucine. The parasites were harvested onto glass fibre filters using a cell harvester. The filters were washed with 1xPBS, followed by 5% TCA to precipitate the proteins. The filters were dried and radioactivity counted.

6.2.5 Hypoxanthine and adenine uptake

Saponin released parasites from 30 ml trophozoite rich culture having 9-10% parasitemia, were resuspended in 800 μ l of culture medium. 100 μ l of this suspension was added to each well in a 96 well plate followed by addition of 1 μ Ci of [3 H]-hypoxanthine or [3 H]-adenine in the presence or absence of 0.5 mM cold adenine and hypoxanthine, respectively. The specific activity of the labels was normalized by adding the cold nucleobase. Uptake was allowed to proceed for one and a half hours after which the cell suspension was transferred into an eppendorf and centrifuged. The pellet was washed thrice with 1xPBS and the cells lysed using distilled water. The solution was completely transferred to 2 ml scintillation fluid containing 9% H₂O₂ and counts measured.

6.2.6 Hadacidin inhibition and adenine supplementation

Saponin released parasites were resuspended in the culture medium and transferred to a 96 well plate with 100 μ l suspension in each well. Parasites were treated with 1.5 mM hadacidin in the presence or absence of 2 mM cold adenine for 2 hours followed by addition of 1 μ Ci of [3 H]-adenine or [3 H]-hypoxanthine to all the wells. After incubation for 8 hours with the label, the contents of each well were harvested onto glass fiber filters using a Combi-12 automated cell harvester, washed extensively with distilled water and dried. The incorporated radioactivity was estimated using liquid scintillation counter. To monitor the effect of increasing concentration of adenine on the viability of hadacidin treated parasites, drug treated parasites were supplemented with 0.1, 0.5, 1 and 2 mM cold adenine and survival assessed by labeled adenine incorporation. All experiments were done in duplicate and repeated atleast thrice. The results obtained were highly reproducible.

6.2.7 Parasite lysate pull down using AMP-affinity beads

Preparation of AMP-affinity beads. The beads were prepared by binding AMP to epoxy-activated Sepharose 6B beads (Amersham Pharmacia, Uppsala, Sweden) (Ikegami *et al.*, 1987). 0.5 g of beads were swollen in distilled water for 6 hours followed by extensive washes with distilled water and 0.1 N NaOH. The beads were

mixed with 1 mmole AMP in 2.5 ml of 0.1 N NaOH and the pH adjusted to 11.5. This was followed by the incubation of the beads at 37°C for 4 days with gentle shaking, after which the supernatant was discarded and the beads washed with water. The unreacted epoxy groups on the beads were blocked by incubation with 1 M ethanolamine for 2 hours at 41°C. The beads were again washed with water followed by 3-4 alternate washes with 0.1 M Tris HCl, pH 8.0 and 0.1 M sodium acetate, pH 4.0. The AMP-affinity beads were stored in 20% alcohol at 4°C till further use.

Parasite lysate pull down. About 100 µl of saponin released free parasites, were resuspended in 500 µl lysis buffer containing 10 mM Tris HCl, pH 7.4, 10 µM PMSF, 10 µM Pepstatin A and 0.025 mg E-64. The cells were lysed by sonication using a microprobe followed by centrifugation at 13,000 rpm for 10 minutes. The supernatant was incubated with AMP affinity beads pre-equilibrated with 10 mM Tris HCl, pH 7.4, for 8 hours at 4°C. The beads were then washed with 10 mM Tris HCl, pH 7.4, boiled with SDS sample buffer, centrifuged and the supernatant loaded on a 12% SDS-PAGE. Assuming 5% RBC contamination in the saponin pellets, 5-10 µl packed erythrocytes were lysed and treated in a similar manner and loaded on the gel. The gel was silver stained, bands excised and subjected to in-gel tryptic digestion followed by MALDI mass spectrometric analysis.

6.3 Results

Parasites in in vitro culture grow in a milieu that is rich in human erythrocytes, which includes both infected and uninfected erythrocytes (whole culture). Thus, the metabolic flux in the parasite is influenced by pathways and processes operating in the erythrocyte in which it resides and also by the surrounding uninfected erythrocytes. To study the parasite metabolism in isolation most of the experiments discussed below were done on saponin released erythrocyte free parasites. The saponin preparations were >95-97% pure and free of intact erythrocytes as judged by microscopic examination of the Giemsa stained smears (Figure 6.2).

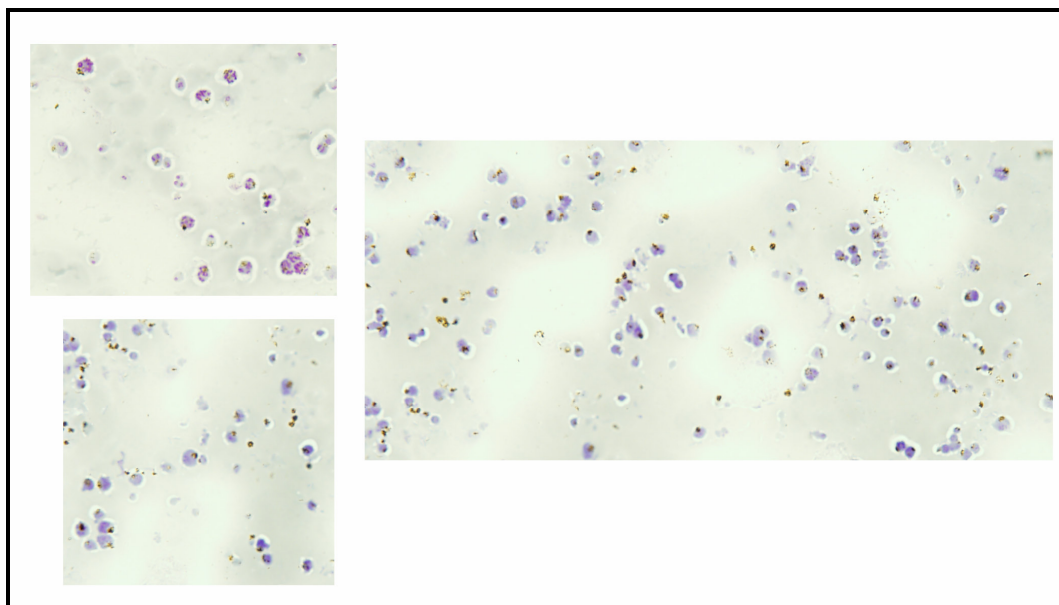


Figure 6.2: Giemsa stained smears of saponin released parasites. The preparations were >95% pure and lacked intact erythrocyte contamination.

6.3.1 Effect of hadacidin and xanthine oxidase on parasite growth

Hadacidin and xanthine oxidase are known inhibitors of parasite growth in culture (Webster *et al.*, 1984; Berman *et al.*, 1991). We examined the effect of hadacidin and xanthine oxidase on whole culture, percoll enriched and saponin released parasites. Hadacidin showed potent antiplasmodial activity (Figure 6.3). While the control cultures showed high ability to incorporate [³H]-hypoxanthine into the nucleic acid pool, the incorporation was markedly impaired in the presence of hadacidin. Almost complete inhibition of growth was observed in percoll enriched and saponin released parasites treated with 5 and 2.5 mM concentration of hadacidin, respectively (Figure 6.3 b,c). Hadacidin exhibited an IC₅₀ value of 133 μM in whole parasite culture (Figure 6.4).

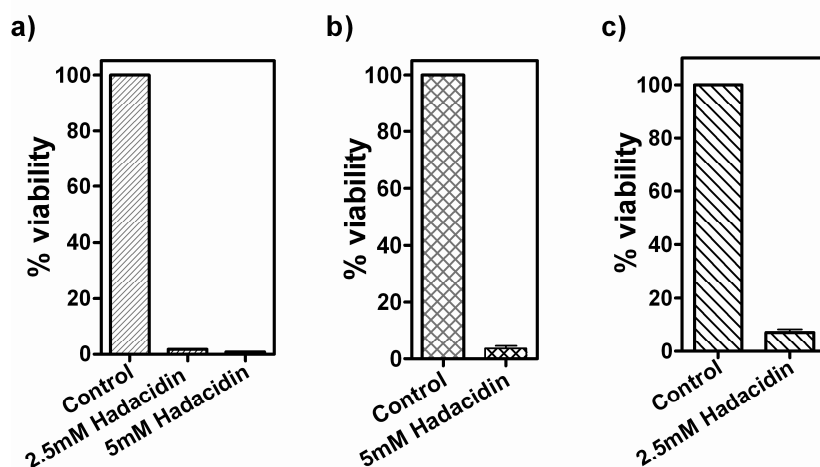


Figure 6.3: Effect of hadacidin on a) whole culture, b) percoll enriched and c) saponin released free parasites. Parasite viability was assessed by [^3H]-hypoxanthine incorporation. Label incorporation in the control cultures was taken as 100%. All experiments were done in duplicate and repeated thrice.

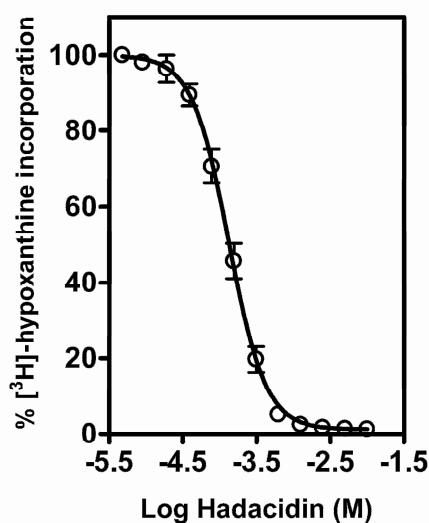


Figure 6.4: Effect of hadacidin on [^3H]-hypoxanthine incorporation by parasitized erythrocytes in culture. The culture was treated with hadacidin for 24 hours, followed by the addition of 1 μCi [^3H]-hypoxanthine to each well. The cells were harvested after another 12 hours and [^3H]-hypoxanthine incorporated in the nucleotide pool estimated by scintillation counting. The graph represents mean of two independent experiments each done in duplicate.

Xanthine oxidase also showed high in vitro toxicity against *P. falciparum*. About 65% inhibition of parasite growth was seen after 24 hours of treatment with 20 mU/ml of xanthine oxidase, with the inhibition being 90% at the end of 36 hours. Parasite growth was completely abolished within 36 hours of treatment with 40 mU/ml xanthine oxidase (Figure 6.5a). In addition, xanthine oxidase treated parasites showed morphological abnormalities as well as developmental arrest. The experiment was started with a culture in which about 75% erythrocytes were infected with trophozoites. After 24 hours, when the control culture showed predominant ring stages, 20 mU/ml xanthine oxidase treated culture showed reduced parasitemia as well as a large proportion of trophozoite and schizonts which were pyknotic. Unlike healthy schizonts which fragment to form 10-20 daughter cells, the schizonts in xanthine oxidase treated cultures failed to show clear fragmentation of the nucleus (Figure 6.6). Xanthine oxidase had a more potent effect on saponin released parasites with complete inhibition of growth seen at 5 mU/ml xanthine oxidase as monitored by [^3H]-isoleucine incorporation (Figure 6.5b).

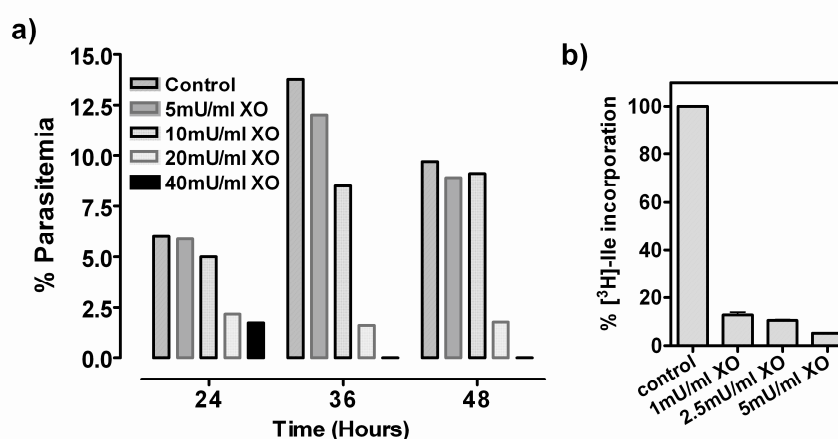


Figure 6.5: Effect of xanthine oxidase treatment on a) whole culture monitored by microscopy and b) saponin released parasites monitored by [^3H]-Ile incorporation. The counts in control cultures were taken as 100%.

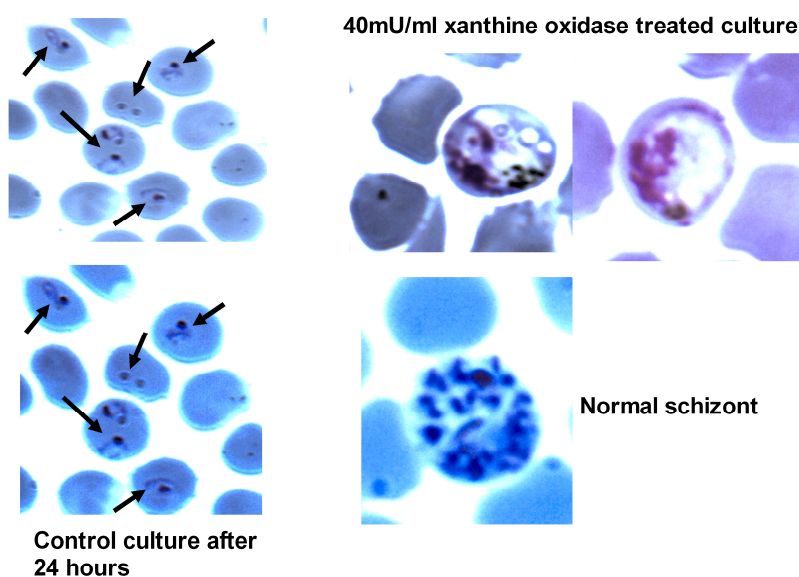


Figure 6.6: Morphological abnormalities and delayed growth in xanthine oxidase treated culture. The experiment was initiated on a trophozoite rich culture. 24 hours post-treatment, control culture showed healthy parasites in the ring stage, whereas xanthine oxidase treated culture showed unhealthy trophozoites and schizonts with a few rings.

6.3.2 Adenine uptake and incorporation in *P. falciparum*

To monitor the uptake of adenine and hypoxanthine, saponin released erythrocyte free parasites were incubated with the labeled nucleobase for 90 minutes, after which the cells were lysed and the total counts in the lysate measured. Saponin released free parasites showed efficient uptake of both adenine as well as hypoxanthine. While the uptake of hypoxanthine was not significantly altered in the presence of 0.5 mM cold adenine, a 9 fold drop in uptake of adenine was evident when the uptake was measured in the presence of 0.5 mM cold hypoxanthine (Figure 6.7).

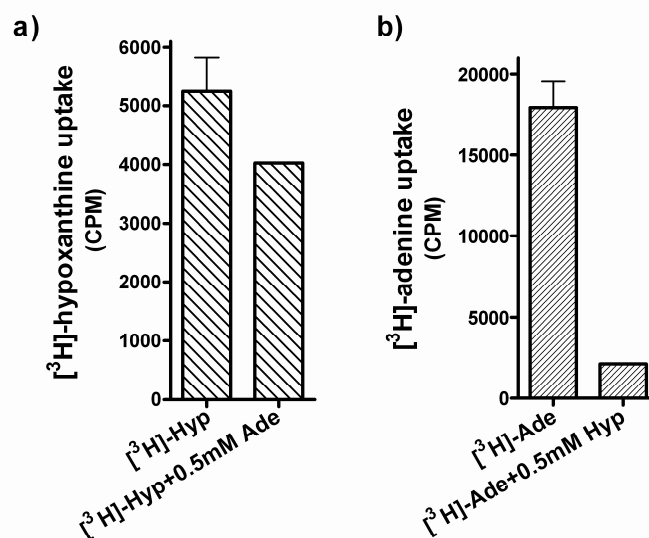


Figure 6.7: Uptake of 5 μM labeled a) hypoxanthine, and b) adenine by saponin released parasites measured over a 90 minute time course in the presence and absence of 500 μM cold adenine and hypoxanthine, respectively. The data set is an average of three independent experiments each done in duplicate.

To check if the adenine taken up by the parasite was metabolized in the cell, the incorporation of adenine into the nucleotide pool of the parasite was examined on whole culture and saponin released parasites. Parasitized erythrocytes were incubated with 0.2, 1.0 and 2.0 μCi of $[^3\text{H}]$ -adenine and the amount of label incorporated in the nucleotide pool assessed after 24 hours. Unlike in uptake experiments where the labeling time was reduced and the entire culture was lysed and counts taken, in the incorporation studies the culture was incubated for longer time periods with the label, passed through glass fiber filter discs that bind only nucleotides and the counts estimated. There was an increase in counts associated with the nucleotide pool of the parasite with increase in labeled adenine (Figure 6.8a). This observation however, did not implicate the role of parasite encoded enzymes in adenine metabolism. To evaluate this, the incorporation was followed in saponin released erythrocyte-free parasites which were incubated with 1 μCi of $[^3\text{H}]$ -adenine for 10 hours. Incorporation of the label in the nucleotide pool of the free parasites implicated the ability of parasite enzymes to metabolize adenine (Figure 6.8b).

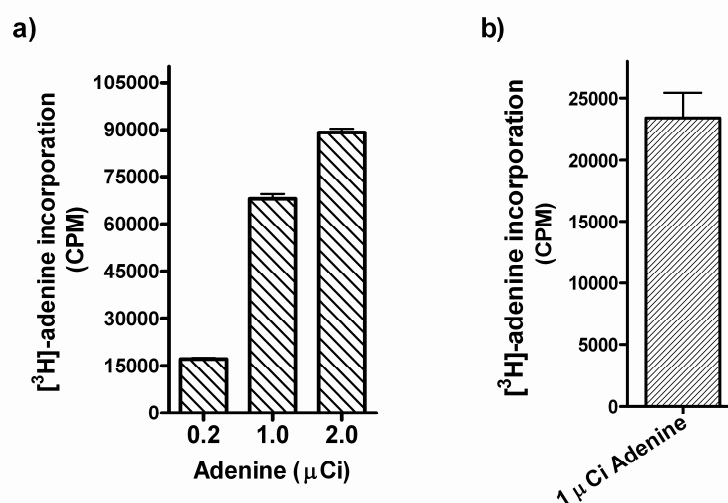


Figure 6.8: Adenine incorporation in a) whole culture and b) saponin released parasites. Each data set is an average of three independent experiments each done in duplicate.

6.3.3 Route of adenine metabolism

There are two possible routes for adenine incorporation in the nucleotide pool of saponin released parasites. First, adenine could be directly converted to AMP by the action of APRT and second, adenine could be converted to hypoxanthine by the enzyme adenine deaminase which would then form AMP via the enzymes HGPRT, AdSS and ASL. Inhibition of AdSS by hadacidin blocks AMP formation in the parasite showing that this is the only known route for AMP production in the parasite (Webster *et al.*, 1984). Thus, hadacidin at 1.5 mM concentration was used to inhibit AdSS in erythrocyte free parasites. To examine if adenine could supplement growth of hadacidin treated parasites, hadacidin treatment was done in the presence of 2 mM cold adenine. After 2 hours, 1 μCi of the appropriate label was added to all the wells. In contrast to hadacidin treated cultures which showed only 12-13% viability at the end of 10 hours, cultures treated with hadacidin in the presence of 2 mM cold adenine showed 35-40% viability. The 25-30% increase in viability of hadacidin treated parasites in the presence of adenine indicates that adenine was able to supplement growth of hadacidin treated saponin released parasites (Figure 6.9a). In the above experiment, the antiparasitic effect of hadacidin was monitored using [³H]-

hypoxanthine, whereas growth supplementation was assessed using [^3H]-adenine. To rule out the possibility of variation between incorporation of labeled adenine and hypoxanthine, the experiment was repeated using [^3H]-adenine alone as reporter for parasite viability. Similar results were obtained, with the presence of adenine resulting in about 30% supplementation of growth in hadacidin treated saponin released parasites.

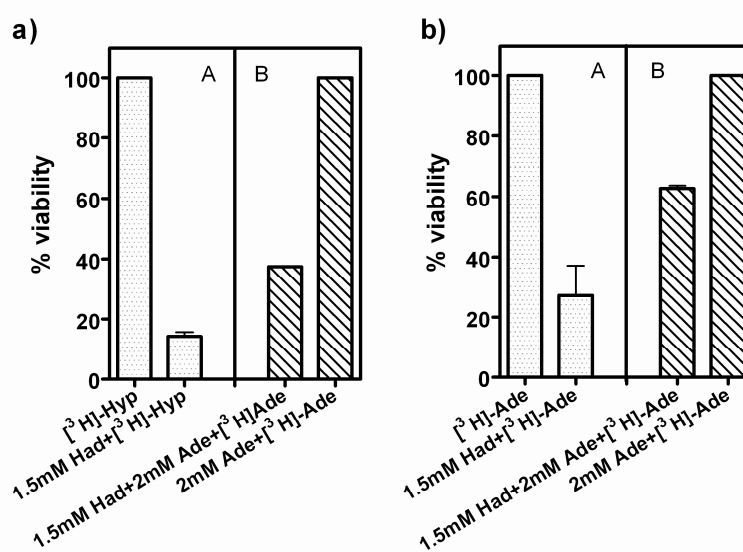


Figure 6.9: Rescue of hadacidin treated saponin released parasites by 2 mM adenine in complete media (RPMI+serum). a) [^3H]-hypoxanthine was used to monitor death and [^3H]-adenine was used to monitor supplementation of growth by adenine, whereas in b) [^3H]-adenine was used to monitor both death and growth supplementation. In both panels, the difference between the two bars in column A, represents the % loss of viability in hadacidin treated parasites and the difference between the two bars in column B, denotes the % loss in viability of hadacidin treated parasites in the presence of 2 mM adenine. A difference of these two numbers gives the increase in viability of the hadacidin treated parasites in the presence of 2 mM adenine. The result was reproducible over five independent experiments each done in duplicate.

Uptake experiments had shown that presence of hypoxanthine significantly reduced adenine uptake (Figure 6.7). Hence, the above experiment was repeated in incomplete media (RPMI-serum) supplemented with glucose. This resulted in an increase in viability of hadacidin treated parasites from 30 to about 50% (Figure 6.10) further indicating that presence of hypoxanthine interferes with adenine uptake by the

parasites. The supplementation of growth of hadacidin treated cultures increased with increase in concentration of adenine (Figure 6.11). However, it was not possible to supplement more than 2 mM adenine due to limited solubility of the base in RPMI.

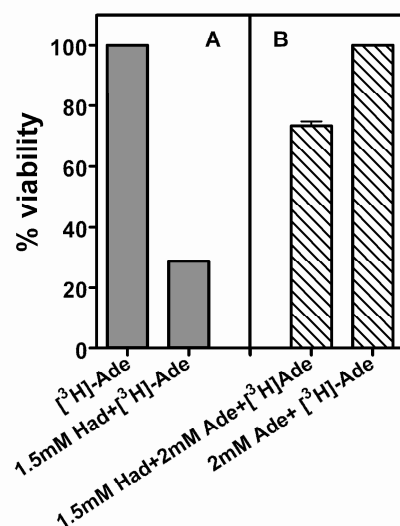


Figure 6.10: Supplementation of growth of hadacidin treated parasites by 2 mM adenine monitored by [³H]-adenine incorporation in incomplete media (RPMI-serum). The difference between the two bars in column A, represents the % loss of viability in hadacidin treated parasites and the difference between the two bars in column B, denotes the % loss in viability of hadacidin treated parasites in the presence of 2 mM adenine. A net difference between the two numbers gives an estimate of adenine's effect in promoting the growth of hadacidin treated parasites. The result was reproducible over five independent experiments each done in duplicate.

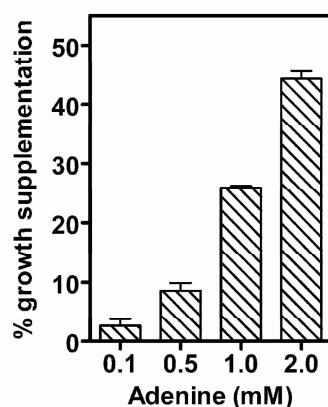


Figure 6.11: Effect of increasing adenine concentration on the growth of 1.5 mM hadacidin treated saponin released parasites in incomplete media supplemented with glucose. The viability of the parasites was assessed by monitoring the incorporation of [³H]-adenine. The data is an average of two independent experiments done in duplicate.

6.3.4 AMP-affinity pull down of *P. falciparum* lysate

The AMP-affinity beads were prepared in the laboratory as described in Section 6.2.7. The efficiency of the beads was evaluated using purified recombinant *P. falciparum* adenylosuccinate lyase (available in the laboratory) which uses AMP as substrate. The parasite lysate was incubated with the AMP-affinity beads for 8 hours, after which the beads were washed and boiled with SDS sample loading buffer. The samples were run on a 12% SDS-PAGE and the gel silver stained. When compared to RBC control treated in a similar manner, several new bands were evident in the parasite lysate pull down samples in the molecular mass range 30-66 kDa. A band at about 18 kDa was consistently observed on repeating the experiment 4-6 times (Figure 6.12). This corresponded to the molecular weight reported for the parasite APRT by Queen *et al.* (Queen *et al.*, 1989). With an aim to identify the proteins binding to the AMP-affinity beads, the bands were excised and an in-gel trypsin digestion was done followed by MALDI mass spectrometry. However, due to poor yield of the proteins, good quality spectra required for protein identification could not be obtained.

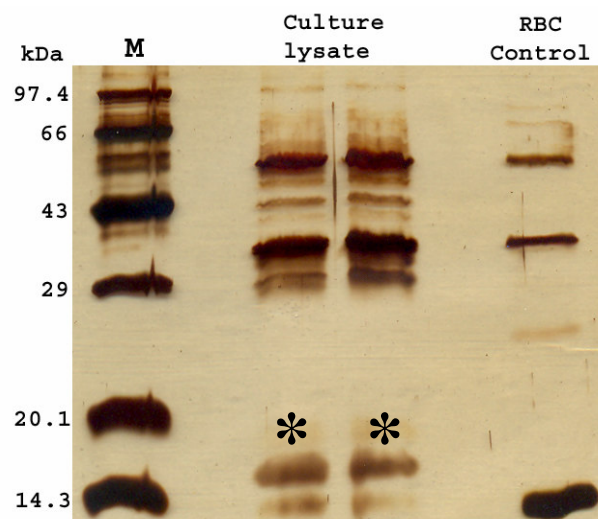


Figure 6.12: Silver stained SDS-PAGE of the AMP-affinity pull down samples. The beads were boiled with SDS-sample buffer and loaded on a 12% polyacrylamide gel. The two stars in black show the 18 kDa band pulled down from the parasite lysate.

6.4 Discussion

One distinctive feature of the biochemistry of parasitic protozoa is their absolute requirement for salvage of preformed purines or their precursors from the host (Sherman, 1979). These nutrients are imported from the host either as nucleobases or nucleosides. The primary step in the salvage pathway is the uptake of the purine precursors from the host milieu using transporters located in the parasite plasma membrane. Hypoxanthine, a nucleobase, serves as the major source of the essential purine groups in the intraerythrocytic malarial parasite. The involvement of enzymes like adenosine kinase and APRT for AMP synthesis has not been implicated in *Plasmodium falciparum*. Our studies also show that the flux through the HGPRT pathway is absolutely essential for parasite survival. Hadacidin or xanthine oxidase that block this pathway completely abolish parasite growth. However, we observed that adenine supplementation of hadacidin treated cultures promoted parasite growth, thereby, implicating a possible alternate, new route for AMP synthesis in *P. falciparum*.

P. falciparum relies entirely on the host for precursors that can be converted to purine nucleotides by enzymes expressed in the parasite. The composition of the purine nucleotides in the erythrocyte is governed by the pathways and enzymes that constitute the purine nucleotide metabolism in the erythrocyte.

6.4.1 Purine metabolism in human erythrocytes

Purine metabolism involves synthesis and degradation of purine nucleotides and in turn regulates the intracellular levels of ATP and GTP. Erythrocytes, like parasitic protozoa, lack *de novo* purine nucleotide biosynthesis pathway. Hence, in erythrocytes, purines are produced by reutilization of existing purine bases (adenine, hypoxanthine and guanine) and nucleosides (adenosine, inosine and guanosine) resulting in the formation of the mononucleotides, IMP, AMP and GMP. The metabolic purpose of these reactions is to introduce these compounds into the high

energy purine nucleotide synthesis pathways (ATP, ADP, GTP, and GDP). Thus purine metabolism involves both salvage and catabolic pathways.

The conversion of purine bases into mononucleotides requires PRPP as a substrate in reactions catalyzed by the phosphoribosyltransferases, APRT and HGPRT. Adenine phosphoribosyltransferase is a non-abundant intracellular enzyme that contributes to the salvage of purine bases by catalyzing the phosphoribosylation of adenine to form AMP. This reaction seems to be the only mechanism through which free adenine is incorporated into its corresponding nucleotide in humans. The polyamine biosynthetic pathway is a basic source of adenine in erythrocytes because the erythrocyte PNP is unable to use adenosine as a substrate. The erythrocyte expresses methylthioadenosine phosphorylase (MTAP) which converts methylthioadenosine to adenine and 5-methylthioribose-1-phosphate (Sahota *et al.*, 1983). The erythrocyte APRT has been purified and characterized (Srivastava & Beutler, 1971; Holden *et al.*, 1979; Wilson *et al.*, 1986).

Nucleosides are also the source of purine nucleotides in the erythrocyte. Adenosine kinase catalyzes the phosphorylation of adenosine to AMP using ATP or GTP as substrates. Thus, adenine nucleotides in the erythrocyte can be synthesized by both APRT and adenosine kinase pathway. Similarly, inosine and guanosine can be converted to IMP and GMP by inosine kinase and guanosine kinase, respectively. IMP can be formed from hypoxanthine by HGPRT. HGPRT from human erythrocyte has been characterized (Muensch & Yoshida, 1977; Zannis *et al.*, 1980; Wilson *et al.*, 1982). In mature erythrocytes, IMP is not a source for AMP, as adenylosuccinate synthetase activity is lacking (Simmonds *et al.*, 1989). AMP produced in erythrocytes is phosphorylated to ADP in a reaction catalyzed by adenylate kinase. The resynthesis of ATP from ADP takes place in substrate phosphorylation reactions involving the enzymes phosphoglycerate kinase and pyruvate kinase and these reactions are the only source of ATP in erythrocytes.

The catabolic pathway may begin with mononucleotide dephosphorylation leading to the formation of nucleosides. These reactions are catalyzed by enzymes known as 5'-nucleotidases (5'-NT). AMP specific 5'-NT (cN-I) and IMP and GMP specific nucleotidase, cN-II, from the erythrocyte have been characterized (Bontemps

et al., 1986; Bontemps *et al.*, 1988; Van den Berghe *et al.*, 1988; Oka *et al.*, 1994; Van den Berghe & Bontemps, 1990). Adenosine is rapidly catabolized to inosine and hypoxanthine through the enzymes, adenosine deaminase and purine nucleoside phosphorylase (Dudzinska *et al.*, 2006). AMP can also be deaminated to form IMP by the enzyme AMP deaminase, which is then dephosphorylated to form inosine. Several of the erythrocyte enzymes involved in the catabolic pathway have also been well characterized (Yun & Suelter, 1978; Ogasawara *et al.*, 1982; Van Heukelom *et al.*, 1976; Zannis *et al.*, 1978). Erythrocyte PNP is more active than adenosine deaminase, hence all inosine gets channeled into hypoxanthine. Thus hypoxanthine is the final products of purine nucleotide metabolism.

In humans, the average concentration of nucleoside and nucleobase is generally in the range of 0.4-6 μM . However, among the purines, hypoxanthine and inosine concentrations are significantly higher (172 and 168 μM , respectively). The intracellular concentrations of bases and nucleosides are generally higher than in the extracellular fluid. Exceptions to this are adenine and adenosine, indicating that adenine nucleotides are readily metabolized so that their precursors do not accumulate in the cell. The most significant intracellular accumulation occurs for guanine, hypoxanthine and inosine (Traut, 1994). Adenine, adenosine and hypoxanthine concentrations in human erythrocyte are 0.3, 0.6 and 8.2 $\mu\text{mol/l}$ of cells, respectively (Werner *et al.*, 1987). It has been demonstrated that *P. berghei* infected erythrocytes possess higher hypoxanthine, adenine and adenosine levels (Werner *et al.*, 1990).

Despite the presence of two adenine transporters, a high affinity and another low affinity/high-capacity, the importance of adenine salvage for *P. falciparum* is unknown (Quashie *et al.*, 2008). Feeble APRT activity has been shown in parasite lysates with the annotation of a gene encoding this activity missing in the Plasmodium genome database (Chaudhary *et al.*, 2004; Ting *et al.*, 2005). Recent reports also implicate the role of adenine deaminase, which converts adenine to hypoxanthine, in adenine metabolism in the parasite (Hyde, 2007). Here again, an annotation of a gene encoding the enzyme is lacking.

Our studies using hadacidin and adenine implicate the presence of an APRT like activity in the parasite. Adenine deaminase activity, if present in the parasite, would result in the conversion of adenine to hypoxanthine. Formation of AMP from hypoxanthine requires the enzymes HGPRT, AdSS and ASL. Hadacidin inhibits adenylosuccinate synthetase which is the first enzyme that commits IMP to the formation of AMP, and hence inhibiting this enzyme blocks the route for AMP production (Shigeura & Gordon, 1962a; Shigeura & Gordon, 1962b). Therefore, the 50% growth supplementation that we see in hadacidin treated cultures in the presence of 2 mM adenine, may imply a direct adenine to AMP conversion reaction in the parasite. However, it is not clear from this study, whether this activity is due to a separate APRT enzyme or due to an APRT like activity being induced as a secondary function in an enzyme at high adenine concentrations. AMP-affinity pull down of *P. falciparum* culture lysate consistently yielded a protein having a molecular mass of about 18 kDa, which corresponds to the molecular mass of the protein reported to have APRT activity in the parasite (Queen *et al.*, 1989). However, repeated attempts to identify the protein using a mass spectrometry based approach proved futile. Purified recombinant *P. falciparum* HGPRT is unable to utilize adenine as a substrate even at 1.5 mM concentration. The physiological significance of our observation and its implication in parasite biochemistry requires further investigation.

References

1. **Abrahamsen MS, Templeton TJ, Enomoto S, Abrahante JE, Zhu G, Lancto CA, Deng M, Liu C, Widmer G, Tzipori S, Buck GA, Xu P, Bankier AT, Dear PH, Konfortov BA, Spriggs HF, Iyer L, Anantharaman V, Aravind L and Kapur V (2004)** Complete genome sequence of the apicomplexan, *Cryptosporidium parvum*. *Science*. 304(5669):441-5.
2. **Albers E, Bakker BM and Gustafsson L (2002)** Modeling response of glycolysis in *S. cerevisiae* cells harvested at diauxic shift. *Mol Biol Rep.*, 29(1-2):119-23.
3. **Alberty RA (1953)** The Relationship between Michaelis Constants, Maximum Velocities and the Equilibrium Constant for an Enzyme-catalyzed Reaction. *J. Am. Chem. Soc.*, 75(8):1928 – 1932.
4. **Alberty RA (1958)** On the Determination of Rate Constants for Coenzyme Mechanisms *J. Am. Chem. Soc.*, 80(8):1777 – 1782.
5. **Al Safarjalani ON, Naguib FN and El Kouni MH (2003)** Uptake of nitrobenzylthioinosine and purine beta-L-nucleosides by intracellular *Toxoplasma gondii*. *Antimicrob Agents Chemother.*, 47(10):3247-51.
6. **Al-Salabi MI, Wallace LJ, Lüscher A, Mäser P, Candlish D, Rodenko B, Gould MK, Jabeen I, Ajith SN and de Koning HP (2007)** Molecular interactions underlying the unusually high adenosine affinity of a novel *Trypanosoma brucei* nucleoside transporter. *Mol Pharmacol.*, 71(3):921-9.
7. **Arai M and Kuwajima K (2000)** Role of the molten globule state in protein folding. *Adv Protein Chem.*, 53:209-82.
8. **Aronow B, Kaur K, McCartan K and Ullman B (1987)** Two high affinity nucleoside transporters in *Leishmania donovani*. *Mol Biochem Parasitol.*, 22(1):29-37.
9. **Auerbach G, Huber R, Grättinger M, Zaiss K, Schurig H, Jaenicke R and Jacob U (1997)** Closed structure of phosphoglycerate kinase from *Thermotoga maritima* reveals the catalytic mechanism and determinants of thermal stability. *Structure.*, 5(11):1475-83.
10. **Auerbach G, Ostendorp R, Prade L, Korndörfer I, Dams T, Huber R and Jaenicke R (1998)** Lactate dehydrogenase from the hyperthermophilic bacterium *thermotoga maritima*: the crystal structure at 2.1 Å resolution reveals strategies for intrinsic protein stabilization. *Structure.*, 6(6):769-81.
11. **Aune KC and Tanford C (1969)** Thermodynamics of the denaturation of lysozyme by guanidine hydrochloride. II. Dependence on denaturant concentration at 25 degrees. *Biochemistry.*, 8:4586-4590.
12. **Bahadur RP, Chakrabarti P, Rodier F and Janin J (2003)** Dissecting subunit interfaces in homodimeric proteins. *Proteins.*, 53(3):708-19.
13. **Bahl A, Brunk B, Crabtree J, Fraunholz MJ, Gajria B, Grant GR, Ginsburg H, Gupta D, Kissinger JC, Labo P, Li L, Mailman MD, Milgram AJ, Pearson DS, Roos DS, Schug**

References

- J, Stoeckert CJ Jr and Whetzel P (2003)** PlasmoDB: the Plasmodium genome resource. A database integrating experimental and computational data. *Nucleic Acids Res.*, 31(1):212-5.
14. **Barford D (2004)** The role of cysteine residues as redox-sensitive regulatory switches. *Curr Opin Struct Biol.*, 14(6):679-86.
 15. **Barnett ME and Zolkiewski M (2002)** Site-directed mutagenesis of conserved charged amino acid residues in ClpB from *Escherichia coli*. *Biochemistry.*, 41(37):11277-83.
 16. **Bass MB, Fromm HJ and Rudolph FB (1984)** The mechanism of the adenylosuccinate synthetase reaction as studied by positional isotope exchange. *J Biol Chem.* 259(20):12330-3.
 17. **Benjwal S, Verma S, Rohm KH, and Gursky O (2006)** Monitoring protein aggregation during thermal unfolding in circular dichroism experiments. *Protein Sci.*, 15:635-639.
 18. **Benkovic SJ and Hammes-Schiffer S (2003)** A perspective on enzyme catalysis. *Science.* 301(5637):1196-202.
 19. **Berman PA, Human L and Freese JA (1991)** Xanthine oxidase inhibits growth of *Plasmodium falciparum* in human erythrocytes in vitro. *J Clin Invest.*, 88(6):1848-55.
 20. **Berman PA and Human L (1990)** Regulation of 5-phosphoribosyl 1-pyrophosphate and of hypoxanthine uptake and release in human erythrocytes by oxypurine cycling. *J Biol Chem.*, 265(12):6562-8.
 21. **Berman PA, Human L and Freese JA (1991)** Xanthine oxidase inhibits growth of *Plasmodium falciparum* in human erythrocytes in vitro. *J Clin Invest.*, 88(6):1848-55
 22. **Bhat JY, Shastri BG and Balaram H (2008)** Kinetic and biochemical characterization of *Plasmodium falciparum* GMP synthetase. *Biochem J.*, 409(1):263-73.
 23. **Bogumil R, Knipp M, Fundel SM and Vasák M (1998)** Characterization of dimethylargininase from bovine brain: evidence for a zinc binding site. *Biochemistry.*, 37(14):4791-8.
 24. **Boitz JM and Ullman B (2006a)** *Leishmania donovani* singly deficient in HGPRT, APRT or XPRT are viable in vitro and within mammalian macrophages. *Mol Biochem Parasitol.*, 148(1):24-30.
 25. **Boitz JM and Ullman B (2006b)** A conditional mutant deficient in hypoxanthine-guanine phosphoribosyltransferase and xanthine phosphoribosyltransferase validates the purine salvage pathway of *Leishmania donovani*. *J Biol Chem.*, 281(23):16084-9
 26. **Bontemps F, Van den Berghe G and Hers HG (1988)** 5'-Nucleotidase activities in human erythrocytes. Identification of a purine 5'-nucleotidase stimulated by ATP and glycerate 2,3-bisphosphate. *Biochem J.*, 250(3):687-96.
 27. **Bourne HR, Sanders DA and McCormick F (1991)** The GTPase superfamily: conserved structure and molecular mechanism. *Nature.*, 349(6305):117-27.
 28. **Bouyoub A, Barbier G, Forterre P and Labedan B (1996)** The adenylosuccinate synthetase from the hyperthermophilic archaeon *Pyrococcus* species displays unusual structural features. *J Mol Biol.*, 261(2):144-54.

29. **Bönisch H, Backmann J, Kath T, Naumann D and Schäfer G (1996)** Adenylate kinase from *Sulfolobus acidocaldarius*: expression in *Escherichia coli* and characterization by Fourier transform infrared spectroscopy. *Arch Biochem Biophys.*, 333(1):75-84.
30. **Bontemps F, Van den Berghe G and Hers HG (1986)** Identification of a purine 5'-nucleotidase in human erythrocytes. *Adv Exp Med Biol.*, 195 Pt B:283-90.
31. **Bonvin J, Aponte RA, Marcantonio M, Singh S, Christendat D, and Turnbull JL (2006)** Biochemical characterization of prephenate dehydrogenase from the hyperthermophilic bacterium *Aquifex aeolicus*. *Protein Sci.*, 15:1417-1432.
32. **Borza T, Iancu CV, Pike E, Honzatko RB and Fromm HJ (2003)** Variations in the response of mouse isozymes of adenylosuccinate synthetase to inhibitors of physiological relevance. *J Biol Chem.*, 278(9):6673-9.
33. **Bradford MM (1976)** A rapid and sensitive method for the quantitation of microgram quantities of protein utilizing the principle of protein-dye binding. *Anal Biochem.*, 72:248-54.
34. **Brinda KV, Kannan N and Vishveshwara S (2002)** Analysis of homodimeric protein interfaces by graph-spectral methods. *Protein Eng.*, 15(4):265-77.
35. **Britton KL, Yip KS, Sedelnikova SE, Stillman TJ, Adams MW, Ma K, Maeder DL, Robb FT, Tolliday N, Vetriani C, Rice DW and Baker PJ (1999)** Structure determination of the glutamate dehydrogenase from the hyperthermophile *Thermococcus litoralis* and its comparison with that from *Pyrococcus furiosus*. *J Mol Biol.*, 293(5):1121-32.
36. **Brock TD. (1967)** Life at high temperatures. Evolutionary, ecological, and biochemical significance of organisms living in hot springs is discussed. *Science*, 158(804):1012-9.
37. **Brown DM, Netting AG, Chun BK, Choi Y, Chu CK and Gero AM (1999)** L-nucleoside analogues as potential antimalarials that selectively target *Plasmodium falciparum* adenosine deaminase. *Nucleosides Nucleotides.*, 18(11-12):2521-32.
38. **Brown JR and Doolittle WF (1995)** Root of the universal tree of life based on ancient aminoacyl-tRNA synthetase gene duplications. *Proc Natl Acad Sci U S A.*, 92(7):2441-5.
39. **Buchholz A, Takors R and Wandrey C (2001)** Quantification of intracellular metabolites in *Escherichia coli* K12 using liquid chromatographic-electrospray ionization tandem mass spectrometric techniques. *Anal Biochem.*, 295(2):129-37.
40. **Bult CJ, White O, Olsen GJ, Zhou L, Fleischmann RD, Sutton GG, Blake JA, FitzGerald LM, Clayton RA, Gocayne JD, Kerlavage AR, Dougherty BA, Tomb JF, Adams MD, Reich CI, Overbeek R, Kirkness EF, Weinstock KG, Merrick JM, Glodek A, Scott JL, Geoghagen NS and Venter JC (1996)** Complete genome sequence of the methanogenic archaeon, *Methanococcus jannaschii*. *Science.*, 273(5278):1058-73.
41. **Burchmore RJ, Wallace LJ, Candlish D, Al-Salabi MI, Beal PR, Barrett MP, Baldwin SA and de Koning HP (2003)** Cloning, heterologous expression, and in situ characterization of the first high affinity nucleobase transporter from a protozoan. *J Biol Chem.*, 278(26):23502-7.
42. **Burmeister WP, Cusack S and Ruigrok RW (1994)** Calcium is needed for the thermostability of influenza B virus neuraminidase. *J Gen Virol.*, 75 (Pt 2):381-8.

References

43. **Cann IK, Kanai S, Toh H and Ishino Y (1998)** Adenylosuccinate synthetase genes: molecular cloning and phylogenetic analysis of a highly conserved archaeal gene. *Syst Appl Microbiol.*, 21(4):478-86.
44. **Carey NH, Mandel HG (1961)** Studies on the inhibition of growth of *Bacillus cereus* by 6-mercaptopurine. *J Biol Chem.*, 236:520-4.
45. **Carter NS and Fairlamb AH (1993)** Arsenical-resistant trypanosomes lack an unusual adenosine transporter. *Nature.*, 361(6408):173-6.
46. **Carter NS, Berger BJ and Fairlamb AH (1995)** Uptake of diamidine drugs by the P2 nucleoside transporter in melarsen-sensitive and -resistant *Trypanosoma brucei brucei*. *J Biol Chem.*, 270(47):28153-7.
47. **Carter NS, Ben Mamoun C, Liu W, Silva EO, Landfear SM, Goldberg DE and Ullman B (2000a)** Isolation and functional characterization of the PfNT1 nucleoside transporter gene from *Plasmodium falciparum*. *J Biol Chem.*, 275(14):10683-91
48. **Carter NS, Drew ME, Sanchez M, Vasudevan G, Landfear SM and Ullman B (2000b)** Cloning of a novel inosine-guanosine transporter gene from *Leishmania donovani* by functional rescue of a transport-deficient mutant. *J Biol Chem.*, 275(27):20935-41
49. **Cha S (1968)** A simple method for derivation of rate equations for enzyme-catalyzed reactions under the rapid equilibrium assumption or combined assumptions of equilibrium and steady state. *J Biol Chem.*, 243(4):820-5.
50. **Chakravarty S and Varadarajan R (2000)** Elucidation of determinants of protein stability through genome sequence analysis. *FEBS Lett.*, 470(1):65-9.
51. **Chan MK, Mukund S, Kletzin A, Adams MW and Rees DC (1995)** Structure of a hyperthermophilic tungstopterin enzyme, aldehyde ferredoxin oxidoreductase. *Science.*, 267(5203):1463-9.
52. **Chaudhary K, Darling JA, Fohl LM, Sullivan WJ Jr, Donald RG, Pfefferkorn ER, Ullman B and Roos DS (2004)** Purine salvage pathways in the apicomplexan parasite *Toxoplasma gondii*. *J Biol Chem.*, 279(30):31221-7.
53. **Chaudhary K, Donald RG, Nishi M, Carter D, Ullman B and Roos DS (2005)** Differential localization of alternatively spliced hypoxanthine-xanthine-guanine phosphoribosyltransferase isoforms in *Toxoplasma gondii*. *J Biol Chem.*, 280(23):22053-9
54. **Chi YI, Martinez-Cruz LA, Jancarik J, Swanson RV, Robertson DE, Kim SH (1999)** Crystal structure of the beta-glycosidase from the hyperthermophile *Thermosphaera aggregans*: insights into its activity and thermostability. *FEBS Lett.*, 445(2-3):375-83.
55. **Chiang CW, Carter N, Sullivan WJ Jr, Donald RG, Roos DS, Naguib FN, el Kouni MH, Ullman B and Wilson CM (1999)** The adenosine transporter of *Toxoplasma gondii*. Identification by insertional mutagenesis, cloning, and recombinant expression. *J Biol Chem.*, 274(49):35255-61
56. **Choe JY, Poland BW, Fromm HJ and Honzatko RB (1999)** Mechanistic implications from crystalline complexes of wild-type and mutant adenylosuccinate synthetases from *Escherichia coli*. *Biochemistry.*, 38(21):6953-61.
57. **Chulay JD, Haynes JD and Diggs CL (1983)** *Plasmodium falciparum*: assessment of in vitro growth by [³H]hypoxanthine incorporation. *Exp Parasitol.*, 55(1):138-46.

58. **Claiborne A, Yeh JI, Mallett TC, Luba J, Crane EJ 3rd, Charrier V and Parsonage D (1999)** Protein-sulfenic acids: diverse roles for an unlikely player in enzyme catalysis and redox regulation. *Biochemistry.*, 38(47):15407-16.
59. **Claiborne A, Mallett TC, Yeh JI, Luba J and Parsonage D (2001)** Structural, redox, and mechanistic parameters for cysteine-sulfenic acid function in catalysis and regulation. *Adv Protein Chem.*, 58:215-76.
60. **Clark AW and Rudolph FB (1976)** Regulation of purine metabolism. Adenylosuccinate synthetase from Novikoff ascites tumor cells. *Biochim Biophys Acta.*, 437(1):87-90
61. **Cleland WW (1979)** Substrate inhibition, *Methods Enzymol.*, 63:500-513.
62. COLLABORATIVE COMPUTATIONAL PROJECT, NUMBER 4. 1994. The CCP4 Suite: Programs for Protein Crystallography. *Acta Cryst. D50*, 760-763
63. **Cooper BF, Fromm HJ and Rudolph FB (1986)** Isotope exchange at equilibrium studies with rat muscle adenylosuccinate synthetase. *Biochemistry.*, 25(23):732-37.
64. **Cross JV and Templeton DJ (2006)** Regulation of signal transduction through protein cysteine oxidation. *Antioxid Redox Signal.*, 8(9-10):1819-27.
65. **Daddona PE, Wiesmann WP, Milhouse W, Chern JW, Townsend LB, Hershfield MS and Webster HK (1986)** Expression of human malaria parasite purine nucleoside phosphorylase in host enzyme-deficient erythrocyte culture. Enzyme characterization and identification of novel inhibitors. *J Biol Chem.*, 261(25):11667-73.
66. **Daniel RM, Cowan DA, Morgan HW and Curran MP (1982)** A correlation between protein thermostability and resistance to proteolysis. *Biochem J.*, 207(3):641-4.
67. **Darling JA, Sullivan WJ Jr, Carter D, Ullman B and Roos DS (1999)** Recombinant expression, purification, and characterization of *Toxoplasma gondii* adenosine kinase. *Mol Biochem Parasitol.*, 103(1):15-23.
68. **Davies MJ, Ross AM and Gutteridge WE (1983)** The enzymes of purine salvage in *Trypanosoma cruzi*, *Trypanosoma brucei* and *Leishmania mexicana*. *Parasitology.*, 87 (Pt 2):211-7.
69. **de Koning HP and Jarvis SM (1997a)** Hypoxanthine uptake through a purine-selective nucleobase transporter in *Trypanosoma brucei* procyclic cells is driven by protonmotive force. *Eur J Biochem.* 247(3):1102-10.
70. **de Koning HP and Jarvis SM (1997b)** Purine nucleobase transport in bloodstream forms of *Trypanosoma brucei* is mediated by two novel transporters. *Mol Biochem Parasitol.*, 89(2):245-58.
71. **de Koning HP and Jarvis SM (1998)** A highly selective, high-affinity transporter for uracil in *Trypanosoma brucei*: evidence for proton-dependent transport. *Biochem Cell Biol.*, 76(5):853-8.
72. **de Koning HP and Jarvis SM (1999)** Adenosine transporters in bloodstream forms of *Trypanosoma brucei*: substrate recognition motifs and affinity for trypanocidal drugs. *Mol Pharmacol.*, 56(6):1162-70.

References

73. **de Koning HP and Jarvis SM (2001)** Uptake of pentamidine in *Trypanosoma brucei brucei* is mediated by the P2 adenosine transporter and at least one novel, unrelated transporter. *Acta Trop.*, 80(3):245-50.
74. **de Koning HP, Al-Salabi MI, Cohen AM, Coombs GH and Wastling JM (2003)** Identification and characterisation of high affinity nucleoside and nucleobase transporters in *Toxoplasma gondii*. *Int J Parasitol.*, 33(8):821-31.
75. **de Koning HP, Bridges DJ and Burchmore RJ (2005)** Purine and pyrimidine transport in pathogenic protozoa: from biology to therapy. *FEMS Microbiol Rev.*, 29(5):987-1020.
76. **DeLano WL.(2002)** The PyMOL Molecular Graphics System .DeLano Scientific, Palo Alto, CA, USA.
77. **den Hertog J, Groen A and van der Wijk T (2005)** Redox regulation of protein-tyrosinephosphatases. *Arch Biochem Biophys.*, 434(1):11-5.
78. **Denu JM and Tanner KG (1998)** Specific and reversible inactivation of protein tyrosine phosphatases by hydrogen peroxide: evidence for a sulfenic acid intermediate and implications for redox regulation. *Biochemistry.*, 37(16):5633-42.
79. **Deppenmeier U, Johann A, Hartsch T, Merkl R, Schmitz RA, Martinez-Arias R, Henne A, Wiezer A, Bäumer S, Jacobi C, Brüggemann H, Lienard T, Christmann A, Bömeke M, Steckel S, Bhattacharyya A, Lykidis A, Overbeek R, Klenk HP, Gunsalus RP, Fritz HJ and Gottschalk G (2002)** The genome of *Methanosarcina mazei*: evidence for lateral gene transfer between bacteria and archaea. *J Mol Microbiol Biotechnol.*, 4(4):453-61.
80. **Desai SA, Krogstad DJ and McCleskey EW (1993)** A nutrient-permeable channel on the intraerythrocytic malaria parasite. *Nature.*, 362(6421):643-6.
81. **Desjardins RE, Canfield CJ, Haynes JD and Chulay JD (1979)** Quantitative assessment of antimalarial activity in vitro by a semiautomated microdilution technique. *Antimicrob Agents Chemother.*, 16(6):710-8.
82. **Dever TE, Glyniadis MJ and Merrick WC (1987)** GTP-binding domain: three consensus sequence elements with distinct spacing. *Proc Natl Acad Sci U S A.*, 84(7):1814-8.
83. **Dixon M.(1953)** The determination of enzyme inhibitor constants. *Biochem J.*, 55(1):170-1.
84. **Donald RG, Carter D, Ullman B and Roos DS (1996)** Insertional tagging, cloning, and expression of the *Toxoplasma gondii* hypoxanthine-xanthine-guanine phosphoribosyltransferase gene. Use as a selectable marker for stable transformation. *J Biol Chem.* 271(24):14010-9.
85. **Dong Q and Fromm HJ (1990)** Chemical modification of adenylosuccinate synthetase from *Escherichia coli* by pyridoxal 5'-phosphate. Identification of an active site lysyl residue. *J Biol Chem.*, 265(11):6235-40.
86. **Dong Q, Liu F, Myers AM and Fromm HJ (1991).** Evidence for an arginine residue at the substrate binding site of *Escherichia coli* adenylosuccinate synthetase as studied by chemical modification and site-directed mutagenesis. *J Biol Chem.*, 266(19):12228-33.
87. **Dong Q, Soans C, Liu F and Fromm HJ (1990)** Identification of different classes of nonessential sulfhydryl groups in *Escherichia coli* adenylosuccinate synthetase. *Arch Biochem Biophys.*, 276(1):77-84.

88. **Downie MJ, Saliba KJ, Bröer S, Howitt SM and Kirk K (2008)** Purine nucleobase transport in the intraerythrocytic malaria parasite. *Int J Parasitol.* 38(2):203-9.
89. **Downie MJ, Saliba KJ, Howitt SM, Bröer S and Kirk K (2006)** Transport of nucleosides across the *Plasmodium falciparum* parasite plasma membrane has characteristics of PfENT1. *Mol Microbiol.*, 60(3):738-48.
90. **Doyle PS, Kanaani J and Wang CC (1998)** Hypoxanthine, guanine, xanthine phosphoribosyltransferase activity in *Cryptosporidium parvum*. *Exp Parasitol.*, 89(1):9-15.
91. **Dudzinska W, Hlynczak AJ, Skotnicka E and Suska M (2006)** The purine metabolism of human erythrocytes. *Biochemistry (Mosc.)*, 71(5):467-75.
92. **Dyann F. Wirth (2002)** The parasite genome: Biological revelations. *Nature.*, 419: 495-496.
93. **Eaazhisai K, Jayalakshmi R, Gayathri P, Anand RP, Sumathy K, Balaram H and Murthy MR (2004)** Crystal structure of fully ligated adenylosuccinate synthetase from *Plasmodium falciparum*. *J Mol Biol.*, 335(5):1251-64.
94. **Eaton P (2006)** Protein thiol oxidation in health and disease: techniques for measuring disulfides and related modifications in complex protein mixtures. *Free Radic Biol Med.* 40(11):1889-99.
95. **Eggers DK and Valentine JS (2001)** Crowding and hydration effects on protein conformation: a study with sol-gel encapsulated proteins. *J Mol Biol.*, 314(4):911-22.
96. **Eisenmesser EZ, Millet O, Labeikovsky W, Korzhnev DM, Wolf-Watz M, Bosco DA, Skalicky JJ, Kay LE and Kern D (2005)** Intrinsic dynamics of an enzyme underlies catalysis. *Nature.*, 438(7064):117-21.
97. **El Bissati K, Zufferey R, Witola WH, Carter NS, Ullman B and Ben Mamoun C (2006)** The plasma membrane permease PfNT1 is essential for purine salvage in the human malaria parasite *Plasmodium falciparum*. *Proc Natl Acad Sci U S A.*, 103(24):9286-91.
98. **Ellis HR and Poole LB (1997)** Novel application of 7-chloro-4-nitrobenzo-2-oxa-1,3-diazole to identify cysteine sulfenic acid in the AhpC component of alkyl hydroperoxide reductase. *Biochemistry.*, 36(48):15013-8.
99. **Ellis RJ (2001)** Macromolecular crowding: an important but neglected aspect of the intracellular environment. *Curr Opin Struct Biol.*, 11(1):114-9.
100. **Englander SW (2000)** Protein folding intermediates and pathways studied by hydrogen exchange. *Annu. Rev. Biophys. Biomol. Struct.*, 29:213-238.
101. **Facchiano AM, Colonna G and Ragone R (1998)** Helix stabilizing factors and stabilization of thermophilic proteins: an X-ray based study. *Protein Eng.*, 11(9):753-60.
102. **Fairlamb AH (1989)** Novel biochemical pathways in parasitic protozoa. *Parasitology.*, 99 Suppl:S93-112.
103. **Fields PA (2001)** Review: Protein function at thermal extremes: balancing stability and flexibility. *Comp Biochem Physiol A Mol Integr Physiol.*, 129(2-3):417-31.
104. **Fonné-Pfister R, Chemla P, Ward E, Girardet M, Kreuz KE, Honzatko RB, Fromm HJ, Schär HP, Grütter MG and Cowan-Jacob SW (1996)** The mode of action and the structure

References

- of a herbicide in complex with its target: binding of activated hydantocidin to the feedback regulation site of adenylosuccinate synthetase. *Proc Natl Acad Sci U S A.*, 93(18):9431-6
105. **Frieden C (1959)** Glutamic dehydrogenase. III. The order of substrate addition in the enzymatic reaction. *J Biol Chem.*, 234:2891-6.
 106. **Fromm HJ (1967)** The use of competitive inhibitors in studying the mechanism of action of some enzyme systems utilizing three substrates. *Biochim Biophys Acta.*, 139(2):221-30.
 107. **Fromm HJ, Nelson DR (1962)** Ribitol dehydrogenase. III. Kinetic studies with product inhibition. *J Biol Chem.*, 237:215-20.
 108. **Fuangthong M and Helmann JD (2002)** The OhrR repressor senses organic hydroperoxides by reversible formation of a cysteine-sulfenic acid derivative. *Proc Natl Acad Sci U S A.*, 99(10):6690-5.
 109. **Fujii T, Hata Y, Oozeki M, Moriyama H, Wakagi T, Tanaka N and Oshima T (1997)** The crystal structure of zinc-containing ferredoxin from the thermoacidophilic archaeon *Sulfolobus* sp. strain 7. *Biochemistry.*, 36(6):1505-13.
 110. **Galazka J, Striepen B and Ullman B (2006)** Adenosine kinase from *Cryptosporidium parvum*. *Mol Biochem Parasitol.*, 149(2):223-30.
 111. **Gallant J, Irr J and Cashel M (1971)** The mechanism of amino acid control of guanylate and adenylate biosynthesis. *J Biol Chem.*, 246(18):5812-6.
 112. **Garbers DL, Hardman JG and Rudolph FB (1974)** Kinetic analysis of sea urchin sperm guanylate cyclase. *Biochemistry.*, 13:4166-4171.
 113. **Geary TG, Divo AA and Jensen JB (1983)** An in vitro assay system for the identification of potential antimalarial drugs. *J Parasitol.*, 69(3):577-83.
 114. **Georlette D, Damien B, Blaise V, Depiereux E, Uversky VN, Gerday C and Feller G (2003)** Structural and functional adaptations to extreme temperatures in psychrophilic, mesophilic, and thermophilic DNA ligases. *J Biol Chem.*, 278(39):37015-23.
 115. **Giles NM, Giles GI and Jacob C (2003a)** Multiple roles of cysteine in biocatalysis. *Biochem Biophys Res Commun.*, 300(1):1-4.
 116. **Giles NM, Watts AB, Giles GI, Fry FH, Littlechild JA and Jacob C (2003b)** Metal and redox modulation of cysteine protein function. *Chem Biol.*, 10(8):677-93.
 117. **Gogarten JP, Kibak H, Dittrich P, Taiz L, Bowman EJ, Bowman BJ, Manolson MF, Poole RJ, Date T and Oshima T, et al. (1989)** Evolution of the vacuolar H⁺-ATPase: implications for the origin of eukaryotes. *Proc Natl Acad Sci U S A.*, 86(17):6661-5.
 118. **Gorrell A, Wang W, Underbakke E, Hou Z, Honzatko RB, Fromm HJ (2002)** Determinants of L-aspartate and IMP recognition in *Escherichia coli* adenylosuccinate synthetase. *J Biol Chem.*, 277(11):8817-21.
 119. **Gouet P, Courcelle E, Stuart DI and Metz F (1999)** ESPript: multiple sequence alignments in PostScript. *Bioinformatics.*, 15:305-8.
 120. **Grabarse W, Vaupel M, Vorholt JA, Shima S, Thauer RK, Wittershagen A, Bourenkov G, Bartunik HD and Ermler U (1999)** The crystal structure of

- methenyltetrahydromethanopterin cyclohydrolase from the hyperthermophilic archaeon *Methanopyrus kandleri*. *Structure.*, 7(10):1257-68.
121. **Graf PC, Martinez-Yamout M, VanHaerents S, Lilie H, Dyson HJ and Jakob U (2004)** Activation of the redox-regulated chaperone Hsp33 by domain unfolding. *J Biol Chem.*, 279(19):20529-38.
 122. **Gray GR and Barker R (1970)** Studies on the substrates of D-fructose 1,6-diphosphate aldolase in solution. *Biochemistry.*, 9:2454-2462.
 123. **Gu Z, Kaul M, Yan B, Kridel SJ, Cui J, Strongin A, Smith JW, Liddington RC and Lipton SA (2002)** S-nitrosylation of matrix metalloproteinases: signaling pathway to neuronal cell death. *Science.*, 297(5584):1186-90.
 124. **Hammes-Schiffer S and Benkovic SJ (2006)** Relating protein motion to catalysis. *Annu Rev Biochem.*, 75:519-41.
 125. **Hampton A and Chu SY (1970)** Specific binding to adenylosuccinate synthetase of analogs of inosinic acid with nitrogen, sulfur, and carbon substituted for phosphate oxygens. *Biochim Biophys Acta.*, 198(3):594-600.
 126. **Haney P, Konisky J, Koretke KK, Luthey-Schulten Z and Wolynes PG (1997)** Structural basis for thermostability and identification of potential active site residues for adenylate kinases from the archaeal genus *Methanococcus*. *Proteins.*, 28(1):117-30.
 127. **Haney PJ, Badger JH, Buldak GL, Reich CI, Woese CR and Olsen GJ (1999)** Thermal adaptation analyzed by comparison of protein sequences from mesophilic and extremely thermophilic *Methanococcus* species. *Proc Natl Acad Sci U S A.*, 96(7):3578-83.
 128. **Hashimoto H, Inoue T, Nishioka M, Fujiwara S, Takagi M, Imanaka T and Kai Y (1999)** Hyperthermostable protein structure maintained by intra and inter-helix ion-pairs in archaeal O6-methylguanine-DNA methyltransferase. *J Mol Biol.*, 292(3):707-16.
 129. **He YZ, Fan KQ, Jia CJ, Wang ZJ, Pan WB, Huang L, Yang KQ and Dong ZY (2007)** Characterization of a hyperthermostable Fe-superoxide dismutase from hot spring. *Appl Microbiol Biotechnol.*, 75(2):367-76.
 130. **Hennig M, Darimont B, Sterner R, Kirschner K and Jansonius JN (1995)** 2.0 Å structure of indole-3-glycerol phosphate synthase from the hyperthermophile *Sulfolobus solfataricus*: possible determinants of protein stability. *Structure.*, 3(12):1295-306.
 131. **Hennig M, Sterner R, Kirschner K and Jansonius JN (1997)** Crystal structure at 2.0 Å resolution of phosphoribosyl anthranilate isomerase from the hyperthermophile *Thermotoga maritima*: possible determinants of protein stability. *Biochemistry.*, 36(20):6009-16.
 132. **Hess D, Krüger K, Knappik A, Palm P and Hensel R (1995)** Dimeric 3-phosphoglycerate kinases from hyperthermophilic Archaea. Cloning, sequencing and expression of the 3-phosphoglycerate kinase gene of *Pyrococcus woesei* in *Escherichia coli* and characterization of the protein. Structural and functional comparison with the 3-phosphoglycerate kinase of *Methanothermus fervidus*. *Eur J Biochem.*, 233(1):227-37.
 133. **Holden JA, Meredith GS and Kelley WN (1979)** Human adenine phosphoribosyltransferase. Affinity purification, subunit structure, amino acid composition, and peptide mapping. *J Biol Chem.*, 254(15):6951-5.

References

134. **Honzatko RB, Stayton MM and Fromm HJ (1999)** Adenylosuccinate synthetase: recent developments. *Adv Enzymol Relat Areas Mol Biol.*, 73:57-102.
135. **Hou Z, Cashel M, Fromm HJ and Honzatko RB (1999)** Effectors of the stringent response target the active site of *Escherichia coli* adenylosuccinate synthetase. *J Biol Chem.*, 274(25):17505-10.
136. **Hou Z, Wang W, Fromm HJ and Honzatko RB (2002)** IMP Alone Organizes the Active Site of Adenylosuccinate Synthetase from *Escherichia coli*. *J Biol Chem.*, 277(8):5970-6.
137. **Housley TJ, Baumann AP, Braun ID, Davis G, Seperack PK and Wilhelm SM (1993)** Recombinant Chinese hamster ovary cell matrix metalloprotease-3 (MMP-3, stromelysin-1). Role of calcium in promatrix metalloprotease-3 (pro-MMP-3, prostromelysin-1) activation and thermostability of the low mass catalytic domain of MMP-3. *J Biol Chem.*, 268(6):4481-7.
138. **Hsiao LL, Howard RJ, Aikawa M and Taraschi TF (1991)** Modification of host cell membrane lipid composition by the intra-erythrocytic human malaria parasite *Plasmodium falciparum*. *Biochem J.*, 274 (Pt 1):121-32.
139. **Hu Z, Ma B, Wolfson H and Nussinov R (2000)** Conservation of polar residues as hot spots at protein interfaces. *Proteins.*, 39(4):331-42.
140. **Huffman JL, Mokashi A, Bächinger HP and Brennan RG (2001)** The basic helix-loop-helix domain of the aryl hydrocarbon receptor nuclear transporter (ARNT) can oligomerize and bind E-box DNA specifically. *J Biol Chem.*, 276(44):40537-44.
141. **Hwang HY and Ullman B (1997)** Genetic analysis of purine metabolism in *Leishmania donovani*. *J Biol Chem.*, 272(31):19488-96.
142. **Hyde JE (2007)** Targeting purine and pyrimidine metabolism in human apicomplexan parasites. *Curr Drug Targets.*, 8(1):31-47.
143. **Iancu CV, Borza T, Choe JY, Fromm HJ and Honzatko RB (2001)** Recombinant mouse muscle adenylosuccinate synthetase: overexpression, kinetics, and crystal structure. *J Biol Chem.*, 276(45):42146-52.
144. **Iancu CV, Borza T, Fromm HJ and Honzatko RB (2002)** IMP, GTP, and 6-phosphoryl-IMP complexes of recombinant mouse muscle adenylosuccinate synthetase.
145. *J Biol Chem.*, 277(30):26779-87.
146. **Iancu CV, Zhou Y, Borza T, Fromm HJ and Honzatko RB (2006)** Cavitation as a mechanism of substrate discrimination by adenylosuccinate synthetases. *Biochemistry.*, 45(38):11703-11.
147. **Imanaka T, Atomi H (2002)** Catalyzing "hot" reactions: enzymes from hyperthermophilic *Archaea*. *Chem Rec.*, 2(3):149-63.
148. **Iovannisci DM, Kaur K, Young L and Ullman B (1984)** Genetic analysis of nucleoside transport in *Leishmania donovani*. *Mol Cell Biol.*, 4(6):1013-9.
149. **Iovannisci DM and Ullman B (1984)** Characterization of a mutant *Leishmania donovani* deficient in adenosine kinase activity. *Mol Biochem Parasitol.*, 12(2):139-51.

150. **Isupov MN, Fleming TM, Dalby AR, Crowhurst GS, Bourne PC and Littlechild JA (1999)** Crystal structure of the glyceraldehyde-3-phosphate dehydrogenase from the hyperthermophilic archaeon *Sulfolobus solfataricus*. *J Mol Biol.*, 291(3):651-60.
151. **Iwabe N, Kuma K, Hasegawa M, Osawa S and Miyata T (1989)** Evolutionary relationship of archaeobacteria, eubacteria, and eukaryotes inferred from phylogenetic trees of duplicated genes. *Proc Natl Acad Sci U S A.*, 86(23):9355-9.
152. **Jaenicke R (1991)** Protein stability and molecular adaptation to extreme conditions. *Eur. J. Biochem.*, 202:715-728.
153. **Jaenicke R and Böhm G (1998)** The stability of proteins in extreme environments. *Curr Opin Struct Biol.*, 8(6):738-48.
154. **Jahngen EG and Rossomando EF (1984)** Adenylosuccinate synthetase from *Dictyostelium discoideum*: effects of hadacidin analogs and binding of [¹⁴C]hadacidin. *Arch Biochem Biophys.*, 229(1):145-54.
155. **Jakob U, Muse W, Eser M and Bardwell JC (1999)** Chaperone activity with a redox switch. *Cell.*, 96(3):341-52.
156. **Jayalakshmi R, Sumathy K and Balaram H (2002)** Purification and characterization of recombinant *Plasmodium falciparum* adenylosuccinate synthetase expressed in *Escherichia coli*. *Protein Expr Purif.*, 25(1):65-72.
157. **Jayalakshmi R (2004)** Structure-function Studies on Successive Purine Salvage Pathway Enzymes-Hypoxanthine Guanine Phosphoribosyltransferase and Adenylosuccinate Synthetase, Ph. D. Thesis. Jawaharlal Nehru Centre for Advanced Scientific Research, Bangalore, India.
158. **Johnson KA (1995)** Rapid quench kinetic analysis of polymerases, adenosinetriphosphates, and enzyme intermediates. *Methods Enzymol.*, 249:38-61.
159. **Jones WJ, Leigh JA, Mayer F, Woese CR, and. Wolfe RS (1983)** *Methanococcus jannaschii* sp. nov., an extremely thermophilic methanogen from a submarine hydrothermal vent. *Arch Microbiol.*, 136:254-261.
160. **Jones S and Thornton JM (1996)** Principles of protein-protein interactions. *Proc Natl Acad Sci U S A.*, 93(1):13-20.
161. **Kaczka EA, Gitterman CO, Dulaney EL and Folkers K (1962)** Hadacidin, a new growth-inhibitory substance in human tumor systems. *Biochemistry.*, 1:340-3.
162. **Kang C, Fromm HJ (1994)** Characterization of the putative GTP-binding site residues of *Escherichia coli* adenylosuccinate synthetase by site-directed mutagenesis. *Arch Biochem Biophys.*, 310(2):475-80.
163. **Kang C and Fromm HJ (1995)** Identification of an essential second metal ion in the reaction mechanism of *Escherichia coli* adenylosuccinate synthetase. *J. Biol. Chem.*, 270:15539-15544.
164. **Kang C, Kim S and Fromm HJ (1996)** Subunit complementation of *Escherichia coli* adenylosuccinate synthetase. *J Biol Chem.*, 271(47):29722-8.

References

165. **Kang C, Sun N, Poland BW, Gorrell A, Honzatko RB and Fromm HJ (1997)** Residues essential for catalysis and stability of the active site of Escherichia coli adenylosuccinate synthetase as revealed by directed mutation and kinetics. *J Biol Chem.*, 272(18):11881-5.
166. **Kang C, Sun N, Honzatko RB and Fromm HJ (1994a)** Replacement of Asp333 with Asn by site-directed mutagenesis changes the substrate specificity of Escherichia coli adenylosuccinate synthetase from guanosine 5'-triphosphate to xanthosine 5'-triphosphate. *J Biol Chem.*, 269(39):24046-9.
167. **Kang C and Fromm HJ (1994b)** Characterization of the putative GTP-binding site residues of E. coli adenylosuccinate synthetase by site-directed mutagenesis. *Arch Biochem Biophys.*, 310 (2): 475-80.
168. **Karlström M, Steen IH, Madern D, Fedöy AE, Birkeland NK and Ladenstein R (2006)** The crystal structure of a hyperthermostable subfamily II isocitrate dehydrogenase from *Thermotoga maritima*. *FEBS J.*, 273(13):2851-68.
169. **Karshikoff A and Ladenstein R (2001)** Ion pairs and the thermotolerance of proteins from hyperthermophiles: a "traffic rule" for hot roads. *Trends Biochem. Sci.*, 26:550-556.
170. **Kauzmann W (1959)** Some factors in the interpretation of protein denaturation. *Adv. Protein Chem.*, 14:1-63.
171. **Keough DT, Ng AL, Winzor DJ, Emmerson BT and de Jersey J (1999)** Purification and characterization of *Plasmodium falciparum* hypoxanthine-guanine-xanthine phosphoribosyltransferase and comparison with the human enzyme. *Mol Biochem Parasitol.*, 98(1):29-41.
172. **Keough DT, Skinner-Adams T, Jones MK, Ng AL, Brereton IM, Guddat LW and de Jersey J (2006)** Lead compounds for antimalarial chemotherapy: purine base analogs discriminate between human and *P. falciparum* 6-oxopurine phosphoribosyltransferases. *J Med Chem.*, 49(25):7479-86.
173. **Khajeh K, Khezre-Barati S and Nemat-Gorgani M (2001)** Proteolysis of mesophilic and thermophilic alpha-amylases: a comparative study. *Appl Biochem Biotechnol.*, 94(2):97-109.
174. **Kicska GA, Tyler PC, Evans GB, Furneaux RH, Kim K and Schramm VL (2002a)** Transition state analogue inhibitors of purine nucleoside phosphorylase from *Plasmodium falciparum*. *J Biol Chem.*, 277(5):3219-25.
175. **Kicska GA, Tyler PC, Evans GB, Furneaux RH, Schramm VL and Kim K (2002b)** Purine-less death in *Plasmodium falciparum* induced by immucillin-H, a transition state analogue of purine nucleoside phosphorylase. *J Biol Chem.*, 277(5):3226-31.
176. **Kim PS and Baldwin RL (1990)** Intermediates in the folding reactions of small proteins. *Annu. Rev. Biochem.*, 59:631-660.
177. **Kirk K (2001)** Membrane transport in the malaria-infected erythrocyte. *Physiol Rev.*, 81(2):495-537.
178. **Knapp S, Kardinahl S, Hellgren N, Tibbelin G, Schäfer G and Ladenstein R (1999)** Refined crystal structure of a superoxide dismutase from the hyperthermophilic archaeon *Sulfolobus acidocaldarius* at 2.2 Å resolution. *J Mol Biol.*, 285(2):689-702.
179. **Kohen A, Cannio R, Bartolucci S and Klinman JP (1999)** Enzyme dynamics and hydrogen tunnelling in a thermophilic alcohol dehydrogenase. *Nature.*, 399:496-469.

180. **Kojoh K, Matsuzawa H and Wakagi T (1999)** Zinc and an N-terminal extra stretch of the ferredoxin from a thermoacidophilic archaeon stabilize the molecule at high temperature. *Eur J Biochem.*, 264(1):85-91.
181. **Korkhin Y, Kalb (Gilboa) AJ, Peretz M, Bogin O, Burstein Y and Frolow F (1999)** Oligomeric integrity--the structural key to thermal stability in bacterial alcohol dehydrogenases. *Protein Sci.*, 8(6):1241-9.
182. **Korn AP and Burnett RM (1991)** Distribution and complementarity of hydrophathy in multisubunit proteins. *Proteins.*, 9(1):37-55.
183. **Kumar S and Nussinov R (2001)** How do thermophilic proteins deal with heat? *Cell Mol Life Sci.*, 58(9):1216-33.
184. **Kumar S, Tsai CJ and Nussinov R (2000)** Factors enhancing protein thermostability. *Protein Eng.*, 13(3):179-91.
185. **Kuwajima K (1996)** The molten globule state of alpha-lactalbumin. *Faseb J.*, 10(1):102-9.
186. **Laemmli UK (1970)** Cleavage of structural proteins during the assembly of the head of bacteriophage T4. *Nature.*, 227:680-685
187. **Lakatos S, Halasz G and Zavodszky P (1978)** Conformational stability of lactate dehydrogenase from *Bacillus thermus-aquaticus*. *Biochem. Soc. Trans.*, 6:1195-1197.
188. **Lassalle MW, Hinz HJ, Wenzel H, Vlasi M, Kokkinidis M and Cesareni G (1998)** Dimer-to-tetramer transformation: loop excision dramatically alters structure and stability of the ROP four alpha-helix bundle protein. *J Mol Biol.*, 279(4):987-1000.
189. **Lawrence MC and Colman PM (1993)** Shape complementarity at protein/protein interfaces. *J Mol Biol.* 234(4):946-50.
190. **Lehrer GM and Barker R (1970)** Conformational changes in rabbit muscle aldolase. Kinetic studies. *Biochemistry.*, 9:1533-1540.
191. **Leskovic V (2003)** *Comprehensive Enzyme Kinetics*, Kulwer Academic/ Plenum Publishers, New York.
192. **Levy HM, Sharon N and Koshland DE (1959)** Purified muscle proteins and the walking rate of ants. *Proc. Natl. Acad. Sci. U.S.A.*, 45:785-791.
193. **Lewandowicz A, Ringia EA, Ting LM, Kim K, Tyler PC, Evans GB, Zubkova OV, Mee S, Painter GF, Lenz DH, Furneaux RH and Schramm VL (2005)** Energetic mapping of transition state analogue interactions with human and *Plasmodium falciparum* purine nucleoside phosphorylases. *J Biol Chem.*, 280(34):30320-8.
194. **Li CM, Tyler PC, Furneaux RH, Kicska G, Xu Y, Grubmeyer C, Girvin ME and Schramm VL (1999)** Transition-state analogs as inhibitors of human and malarial hypoxanthine-guanine phosphoribosyltransferases. *Nat Struct Biol.*, 6(6):582-7.
195. **Li WF, Zhou XX and Lu P (2005)** Structural features of thermozymes. *Biotechnol Adv.*, 23(4):271-81.
196. **Li WT, Grayling RA, Sandman K, Edmondson S, Shriver JW and Reeve JN (1998)** Thermodynamic stability of archaeal histones. *Biochemistry.*, 37(30):10563-72.

References

197. **Li WT, Shriver JW and Reeve JN (2000)** Mutational analysis of differences in thermostability between histones from mesophilic and hyperthermophilic archaea. *J Bacteriol.*, 182(3):812-7.
198. **Lieberman I (1956)** Enzymatic synthesis of adenosine-5'-phosphate from inosine-5'-phosphate. *J. Biol. Chem.*, 223:327-339.
199. **Lijnzaad P and Argos P (1997)** Hydrophobic patches on protein subunit interfaces: characteristics and prediction. *Proteins.*, 28(3):333-43.
200. **Lim JK, Lee HS, Kim YJ, Bae SS, Jeon JH, Kang SG and Lee JH (2007)** Critical factors to high thermostability of an alpha-amylase from hyperthermophilic archaeon *Thermococcus onnurineus* NA1. *J Microbiol Biotechnol.*, 17(8):1242-8.
201. **Lipps G and Krauss G (1999)** Adenylosuccinate synthase from *Saccharomyces cerevisiae*: homologous overexpression, purification and characterization of the recombinant protein. *Biochem J.*, 341 (Pt 3):537-43.
202. **Liu F, Dong Q and Fromm HJ (1992)** Site-directed mutagenesis of the phosphate-binding consensus sequence in *Escherichia coli* adenylosuccinate synthetase. *J Biol Chem.*, 267(4):2388-92.
203. **Liu W, Boitz JM, Galazka J, Arendt CS, Carter NS and Ullman B (2006)** Functional characterization of nucleoside transporter gene replacements in *Leishmania donovani*. *Mol Biochem Parasitol.*, 150(2):300-7.
204. **Lo Conte L, Chothia C and Janin J (1999)** The atomic structure of protein-protein recognition sites. *J Mol Biol.*, 285(5):2177-98.
205. **Lokanath NK, Shiromizu I, Ohshima N, Nodake Y, Sugahara M, Yokoyama S, Kuramitsu S, Miyano M and Kunishima N (2004)**. Structure of aldolase from *Thermus thermophilus* HB8 showing the contribution of oligomeric state to thermostability. *Acta Crystallogr D Biol Crystallogr.*, (Pt 10):1816-23.
206. **Londesborough J (1980)** The causes of sharply bent or discontinuous Arrhenius plots for enzyme-catalyzed reactions. *Eur. J. Biochem.*, 105:211-215.
207. **Lowenstein JM (1972)** Ammonia production in muscle and other tissues: the purine nucleotide cycle. *Physiol Rev.*, 52(2):382-414.
208. **Lüscher A, Onal P, Schweingruber AM and Mäser P (2007)** Adenosine kinase of *Trypanosoma brucei* and its role in susceptibility to adenosine antimetabolites. *Antimicrob Agents Chemother.*, 51(11):3895-901.
209. **Ma JC and Dougherty DA (1997)** The Cation- π Interaction. *Chem Rev.*, 97(5):1303-1324.
210. **MacBeath G, Kast P and Hilvert D (1998)** A small, thermostable, and monofunctional chorismate mutase from the archaeon *Methanococcus jannaschii*. *Biochemistry.*, 37:10062-10073.
211. **Macedo-Ribeiro S, Darimont B, Sterner R and Huber R (1996)** Small structural changes account for the high thermostability of 1[4Fe-4S] ferredoxin from the hyperthermophilic bacterium *Thermotoga maritima*. *Structure.*, 4(11):1291-301.

212. **Markham GD and Reed GH (1977)** Adenylosuccinate synthetase from *Azotobacter vinelandii*: purification, properties and steady-state kinetics. *Arch Biochem Biophys.*, 184(1):24-35.
213. **Markham GD and Reed GH (1978)** Reactions of phosphorothioate compounds catalyzed by adenylosuccinate synthetase. Steady state and pre-steady state kinetic studies. *J Biol Chem.*, 253(17):6184-9.
214. **Martin RE, Henry RI, Abbey JL, Clements JD and Kirk K (2005)** The 'permeome' of the malaria parasite: an overview of the membrane transport proteins of *Plasmodium falciparum*. *Genome Biol.*, 6(3):R26.
215. **Mäser P, Sütterlin C, Kralli A and Kaminsky R (1999)** A nucleoside transporter from *Trypanosoma brucei* involved in drug resistance. *Science.*, 285(5425):242-4.
216. **Massey V, Curti B and Ganther H (1966)** A temperature-dependent conformational change in D-amino acid oxidase and its effect on catalysis. *J. Biol. Chem.*, 241:2347-2357.
217. **Massova I, Kotra LP, Fridman R and Mobashery S (1998)** Matrix metalloproteinases: structures, evolution, and diversification. *FASEB J.*, 12(12):1075-95.
218. **Matovu E, Stewart ML, Geiser F, Brun R, Mäser P, Wallace LJ, Burchmore RJ, Enyaru JC, Barrett MP, Kaminsky R, Seebeck T and de Koning HP (2003)** Mechanisms of arsenical and diamidine uptake and resistance in *Trypanosoma brucei*. *Eukaryot Cell.*, 2(5):1003-8.
219. **Matsuda Y, Ogawa H, Fukutome S, Shiraki H and Nakagawa H (1977)** Adenylosuccinate synthetase in rat liver: the existence of two types and their regulatory roles. *Biochem Biophys Res Commun.*, 78(2):766-71.
220. **Matsuda Y, Shimura K, Shiraki H and Nakagawa H (1980)** Purification and properties of adenylosuccinate synthetase from Yoshida sarcoma ascites tumor cells. *Biochim Biophys Acta.*, 616(2):340-50.
221. **Matsui I and Harata K (2007)** Implication for buried polar contacts and ion pairs in hyperthermostable enzymes. *FEBS J.*, 274(16):4012-22.
222. **McConkey GA (2000)** *Plasmodium falciparum*: isolation and characterisation of a gene encoding protozoan GMP synthase. *Exp Parasitol.*, 94(1):23-32.
223. **McCoy AJ, Chandana Epa V and Colman PM (1997)** Electrostatic complementarity at protein/protein interfaces. *J Mol Biol.*, 268(2):570-84.
224. **Mehrotra S and Balaram H (2007)** Kinetic characterization of adenylosuccinate synthetase from the thermophilic archaea *Methanocaldococcus jannaschii*. *Biochemistry.*, 46:12821-12832.
225. **Merz A, Yee MC, Szadkowski H, Pappenberger G, Cramer A, Stemmer WP, Yanofsky C and Kirschner K (2000)** Improving the catalytic activity of a thermophilic enzyme at low temperatures. *Biochemistry.*, 39(5):880-9.
226. **Miller RW and Buchanan JM (1962)** Biosynthesis of the purines. 27. N-(5-Amino-1-ribose-4-imidazolylcarbonyl)-L-aspartic acid 5'-phosphate kinosynthetase. *J Biol Chem.*, 237:485-90.

References

227. **Miyazono K, Sawano Y and Tanokura M (2005)** Crystal structure and structural stability of acylphosphatase from hyperthermophilic archaeon *Pyrococcus horikoshii* OT3. *Proteins.*, 61(1):196-205.
228. **Muensch H and Yoshida A (1977)** Purification and characterization of human hypoxanthine/guanine phosphoribosyltransferase. *Eur J Biochem.*, 76(1):107-12
229. **Muirhead KM and Bishop SH (1974)** Purification of adenylosuccinate synthetase from rabbit skeletal muscle. *J. Biol. Chem.*, 249: 459-464.
230. **Nagy M, Djembo-Taty M and Heslot (1973)** Regulation of the biosynthesis of purine nucleotides in *Schizosaccharomyces pombe*. 3. Kinetic studies of adenylosuccinate synthetase. *Biochim Biophys Acta.*, 309(1):1-10.
231. **Nelson KE, Clayton RA, Gill SR, Gwinn ML, Dodson RJ, Haft DH, Hickey EK, Peterson JD, Nelson WC, Ketchum KA, McDonald L, Utterback TR, Malek JA, Linher KD, Garrett MM, Stewart AM, Cotton MD, Pratt MS, Phillips CA, Richardson D, Heidelberg J, Sutton GG, Fleischmann RD, Eisen JA, White O, Salzberg SL, Smith HO, Venter JC and Fraser CM (1999)** Evidence for lateral gene transfer between Archaea and bacteria from genome sequence of *Thermotoga maritima*. *Nature.*, 399(6734):323-9.
232. **Ogasahara K, Khechinashvili NN, Nakamura M, Yoshimoto T and Yutani K (2001)** Thermal stability of pyrrolidone carboxyl peptidases from the hyperthermophilic Archaeon, *Pyrococcus furiosus*. *Eur J Biochem.*, 268(11):3233-42.
233. **Ogasawara N, Goto H, Yamada Y, Watanabe T and Asano T (1982)** AMP deaminase isozymes in human tissues. *Biochim Biophys Acta.*, 714(2):298-306.
234. **Ogawa H, Shiraki H, Matsuda Y, Kakiuchi K and Nakagawa H (1977)** Purification, crystallization, and properties of adenylosuccinate synthetase from rat skeletal muscle. *J Biochem.*, 81(4):859-69.
235. **Ogawa H, Shiraki H and Nakagawa H (1976)** Study on the regulatory role of fructose-1,6-diphosphate in the formation of AMP in rat skeletal muscle. A mechanism for synchronization of glycolysis and the purine nucleotide cycle. *Biochem Biophys Res Commun.*, 68(2):524-8.
236. **Ogbunude PO and Ikediobi CO (1983)** Comparative aspects of purine metabolism in some African trypanosomes. *Mol Biochem Parasitol.*, 9(4):279-87.
237. **Oka J, Matsumoto A, Hosokawa Y and Inoue S (1994)** Molecular cloning of human cytosolic purine 5'-nucleotidase. *Biochem Biophys Res Commun.*, 205(1):917-22.
238. **Ortiz D, Sanchez MA, Pierce S, Herrmann T, Kimblin N, Archie Bower HG and Landfear SM (2007)** Molecular genetic analysis of purine nucleobase transport in *Leishmania major*. *Mol Microbiol.*, 64(5):1228-43.
239. **Pace CN (1979)** The stability of globular proteins. *CRC Crit. Rev. Biochem.*3, 1-43.
240. **Pace CN (1986)** Determination and analysis of urea and guanidine hydrochloride denaturation curves. *Methods Enzymol.*, 131:266-280.
241. **Pace CN (1990)** Conformational stability of globular proteins. *Trends Biochem. Sci.*, 15:14-17.

242. **Pack SP and Yoo YJ (2004)** Protein thermostability: structure-based difference of amino acid between thermophilic and mesophilic proteins. *J Biotechnol.*, 111(3):269-77.
243. **Pao CC and Dyess BT (1981)** Effect of unusual guanosine nucleotides on the activities of some *Escherichia coli* cellular enzymes. *Biochim Biophys Acta.*, 677(3-4):358-62
244. **Papageorgiou IG, Yakob L, Al Salabi MI, Diallinas G, Soteriadou KP and De Koning HP (2005)** Identification of the first pyrimidine nucleobase transporter in *Leishmania*: similarities with the *Trypanosoma brucei* U1 transporter and antileishmanial activity of uracil analogues. *Parasitology.*, 130(Pt 3):275-83.
245. **Parker MD, Hyde RJ, Yao SY, McRobert L, Cass CE, Young JD, McConkey GA and Baldwin SA (2000)** Identification of a nucleoside/nucleobase transporter from *Plasmodium falciparum*, a novel target for anti-malarial chemotherapy. *Biochem J.*, 349(Pt 1):67-75.
246. **Parkin DW (1996)** Purine-specific nucleoside N-ribohydrolase from *Trypanosoma brucei brucei*. Purification, specificity, and kinetic mechanism. *J Biol Chem.*, 271(36):21713-9.
247. **Pellé R, Schramm VL and Parkin DW (1998)** Molecular cloning and expression of a purine-specific N-ribohydrolase from *Trypanosoma brucei brucei*. Sequence, expression, and molecular analysis. *J Biol Chem.*, 273(4):2118-26.
248. **Penny JI, Hall ST, Woodrow CJ, Cowan GM, Gero AM and Krishna S (1998)** Expression of substrate-specific transporters encoded by *Plasmodium falciparum* in *Xenopus laevis* oocytes. *Mol Biochem Parasitol.* 93(1):81-9.
249. **Petsko GA (2001)** Structural basis of thermostability in hyperthermophilic proteins, or "there's more than one way to skin a cat". *Methods Enzymol.*, 334:469-478.
250. **Poland BW, Silva MM, Serra MA, Cho Y, Kim KH, Harris EM and Honzatko RB (1993)** Crystal structure of adenylosuccinate synthetase from *Escherichia coli*. Evidence for convergent evolution of GTP-binding domains. *J Biol Chem.*, 268(34):25334-42.
251. **Poland BW, Fromm HJ and Honzatko RB (1996a)** Crystal structures of adenylosuccinate synthetase from *Escherichia coli* complexed with GDP, IMP hadacidin, NO_3^- , and Mg^{2+} . *J Mol Biol.*, 264(5):1013-27.
252. **Poland BW, Lee SF, Subramanian MV, Siehl DL, Anderson RJ, Fromm HJ and Honzatko RB (1996b)** Refined crystal structure of adenylosuccinate synthetase from *Escherichia coli* complexed with hydantocidin 5'-phosphate, GDP, $\text{HPO}_4(2-)$, Mg^{2+} , and hadacidin. *Biochemistry.*, 35(49):15753-9.
253. **Poland BW, Hou Z, Bruns C, Fromm HJ and Honzatko RB (1996c)** Refined crystal structures of guanine nucleotide complexes of adenylosuccinate synthetase from *Escherichia coli*. *J Biol Chem.*, 271(26):15407-13.
254. **Poland BW, Bruns C, Fromm HJ and Honzatko RB (1997)** Entrapment of 6-thiophosphoryl-IMP in the active site of crystalline adenylosuccinate synthetase from *Escherichia coli*. *J Biol Chem.*, 272(24):15200-5.
255. **Poland BW, Hou Z, Bruns C, Fromm HJ and Honzatko RB (2002)** Refined crystal structures of guanine nucleotide complexes of adenylosuccinate synthetase from *Escherichia coli*. *J Biol Chem.*, 271(26):15407-13

References

256. **Pollack Y, Shemer R, Metzger S, Spira DT and Golenser J (1985)** Plasmodium falciparum: expression of the adenine phosphoribosyltransferase gene in mouse L cells. *Exp Parasitol.*, 60(3):270-5.
257. **Poole LB, Karplus PA and Claiborne A (2004)** Protein sulfenic acids in redox signaling. *Annu Rev Pharmacol Toxicol.*, 44:325-47.
258. **Poole LB, Zeng BB, Knaggs SA, Yakubu M and King SB (2005)** Synthesis of chemical probes to map sulfenic acid modifications on proteins. *Bioconjug Chem.*, 16(6):1624-8.
259. **Poole LB, Klomsiri C, Knaggs SA, Furdui CM, Nelson KJ, Thomas MJ, Fetrow JS, Daniel LW and King SB (2007)** Fluorescent and affinity-based tools to detect cysteine sulfenic acid formation in proteins. *Bioconjug Chem.*, 18(6):2004-17.
260. **Poole LB (2003)** Formation and Functions of Protein Sulfenic Acids, *Current Protocols in Toxicology* 17.1.1-17.1.15
261. **Poole LB (2003)** Measurement of protein sulfenic acid content. *Current Protocols in Toxicology* 17.2.1-17.1.20
262. **Porter DJ, Rudie NG and Bright HJ (1983)** Nitro analogs of substrates for adenylosuccinate synthetase and adenylosuccinate lyase. *Arch Biochem Biophys.*, 225(1):157-63.
263. **Potter SZ, Zhu H, Shaw BF, Rodriguez JA, Doucette PA, Sohn SH, Durazo A, Faull KF, Gralla EB, Nersissian AM and Valentine JS (2007)** Binding of a single zinc ion to one subunit of copper-zinc superoxide dismutase apoprotein substantially influences the structure and stability of the entire homodimeric protein. *J Am Chem Soc.*, 129(15):4575-83.
264. **Prade L, Cowan-Jacob SW, Chemla P, Potter S, Ward E and Fonne-Pfister R (2000)** Structures of adenylosuccinate synthetase from *Triticum aestivum* and *Arabidopsis thaliana*. *J Mol Biol.*, 296(2):569-77.
265. **Privalov PL (1979)** Stability of proteins: small globular proteins. *Adv. Protein Chem.*, 33:167-241.
266. **Privalov PL (1996)** Intermediate states in protein folding. *J. Mol. Biol.*, 258:707-725.
267. **Ptitsyn OB (1995)** Structures of folding intermediates. *Curr. Opin. Struct. Biol.*, 5:74-78.
268. **Ptitsyn OB (1995)** Molten globule and protein folding. *Adv Protein Chem.*, 83-229.
269. **Quashie NB, Dorin-Semblat D, Bray PG, Biagini GA, Doerig C, Ranford-Cartwright LC and De Koning HP (2008)** A comprehensive model of purine uptake by the malaria parasite *Plasmodium falciparum*: identification of four purine transport activities in intraerythrocytic parasites. *Biochem J.*, 411(2):287-95.
270. **Queen SA, Vander Jagt D and Reyes P (1988)** Properties and substrate specificity of a purine phosphoribosyltransferase from the human malaria parasite, *Plasmodium falciparum* *Mol Biochem Parasitol.*, 30(2):123-33.
271. **Queen SA, Vander Jagt DL and Reyes P (1989)** Characterization of adenine phosphoribosyltransferase from the human malaria parasite, *Plasmodium falciparum*. *Biochim Biophys Acta.*, 996(3):160-5.

272. **Rahman RN, Fujiwara S, Nakamura H, Takagi M and Imanaka T (1998)** Ion pairs involved in maintaining a thermostable structure of glutamate dehydrogenase from a hyperthermophilic archaeon. *Biochem Biophys Res Commun.*, 248(3):920-6.
273. **Raman B, Siva Kumar LV, Ramakrishna T and Mohan Rao C (2001)** Redox-regulated chaperone function and conformational changes of *Escherichia coli* Hsp33. *FEBS Lett.*, 489(1):19-24.
274. **Raman J, Mehrotra S, Anand RP and Balaram H (2004)** Unique kinetic mechanism of *Plasmodium falciparum* adenylosuccinate synthetase. *Mol Biochem Parasitol.*, 138(1):1-8
275. **Raman J, Ashok CS, Subbayya SI, Anand RP, Selvi ST and Balaram H (2005)** *Plasmodium falciparum* hypoxanthine guanine phosphoribosyltransferase. Stability studies on the product-activated enzyme. *FEBS J.*, 272(8):1900-11.
276. **Rager N, Mamoun CB, Carter NS, Goldberg DE and Ullman B (2001)** Localization of the *Plasmodium falciparum* PfNT1 nucleoside transporter to the parasite plasma membrane. *J Biol Chem.* 276(44):41095-9.
277. **Reyes P, Rathod PK, Sanchez DJ, Mrema JE, Rieckmann KH and Heidrich HG (1982)** Enzymes of purine and pyrimidine metabolism from the human malaria parasite, *Plasmodium falciparum*. *Mol Biochem Parasitol.*, 5(5):275-90
278. **Rudolph FB (1979a)** Product inhibition and abortive complex formation. *Methods Enzymol.*, 63:411-36.
279. **Rudolph FB and Fromm HJ (1969)** Initial rate studies of adenylosuccinate synthetase with product and competitive inhibitors. *J Biol Chem.*, 244(14):3832-9.
280. **Rudolph FB and Fromm HJ (1979b)** Plotting methods for analyzing enzyme rate data. *Methods Enzymol.*, 63:138-59.
281. **Russell RJ, Ferguson JM, Hough DW, Danson MJ and Taylor GL (1997)** The crystal structure of citrate synthase from the hyperthermophilic archaeon *pyrococcus furiosus* at 1.9 Å resolution. *Biochemistry*, 36(33):9983-94.
282. **Sadeghi M, Naderi-Manesh H, Zarrabi M and Ranjbar B (2006)** Effective factors in thermostability of thermophilic proteins. *Biophys Chem.*, 119(3):256-70.
283. **Sahota A, Webster DR, Potter CF, Simmonds HA, Rodgers AV and Gibson T (1983)** Methylthioadenosine phosphorylase activity in human erythrocytes. *Clin Chim Acta.*, 128(2-3):283-90
284. **Sakuraba H, Yoneda K, Asai I, Tsuge H, Katunuma N and Ohshima T (2008)** Structure of L-aspartate oxidase from the hyperthermophilic archaeon *Sulfolobus tokodaii*. *Biochim Biophys Acta.*, 3:563-71.
285. **Salmeen A and Barford D (2005)** Functions and mechanisms of redox regulation of cysteine-based phosphatases. *Antioxid Redox Signal.*, 7(5-6):560-77.
286. **Salminen T, Teplyakov A, Kankare J, Cooperman BS, Lahti R and Goldman A (1996)** An unusual route to thermostability disclosed by the comparison of *Thermus thermophilus* and *Escherichia coli* inorganic pyrophosphatases. *Protein Sci.*, 5(6):1014-25.

References

287. **Sanchez MA, Ullman B, Landfear SM and Carter NS (1999)** Cloning and functional expression of a gene encoding a P1 type nucleoside transporter from *Trypanosoma brucei*. *J Biol Chem.*, 274(42):30244-9.
288. **Sanchez MA, Tryon R, Green J, Boor I and Landfear SM (2002)** Six related nucleoside/nucleobase transporters from *Trypanosoma brucei* exhibit distinct biochemical functions. *J Biol Chem.*, 277(24):21499-504.
289. **Sanchez MA, Tryon R, Pierce S, Vasudevan G and Landfear SM (2004a)** Functional expression and characterization of a purine nucleobase transporter gene from *Leishmania major*. *Mol Membr Biol.*, 21(1):11-8.
290. **Sanchez MA, Drutman S, van Ampting M, Matthews K and Landfear SM (2004b)** A novel purine nucleoside transporter whose expression is up-regulated in the short stumpy form of the *Trypanosoma brucei* life cycle. *Mol Biochem Parasitol.*, 136(2):265-72.
291. **Saraste M, Sibbald PR and Wittinghofer A (1990)** The P-loop--a common motif in ATP- and GTP-binding proteins. *Trends Biochem Sci.*, 15(11):430-4.
292. **Sarkar Gand Sommer SS (1990)** The "megaprimer" method of site-directed mutagenesis. *Biotechniques.*, 8(4):404-7.
293. **Saxena VP and Wetlaufer DB (1971)** A new basis for interpreting the circular dichroic spectra of proteins. *Proc. Natl. Acad. Sci. U.S.A.*, 68:969-972.
294. **Schmalhausen EV, Nagradova NK, Boschi-Muller S, Branlant G and Muronetz VI (1999)** Mildly oxidized GAPDH: the coupling of the dehydrogenase and acyl phosphatase activities. *FEBS Lett.*, 452(3):219-22.
295. **Schultes V and Jaenicke R (1991)** Folding intermediates of hyperthermophilic D-glyceraldehyde-3-phosphate dehydrogenase from *Thermotoga maritima* are trapped at low temperature. *FEBS Lett.*, 290:235-238.
296. **Schwab JC, Afifi Afifi M, Pizzorno G, Handschumacher RE and Joiner KA (1995)** *Toxoplasma gondii* tachyzoites possess an unusual plasma membrane adenosine transporter. *Mol Biochem Parasitol.*, 70(1-2):59-69
297. **Scopes DA, Bautista JM, Naylor CE, Adams MJ and Mason PJ (1998)** Amino acid substitutions at the dimer interface of human glucose-6-phosphate dehydrogenase that increase thermostability and reduce the stabilising effect of NADP. *Eur J Biochem.*, 251(1-2):382-8.
298. **Segel IH (1975)** *Enzyme Kinetics. Behaviour and Analysis of Rapid Equilibrium and Steady-state Enzyme Systems.* John Wiley & Sons Inc., New York.
299. **Sherman IW (1979)** *Biochemistry of Plasmodium (malarial parasites).* *Microbiol Rev.*, 43(4):453-95.
300. **Shi W, Ting LM, Kicska GA, Lewandowicz A, Tyler PC, Evans GB, Furneaux RH, Kim K, Almo SC and Schramm VL (2004)** *Plasmodium falciparum* purine nucleoside phosphorylase: crystal structures, immucillin inhibitors, and dual catalytic function. *J Biol Chem.*, 279(18):18103-6.
301. **Shigeura HT (1963)** Structural modifications of hadacidin and their effects on the activity of adenylosuccinate synthetase. *J Biol Chem.*, 238:3999-4001.

302. **Shigeura HT and Gordon CN (1962b)** The mechanism of action of hadacidin. *J Biol Chem.*, 237:1937-40.
303. **Shigeura HT, Gordon CN (1962a)** Hadacidin, a new inhibitor of purine biosynthesis. *J Biol Chem.*, 237:1932-6.
304. **Shivashankar K, Subbayya IN and Balaram H (2001)** Development of a bacterial screen for novel hypoxanthine-guanine phosphoribosyltransferase substrates. *J Mol Microbiol Biotechnol.*, 3(4):557-62.
305. **Silva MM, Poland BW, Hoffman CR, Fromm HJ and Honzatko RB (1995)** Refined crystal structures of unligated adenylosuccinate synthetase from *Escherichia coli*. *J Mol Biol.*, 254(3):431-46.
306. **Simmonds HA, Fairbanks LD, Duley JA and Morris GS (1989)** ATP formation from deoxyadenosine in human erythrocytes: evidence for a hitherto unidentified route involving adenine and S-adenosylhomocysteine hydrolase. *Biosci Rep.*, 9(1):75-85.
307. **Smith CA, Toogood HS, Baker HM, Daniel RM and Baker EN (1999)** Calcium-mediated thermostability in the subtilisin superfamily: the crystal structure of *Bacillus Ak.1* protease at 1.8 Å resolution. *J Mol Biol.*, 294(4):1027-40.
308. **Spector T and Miller RL (1976)** Mammalian adenylosuccinate synthetase. Nucleotide monophosphate substrates and inhibitors. *Biochim Biophys Acta.*, 445(2):509-17.
309. **Spector T, Jones TE and Elion GB (1979)** Specificity of adenylosuccinate synthetase and adenylosuccinate lyase from *Leishmania donovani*. Selective amination of an antiprotozoal agent. *J Biol Chem.*, 254(17):8422-6.
310. **Srivastava SK and Beutler E (1971)** Purification and kinetic studies of adenine phosphoribosyltransferase from human erythrocytes. *Arch Biochem Biophys.*, 142(2):426-34
311. **Stayton MM and Fromm HJ (1979)** Guanosine 5'-diphosphate-3'-diphosphate inhibition of adenylosuccinate synthetase. *J Biol Chem.*, 254(8):2579-81.
312. **Stayton MM, Rudolph FB and Fromm HJ (1983)** Regulation, genetics, and properties of adenylosuccinate synthetase: A review. *Curr Top Cell Regul.*, 22:103-41.
313. **Stein A, Vaseduvan G, Carter NS, Ullman B, Landfear SM and Kavanaugh MP (2003)** Equilibrative nucleoside transporter family members from *Leishmania donovani* are electrogenic proton symporters. *J Biol Chem.*, 278(37):35127-34.
314. **Sterner R, Kleemann GR, Szadkowski H, Lustig A, Hennig M and Kirschner K (1996)** Phosphoribosyl anthranilate isomerase from *Thermotoga maritima* is an extremely stable and active homodimer. *Protein Sci.*, 5(10):2000-8.
315. **Stieglitz KA, Yang H, Roberts MF and Stec B (2005)** Reaching for mechanistic consensus across life kingdoms: structure and insights into catalysis of the myo-inositol-1-phosphate synthase (mIPS) from *Archaeoglobus fulgidus*. *Biochemistry.*, 44(1):213-24.
316. **Striepen B, Pruijssers AJ, Huang J, Li C, Gubbels MJ, Umejiro NN, Hedstrom L and Kissinger JC (2004)** Gene transfer in the evolution of parasite nucleotide biosynthesis. *Proc Natl Acad Sci U S A.*, 101(9):3154-9.
317. **Stryer L and Bourne HR (1986)** G proteins: a family of signal transducers. *Annu Rev Cell Biol.*, 2:391-419.

References

318. **Sullivan WJ Jr, Chiang CW, Wilson CM, Naguib FN, el Kouni MH, Donald RG and Roos DS (1999)** Insertional tagging of at least two loci associated with resistance to adenine arabinoside in *Toxoplasma gondii*, and cloning of the adenosine kinase locus. *Mol Biochem Parasitol.*, 103(1):1-14.
319. **Sullivan WJ Jr, Dixon SE, Li C, Striepen B and Queener SF (2005)** IMP dehydrogenase from the protozoan parasite *Toxoplasma gondii*. *Antimicrob Agents Chemother.*, 49(6):2172-9.
320. **Szilágyi A and Závodszy P (2000)** Structural differences between mesophilic, moderately thermophilic and extremely thermophilic protein subunits: results of a comprehensive survey. *Structure.*, 8(5):493-504.
321. **Tahirov TH, Oki H, Tsukihara T, Ogasahara K, Yutani K, Ogata K, Izu Y, Tsunasawa S and Kato I (1998)** Crystal structure of methionine aminopeptidase from hyperthermophile, *Pyrococcus furiosus*. *J Mol Biol.*, 284(1):101-24.
322. **Tainer JA, Roberts VA and Getzoff ED (1992)** Protein metal-binding sites. *Curr Opin Biotechnol.*, 3(4):378-87.
323. **Takagi Y and Taira K (1995)** Temperature-dependent change in the rate-determining step in a reaction catalyzed by a hammerhead ribozyme. *FEBS Lett.*, 361:273-276.
324. **Tanford C (1968)** Protein denaturation. *Adv. Protein Chem.*, 23:121-282.
325. **Tanford C (1970)** Protein denaturation. C. Theoretical models for the mechanism of denaturation. *Adv. Protein Chem.*, 24:1-95.
326. **Talsky G (1971)** The anomalous temperature dependence of enzyme-catalyzed reactions. *Angew. Chem. Int. Ed. Engl.*, 10:548-554.
327. **Tanner JJ, Hecht RM and Krause KL (1996)** Determinants of enzyme thermostability observed in the molecular structure of *Thermus aquaticus* D-glyceraldehyde-3-phosphate dehydrogenase at 25 Angstroms Resolution. *Biochemistry.*, 35(8):2597-609.
328. **Tansey MR and Brock TD (1972)** The upper temperature limit for eukaryotic organisms. *Proc Natl Acad Sci U S A*, 69(9):2426-8.
329. **Tehei M and Zaccai G (2007)** Adaptation to high temperatures through macromolecular dynamics by neutron scattering. *FEBS J.*, 274(16):4034-43.
330. **Tekaia F, Yeramian E and Dujon B (2002)** Amino acid composition of genomes, lifestyles of organisms, and evolutionary trends: a global picture with correspondence analysis. *Gene.*, 297(1-2):51-60.
331. **Thoma R, Hennig M, Sterner R and Kirschner K (2000)** Structure and function of mutationally generated monomers of dimeric phosphoribosylanthranilate isomerase from *Thermotoga maritima*. *Structure.*, 8(3):265-76.
332. **Thompson JD, Higgins DG, Gibson TJ (1994)** CLUSTAL W: improving the sensitivity of progressive multiple sequence alignment through sequence weighting, position-specific gap penalties and weight matrix choice. *Nucleic Acids Res.*, 22(22):4673-80.
333. **Thompson MJ and Eisenberg D (1999)** Transproteomic evidence of a loop-deletion mechanism for enhancing protein thermostability. *J Mol Biol.*, 290(2):595-604.

334. **Thompson J, Shirley B, Grimsley G and Pace CN (1989)** Conformational stability and mechanism of folding of ribonuclease T1. *J Biol Chem.*, 264(20):11614-11620.
335. **Ting LM, Shi W, Lewandowicz A, Singh V, Mwakingwe A, Birck MR, Ringia EA, Bench G, Madrid DC, Tyler PC, Evans GB, Furneaux RH, Schramm VL and Kim K (2005)** Targeting a novel Plasmodium falciparum purine recycling pathway with specific immucillins. *J Biol Chem.*, 280(10):9547-54.
336. **Tipton KF and Dixon HB (1979)** Effects of pH on enzymes. *Methods Enzymol.*, 63:183-234.
337. **Tomazic SJ and Klibanov AM (1988)** Why is one Bacillus alpha-amylase more resistant against irreversible thermoinactivation than another? *J Biol Chem.*, 263(7):3092-6.
338. **Tornheim K and Lowenstein JM (1974)** The purine nucleotide cycle. IV. Interactions with oscillations of the glycolytic pathway in muscle extracts. *J Biol Chem.*, 249(10):3241-7.
339. **Trager W (1970)** Recent progress in some aspects of the physiology of parasitic protozoa. *J Parasitol.*, 56(4):627-33.
340. **Trager W and Jensen JB (1976)** Human malaria parasites in continuous culture. *Science.*, 193(4254):673-5.
341. **Traut TW (1994)** Physiological concentrations of purines and pyrimidines. *Mol Cell Biochem.*, 140(1):1-22.
342. **Valdar WS and Thornton JM (2001)** Protein-protein interfaces: analysis of amino acid conservation in homodimers. *Proteins.*, 42(1):108-24.
343. **Van den Berghe G, Bontemps F and Vincent MF (1988)** Cytosolic purine 5'-nucleotidases of rat liver and human red blood cells: regulatory properties and role in AMP dephosphorylation. *Adv Enzyme Regul.*, 27:297-311.
344. **Van den Berghe G and Bontemps F (1990)** Adenine nucleotide catabolism in human erythrocytes: pathways and regulation. *Biomed Biochim Acta.*, 49(2-3):S117-22.
345. **Van der Weyden MB and Kelly WN (1974)** Human adenylosuccinate synthetase. Partial purification, kinetic and regulatory properties of the enzyme from placenta. *J Biol Chem.*, 249(22):7282-9.
346. **Van Heukelom LH, Boom A, Bartstra HA and Staal GE (1976)** Characterization of adenosine deaminase isozymes from normal human erythrocytes. *Clin Chim Acta.*, 72(1):109-15.
347. **Vargo MA, Nguyen L and Colman RF (2004)** Subunit interface residues of glutathione S-transferase A1-1 that are important in the monomer-dimer equilibrium. *Biochemistry.*, 43(12):3327-35.
348. **Vasudevan G, Carter NS, Drew ME, Beverley SM, Sanchez MA, Seyfang A, Ullman B and Landfear SM (1998)** Cloning of Leishmania nucleoside transporter genes by rescue of a transport-deficient mutant. *Proc Natl Acad Sci U S A.*, 95(17):9873-8.
349. **Vermeer AW and Norde W (2000)** The thermal stability of immunoglobulin: unfolding and aggregation of a multi-domain protein. *Biophys. J.*, 78:394-404.

References

350. **Vieille C, Epting KL, Kelly RM and Zeikus JG (2001)** Bivalent cations and amino-acid composition contribute to the thermostability of *Bacillus licheniformis* xylose isomerase. *Eur J Biochem.*, 268(23):6291-301.
351. **Vieille C and Zeikus GJ (2001)** Hyperthermophilic enzymes: sources, uses, and molecular mechanisms for thermostability. *Microbiol Mol Biol Rev.*,65(1):1-43.
352. **Villeret V, Clantin B, Tricot C, Legrain C, Roovers M, Stalon V, Glansdorff N and Van Beeumen J (1998)** The crystal structure of *Pyrococcus furiosus* ornithine carbamoyltransferase reveals a key role for oligomerization in enzyme stability at extremely high temperatures. *Proc Natl Acad Sci U S A.*, 95(6):2801-6.
353. **Vetriani C, Maeder DL, Tolliday N, Yip KS, Stillman TJ, Britton KL, Rice DW, Klump HH and Robb FT (1998)** Protein thermostability above 100 degreesC: a key role for ionic interactions. *Proc Natl Acad Sci U S A.*, 95(21):12300-5.
354. **Vieille C, Burdette DS and Zeikus JG (1996)** Thermozyms. *Biotechnol Annu Rev.*, 2:1-83.
355. **Vihinen M (1987)** Relationship of protein flexibility to thermostability. *Protein Eng.*, 1(6):477-80.
356. **Vitali J, Colaneri MJ, Kantrowitz E (2007)** Crystal structure of the catalytic trimer of *Methanococcus jannaschii* aspartate transcarbamoylase. *Proteins.*,71(3):1324-1334.
357. **Vodnala M, Fijolek A, Rofougaran R, Mosimann M, Mäser P and Hofer A (2008)** Adenosine kinase mediates high affinity adenosine salvage in *Trypanosoma brucei*. *J Biol Chem.*, 283(9):5380-8.
358. **Vogt G, Woell S and Argos P (1997)** Protein thermal stability, hydrogen bonds, and ion pairs. *J. Mol. Biol.*, 269:631-643.
359. **Wallace LJ, Candlish D, Hagos A, Seley KL and de Koning HP (2004)** Selective transport of a new class of purine antimetabolites by the protozoan parasite *Trypanosoma brucei*. *Nucleosides Nucleotides Nucleic Acids.*, 23(8-9):1441-4.
360. **Wang W, Gorrell A, Honzatko RB and Fromm HJ (1997a)** A study of *Escherichia coli* adenylosuccinate synthetase association states and the interface residues of the homodimer. *J Biol Chem.*, 272(11):7078-84.
361. **Wang W, Hou Z, Honzatko RB and Fromm HJ (1997b)** Relationship of conserved residues in the IMP binding site to substrate recognition and catalysis in *Escherichia coli* adenylosuccinate synthetase. *J Biol Chem.*, 272(27):16911-6.
362. **Wang W, Gorrell A, Hou Z, Honzatko RB and Fromm HJ (1998)** Ambiguities in mapping the active site of a conformationally dynamic enzyme by directed mutation. Role of dynamics in structure-function correlations in *Escherichia coli* adenylosuccinate synthetase. *J Biol Chem.*, 273(26):16000-4.
363. **Wang W, Poland BW, Honzatko RB and Fromm HJ (1995)** Identification of arginine residues in the putative L-aspartate binding site of *Escherichia coli* adenylosuccinate synthetase. *J Biol Chem.*, 270(22):13160-3.
364. **Webster HK and Whaun JM (1981)** Purine metabolism during continuous erythrocyte culture of human malaria parasites (*P. falciparum*). *Prog Clin Biol Res.*, 55:557-73.

365. **Webster HK, Whaun JM, Walker MD and Bean TL (1984)** Synthesis of adenosine nucleotides from hypoxanthine by human malaria parasites (*Plasmodium falciparum*) in continuous erythrocyte culture: inhibition by hadacidin but not alanosine. *Biochem Pharmacol.*, 33(9):1555-7.
366. **Werner A, Siems W, Schmidt H, Rapoport I, Gerber G, Toguzov RT, Tikhonov YV and Pimenov AM (1987)** Determination of nucleotides, nucleosides and nucleobases in cells of different complexity by reversed-phase and ion-pair high-performance liquid chromatography. *J Chromatogr.*, 421(2):257-65.
367. **Werner A, Jacobasch G, Siems W, Gerth C and Schreiter C (1990)** Nucleotide status in erythrocytes of rats infected with *Pl. berghei*. *Biomed Biochim Acta.*, 49(2-3):S301-4.
368. **White EL, Ross LJ, Davis RL, Zywno-Van Ginkel S, Vasanthakumar G and Borhani DW (2000)** The two *Toxoplasma gondii* hypoxanthine-guanine phosphoribosyltransferase isozymes form heterotetramers. *J Biol Chem.*, 275(25):19218-23.
369. **Wilson JM, O'Toole TE, Argos P, Shewach DS, Daddona PE and Kelley WN (1986)** Human adenine phosphoribosyltransferase. Complete amino acid sequence of the erythrocyte enzyme. *J Biol Chem.*, 261(29):13677-83.
370. **Wilson JM, Tarr GE, Mahoney WC and Kelley WN (1982)** Human hypoxanthine-guanine phosphoribosyltransferase. Complete amino acid sequence of the erythrocyte enzyme. *J Biol Chem.*, 257(18):10978-85.
371. **Witzmann S and Bisswanger H (1998)** The pyruvate dehydrogenase complex from thermophilic organisms: thermal stability and re-association from the enzyme components. *Biochim. Biophys. Acta*, 1385:341-352.
372. **Woese CR and Fox GE (1977)** Phylogenetic structure of the prokaryotic domain: the primary kingdoms. *Proc Natl Acad Sci U S A.*, 74(11):5088-90.
373. **Woese CR, Kandler O and Wheelis ML (1990)** Towards a natural system of organisms: proposal for the domains Archaea, Bacteria, and Eucarya. *Proc Natl Acad Sci U S A.*, 87(12):4576-9.
374. **Wolf-Watz M, Thai V, Henzler-Wildman K, Hadjipavlou G, Eisenmesser EZ and Kern D (2004)** Linkage between dynamics and catalysis in a thermophilic-mesophilic enzyme pair. *Nat Struct Mol Biol.*, 11(10):945-9.
375. **Wrba A, Schweiger A, Schultes V, Jaenicke R and Zavodsky P (1990)** Extremely thermostable D-glyceraldehyde-3-phosphate dehydrogenase from the eubacterium *Thermotoga maritima*. *Biochemistry.*, 29:7584-7592.
376. **Xanthoudakis S and Curran T (1996)** Redox regulation of AP-1: a link between transcription factor signaling and DNA repair. *Adv Exp Med Biol.*, 387:69-75.
377. **Yang M, Horii K, Herr AB and Kirley TL (2008)** Characterization and importance of the dimer interface of human calcium-activated nucleotidase. *Biochemistry.*, 47(2):771-8.
378. **Yip KS, Stillman TJ, Britton KL, Artymiuk PJ, Baker PJ, Sedelnikova SE, Engel PC, Pasquo A, Chiaraluce R and Consalvi V (1995)** The structure of *Pyrococcus furiosus* glutamate dehydrogenase reveals a key role for ion-pair networks in maintaining enzyme stability at extreme temperatures. *Structure.*, 3(11):1147-58.

References

379. **Yun S and Suelter CH (1978)** Human erythrocyte 5'-AMP aminohydrolase. Purification and characterization. *J Biol Chem.*, 253(2):404-8.
380. **Zannis V, Doyle D and Martin DW Jr (1978)** Purification and characterization of human erythrocyte purine nucleoside phosphorylase and its subunits. *J Biol Chem.*, 253(2):504-10.
381. **Zannis VI, Gudas LJ and Martin DW Jr (1980)** Characterization of the subunit composition of HGPRTase from human erythrocytes and cultured fibroblasts. *Biochem Genet.*, 18(1-2):1-19.
382. **Závodszy P, Kardos J, Svingor and Petsko GA (1998)** Adjustment of conformational flexibility is a key event in the thermal adaptation of proteins. *Proc Natl Acad Sci U S A.*, 95(13):7406-11.
383. **Zeidler R, Hobert O, Johannes L, Faulhammer H and Krauss G (1993)** Characterization of two novel single-stranded DNA-specific autonomously replicating sequence-binding proteins from *Saccharomyces cerevisiae*, one of which is adenylosuccinate synthetase. *J. Biol. Chem.*, 268:20191-20197.
384. **Zewe V and Fromm HJ (1962)** Kinetic studies of rabbit muscle lactate dehydrogenase. *J Biol Chem.*, 237:1668-75.
385. **Zhanhua C, Gan JG, Lei L, Sakharkar MK and Kanguane P (2005)** Protein subunit interfaces: heterodimers versus homodimers. *Bioinformation.*, 1(2):28-39.
386. **Zhou XX, Wang YB, Pan YJ and Li WF (2008)** Differences in amino acids composition and coupling patterns between mesophilic and thermophilic proteins. *Amino Acids.*, 34(1):25-33.
387. **Zolg JW, MacLeod AJ, Dickson IH and Scaife JG (1982)** Plasmodium falciparum: modifications of the in vitro culture conditions improving parasitic yields. *J Parasitol.*, 68(6):1072-80.